REPORT NO.
UCB/EERC-88/17
NOVEMBER 1988

EARTHQUAKE ENGINEERING RESEARCH CENTER

EARTHQUAKE ENGINEERING RESEARCH AT BERKELEY – 1988

Papers presented by faculty participants and research personnel associated with the Earthquake Engineering Research Center at the Ninth World Conference on Earthquake Engineering, Tokyo-Kyoto, Japan, August 1988.

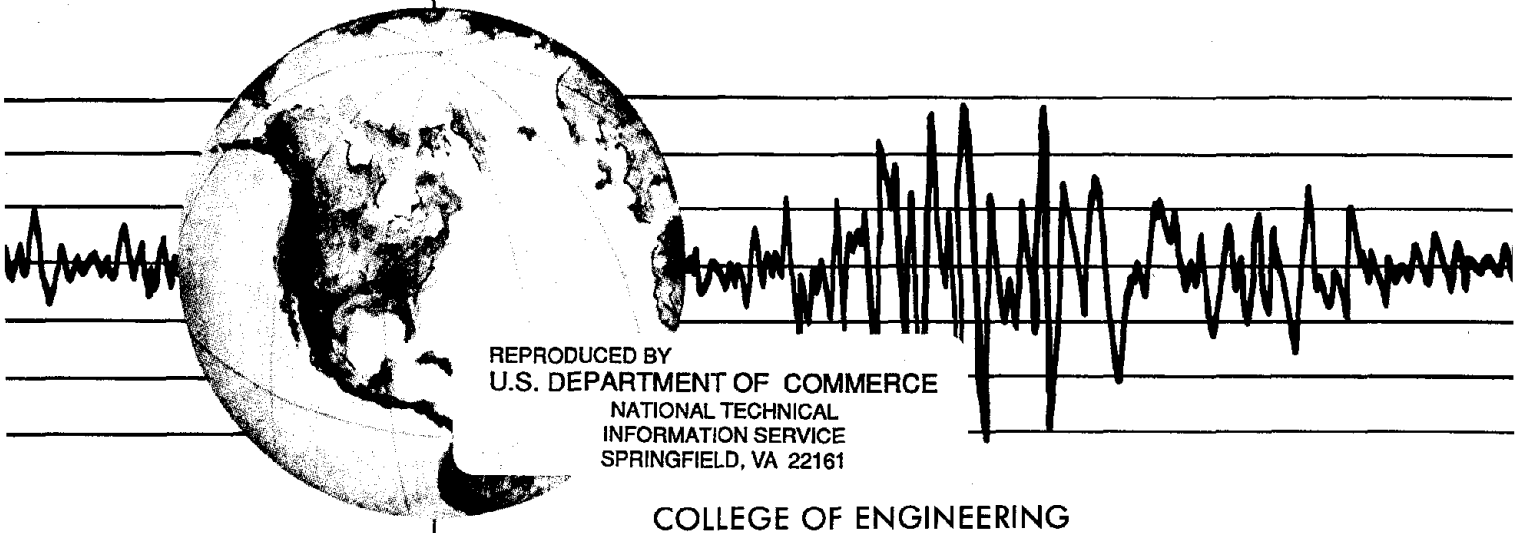

COLLEGE OF ENGINEERING

UNIVERSITY OF CALIFORNIA AT BERKELEY

For sale by the National Technical Information Service, U.S. Department of Commerce, Springfield, Virginia 22161

See back of report for up to date listing of EERC reports.

50272-101

REPORT DOCUMENTATION PAGE	1. REPORT NO. NSF/ENG-88056	2.	3. PB91-210864

4. Title and Subtitle
"Earthquake Engineering Research at Berkeley - 1988."

5. Report Date
November 1988

6.

7. Author(s)
Faculty participants and research personnel at EERC

8. Performing Organization Rept. No.
UCB/EERC-88/17

9. Performing Organization Name and Address
Earthquake Engineering Research Center
University of California
1301 South 46th Street
Richmond CA 94804

10. Project/Task/Work Unit No.

11. Contract(C) or Grant(G) No.
(C)
(G) ECE 8419739
ECE 8414036
CEE 8402271

12. Sponsoring Organization Name and Address

13. Type of Report & Period Covered

14.

15. Supplementary Notes

16. Abstract (Limit: 200 words)

At the Ninth World Conference on Earthquake Engineering held in Tokyo and Kyoto, Japan, August 2-9, 1988 twenty-six papers were presented by faculty participants and research personnel associated with the Earthquake Engineering Research Center, University of California at Berkeley. The papers have been compiled in this report to illustrate some of the research work in earthquake engineering being conducted at the University of California at Berkeley.

The research work has been sponsored by the following agencies:

National Science Foundation
Electric Power Research Institute
The Tinker Foundation
Italian Research Council (C.N.R.)
Research Division of the Catholic University of Chile
Computer Center at the University of California at Berkeley
American Institute of Steel Construction Fellowship Program
Nishkian Professorship in Structural Engineering at the University of California at Berkeley
Tokyo Electric Power-Service Company
Taiwan Power Company, R.O.C.
American Iron and Steel Institute

17. Document Analysis a. Descriptors

b. Identifiers/Open-Ended Terms

c. COSATI Field/Group

18. Availability Statement:	19. Security Class (This Report)	21. No. of Pages
Release Unlimited	Release Unlimited	200
	20. Security Class (This Page)	22. Price

EARTHQUAKE ENGINEERING RESEARCH AT BERKELEY — 1988

Papers presented by faculty participants and
research personnel associated with the
Earthquake Engineering Research Center at the
Ninth World Conference on Earthquake Engineering
Tokyo—Kyoto, Japan
August 1988

Report No. UCB/EERC-88/17
Earthquake Engineering Research Center
College of Engineering
University of California at Berkeley

November 1988

FOREWORD

At the Ninth World Conference on Earthquake Engineering held in Tokyo and Kyoto, Japan, August 2—9, 1988 twenty-six papers were presented by faculty participants and research personnel associated with the Earthquake Engineering Research Center, University of California at Berkeley. The papers have been compiled in this report to illustrate some of the research work in earthquake engineering being conducted at the University of California at Berkeley. The research work has been sponsored by the following agencies:

National Science Foundation
Tokyo Electric Power Service Company
Electric Power Research Institute (EPRI)
Taiwan Power Company, ROC
Research Division of the Catholic University of Chile
The Tinker Foundation
Computer Center, University of California at Berkeley
American Iron and Steel Institute
American Institute of Steel Construction Fellowship Program
Nishkian Professorship in Structural Engineering, University of California at Berkeley
Italian Research Council (C.N.R.)

TABLE OF CONTENTS

SEISMIC RESPONSE OF A NINE-STORY STEEL FRAME WITH FRICTION DAMPED CROSS-BRACING

Ian D. Aiken[1], James M. Kelly[2], and Avtar S. Pall[3]

1 Graduate Student, Dept. of Civil Engineering, University of California, Berkeley, USA
2 Professor, Dept. of Civil Engineering, University of California, Berkeley, USA
3 President, Pall Dynamics Limited, Montreal, Quebec, Canada

SUMMARY

A passive energy dissipation system that incorporates friction damping devices in the cross-bracing of a medium-rise steel moment resisting frame is investigated. Earthquake simulator tests and an analytical study of the system are performed and the response characteristics compared with those of equivalent moment resisting and eccentric braced frames.

An existing scale model 9 story steel moment resisting frame (MRF) was modified to include friction damped bracing as part of the lateral load resisting system. The frame is one bay wide and three bays long and represents a typical section in the weak direction of a steel frame building of approximately one-quarter scale.

It was observed that the friction damped braced frame (FDBF) system had the ability to behave in a nonlinear fashion without demanding inelastic behavior in the frame itself. This implied continued integrity of the structure during and after a seismic event. Analytical results and experimental observations confirmed that for small variations of the slip loads from the optimum loads the overall response of the frame remained essentially unchanged.

INTRODUCTION

It is generally accepted that the performance of a structure subject to earthquake attack is enhanced by an increase in internal damping in that structure. The damping absorbs kinetic energy induced in the structure and prevents the build-up of resonant vibrations should the natural frequency of the structure coincide with a strong frequency present in the ground motion. In conventional structural design for earthquake resistance the damping in the structure is produced by inelastic action at beam-column connections and to develop significant damping the amount of inelastic action can produce damage at the connections. For long duration earthquake attack, such as, for example, the recent Mexico City earthquake, this damage at the connections over many cycles can lead to collapse of the structure even for a relatively low peak ground acceleration.

There have been attempts in recent years to introduce special structural details such as the eccentrically braced frame, or special energy absorbing devices which can increase the damping of the system but still sustain many cycles of action without leading to collapse. The action in the eccentric braced frame and in many of the devices so far proposed is still cyclic plastic deformation and as such is irrevocably associated with the development of local damage. While the devices could in principle be replaced after a severe earthquake, eccentric bracing is an integral part of the structure and could not be replaced. Further, in both cases the response of the element and of the entire structural system can be complex and there are as yet unresolved problems in designing structures using design spectrum methods (which are the most widely used techniques and which are intrinsically linear).

The use of frictional damping elements for a variety of structural systems has been proposed by Pall, ranging from braced frames [1,2] to concrete shear walls [3] and panel structures [4]. Frictional elements have the advantage of being amenable to a particularly simple form of mechanical modelling and their response should be repeatable and fatigue resistant. The system which is the subject of this experimental study also has the added advantage that it can be incorporated directly in the bracing of a structural frame. The energy dissipated by a typical friction damping device is proportional to the slip load and the slip deformations of that device. For some specific slip load, or combination of device slip loads within a structure, an optimum (minimum) response for the FDBF can be achieved.

TEST PROGRAM

Experimental Model

The earthquake simulator tests were performed on a nine story 1/4-scale steel frame structure which was 28ft high and 18ft wide. To satisfy similitude requirements the structure was loaded with additional mass, consisting of 10 kips of concrete and lead ballast per level, giving a total structure weight of approximately 99 kips. The scale model was originally constructed for an experimental investigation into the effects of column uplift on the seismic preformance of structures [5] and has also been used in a previous series of base isolation tests [6]. The structure was modified for the friction damping tests by providing suitable connection details at the interior beam-column joints to allow the installation of the friction devices. The structure with the friction damping devices installed in the bracing is shown in Figure 1.

Friction Damping Devices

The friction damping devices used in the test series were of a design originally proposed by Pall. A typical friction damping device is shown in Figure 2, and consists of diagonal brace elements that have a friction interface at their intersection point and which are connected together by horizontal and vertical link elements. The friction interface is a simple brake-pad lining/stainless steel couple which is activated by a specified preload normal force. The link elements ensure that when the load applied to the device via the braces is sufficient to initiate slip of the tension arm then the compression arm will also slip an equal amount in the opposite direction. Deformation fields of a friction damping device are shown in Figure 3. Implicit with these slip deformations, and hence energy dissipation by the devices, is that the structural frame must undergo geometric deformations. The design intent, therefore, is to select the loads required to cause slip in the devices within the frame to correspond to the range of elastic deformations of the structure. The criteria used to determine the slip loads for the devices are outlined below:

- The damping devices should not slip for wind and low to moderate earthquake loadings or shear forces calculated on the basis of a quasi-static approach as typically specified by the building codes. This requirement leads to a minimum value for the slip load.
- The devices should start slipping before the yield limit of any member of the structure is reached. This places an upper bound on the device slip load.
- The slip loads of the devices should be such that the energy dissipated within the structural system due to friction is maximized.

These criteria were used to obtain an approximate value for the slip loads required in the devices, and then the opitmization of the loads was achieved by performing a series of nonlinear time history analyses, varying the slip loads and evaluating response amplitudes. It has been observed previously by Filiatrault and Cherry [7] that variations of +/- 20% in the optimum slip load do not significantly alter the overall response of a friction damped structure; and with the above criteria as a basis for selection, slip loads as shown in Figure 4 were chosen. The slip load in a device is obtained by varying the applied preload normal force, and for experimental purposes, preliminary tests of a single device in a static test rig were performed to calibrate device slip load (P_s) against preload normal force (which was measured in terms of the torque applied to the center bolt). Hence, specified slip loads could be easily obtained or changed within the model structure as necessary during testing.

Preliminary Tests of Model

Following the modifications to the frame and the installation of the friction damping devices, preliminary tests were conducted to determine the dynamic characteristics of the model structure. These initial tests consisted of white noise base motion and an impulse excitation, and from the data collected modal frequencies and an estimate of the initial damping of the structure were calculated.

The white noise input motion had an almost constant Fourier amplitude for the frequency range of 0 to 10 Hz. By taking transfer functions of the roof acceleration time history the modal frequencies were estimated. The fundamental frequency of the FDBF was estimated to be 2.23 Hz and the second mode frequency to be 8.34 Hz. The same method was used for the frame in the MRF configuration and the first two frequencies were found to be $f_1 = 2.00$ Hz and $f_2 = 6.61$ Hz.

The impulse loading consisted of a square wave input to the shaking table and was used to excite free vibration responses in the model. These tests were used to obtain an estimate of the damping of the structural system. By evaluating the logarithmic free vibration decay of the 9th floor displacement signal damping in the FDBF was found to be $\xi = 5.6\%$ and $\xi = 2.4\%$ for the MRF. The damping in the FDBF was dependent on the level of excitation and the amount of slip in the friction devices and so the value of 5.6% was only applicable for low levels of excitation during which there was essentially no slip in the devices. As soon as the level of excitation was such that the devices began to slip the amount of damping in the structural system increased significantly.

Earthquake Tests of Model

Earthquake testing of the model was conducted using 10 different real and synthesized earthquake signals that provided a wide range of characteristics of earthquake motion. The earthquake signals used for testing were El Centro, 1940; Kern County Taft, 1952; San Francisco, 1957; Parkfield, 1966; Pacoima Dam, 1971; Bucharest, 1977; Miyagi-Ken-Oki (MKO), 1978; Mexico City, 1985 and two synthesized signals with response spectra equivalent to the ATC 3-06 spectrum for soil type 1. A range of magnitudes of excitation were used for the El Centro, Mexico City, Taft and Miyagi-Ken-Oki earthquakes to gain an insight to the change in response of the structure with varying level of disturbing force.

Tests using the Mexico City signal were also performed using modified time-scale factors. Similitude laws require that for the 1/4-scale model the earthquake signals be time scaled by a factor of $\frac{1}{\sqrt{\text{scale factor}}} = 1/2$. However, a modified time scale factor was arbitrarily imposed on the Mexico City signal to move the predominant frequency of the signal to coincide with (or be very close to) the first frequency of the FDBF structure. This resulted in a quasi-resonance excitation and very large responses were obtained in the structure. This technique was used for tests of both the FDBF and the MRF, and the effects on response due to the friction devices were able to be evaluated.

For the remaining earthquake signals, the tests performed were moderate level excitations, and these were intended for comparisons with previous tests conducted on the model as an eccentrically braced frame (EBF) and in the MRF configuration.

TEST RESULTS

Hysteresis Loops And Damping

For any frictional system the amount of energy dissipated by the system and the damping in the system are proportional to the slip excursions of the frictional elements. This means that frictional damping elements in a structural system will become relatively more effective as the magnitude of the input force increases. This pattern was observed in the series of tests using the El Centro, Taft, Mexico City and Miyagi-Ken-Oki signals for a range of increasing input accelerations. The gradual decrease in the transmissibility (roof acceleration/table acceleration) with increasing peak table acceleration (PGA) can be seen from the data in Table 1.

As a result, values for damping calculated from hysteresis loops for the devices increased as PGA increased. A typical hysteresis loop for a device at the bottom level of the structure is shown in Figure 5. This loop is plotted for the Miyagi-Ken-Oki PGA = 0.447g test. The total force in the device is the sum of the forces in the tension and the compression braces, and this is plotted against the slip deformation time history of the device to obtain a hysteresis loop. The equivalent viscous damping ratio for this loop is $\xi = 37.6\%$, and the effective stiffness of the device at this level of excitation is $k_{eff} = 31.8$ kips/inch. Similar loops for the same device for the El Centro PGA = 0.170g test yielded values of $\xi = 22.4\%$ and $k_{eff} = 47.2$ kips/inch, and for the El Centro PGA = 0.838g test, $\xi = 32.2\%$ and $k_{eff} = 29.9$ kips/inch. Clearly, there is a significant increase in damping and decrease in device effective stiffness with the increase in magnitude of the input motion. For other earthquakes, damping provided by individual friction devices was observed to be in the range of 8.5% — 37.6%.

To obtain an estimate of the total damping in the FDBF, hysteresis loops of base shear plotted against first floor relative displacement were evaluated for equivalent viscous damping. Such a hysteresis

loop is shown in Figure 6 for the Miyagi-Ken-Oki PGA = 0.447g test. The damping ratio for this test is ξ = 16.7%. During the preliminary tests damping of about ξ = 2.4% was calculated for the MRF. Thus, the addition of the frictional elements has added approximately a further 14% to the damping in the structure. This is a significant increase in damping in a structure. For other large magnitude tests damping in the range of 15% to 16.7% was observed, and for smaller magnitude tests typical values of damping were 7% to 10%.

Energy Dissipation

A clear indication of the effectiveness of the friction damping devices in the structural system is given by a consideration of energy dissipation in the structure. Two approaches were taken for the evaluation of the amount of energy dissipated. These were: (a) calculating the amount of the total energy in the structure at a particular level by integrating the inertial story shear force (the sum of all the inertial story forces above the level in question) with respect to the story drift time history and comparing this value with the amount of energy dissipated by the friction devices at that level, and (b) determining the total energy input to the structure by integrating the base shear force with respect to the shaking table displacement and comparing this energy with the total energy dissipated by all the devices in the structure.

A typical energy time history for a level 1 device obtained using the first approach is given in Figure 7. At the completion of the earthquake the device has absorbed 93% of the energy input to that level. For devices at other levels and other earthquake inputs this value varied between about 93% for the bottom level to about 60 — 70% for the upper levels of the structure. To obtain the total energy dissipated by the devices during an earthquake the known values were interpolated to give approximate values of dissipation at the other levels. Time histories of total input energy and approximate energy dissipated by all devices during the Mexico City PGA = 0.651g test are shown in Figure 8. The total energy dissipated by all the friction devices is approximately 70% of the total input energy. The fact that this ratio is not higher reflects that the distribution of device slip forces in the model was not optimized for this earthquake motion.

Negligible change in structure frequency was observed (even for very large magnitude tests) due to the nonlinear slip behavior of the friction devices. Changes in frequency of the order of 1 — 2% at most were observed during testing.

Comparison to MRF Test Results

The most significant comparisons of response between the FDBF and the MRF are found for the tests performed using the modified Mexico City signal. For both structural systems the magnitude of the input signal was increased until a maximum relative displacement of 2.8 — 3.0 inches was achieved. Any displacements beyond this would have caused excessive damage to the frame, and thus were undesirable because of the need for further tests.

The maximum peak input acceleration experienced by the FDBF was PGA = 0.651g, and corresponding to this motion was a maximum relative displacement in the model of 2.80 inches. A comparable test of the MRF had a PGA = 0.249g and for this test the model underwent a maximum relative displacement of 3.11 inches. Figure 9 shows the profile of peak story accelerations normalized to PGA for these two tests, and in Figure 10 the profiles of maximum story drift normalized to PGA are given. The ratios of $\frac{\text{MRF response}}{\text{FDBF response}}$ for these two tests are 2.91 for displacement and 2.02 for acceleration.

Story Shears

For the PGA = 0.651g test the FDBF experienced a peak base shear of 69.9 kips. The story shear profile determined at the time of peak base shear is shown in Figure 11. Also shown in this figure is the profile of shear force resisted by the friction damping devices. Figure 12 gives the profile of story shears at the time of peak base shear for the MRF subjected to the PGA = 0.249g test. For this test the peak base shear was 64.2 kips, all of which was required to be resisted by damaging inelastic action of the MRF elements.

CONCLUSIONS

The seismic performance of the frame is considerably enhanced by the inclusion of the friction damping devices in the structural system. It is clear that the devices provide a significant increase in the available damping within the structure and that this leads to a direct improvement in performance. The dissipation characteristics of the friction damping mechanisms are reliable and the devices are not damaged by large loads. The devices become more effective in absorbing energy as the magnitude of the disturbing force increases. By confining the energy dissipation to the friction devices which are specifically designed to perform under extreme loading conditions without sustaining damage, the main structural elements are able to remain elastic.

The difference between structural systems appears less dramatic from considerations of shear force, but it is still shown that a large portion of the base shear force in a structure can be resisted in a controlled manner and not be required to be resisted by inelastic action of primary structural elements.

REFERENCES

[1] Pall, A. S., Marsh, C., "Response of Friction Damped Braced Frames", Journal of the Structural Division, American Society of Civil Engineers, Vol. 108, No. ST6, June 1982.

[2] Pall, A. S., "Response of Friction Damped Buildings", Proceedings of the Eighth World Conference on Earthquake Engineering, San Francisco, Vol. V, 1984.

[3] Pall, A. S., Marsh, C., "Friction Damped Concrete Shear Walls", Journal of the American Concrete Institute", No. 3, Proceedings Vol. 78, 1981.

[4] Pall, A. S., Marsh, C., Fazio, P., "Friction Joints for Seismic Control of Large Panel Structures", Journal of the Prestressed Concrete Institute, Vol. 25, No. 6, 1980.

[5] Arthur A. Huckelbridge, "Earthquake Simulation Tests of a Nine Story Steel Frame with Columns Allowed to Uplift", Report No. UCB/EERC-77/23, Earthquake Engineering Research Center, University of California, Berkeley, (1977).

[6] Griffith, M. C., Aiken, I. D., Kelly, J. M., "Experimental Evaluation of Seismic Isolation of a Nine Story Braced Steel Frame Subject to Uplift", Report No. UCB/EERC-87/03.

[7] Filiatrault, A. and Cherry, S., "Performance Evaluation of Friction Damped Steel Frames Under Simulated Earthquake Loads", Earthquake Engineering Laboratory Report, Dept. of Civil Engineering, University of British Columbia, Vancouver, B. C., Canada, 1985.

EARTHQUAKE SIGNAL	SPAN	TIME SCALE	PK. TABLE ACCEL.(g's)	PK. MODEL ACCEL.(g's)	MODEL/TABLE
El Centro	150	1/2	0.301	0.913	3.102
	225	1/2	0.422	1.219	2.889
	300	1/2	0.532	1.456	2.638
	350	1/2	0.716	1.549	2.163
	400	1/2	0.838	1.682	2.007
Taft	200	1/2	0.409	0.953	2.330
	300	1/2	0.612	1.330	2.072
	350	1/2	0.777	1.602	2.062
Mexico	40	1/5	0.115	0.695	6.013
	80	1/5	0.219	1.089	4.373
	120	1/5	0.428	1.359	3.214
	160	1/5	0.687	1.516	2.207
Miyagi	150	1/2	0.170	0.847	4.982
	200	1/2	0.206	1.002	4.864
	275	1/2	0.307	1.383	4.505
	350	1/2	0.447	1.308	2.926

Table 1 Reduction In Transmissibility Ratio With Increasing Peak Table Acceleration

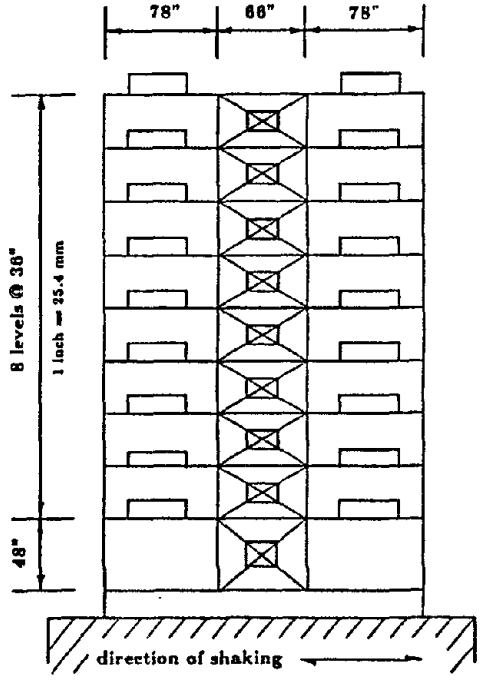

Figure 1 9-Story Steel Friction Damped Braced Frame

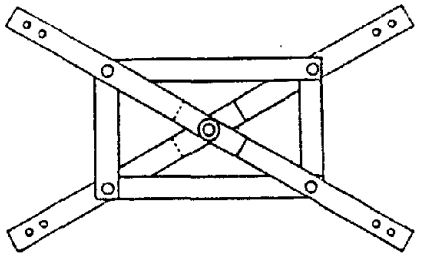

Figure 2 Friction Damping Device

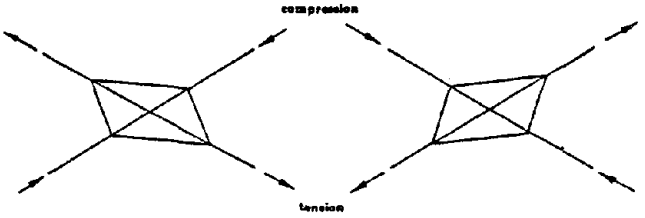

Figure 3 Deformed Configurations of a Friction Damping Device

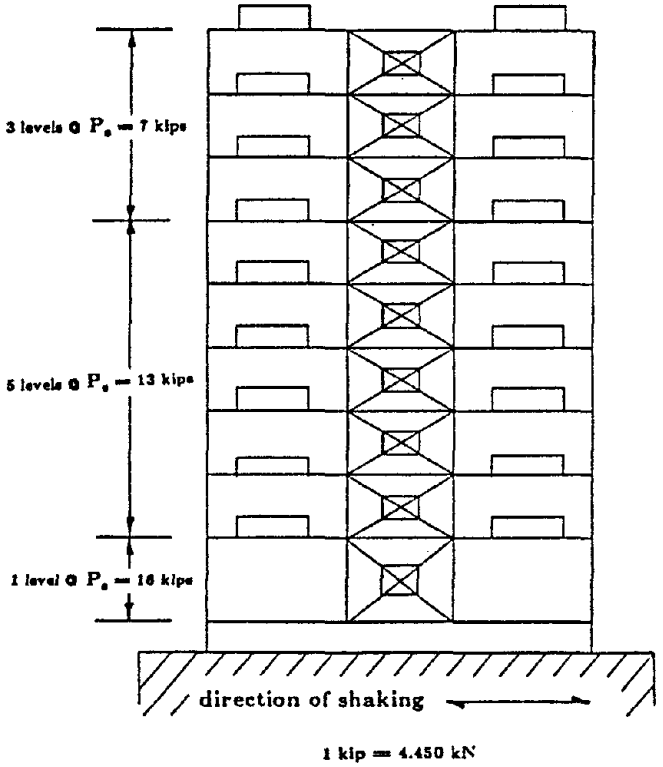

Figure 4 Distribution of Slip Forces

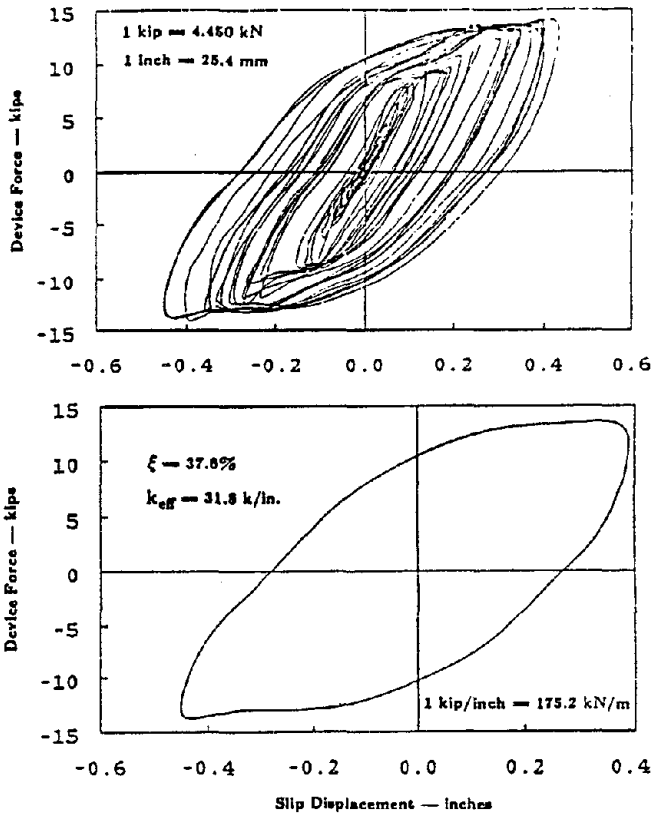

Figure 5 Device Hysteresis Loop — MKO, pga = 0.447g

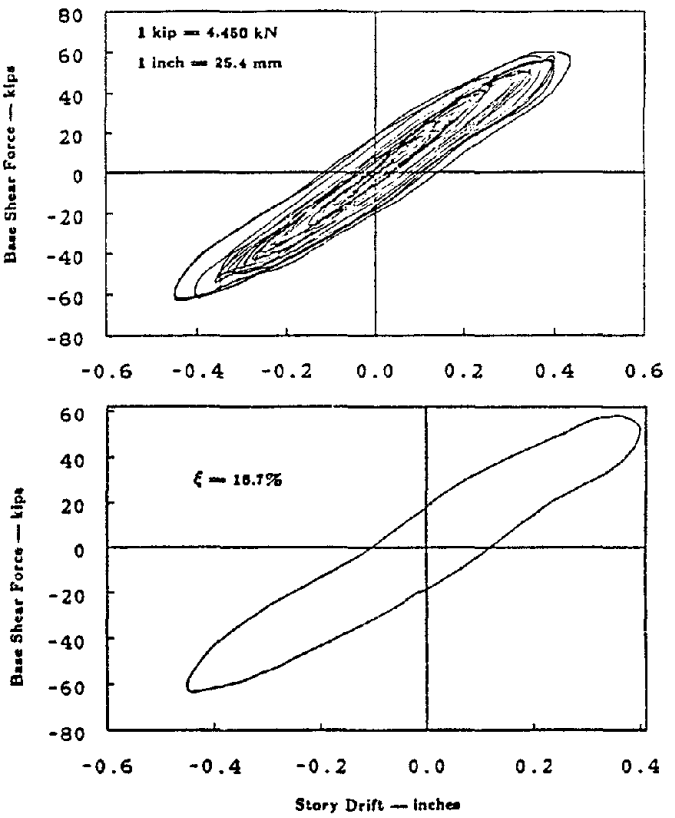

Figure 6 Base Shear vs. First Floor Drift — MKO, pga = 0.447g

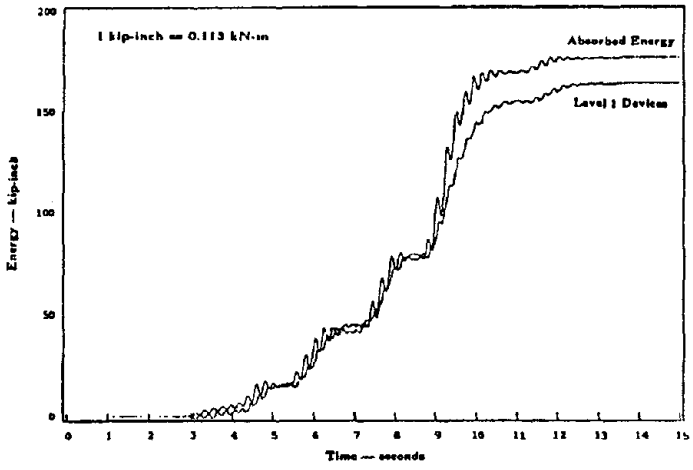

Figure 7 Level 1 Energy Time History — Mexico City, pga = 0.651g

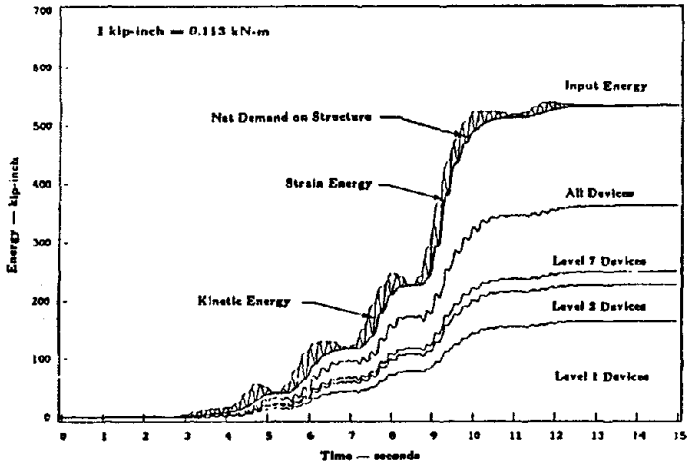

Figure 8 Total Energy Time History — Mexico City, pga = 0.651g

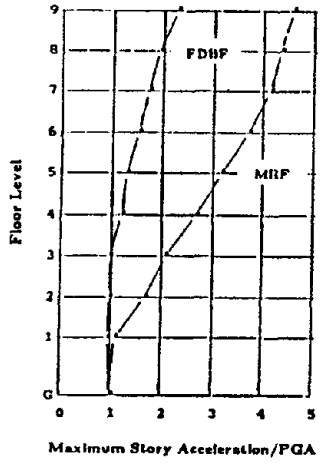

Figure 9 Peak Story Acceleration Profiles

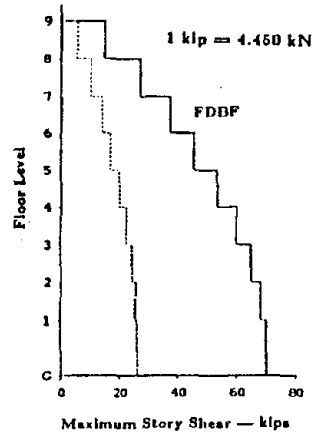

Figure 11 Story Shear Profile — Mexico, pga = 0.651g

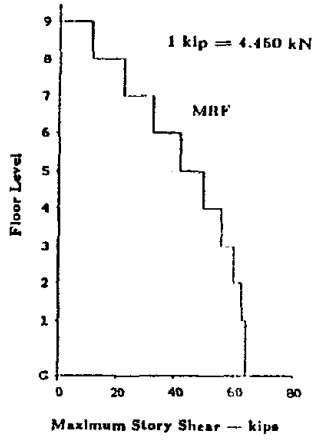

Figure 12 Story Shear Profile — Mexico, pga = 0.240g

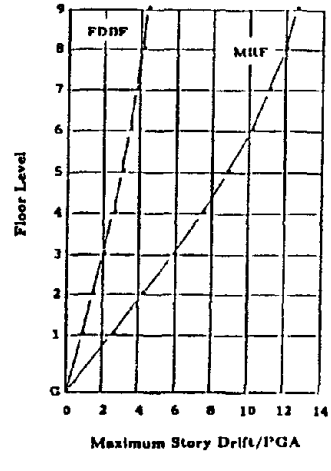

Figure 10 Peak Story Drift Profiles

PROBABILISTIC SEISMIC HAZARD ANALYSIS WITH IMPROVED SOURCE MODELING

Rodrigo Araya[1] and Armen Der Kiureghian[2]

[1] Department of Civil Engineering, University of Chile
Santiago, Chile
[2] Department of Civil Engineering, University of California
Berkeley, California, 94720, U.S.A.

SUMMARY

A new formulation and fast probability integration techniques are employed to assess seismic hazard with refined models of the earthquake source. The source geometry and rupture characteristics can be defined at any desired level of refinement and using as many random variables as necessary. The approach readily provides sensitivities of the hazard with respect to the model parameters. A simple formula is given to determine confidence bounds on the estimated hazard for uncertain model parameters.

INTRODUCTION

Stochastic models used in seismic hazard analysis (SHA) can be classified in four groups: (1) models used to describe random occurrences of earthquakes in time and space; (2) models used to describe the energy release mechanism at the earthquake source; (3) models used to describe the propagation of seismic waves through the ground medium; and (4) models used to describe the damagability of the ground motion at a specific site and for a given structure or other constructed facility. The level of refinement used for each of these models depends on our understanding of the physical processes involved, our access to appropriate mathematical models to describe these processes, the availability of data to estimate the model parameters, and the availability of efficient techniques to compute the hazard for a given set of models. Refined models normally provide more realistic representation of complex physical processes, but require more data to predict and make the hazard computation more difficult.

Regardless of the level of model refinement used, it is essential that all relevant sources of model uncertainty be accounted for in the estimation of seismic hazard. These include uncertainties due to model imperfection, i.e., departure of the model from reality, and uncertainties in the estimation of model parameters due to limited sample size. Normally, more refined models have less of the first and more of the second kind of uncertainty. The use of a refined model in SHA is justified when such use results in a reduced overall uncertainty in the estimated hazard.

In the past two decades, SHA has become a standard tool of practice in earthquake engineering. Nevertheless, while our understanding of the earthquake phenomenon has significantly increased during the same period, and a large data base for earthquake events throughout the world has been gathered, the sophistication of models used in SHA has essentially remained unchanged from the earliest applications (Refs. 2,3). For example, while the significance of the source geometry and the dynamic characteristics of the fault rupture mechanism (e.g., rupture velocity and direction) on the ground motion have become evident, the current SHA methods typically model the source as only a point (Ref. 2) or a line (Ref. 3) and employ a single parameter to characterize the event, namely the magnitude. Clearly, there is a gap between the level of sophistication of models used in SHA and our understanding of the physics of earthquakes.

One reason for the above gap is the difficulty in computing the hazard with refined source models. Presently, all SHA methods employ direct numerical integration (over the magnitude and distance of the earthquake and one or two uncertainty parameters) to compute the seismic hazard for a site. More refined models introduce additional variables and require further integration, thus hampering the direct integration approach. Therefore, a new approach to formulating and computing seismic hazard is necessary to facilitate the use of refined models in SHA.

In this paper, a new and general formulation of SHA is presented which allows the incorporation of refined models with arbitrary number of random variables. Fast probability integration methods adopted from structural reliability theory are used to compute the hazard. In addition to providing the hazard, these methods yield the sensitivities of the hazard (i.e., partial derivatives) with respect to any set of desired parameters. The sensitivities are useful in identifying model parameters which have significant influence on the computed hazard. Furthermore, it is shown that they can be used to compute confidence bounds on the estimated hazard, reflecting the effect of model uncertainties. An example application with a refined source model is presented. Further details on the method and other applications can be found in Ref. 1. It is hoped that the proposed method will encourage and enable other investigators to incorporate more refined models in their SHA applications.

A NEW FORMULATION OF SEISMIC HAZARD

Attention is focused here on the probability that a given measure of ground motion damagability, expressed as a function $A(\mathbf{Y})$ of ground motion variables $\mathbf{Y} = (Y_1, Y_2, \cdots)$ at a site, will exceed a specified threshold, a, during a given earthquake event. The ground motion variables $\mathbf{Y}$ (e.g., peak acceleration, velocity, displacement; duration; measures of frequency content) are given as functions of earthquake variables $\mathbf{X} = (X_1, X_n, \ldots)$ (e.g., geometry of the source, location coordinates, magnitude, seismic moment, dimensions of rupture, velocity and angle of rupture propagation) in the form

$$\mathbf{Y} = \mathbf{Y}(\mathbf{X}, \tilde{\boldsymbol{\theta}}) \tag{1}$$

in which $\tilde{\boldsymbol{\theta}} = (\tilde{\theta}_1, \tilde{\theta}_2, \cdots)$ denotes a set of (unknown) model parameters. A single row of the above matrix relation may resemble the conventional attenuation law for the peak ground acceleration expressed as a function of the earthquake magnitude and distance. However, the above relations are general and may employ as many earthquake variables as necessary. It is assumed that the available statistical data is an observed sample of the earthquake variables, $\mathbf{X}$, such that a joint probability density function $f_{\mathbf{X}}(\mathbf{x}, \hat{\boldsymbol{\theta}})$ can be assigned, in which $\hat{\boldsymbol{\theta}} = (\hat{\theta}_1, \hat{\theta}_2, \cdots)$ represents the set of (unknown) distribution parameters. We will use the notation $\boldsymbol{\theta} = (\tilde{\boldsymbol{\theta}}, \hat{\boldsymbol{\theta}})$ to denote the combined vector of parameters. The lack of precise knowledge of $\boldsymbol{\theta}$ will give rise to uncertainty in the estimated hazard. Well known Bayesian estimation methods can be used to determine the probability distribution of $\boldsymbol{\theta}$, employing both subjective (in the form of priors) and objective (in the form of observed data) information.

The probability of interest is the multifold integral

$$P(A > a \,|\, \boldsymbol{\theta}) = \int_{A(\mathbf{y}(\mathbf{x}, \tilde{\boldsymbol{\theta}})) > a} f_{\mathbf{X}}(\mathbf{x}, \hat{\boldsymbol{\theta}})\, d\mathbf{x} = h(a, \boldsymbol{\theta}) \tag{2}$$

where the integration domain is the set of outcomes of $\mathbf{x}$ for which the damagability measure exceeds the specified threshold. The above probability is conditioned on the selected set of parameters, $\boldsymbol{\theta}$. A simple method to compute confidence bounds on the conditional hazard to reflect uncertainty in $\boldsymbol{\theta}$ will be described shortly. If, however, the uncertainty in $\boldsymbol{\theta}$ is to be incorporated in the hazard estimate, with the above formulation one only needs to carry out further integration on $\boldsymbol{\theta}$ to obtain the unconditional hazard. In that case, one may view $\boldsymbol{\theta}$ as only additional random variables.

As indicated earlier, the above probability is for a given earthquake event. In practice, one is usually interested in the seismic hazard for all earthquakes occurring during a specified time period. If the usual Poisson model for occurrences of earthquakes in time is employed, the lifetime hazard becomes $1 - \exp(-\nu t h)$, where ν denotes the mean rate of occurrences and t denotes the duration of time.

Computation of the Seismic Hazard Integrals of the type shown in Eq. 2 have been of interest in structural reliability for a long time, and efficient computational schemes for their evaluation have been developed. These include the first and second-order reliability methods (FORM and SORM) and the directional simulation (DS) method, which will be briefly presented here. Other methods, such as various importance sampling schemes, are also available but will not be addressed.

In all three methods, FORM, SORM, and DS, computations are carried out in a standard normal space obtained by a nonlinear mapping of the basic variables, $\mathbf{U} = \mathbf{U}(\mathbf{X})$, such that the transformed variables $\mathbf{U}$ have the normal distribution with zero mean and unit covariance matrix. The transformation depends on the probability distribution of $\mathbf{X}$, and for different classes of distributions is given in Refs. 4 and 7.

The main idea in FORM and SORM is to replace the surface $A(\mathbf{y}) = a$, known as the limit-state surface, with a first or second-order approximating surface for which a simple estimate of the probability integral is available. These approximating surfaces are fitted in the standard normal space and at a point of the surface, denoted the design point, which has minimum distance from the origin. The resulting approximations are:

$$h(a,\theta)_1 = \Phi(-\beta) \tag{3}$$

$$h(a,\theta)_2 \approx \Phi(-\beta) \prod_{i=1}^{n-1} (1 + \beta \kappa_i)^{-1/2} \tag{4}$$

where $\Phi(.)$ is the standard normal density, β is the distance of the design point from the origin, and κ_i are the main curvatures of the approximating second-order surface. Thus, the FORM approximation of the hazard only requires finding the design point, whereas the SORM approximation additionally requires computing the curvatures of the approximating surface. These curvatures are determined either by fitting to the curvatures of the actual surface (curvature-fitting, SORM-CF, method), or by fitting to discrete points on the surface (point-fitting, SORM-PF, method). In either case, the SORM evaluation requires repeated computations of the function $A(\mathbf{y})$ for points around the design point (see Ref. 5).

The design point is obtained as the solution of an optimization problem that minimizes the distance from the origin to a point constrained to remain on the limit-state surface. Several standard algorithms for this purpose are available. Most these algorithms find the design point by repeated computations (usually of the order of 10 to 50 times) of the function $A(\mathbf{y}(\mathbf{x}(\mathbf{u})))$ and its gradient, $\nabla_{\mathbf{u}} A$, in the standard normal space. Due to the properties of the standard normal space, the design point has the highest density of all points satisfying the condition $A(\mathbf{y}) > a$. Thus, the corresponding points in the $\mathbf{X}$ and $\mathbf{Y}$ spaces can be considered as the most likely values of the earthquake and ground motion variables that give rise to the event $A(\mathbf{Y}) > a$. Obviously, this information would be useful in practice in specifying the design earthquake.

The DS method is based on the following total probability formulation of the hazard ($\boldsymbol{\theta}$ is deleted for clarity):

$$P(A > a) = \int_{\Omega} P(A > a \mid \boldsymbol{\alpha}) f_{\boldsymbol{\alpha}}(\boldsymbol{\alpha})\, d\boldsymbol{\alpha} \tag{5}$$

in which $\boldsymbol{\alpha}$ denotes a unit direction vector in the standard normal space with a uniform distribution on the unit sphere Ω centered at the origin. Since the square of the radial distance in the standard normal space has the chi-square distribution, the conditional probability is given by

$$P(A > a \mid \boldsymbol{\alpha}) = 1 - \chi_n^2(r^2) \tag{6}$$

where $\chi_n^2(.)$ is the chi-square distribution with n degrees of freedom, n is the number of random variables, and r is the distance from the origin to the limit-state surface in direction $\boldsymbol{\alpha}$. The DS method, thus, proceeds as follows: (a) a set of direction vectors $\boldsymbol{\alpha}$ are generated; (b) for each direction, the distance r and the conditional probability in Eq. 6 are computed; (c) an estimate of the hazard is given by the sample mean of the computed conditional probabilities, and a measure of the error in the estimate is given by the sample variance; (d) the simulation is repeated until the sample variance is sufficiently small. The chief advantage of this simulation scheme over the conventional Monte Carlo method is that the required number of simulations to achieve a given level of accuracy is

independent of the probability of interest and can be significantly smaller than that required in the Monte Carlo method.

Sensitivities of the Hazard One important advantage of the FORM and DS methods is that they readily provide the sensitivities of the computed probability with respect to any set of parameters. In FORM, the partial derivatives of $h(a,\boldsymbol{\theta})_1$ with respect to $\boldsymbol{\theta}$ are given in terms of β, $\nabla_{\mathbf{u}} A$, and the derivatives of $A(\mathbf{y}(\mathbf{x},\tilde{\boldsymbol{\theta}}))$ and $\mathbf{U} = \mathbf{U}(\mathbf{X})$ with respect to $\tilde{\boldsymbol{\theta}}$ and $\hat{\boldsymbol{\theta}}$, respectively, both evaluated at the design point (Ref. 7). In the DS method, the sensitivities with respect to $\tilde{\boldsymbol{\theta}}$ are computed as the expectation of the partial derivative of the conditional probability in Eq. 6 (Ref. 6). This is an important advantage over the conventional SHA method, where the sensitivities are computed by repeated hazard analysis with perturbed parameters. For example, in PRA studies of nuclear power plants, it is not unusual to carry out thousands of repeated hazard analysis to determine the parameter sensitivities. Clearly, the FORM and DS methods present attractive alternatives from this standpoint.

Confidence Bounds on the Computed Hazard As mentioned in the introduction, uncertainties in the assessment of seismic hazard arise from imperfections in the assumed models and from errors in the estimation of model parameters due to limited sample size. These uncertainties are represented herein as uncertainties in the parameters $\tilde{\boldsymbol{\theta}}$ and $\hat{\boldsymbol{\theta}}$, respectively. Let $\mathbf{M}_{\boldsymbol{\theta}}$ and $\boldsymbol{\Sigma}_{\boldsymbol{\theta\theta}}$ denote the mean vector and covariance matrix of $\boldsymbol{\theta}$. Using first-order approximations, estimates of the mean and variance of the hazard are given by

$$\mu_h \approx h(a,\mathbf{M}_{\boldsymbol{\theta}}) \tag{7}$$

$$\sigma_h^2 \approx \nabla_{\boldsymbol{\theta}} h \, \boldsymbol{\Sigma}_{\boldsymbol{\theta\theta}} \nabla_{\boldsymbol{\theta}} h^{\mathrm{T}} \tag{8}$$

in which $\nabla_{\boldsymbol{\theta}} h$ denotes the sensitivities of $h(a,\boldsymbol{\theta})$ with respect to $\boldsymbol{\theta}$, which are evaluated at the mean point. Using these estimates, the k-sigma band of the hazard is computed as $\mu_h \pm k\,\sigma_h$. Note that a single hazard analysis with the mean values of parameters is all that is necessary to compute these estimates.

MODELING OF THE SEISMIC SOURCE

Potential sources of seismic threat for a site can be of various natures. Geologic faults are common sources of seismic activity. In certain cases, the geometry of the fault or a system of faults is well defined, as is the case for the San Andreas fault in California. In other cases the fault geometry is uncertain or unknown. There are also seismically active areas without clearly defined features, as in the Charleston region in the Eastern United States and in Japan. Thus, a comprehensive seismic hazard methodology must include source models with known, partially known and unknown fault geometry, as well as area sources. The formulation presented in the preceding section is particularly attractive since it provides maximum flexibility in modeling the earthquake source.

General Fault Source Model A general fault model is shown in Fig. 1. The fault plane is defined by the coordinates of the end points A and C of its trace on the ground surface and the dip angle ϕ. Generalizing the original ideas of Ref. 3, an earthquake on the fault is assumed to originate as a rectangular rupture of length l_r, width w_r, plunge ψ, and depth z. All these parameters, as well as the location coordinate of the rupture along the fault, are considered as random variables. Furthermore, the direction of propagation of the rupture (i.e., $A \rightarrow C$ or $C \rightarrow A$) and its velocity may also be considered as random variables.

By proper selection of the probability distributions, the above model can be used to account for all kinds of uncertainties relative to the geometry of the fault source. For example, uncertainty in the fault length alone can be modeled by selecting the x-coordinates of A and C as deterministic and the y-coordinates random. Also, uncertainty about the distance and/or orientation of the fault can be modeled by allowing the x-coordinates to be random. In particular, strong positive correlation between the x-coordinates would imply uncertain distance from the site, whereas strong negative correlation between the x-coordinates would imply uncertain orientation (strike) of the fault. The random position of the rupture within the fault plane is specified by the probability distribution of the coordinates of the center point H. This distribution can be defined such that the rupture is confined within the edges of the fault plane (in which case the distribution is conditional on the dimensions, l_r and w_r, of the rupture), or it is allowed to propagate beyond the specified edges of the fault plane.

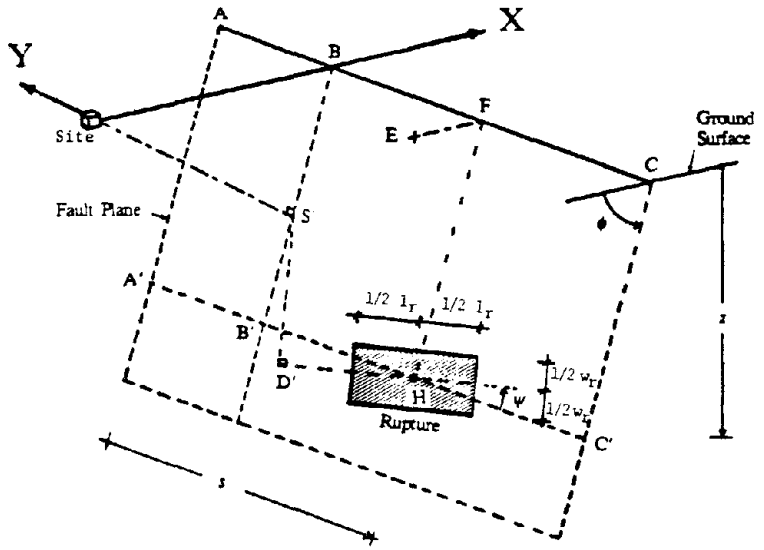

Fig. 1. Fault Source Model

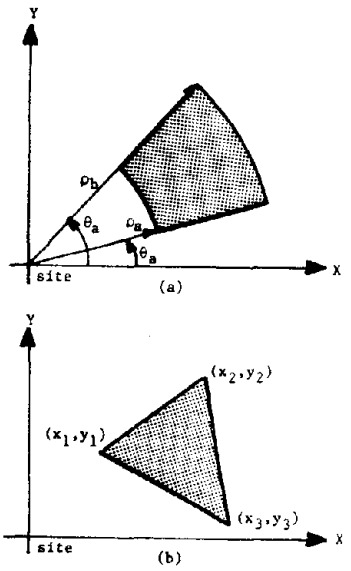

Fig. 2. Area Source Modules: (a) Annular, (b) Triangular

Probability distributions for the dimensions of the rupture, l_r and w_r, are available from regressions on the earthquake magnitude (Ref. 1). Distributions on other variables, such as ϕ and ψ, can be assigned based on studies of previous earthquakes on the fault.

General Area Source Model The two area source modules in Fig. 2 are considered. Any general area source can be synthesized by a combination of these modules. An earthquake in the area source is modeled as a rupture occurring in a fault plane of unknown location, strike, and dip angle. The position of the rupture within the area source is specified by the probability distribution of the coordinates of its center. As an example, if the earthquake is equally likely to occur anywhere within the annular area, the joint probability density of the polar coordinates of the center of the rupture is given by

$$f_{\rho\theta}(\rho,\theta) = \frac{2\rho}{(\rho_b^2-\rho_a^2)(\theta_b-\theta_a)} \qquad \rho_a<\rho<\rho_b\ ,\quad \theta_a<\theta<\theta_b \tag{9}$$

A similar expression for the triangular area source module is available (Ref. 1).

For each of the above source models various source-to-site distance terms have been derived in Ref. 1. These include focal and epicentral distances as well as the shortest distance to the rupture, which are given in terms of the variables defined above. Other distance terms appropriate for refined attenuation laws that account for the geometry of the source can also be easily developed. One such attenuation law which includes the effect of the rupture directivity is introduced in Ref. 1.

EXAMPLE APPLICATION

In Ref. 1, a number of example applications are presented aimed at examining the accuracy and versatility of the FORM, SORM and DS methods for SHA, including the analysis of sensitivities and uncertainties. Because of page limitations, only one example is presented here. It represents the seismic hazard at a site from a given event on a fault with a known trace. Quantities considered random include the dip angle of the fault, the upper-bound magnitude of the fault, the magnitude of the given event (with a distribution conditioned on the upper-bound magnitude), the length and width of the rupture (with the joint distribution conditioned on the magnitude of the event), the depth of the rupture, the horizontal coordinate of the rupture in the fault plane, the seismicity parameter of the region (the b value), and the uncertainty in the attenuation law for a given magnitude and distance. Thus, the problem includes nine random variables, several of which are statistically dependent. Details concerning the distributions of these variables and other data can be found in Ref. 1. Clearly, conventional SHA methods using direct integration would be inappropriate for solving this problem.

Figure 3 shows the hazard estimates based on FORM, SORM, and DS. For the DS method, the figure shows the 95% confidence interval of the estimated hazard. From this example and similar

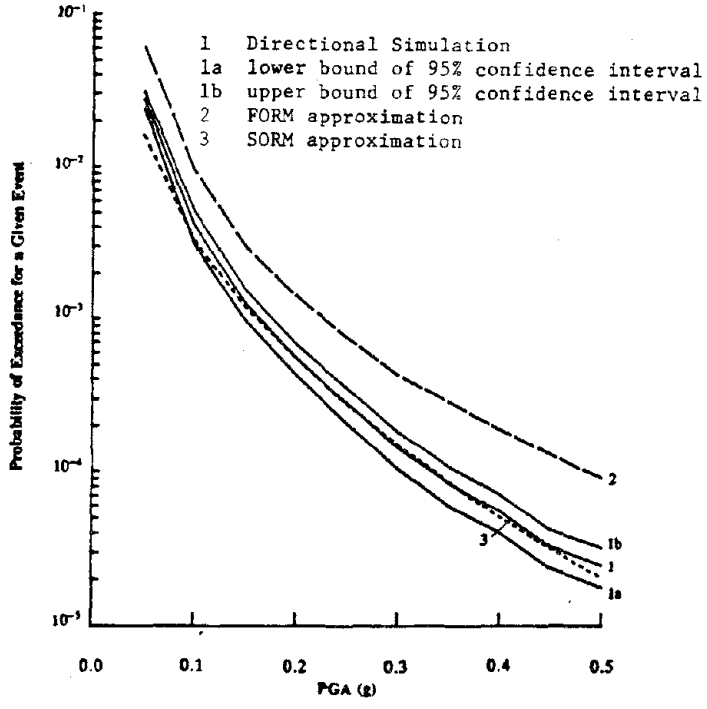

Fig. 3. Comparison of Hazard Estimates Based on DS, FORM, and SORM

results in Ref. 1, it is concluded that the FORM approximation is not sufficiently accurate for the purpose of SHA. The reason lies in the strong nonlinearity of the limit-state surface in the standard normal space, which partly arises from the nonnormal distribution of certain variables, such as the magnitude and the location coordinate of the rupture. The SORM approximation, on the other hand, appears to give reasonably accurate results over a wide range of probability values. Experience also shows that FORM estimates of the sensitivities are reasonably accurate. Thus, SORM estimates of the hazard together with FORM estimates of the sensitivities can be used in Eq. 8 to determine confidence bounds on the estimated hazard. The DS results, which requires relatively small number of simulations (of the order of several hundred at all probability levels), can be considered "exact".

Further examples in Ref. 1 demonstrate results for the analysis of hazard sensitivities and uncertainties. These will be reported in a forthcoming paper.

ACKNOWLEDGMENT

The work presented in this paper is part of a study supported by the National Science Foundation under Grant No. CES-8618905, with Dr. S-C. Liu as Program Director. This support is gratefully acknowledged.

REFERENCES

1. Araya, R., "Seismic Hazard Analysis: Improved Models, Uncertainties and Sensitivities," Doctoral Thesis, Department of Civil Engineering, University of California, Berkeley, CA, 1988.
2. Cornell, C. A., "Engineering Seismic Risk Analysis," *Bull. Seism. Soc. Am.*, 58(5), 1583-1606, (1968).
3. Der Kiureghian, A. and A. H-S. Ang, "A Fault Rupture Model for Seismic Risk Analysis," *Bull. Seism. Soc. Am.*, 67(4), 1173-1194, (1977).
4. Liu, P-L. and Der Kiureghian, A., "Multivariate Distribution Models with Prescribed Marginals and Covariances," *Prob. Eng. Mech.*, 1(2), 105-112, (1986).
5. Der Kiureghian, A., Lin, H-Z. and Hwang, S-J., "Second-Order Reliability Approximations," *J. Eng. Mech.*, ASCE, 113(8), 1208-1225, (1987).
6. Ditlevsen, O. and Bjerager, P., "Plastic Reliability Analysis by Directional Simulation," CAMM Report 353, Technical Univ. of Denmark, Lyngby, Denmark, (1987).
7. Madsen, H., Krenk, S. and Lind, N., *Methods of Structural Safety*, Prentice-Hall, Inc., Englewood Cliffs, N.J., (1986).

USE OF ARMA MODELS FOR THE INVESTIGATION OF EARTHQUAKE-INDUCED DAMAGE MECHANISMS IN STRUCTURES

Mark A. AUSTIN[1], Joel P. CONTE[2],
Stephen A. MAHIN[3] and Karl S. PISTER[4]

[1]Assistant Professor, Systems Research Center, University of Maryland, College Park, MD 20742, USA
[2]Research Assistant,
[3]Professor of Civil Engineering,
[4]Dean and Roy W. Carlson Professor of Engineering,
University of California, Berkeley, CA 94720, USA

SUMMARY

The design of earthquake resistant structures is often complicated by an inadequate number of suitably recorded ground motions, and by our limited understanding of the basic cause and effect relationships coupling the structural response to the details of a ground motion excitation. The use of ARMA models in design has recently been proposed as a means of mitigating these difficulties. This paper describes preliminary results of an investigation aimed at identifying the key factors affecting the response and behavior of a linear viscously damped SDOF structural model excited by a low order ARMA(2,1) ground motion model.

INTRODUCTION

Although it is possible to design a structure to resist severe lateral earthquake loads elastically, economic factors usually dictate that it is more feasible to design a system having the largest energy dissipation capacity consistent with tolerable deformations. For such a structure to survive these motions without collapse, its members should reach full plastic yielding before maximum lateral displacements are attained. Unfortunately, the problem of enforcing these design requirements is often complicated by the scarcity of suitable recorded ground motions, and the large uncertainty in predicting the spatial and temporal nature of future seismic events. Further uncertainties are introduced due to the limited ability of analytical models to describe nonlinear behavior, and by the high sensitivity of inelastic structural response to the overall intensity, duration and frequency content of earthquake excitations.

Most current design codes (Refs. 1,2) circumvent these difficulties by approaching the conventional design problem indirectly via load and resistance factors, simplified equivalent loads, and elastic analyses. Such approaches to design are inadequate for the design of complex or irregular systems, those composed of a new materials, or ones requiring an enhanced level of post-earthquake functionality. What they require instead, is the formulation and use of design methodologies that explicitly evaluate design performance in a manner consistent with expected design behavior.

Past Work At the University of California, Berkeley, the thrust of the early research in this area focussed on the development of DELIGHT.STRUCT (Refs. 3,4) and a design methodology that includes linear and nonlinear time history analyses, and reliability-based ideas within the design process itself (Refs. 5,6). The essential steps of this statistically-based design method are:

[a] Choose the design parameters, ie: structural system, geometrical configuration, stiffness, strength and mass distribution, etc.

[b] Generate a family of real or artificial ground motion records for each limit state considered, and perform dynamic analyses for each input motion, to explicitly account for the scatter in structural

response outputs due to earthquake loads. A realistic nonlinear mathematical model (e.g., finite element model) of the structure is used for those limit states where extensive inelastic deformations are expected.

[c] Evaluate the design based on criteria expressed in terms of the statistics of key response parameters of the model. Typical quantities are maximum ductility, cumulative plastic deformation, hysteretic energy dissipation, and story drift. The design criteria ensure that the structure behaves according to the accepted design philosophy.

Research Objectives Our preliminary results (Ref. 7) indicate that the reliable reproduction of mean extreme frame response levels and their variations is essential to the effective implementation of the proposed statistical design method. Currently, this goal is difficult to achieve because the basic cause and effect mechanisms existing between the features of a ground motion, the properties of a structure, and the resulting structural damage are poorly understood. Additional complications occur when the number of available ground motions is insufficient. One way of mitigating the latter difficulty is to use Auto-Regressive Moving Average (ARMA) models to generate supplementary families of ground motions that are statistically similar to a real target earthquake. In an effort to work towards a solution of these problems, we have initiated a study to identify the key factors affecting the response and behavior of a linear viscously damped SDOF structural model excited by a low order ARMA(2,1) ground motion model. This paper reports on our preliminary findings.

DESCRIPTION OF THE ARMA MODEL

Discrete ARMA models lend themselves to digital simulation in the time domain and can easily be adapted to include changes in frequency content of earthquake ground motions (EGM's). The ARMA(2,1) model is particularly attractive because of its simplicity, and demonstrated ability to provide a best-fit to many California earthquakes (Refs. 8,9,10). The second order autoregressive - first order moving average difference equation is:

$$a_t - \phi_1 a_{t-1} - \phi_2 a_{t-2} = w_t - \theta_1 w_{t-1} \tag{1}$$

where $\{w_t\}$ represents an input discrete white-noise process and $\{a_t\}$ the output process simulating the digitized ground acceleration process at time t. Considerations of stability and finite energy require that the autoregressive coefficients ϕ_1 and ϕ_2 lie inside the triangular region defined by:

$$\phi_1 + \phi_2 < 1 \quad , \quad \phi_2 - \phi_1 < 1 \quad , \quad |\phi_2| < 1 \tag{2}$$

In addition, the moving average coefficient θ_1 has to satisfy $|\theta_1| < 1$ for the process to be invertible. While the nonstationary intensity of EGM's may be accounted for by multiplying the white noise by a non-negative function $\Psi(t)$, the ARMA parameters may be varied as a function of time to account for the transient frequency content of real ground motions.

An interesting duality exists between the ARMA parameters and the physical parameters of an underlying continuous dynamic system whose stochastic process corresponds to the output from a discrete linear dynamic system driven by white-noise. Indeed, in Ref. 7. it is shown that the autocorrelation functions of the ARMA(2,1) model and SDOF linear oscillator shown in Fig. 1. are discretely coincident when the roots of the characteristic equation:

$$r^2 - \phi_1 r - \phi_2 = 0 \tag{3}$$

are either complex conjugates or both real positive. Whereas the underlying system is underdamped ($\xi_g < 1$) in the former case, it is overdamped ($\xi_g > 1$) when both of the roots are real positive. If at least one root of the characteristic equation is negative, then the corresponding ARMA(2,1) model is not physically realizable, i.e., not discretely coincident with an unique underlying physical system at all discrete time lags ($k\Delta t$, $k = 0 , 1 , 2 , \cdots$).

Moreover, the discrete/continuous model relationships are defined by a (3 x 3) nonlinear one-to-one mapping between the ARMA parameters ($\phi_1 , \phi_2 , \theta_1$) and the physical parameters (T_g , ξ_g , (C_0/C_1)). Figs. 2., 3. and 4. show these relationships in the form of contour maps of the physical parameters T_g , ξ_g , (C_0/C_1) in the autoregressive plane (ϕ_1 , ϕ_2). T_g and ξ_g are independent of θ_1, but C_0/C_1 depends on θ_1 and Fig. 4. corresponds to $\theta_1 = 0$. In ground motion modeling, T_g is the

site predominant period, and ξ_g a damping coefficient that governs the spectral bandwidth of the ground motion process. It is interesting to note that the Kanai-Tajimi filter (Ref. 11) widely used for earthquake simulation corresponds to the particular case $C_0/C_1 = 1$.

NUMERICAL SIMULATION

Ensembles of artificial EGM's were systematically generated for ARMA parameters ϕ_1 and ϕ_2 lying on the triangular grid of constant mesh size shown in Fig. 5. For all the simulations the moving-average parameter θ_1 was set to zero, and a time-dependent envelope, $\Psi(t)$, of the form:

$$\Psi(t) = A_0 \alpha \left(\frac{t}{\tau} \right)^3 \exp\left[-A_1 \left(\frac{t}{\tau} \right) \right] \tag{4}$$

where $A_0 = \left(\frac{8e^3}{3\sqrt{3}} \right)$

$A_1 = 2\sqrt{3}$

t = *time (seconds)*

α = *max amplitude of* $\Psi(t)$

τ = *duration of strong shaking (seconds)*

assumed. At each grid point, families of twenty non cross-correlated EGM's were generated by working through the following sequence of operations: (a) generation of discrete Gaussian white-noise, (b) time modulation and amplitude scaling (c) ARMA filtering, and (d) baseline correction. Although τ was held constant at 5 *seconds* for all the simulations, parameter values for α were automatically adjusted so that the maximum value of the ground motion variance envelope would be constant for all the grid points.

Both ground motion and structural response parameters were evaluated for each simulated input motion. Among the traditional ground motion parameters computed were: peak ground acceleration (PGA), velocity (PGV) and displacement (PGD), Arias intensity, Housner spectral intensity (S.I.). Similarly, the spectra of various response quantities (relative and absolute, real and pseudo, displacement,velocity and acceleration) of the linear SDOF structure were computed using the piecewise exact method of integration of the differential equation of motion.

The results of interest are the second order statistics (mean and standard deviation) of the ground motions and structural response parameters associated with each family of ARMA generated earthquakes. A sample of these results is presented in Figs. 6-9 for the ground motion parameters, and in Figs. 10-13 for the structural response parameters. These figures indicate (i) evidence of the resonance condition effect for elastic stuctures and (ii) that the coefficient of variation (C.O.V.) of the structural response parameters are almost insensitive to the ARMA parameters and hence to the spectral properties of the input motion.

CONCLUSIONS AND FUTURE WORK

The long term objectives of this research project are to formulate design methodologies and develop computer software that links the components: (a) seismology, (b) earthquake ground motion modeling, and (c) structural response and structural reliability, into a single design process. Ideally, these methodologies should take into account the statistical information available on previous earthquake ground motions at the design site, together with information on the multi-source character of the seismic environment, and the relative probability of occurrence of earthquakes being generated at the various known sources.

However, these goals will not be reached without an improved understanding of the basic interaction mechanisms existing between an earthquake ground motion, the properties of a structure, and the resulting structural response. Although discussion in this paper has been restricted to the statistical response of linear structures to a small class of ARMA generated ground motions, our problem solving approach is in fact quite general. In the immediate future, the thrust of our work will be directed towards the identification of cause and effect relations existing between low order ARMA model ground motions, and their effect on nonlinear hysteretic SDOF structures. Careful attention will be given to the characterization of damage in a statistical setting. Because real earthquakes exhibit considerable variations in both the shape and magnitude of the variance envelope, as well as the frequency content of ground shaking itself, further work is also needed to extend the basic ARMA models used in this study, so that the expected ground shaking at a site is more realistically modeled.

REFERENCES

1. Applied Technology Council, "Working Draft of Recommended Seismic Design Provisions for Buildings," January 1976.

2. Uniform Building Code, International Conference of Building Officials, Whittier, CA, 1979 Edition.

3. Austin M.A., Pister K.S., Mahin S.A., "Probabilistic Limit States Design of Moment-Resistant Frames under Seismic Loading," *Journal of the Structural Division*, ASCE, August 1987.

4. Balling R.J., Ciampi V., and Pister K.S., "Interactive Optimization-Based Design of Seismically Loaded Structures," *Proceedings*, 7th European Conference on Earthquake Engineering, Athens, Greece, September, 1982.

5. Austin M.A., Pister K.S., Mahin S.A., "A Methodology for the Computer-Aided Design of Seismic-Resistant Steel Structures," *Report* No UCB/EERC-85/13, Earthquake Engineering Research Center, University of California, Berkeley, December 1985.

6. Austin M.A., Pister K.S., Mahin S.A., "A Methodology for the Probabilistic Limit States Design of Earthquake-Resistant Structures," *Journal of the Structural Division*, ASCE, August 1987.

7. Conte J., "ARMA Models for Earthquake Excitation and Structural Response Simulation," *CE299 Report*, Department of Civil Engineering, University of California, Berkeley, 1988.

8. Cakmak A.S., Sherif R.L. and Ellis G., "Modelling Earthquake Ground Motions in California using Parametric Time Series Methods," *Soil Dynamics and Earthquake Engineering*, Vol 4, No 3, 1985.

9. Chang M.K., Kwiakowski J.W., Nau R.F., Oliver R.M. and Pister K.S. "ARMA Models for Earthquake Ground Motions," *Earthquake Engineering and Structural Dynamics*, Vol 10, pp 651-662, 1982.

10. Nau R.F., Oliver R.M. and Pister K.S., "Simulating and analyzing artificial non-stationary earthquake ground motions," *Bulletin of the Seismological Society of America*, Vol. 72, pp 625-636, 1982.

11. Tajimi, H., "A Statistical Method of Determining the Maximum Response of a Building During an Earthquake," *Proceedings*, 2nd World Conference on Earthquake Engineering, Tokyo, 1960.

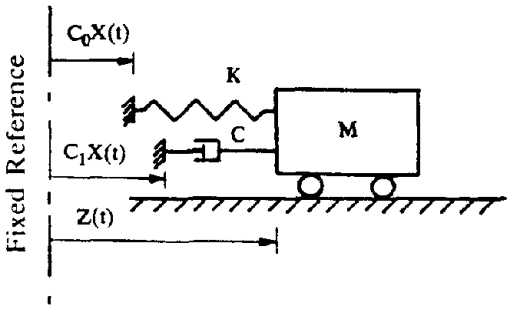

$X(t)$: input displacement

$C_0X(t)$: spring support displacement

$C_1X(t)$: dashpot support displacement

$Z(t)$: SDOF absolute displacement

Fig. 1 Underlying Physical System

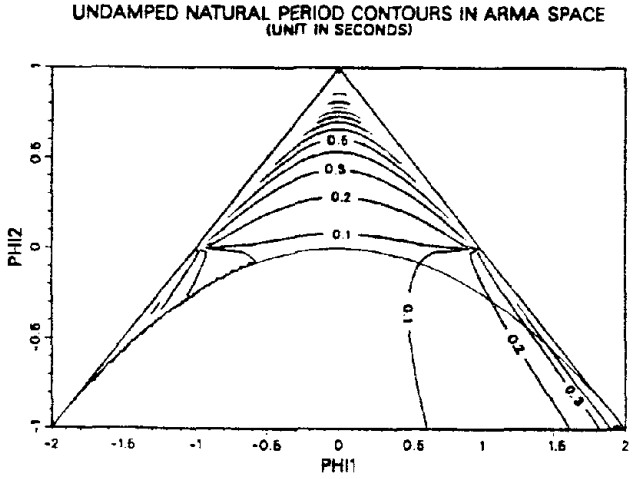

Fig. 2

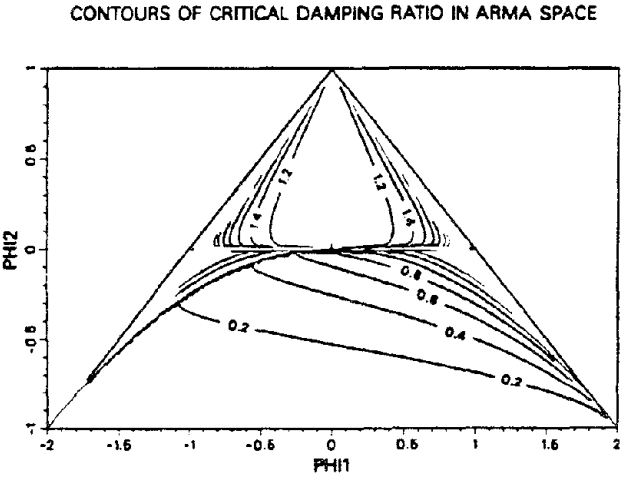

Fig. 3

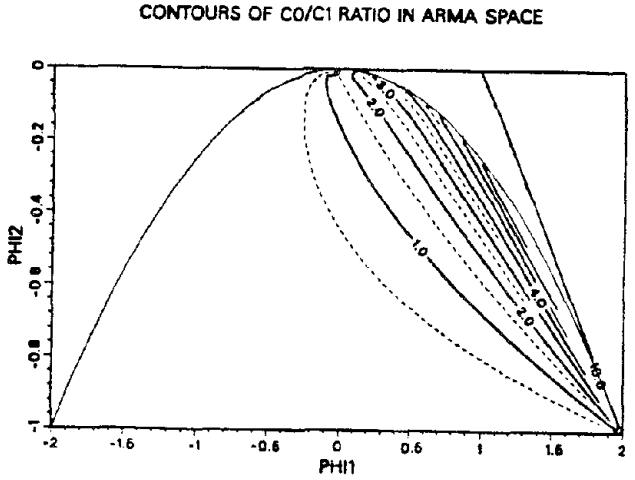

Fig. 4

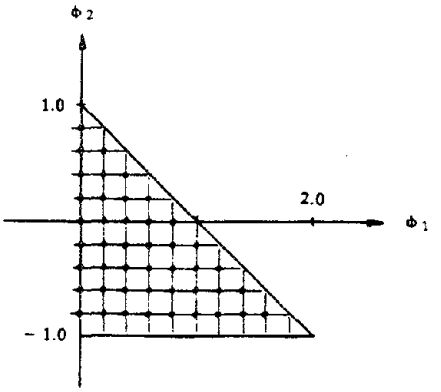

Fig. 5 Grid for Generation of Earthquake Families

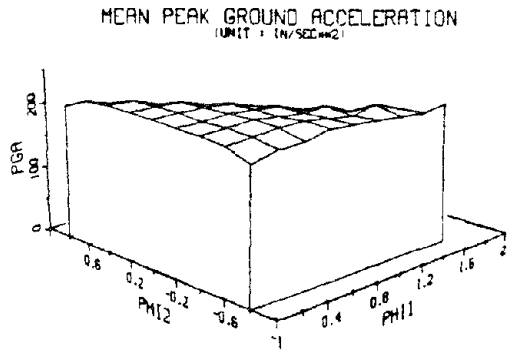

Fig. 6

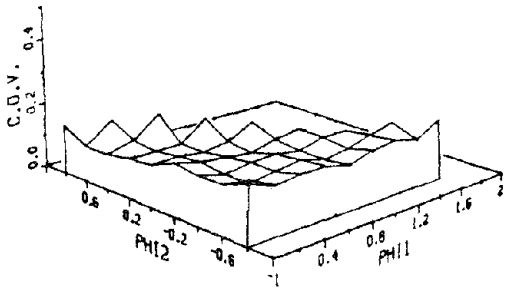

Fig. 7

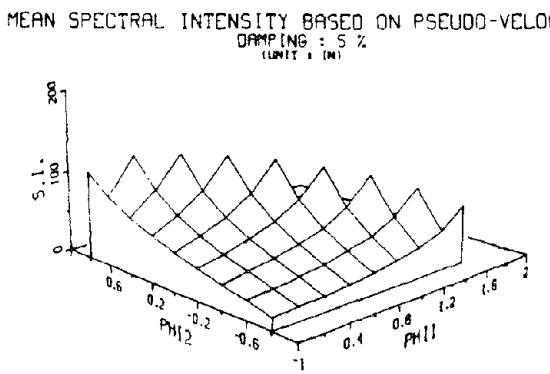

Fig. 8

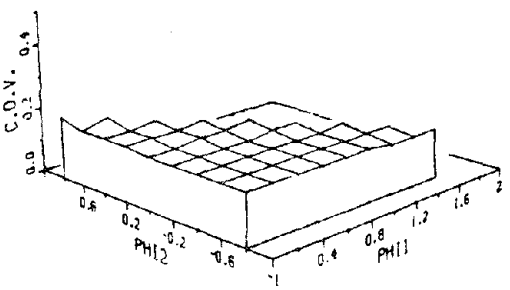

Fig. 9

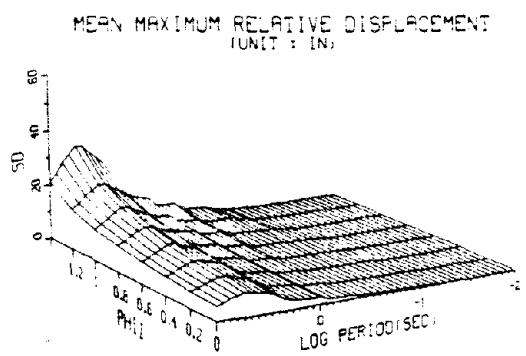

Fig. 10

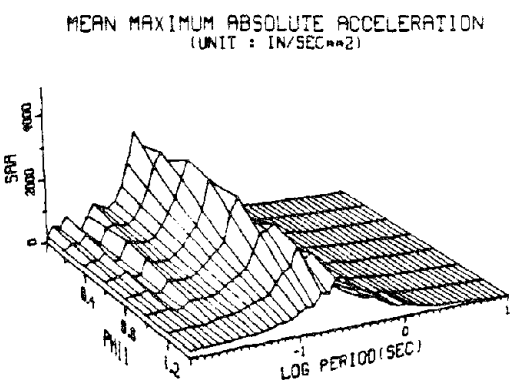

Fig. 11

PHI2 = -0.60
THETA = 0.00
DAMPING = 0 %

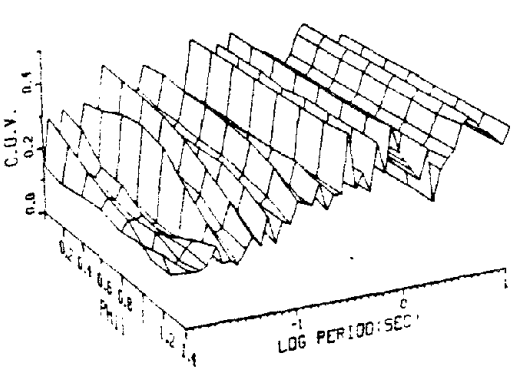

Fig. 13

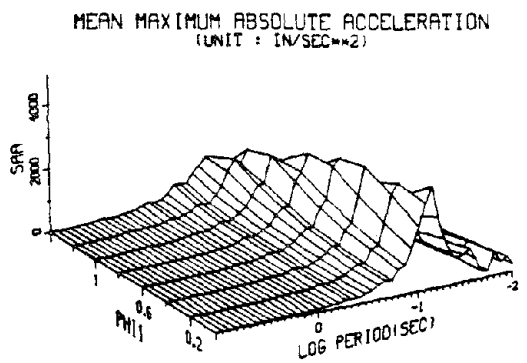

Fig. 12

DUCTILITY BASED STRUCTURAL DESIGN

Vitelmo V. BERTERO[1]

[1]Department of Civil Engineering, University of California, Berkeley, California, United States of America

SUMMARY

After discussing the differences in the concepts of **deformability, ductility and ductility ratio,** the importance of the proper use of these concepts is emphasized. The state-of-the-practice and particularly of-the-art in the use of the concept of ductility ratio for attaining efficient earthquake-resistant design is reviewed, and the various methodologies are discussed. The implications of lessons learned during recent earthquakes and research for improving earthquake-resistant design is assessed and used to identify further research, development and educational needs. Short and long-term solutions are formulated for the proper use of the concept of ductility.

INTRODUCTION

Introductory Remarks One of the most promising approaches for developing efficient methods for improving earthquake (EQ)-resistant construction is by approaching the solution of predicting the response of structures to EQ ground motions through an energy approach. In this approach, it is recognized that the total Energy Input, E_I, can be resisted by the sum of the Kinetic Energy, E_K, the Elastic Strain Energy, E_{ES}, and the Energy Dissipated, E_D, through Plastic Deformations (Hysteretic Damping), E_H; and the equivalent viscous damping, E_ξ. The energy equation for a single-mass oscillatory system can be written as:

$$E_I = E_K + E_{ES} + E_H + E_\xi \qquad (1)$$

The sum of kinetic energy and the linear elastic strain energy constitutes the elastic vibrational energy. If it is assumed that for a given structure the E_I has a constant value, it is clear from the above equation that to achieve economical EQ-resistant construction it will be necessary to dissipate part of the total input energy E_I by nonlinear behavior, i.e., by either E_H or E_ξ or a combination of both. Although the advantages of controlling the seismic response of civil engineering structures by increasing damping has long been recognized, the concept of using plastic deformation of the structural material to dissipate part of the input energy does not appear in the U.S. literature until the 1950s. In 1956 Housner discussed the use of limit design for EQ-resistant design [Ref. 1]. Although the advantage of using ductile material and ductile type structures in seismic-resistant design was demonstrated early in the 1950s, the use of the concept of ductility and ductility ratio in EQ-resistant design of reinforced concrete (RC) structures was introduced in the U.S. for the first time in 1961 with the publication of the Portland Cement Association (PCA) Manual "Design of

Multistory Reinforced Concrete Buildings for Earthquake Motions" [Ref. 2].

Since the publication of the PCA Manual, significant experimental and analytical research efforts have been devoted to the development of reliable methods of EQ-resistant design based on economic combination of strength and ductility. Even though as early as 1977, computer programs for earthquake-resistant inelastic design of RC, ductile moment-resistant space frames (DMRSF) based on the use of the concept of ductility, had been developed and proposed for its use in practice [Ref. 3], the practical application of EQ-resistant inelastic design in the U.S. today is more an exception than a rule. This also seems to be the case world-wide, except for countries like Mexico and New Zealand, where their building codes have introduced explicitly the use of ductility ratio, μ, in the estimation of seismic design forces and allowed the use of limit design method. In New Zealand, the seismic code is based on a "capacity design" procedure.

The slow progress in the use of limit design or capacity design procedure for EQ-resistant design of RC structures (or in general for any kind of structural material) it is not surprising. The definition of ductility ratio, μ, and its evaluation is only precise for the case of ideal linear elastic-perfectly plastic behavior. In reality, such behavior is more an exception than a rule. Furthermore, even though the advantages of providing the EQ-resistant design of a structure with the largest ductility that is economically feasible are generally recognized, the term ductility is used very loosely to express the deformability of the structure or the ductility ratio. Although the deformability, ductility and ductility ratio are parameters that are interrelated, their values and significance in the real behavior of structures can be quite different. There is an urgent need to get a worldwide agreement regarding the proper use of these technical terms, and of their evaluation and application to EQ-resistant design of structures.

Objectives The ultimate goal of this paper is to review the states-of-the-practice and, particularly, of-the-art in the use of the concepts of ductility and ductility ratio for attaining efficient EQ-resistant construction, and to identify the research, development and educational needs to improve the proper use of these ductility concepts.

Scope To achieve this goal, the needs for ductility and its proper use are discussed first, emphasizing the importance of recognizing the differences between deformability, ductility, and ductility ratio, as well as their inter-relationship, and of unifying the ways in which the different types of ductility ratios are estimated from the real seismic response of structures. Then it is shown that to achieve high energy dissipation capacity and overall effective seismic performance, it is advantageous to select highly redundant combined (hybrid) structural systems (several structural defense lines) and to provide their critical elements (i.e. those controlling the inelastic behavior of these systems) with the highest ductility ratio that is economically feasible. After a brief statement of the EQ-resistant design and construction problems, the states-of-the-practice and of-the-art are reviewed showing that there is a dangerous tendency in reducing the yielding strength required on the basis of linear elastic response to critical ground shaking, by means of using higher and higher values of ductility ratios, and to try to provide the constructed structure with just the minimum code required yielding strength. Finally, the implications of lessons learned during recent earthquakes and research for improving EQ-resistant design and construction are assessed and used to identify further research, development and educational needs. Short- and long-term solutions are formulated for the proper use of the concept of ductility and of energy dissipation capacity.

NEEDS FOR DUCTILITY AND ITS PROPER USE IN EQ-RESISTANT DESIGN

General Remarks It is well recognized and accepted that in EQ-resistant design, all structural members and their connections and supports should be designed (sized and detailed) with large ductility and stable hysteretic behavior so that the entire structure will also be ductile and display stable hysteretic behavior. There are two main reasons for this requirement: first, it allows the structure as a whole to develop its maximum potential strength which is given by the summation of the maximum strength of each component; and secondly, large structural ductility allows the structure to move as a mechanism under its maximum potential strength and this will result in dissipation of large amounts of energy. While these reasons have been recognized in the past, only the second has been emphasized because the large dissipation of energy was used to justify the reduction of the design strength that would be required if only linear elastic behavior were permitted. Although this reduction is justifiable in certain cases, the author has previously expressed his concerns about too large reductions of the required elastic strength or the linear elastic design response spectra (LEDRS) through the indiscriminate use of large values for the structural ductility ratio. For clarity and convenience in discussing the reasons for this concern, a glossary of the terms to be used in the discussion is given below.

Deformability: Capability of a material, structural component, or entire structure to deform before rupture.

Ductility: The ability of a material, structural component, or entire structure to undergo deformation after its initial yield without any significant reduction in yield strength.

Ductility Ratio or Ductility Factor, μ: The ratio of the **maximum deformation** that a structure or element can undergo without a significant loss of initial yielding resistance **to the initial yield deformation.**

The above definitions are illustrated in Fig. 1 for the case of DMRSF.

Needs to Recognize the Differences Between Deformability, Ductility and Ductility Ratio Although the ductility ratio depends on the ductility and the ductility depends on the plastic deformability (in other words, the three terms are interrelated), there are essential differences in their quantification that need to be recognized.

Deformability vs Ductility: While one structure can have significantly greater deformability than another, its ductility (particularly its usable ductility) can be smaller. For example, this can be the case of **a very flexible RC-DMRSF vs a stiff but very ductile shear wall.** It is clear from analysis of Fig. 2 that if the DMRSF is too flexible, i.e. the Δ_{Fy} is very large, and the maximum lateral deformation, Δ_{Fult}, that can be accepted or tolerated is limited, then the DMRSF ductility that can be used could be smaller than the available and usable shear wall ductility.

Ductility vs Ductility Ratio: The difference between these two terms is clearly illustrated in Fig. 2. While the shear wall usually has smaller ductility than a DMRSF, it can have a ductility ratio significantly higher.

Advantages of Providing Structural Components and Their Connections with the Largest Ductility Economically Feasible The minimum ductility desirable for each component should be that required to provide the structure the opportunity to develop its maximum potential strength according to the maximum strength of its components. The need for this is illustrated in Fig. 3 where the strengths of a simple structure composed of a ductile moment-resisting frame and two coupled walls are depicted as the sum of the resistance functions of each of

their components. This figure illustrates that in order for a structure to develop its maximum potential strength R_T as determined by the sum of the maximum strength of each component ($R_T = R_{W1} + R_{W2} + R_F$), it is necessary that $\mu_{W1} \geq 4.3$, $\mu_{W2} \geq 2.8$, and $\mu_F \geq 1.0$. To allow the structure to move as a mechanism under its maximum potential strength, the ductility ratio of the walls, particularly wall W_1 must be significantly higher. This figure also illustrates the difference between ductility ratio and deformability. While the ductile moment-resisting frame has a larger deformability than the walls, its ductility ratio can be smaller than that of the individual walls and this frame ductility ratio cannot be used effectively because of its significantly larger deformability (flexibility) than the wall components, resulting in a relatively earlier failure of the wall components.

It should be noted that by providing large ductility and due to three-dimensional (3-D) interaction between DMRF and walls, it is possible that the maximum strength of the entire structure will exceed the summation of the components if the strength of each is determined considering it as acting independently. This is illustrated in the schematic representation (Fig. 4) of the behavior observed in the experiments conducted on the 7-story RC DMRSF-wall structures of the US-Japan Cooperative Research Program. Results of these experiments are discussed in detail in Ref. 4. The beneficial 3-D interaction was identified to be a consequence of the effects of outrigging action of frames on the wall, as illustrated in the isometric view of Fig. 5. The wall rocking around the compressive edge during its ductile axial-flexural behavior tends to lift up the surrounding girders of the DMRSF that frame into the walls. These girders resist this movement and in doing so, act as prestressing cables, which by increasing the axial compression in the wall, increase its axial-flexural capacity. Thus, this outrigging action results in a significant enhancement of the lateral strength of the whole structure.

Quantification of the Ductility Ratio Though the use of the concept of ductility ratio for the EQ-resistant design of structures was introduced in the U.S. EQ Engineering literature in the early part of the 1950s and its application to R.C. structures was presented in 1961 in the PCA Manual "Design of Multistory Reinforced Concrete Buildings for Earthquake Motions" [2], and that tremendous experimental and analytical research efforts have since been devoted to its evaluation and application, even today it continues to be an ambiguous parameter. In a workshop conducted in 1977 [5] a group of experts, including professors, researchers and practicing engineers, after recognizing the need to survey, analyze, and evaluate the main parameters (as well as their definitions) that are presently used in research (analytical and experimental) and in practice to describe the inelastic mechanical characteristics of reinforced concrete materials, sections, regions, members, subassemblages, structures and whole soil-building systems, made the following statement:

"One parameter of particular concern is ductility. While ductility is a useful concept, it has a precise definition and quantitative meaning only for the idealized case of monotonic, linear elasto-perfectly plastic behavior. Its use in real cases where behavior significantly differs from this idealized case leads to much ambiguity and confusion. It is thus difficult to make valid comparisons of "available" ductility values reported by different researchers because they are often based on different response parameters or on yielding values determined using different and/or unexplained definitions. These experimentally obtained "available" ductility values are also often misused in analytical studies of the "demand" or "required" ductility due to the difficulty of establishing realistic values for the "linear-elastic stiffness and yielding strength." Attempts should be made to integrate the definitions of response parameters that are used in experimental test programs and in analytical investigations. Furthermore, it is highly questionable whether the performance of different building systems can be properly described and evaluated on the sole basis of elastic stiffness, yielding

strength, and ductility. Consequently, there is a need to introduce additional parameters for describing the total hysteretic energy dissipation, number of cycles of reversed deformations, and the degradation in stiffness and strength that has been observed under seismic conditions."

The needs stated above are still valid today.

Concluding Remarks While in discussing the **Philosophy** of ductility based design it is possible to use the concept of ductility and/or ductility ratio in a vague manner when such philosophy has to be applied in the EQ-resistant design of real structures, the philosophy has to be quantified, and therefore, it is necessary to use unambiguous parameters that can be reliably evaluated numerically. Such parameters are usually the displacement ductility ratio, μ_δ, and/or rotation ductility ratio, μ_θ. Preliminary designs are usually based on a selected maximum μ_δ which is determined based on the maximum values of μ_θ, that can be developed or that can be accepted at the critical regions of the structural members.

Assuming that the values of μ_δ can be selected and reliably evaluated, the problem that remains is to correctly use this ratio or parameter in the design process of a structure. To discuss the solution of this problem it is advisable to review briefly the states-of-the-practice and of-the-art in EQ-resistant design of RC structures.

STATES-OF-THE-PRACTICE AND OF-THE-ART OF EQ-RESISTANT DESIGN OF RC STRUCTURES

Problems in Design and Construction of EQ-Resistant Structures The problem areas have been identified and discussed in detail by the author in a series of publications [6-8]. Because of the length limitation of this paper, the main problems that have been identified are simply enumerated: The first problematical area in EQ-resistant design is in establishing the critical earthquake input (**Design Earthquakes**). The second includes problems involved in determining the **demands** on the entire soil-foundation-building (superstructure and nonstructural components) systems by the critical earthquake. The third involves the visualization (for preliminary design) and prediction of the real **supplies** to the building at the moment that an earthquake strikes.

The supplies and demands, in general, involve the mechanical characteristics of stiffness, strength, stability, and energy absorption and dissipation capacities. Evaluation of the **demands** and prediction of the **supplies** are not straightforward. Determination of the **demands**, usually by numerical analysis using mathematical models of the entire soil-foundation-building system, depends on the interaction of this system as a whole with the excitations that originate from changes in the system environment and on the **intimate interrelation between the demand and supply itself**. Specific problems encountered in the three problematical areas of the earthquake-resistant design of structures -- **critical earthquake input, demands on the building, and supply capacities to the building** -- are discussed in Refs. 6-8.

While a sound preliminary structural design and reliable analyses of this design are necessary, they do not ensure an efficient EQ-resistant structure. The seismic response of a structure depends on the state of the entire soil-foundation and superstructure system at the time that earthquake shaking occurs, i.e., response depends not only on construction, but on maintenance as well. A design will only be effective if the model used can be constructed and maintained. Although the importance of construction and maintenance in the seismic performance of structures has been recognized, insufficient effort has been made to improve these practices through, for example, supervision and inspection.

State-of-the-Practice This review will focus on just the state-of-the-practice of EQ-resistant design of buildings as reflected by present building seismic codes and emphasize how the concept of μ is used and/or how it could be used to improve the state-of-the-practice according to present knowledge.

Estimation of Demands in Present Seismic Codes: Although the review has been focused on U.S. seismic codes, the problems identified below are common to most codes in the world. There are several sources of uncertainty in code-specified procedures for the estimation of demands, uncertainties that can be grouped in two categories: (1) specified seismic forces; and (2) methods used to estimate response to these seismic forces.

For regular buildings, statically equivalent lateral seismic forces can be derived as follows. **For base shear:** $V = C_s W = (C_{sp}/R)W$ [Eq. (2)] where V is base shear, C_s is defined as the design seismic coefficient, W is the weight of the reactive mass (i.e., the mass that can induce inertial forces), C_{sp} is the seismic coefficient equivalent to a linear elastic response spectral (LERS) acceleration, S_a, ($C_{sp} = C_s R = S_a/g$), and R is the reduction factor. Although in most of the codes the values of R are given without any explicit relation to μ_δ, these values implicitly depend on μ_δ.

Structural response is usually estimated using linear elastic analyses of the effects induced directly by the above statically equivalent lateral forces or by these forces multiplied by load factors depending on whether the design will be performed using allowable (service) stress or the strength method. There are only very few countries in which their codes recommend or encourage the use of limit analysis and limit design methods.

Code Procedure to Estimate Supplies Provided to the Structure Stiffness: **Stiffness** Most of the RC codes give only empirical expressions to estimate the so-called "initial" or "linear elastic stiffness."

Strength Most of the RC EQ-resistant design codes require that the provided supplied strength be estimated using a strength method in which nominal strength of critical sections are evaluated in function of just the minimum specified strength of the materials, and then it is reduced by a strength reduction factor. There are few codes, like the New Zealand Code, in which the design and detailing of the critical regions of the structure is based on the probable supplied strength capacity to the members. Although most of the present RC EQ-resistant design codes specify minimum size and reinforcement detailing according to the ductility ratio that is expected to be developed, this is done in an implicit way. Thus, it can be concluded that the state-of-the-practice, as reflected by most of present EQ-resistant design codes for RC buildings, do not appear to have included in a rational and reliable way the use of the concept of energy dissipation capacity through the use of the ductility ratio.

State-of-the-Art in Ductility Based EQ-Resistant Design The state-of-the-art, with respect to each of the problem areas identified above, is discussed in detail in Refs. 7-8. Here only the state-of-knowledge regarding the proper use of the concept of ductility ration in the EQ-resistant design process will be discussed. It is well recognized that EQ-resistant design requires an iterative procedure in which a preliminary design is improved through a series of analysis. The importance of a proper preliminary design should be overemphasized, because, if the design procedure is started with a poor preliminary design, the only thing that will be achieved at the end through its repeated analyses will be an improved bad design.

State-of-the-Art in Using Ductility Ratio μ_δ, in Preliminary EQ-Resistant Design The first question that arises is where μ_δ should be used, i.e. in what steps of the whole design procedure? According to previous discussion, the answer is

obvious: Throughout the whole procedure, particularly in the final step, i.e. in the final designing and detailing of the critical regions of the structures. However as the importance of this last step is the main theme of the first part of this special session of the Conference, only the use of in estimating the demands will be discussed herein, specifically in (1) establishing the design EQs, and (2) in the preliminary design of the structure.

Use of μ_δ in Establishing the Design of EQs The following two main different methods are being used:

A. REDUCTION OF THE LINEAR ELASTIC DESIGN RESPONSE SPECTRA, (LEDRS) THROUGH THE DIRECT USE OF THE VALUE OF μ_δ (NEWMARK AND HALL PROCEDURE [9]), OR THROUGH THE USE OF R (ATC-3 PROCEDURE) R is a function of not only μ_δ but also of the provided overstrength, OVS, and increase in damping, ξ, due to plastic deformations.

B. DERIVATION OF IDRS THROUGH STATISTICAL STUDIES OF THE INELASTIC RESPONSE SPECTRA (IRS) OF STRUCTURES TO AVAILABLE RECORDED OR EXPECTED (PREDICTED) CRITICAL GROUND MOTIONS. These IRS are obtained through time history nonlinear dynamic analysis of structures with different yielding strengths (C_y), (or different degrees of μ_δ) and of ξ [10]. This method can be considered as a part of the overall energy approach to the design of EQ-resistant design [11].

Method A which is very simple, is already widely used and has been included in codes of several countries. However, as the proposers of this method pointed out, the method is only valid for very limited types of structures. The application of this method to the design of most real buildings is highly questionable [10-12].

Method B can be considered as the method of the future. Although it has already been applied to simple cases, its general application in practice will require extensive integrated analytical and experimental studies on real 3-D soil-foundation superstructure and nonstructural component systems. Once a reliable IDRS has been attained, the next problem is how to use μ_δ in the preliminary design of the structure.

Use of μ_δ in Preliminary Design For the purposes of this discussion, the different ways of conducting the preliminary design of EQ-resistant structures as far as the use of the ductility concept in the sizing of the structural members can be classified in the following three groups: **(a) μ_δ is not used at all.** The critical internal forces in the members are obtained through linear elastic distribution (LED) of forces. **(b) Implicit and Partial Use of μ_δ.** Usually this is done by allowing a limited amount of redistribution of the internal moments that have been obtained through a LED of forces. **(c) Use of Limit Design Approach.** Different methods, varying from the one based on simple plastic theory, which assumes infinity ductility, to those based on a more general plastic theory which consider "linear elastic serviceability conditions," as well as realistic limitation of μ_θ and μ_δ, incorporating also stability considerations. These methods are usually classified as **compatibility** and **serviceability** methods, with serviceability methods being the most promising of the two. This group also covers methods that include the possible occurrence of shakedown phenomena, which are, at present, being developed.

Concluding Remarks In summary, the author believe that the future of EQ-resistant design is on an energy approach in which the concept of ductility is used by combining the methods B and c, i.e., Bc, with proper consideration of the possibility of shakedown phenomena. However, this is considered a long-term approach. In present practice, most of the methods that are used can be classified as under the combination Aa. Although methods that can be classified

as combined Ab are being used and have been investigated recently [13-15], the results of these investigations indicate the need for further studies regarding the: (1) proper limits in the amount of redistribution; and (2) the adequate redistribution pattern through the height of the structures.

In view of the above remarks, and the fact that it is very difficult to change radically the state-of-the-practice, the author would like to formulate for the immediate or very near future the following compromise solution: To conduct the preliminary design using improved Ab or Ac (or even Aa) methods; but, this should be complemented with time history nonlinear dynamic analyses of the response of the preliminary designed structure to the predicted probable maximum credible earthquake (MCEQ) ground shakings that can occur at the site of the structure during its service life. Before this compromise solution can be applied in practice, it is necessary to first identify the improvements that are needed, and then to carry out the studies required to achieve such improvements.

RESEARCH, DEVELOPMENT AND EDUCATIONAL NEEDS TO IMPROVE EQ-RESISTANT DESIGN

Improvement of Methods Based on the Use of LEDRS The compromise solution formulated above, i.e. the use of Aa, Ab, or Ac methods for preliminary design involves the combination of the use of an IDRS which is derived from a selected LEDRS through the use of μ_δ or R. Thus, there is a need to look at how each of these two ingredients can be improved.

Seismic Code Procedures to Determine LEDRS Because reliable, measured data on earthquake ground motions are scarce, design spectra are currently formulated using inadequate statistical information. Data from records of the severe ground motions of earthquakes that have occurred during the last seventeen years has altered the previous statistical base so dramatically that drastic changes in the LEDRS and, therefore, in the code-specified C_s have been required. Examples of such ground motions are: the 1971 San Fernando earthquake; the 1979 Imperial Valley earthquake; the recent 1985 Chilean and Mexican earthquakes, the latter being perhaps the most dramatic, and the 1986 San Salvador earthquake. Until 1971, the recorded NS component of the 1940 El Centro earthquake was considered the most extreme earthquake ground motion. The records obtained during the 1971 San Fernando Valley earthquake demonstrated, however, that the damage potential of this El Centro component was very low compared with that of some of the recorded San Fernando motions.

The author and his research associates have recently conducted a series of studies regarding the implications of recorded ground motions regarding the rationality and reliability of code LEDRS [7, 8, 11]. These studies clearly demonstrated that EQs like the 1940 El Centro (which is usually used as a MCEQ to check the safety of designed structures) have a damage potential to structures (as measured by its energy input, E_I) that are significantly smaller than that of recently recorded motions. This is illustrated in Fig. 6. Furthermore, as illustrated in Fig. 7 and 8, the LEDRS assumed by the 1985 SEAOC (which is the one used in the 1988 UBC) and ATC-3 are significantly smaller than the LERS corresponding to the recorded ground motions during the 1985 earthquakes in Mexico and in Chile, and in other earthquakes such as the 1986 San Salvador and the 1971 San Fernando earthquakes. Thus, if such ground motions were to occur in the U.S. in the future, the values of the LEDRS adopted by present U.S. code requirements will underestimate significantly the response that could occur.

Improvement of the Values of R. **Rationale for R Code Values** The author has recently analyzed the values of R that ATC-3 and the values of R_W that the 1985 SEAOC (1988 UBC) have recommended for reducing the LEDRS to the recommended IDRS. As discussed in more detail in Refs. 7 and 8, it is very difficult to judge the rationale for the values recommended for these R and R_W factors due to a lack of

discussion or even any indication of how these values have been derived and what they are meant physically to represent. In Chapter 4 of the ATC-3 Commentary, it is stated that R "is an empirical response reduction factor intended to account for both damping and the ductility inherent in the structural system at displacements great enough to surpass initial yield and approach the ultimate load displacement of the structural system." In evaluating this statement, it should be noted that the LEDRS selected by ATC is already based on a 5% damped LEDRS. Therefore, the equivalent viscous damping expected in clean structures should not be significantly greater. If the values of R and R_W will depend only on μ_δ then the studies reported in Refs. 6-9 clearly demonstrate that for any selected resistance function, damping ratio, and ductility, the reduction factor varies with the period of the structure, decreasing as T decreases. It therefore appears that the recommendation of a constant value for R (or R_W), i.e., that the value be independent of T for the structure, cannot be justified solely on the basis of the ductility built up in a structure. The values recommended for R (or R_W) appear too high, particularly for short period structures (say, T less than 0.5 seconds) if the designer attempts to provide the structure with only the strength required by the code. Fortunately, as shown in previous publications [7, 8], the resulting code design generally produces a significant overstrength.

A better explanation of R is given in Chapter 3 of the ATC-3 Commentary. "The response modification factor, R, and ... have been established considering that structures generally have additional overstrength capacity, above that whereby the design loads cause significant yield." The author believes that this overstrength, OVS, together with built-in toughness is a "blessing" because of which structures designed according to presently specified design seismic forces (UBC or recommended ATC values) are able or would be able to withstand MCEQ shaking safely. The first "significant effective yielding" of properly designed (sized), detailed, constructed and maintained structures is not only considerably higher than that on which the code design is based, but such structures also have a significant overstrength beyond their first effective yielding. The resulting overstrength usually totals 2 to 3 times the minimum code-specified effective yield strength.

Implications of Recent Research Results with Respect to Rationale for R Code Values In Refs. 7 and 8 the author has analyzed the implications of the results obtained in shaking-table experiments on a seven-story RC frame-wall test structure, and after comparing ATC minimum required design strengths, the design strength used, ATC 5% damped LEDRS, 5% damped LERS for shaking table motion and measured strengths (Fig. 9), the actual value of R, termed R_a, could not have been larger than 2.7. Therefore, it was also concluded that "It is very difficult to rationalize (justify) quantitatively the values recommended by ATC and R. If the value of R alone is used in the design of reinforced concrete frame-wall dual systems, i.e., **without any other requirements**, the resulting design will not be reliable. The use of a specific value for R should be tied to other requirements. In the present ATC recommendations, the value of R is tied to stringent requirements for detailing reinforced concrete ductile moment-resisting space frame members and structural walls. The author believes that this is not enough, and suggests that the preliminary design using ATC-recommended approach (or that of the UBC) be subjected to a limit analysis to obtain an estimate of the **actual maximum resistance** of the structure as it will be constructed, and that a value approximately 3 to 5 (depending on the structural type and fundamental period T) times the minimum yielding strength required by ATC be ensured. Furthermore, the design of the wall (sizing and detailing) against shear (as well as against shear of members of ductile moment-resisting space frames) should be based on this maximum resistance.

Figure 10 [11] clearly shows that structures with $T \leq 1.5$ sec. which have been designed according to ATC-3 ($\mu_\delta = 5.5$ and $\xi = 5\%$) will be required to have a yielding strength (represented by C_y) significantly higher than that required by

ATC (represented by C_s) or a strength capacity (defined in the figure as Overstrength Factor OVF (req'd) = required C_y / ATC's C_s) significantly higher than that required by the ATC-3 provisions. Reference 11 shows that a structure with $T \leq 1.0$ sec. that has been designed and constructed to just satisfy the minimum required resistance (C_s) by the ATC-3 provisions will be required to develop ductility displacement ratios, μ, well beyond the value usually considered as acceptable ($\mu = 5$). Lessons learned from analysis of performance of buildings during recent destructive EQs and results from recent research clearly indicate that low-rise buildings (less than 4 stories) usually have large overstrength with respect to that required by code. Thus, it appears that in U.S. cities the buildings with between 4 and 12 stories are the ones that have to be suspected of becoming a serious threat to life and/or of incurring large economic losses in the case of a major EQ.

Research Development and Educational Needs The assessment presented above clearly indicates that there are gaps in the knowledge necessary for reliable use of the concept of ductility in EQ-resistant design of structures. In particular, the following further research, development, and education are needed.

1. To develop practical methods of EQ-resistant design based on an energy approach.

2. More reliable engineering parameters than are presently used to define the damage potential of recorded ground motions are needed. The E_I is a promising parameter that should be investigated further.

3. To improve quantification of ductility ratios.

4. To attain more reliable LEDRS, it will be necessary to install appropriate instruments, networks and array to record strong motions in the free field and at the foundation of structures. Research should be carried to improve processing and probabilistic methods of analyzing strong motion data and quantifying seismic hazard.

5. To develop more reliable methods for estimating the values of R. This requires a more precise definition of R. The definition illustrated in Fig. 11 is proposed as a basis for improving the evaluation of R. For the proper use of this definition in evaluating reliable values of R, there is an urgent need for calibration of the real strength of structures that have been designed according to present code.

6. The lag time for research and development to be reflected in codes should be reduced. This will require a broad educational effort. Efforts should be made to synthesize research results in EQ hazards and EQ-resistant design and construction of structures and to put them in an easily understandable, simplified form that can be applied in practice.

REFERENCES

1. Housner, G.W., "Limit Design of Structures to Resist Earthquakes," Proceedings, World Conference on Earthquake Engineering, Berkeley, California, June 1956, pp. 5.1-511.

2. Blume, J.A., Newmark, N.M. and Corning, L.H., "Design of Multistory Reinforced Concrete Buildings for Earthquake Motions," Portland Cement Association, Chicago, Illinois, 1961.

3. Zagajeski, S., and Bertero, V.V., "Computer-Aided Optimum Design of Ductile R/C Moment-Resistant Frame," Proceedings, Workshop of Earthquake-Resistant

Reinforced Concrete Building Construction, University of California, Berkeley, California, July 1977, II, pp. 1140-1174.

4. Bertero, V.V., et al., "Earthquake Simulator Tests and Associated Experimental, Analytical, and Correlation Studies of One-fifth Scale Model, SP-84 American Concrete Institute, Detroit, Michigan, 1985, pp. 375-424.

5. Bertero, V.V., "Earthquake Resistant Reinforced Concrete Building Construction," Proceedings, Workshop, University of California, University Extension, Berkeley, California, I, pp. 38-39.

6. Bertero, V.V., "State-of-the-Art in the Seismic Resistant Construction of Structures," Proceedings, Third International Microzonation Conference, University of Washington, Seattle, Washington, June 28-July 1, 1982, II, pp. 767-808.

7. Bertero, V.V., "Lessons Learned from Recent Earthquakes and Research Implications for Earthquake-Resistant Design of Building Structures in U.S.," Report No. UCB/EERC-86/03, Earthquake Engineering Research Center, University of California, Berkeley, California, April 1986.

8. Bertero, V.V., "Evaluation of Response Reduction Factors Recommended by ATC and SEAOC," Proceedings, Third U.S. National Conference on Earthquake Engineering, Charleston, South Carolina 1986. Earthquake Engineering Research Institute, El Cerrito, California, III, pp. 1663-1673.

9. Newmark, N.N. and Hall, W.J., "Procedures and Criteria for Earthquake Resistant Design," Building Practices for Disaster Mitigation, Building Science Series 46, U.S. Department of Commerce, National Bureau of Standards, Washington, D.C., Feb. 1973 and "Earthquake Spectra and Design," Earthquake Engineering Research Institute, Berkeley, California, 1982.

10. Bertero, V.V., et al., "Establishment of Design Earthquakes-Evaluation of Present Methods," Proceedings, International Symposium on Earthquake Structural Methods, St. Louis, Missouri, Aug. 1976, pp. 551-580.

11. Uang, C-M and Bertero, V.V., "Identification of Research Needs in Seismic Resistant Design of Structures," UBC/EERC Report, Earthquake Engineering Research Center, University of California, Berkeley, California, May 1988.

12. Mahin, S.A. and Bertero, V.V., "An Evaluation of Inelastic Seismic Design Spectra," Journal, Structural Division of the ASCE, 107, No. ST9, Sept. 1981, pp. 1177-1195.

13. Fenwick, R.C. and Davidson, B.J., "Moment Redistribution in Seismic Resistant Concrete Frames," Proceedings, Pacific Conference on Earthquake Engineering, New Zealand, Aug. 1987, pp. 95-106.

14. Cili, F., "Appropriate Yield Strength Distribution for Low-Rise Reinforced Concrete Structures," Proceedings, 8th European Conference on Earthquake Engineering, Lisbon, Portugal, 1986, Vol. 5, pp. 8.1/95-8.1/108.

15. Otani, S., et al. "Moment Redistribution in Earthquake Resistant Design of Reinforced Concrete Frames," Proceedings, 9WCEE, Tokyo-Kyoto, Japan, Aug. 1988.

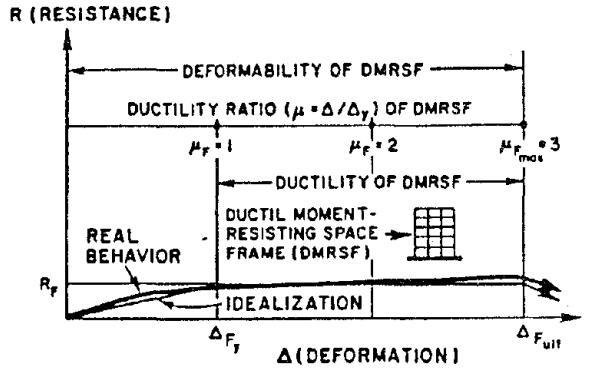

Fig. 1 Definitions of Deformability, Ductility and Ductility Ratio

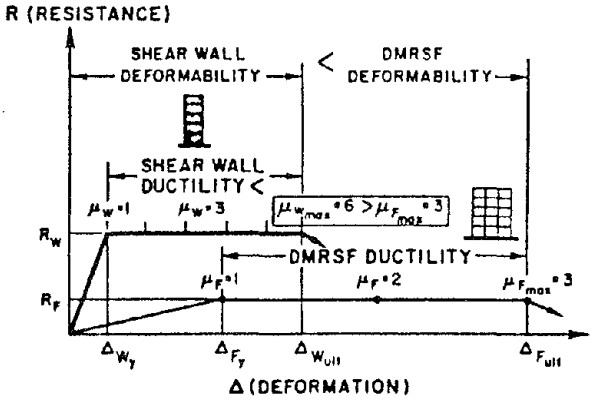

Fig. 2 Deformability and Ductility of an RC Wall and an RC DMRSF

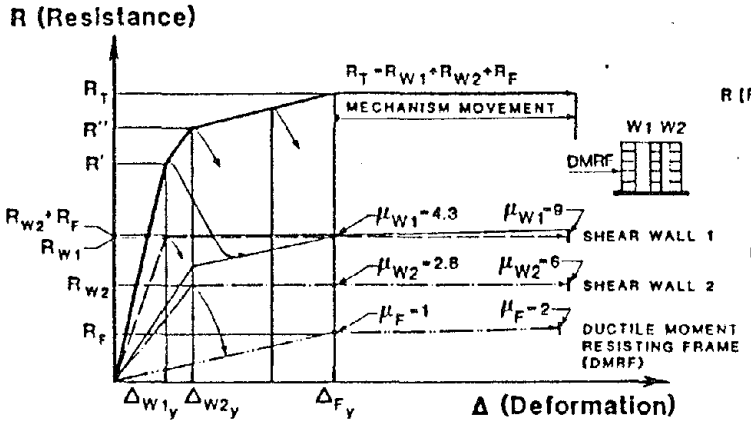

Fig. 3 Ductility Requirements for both Walls and Frames in an RC Frame-Wall System

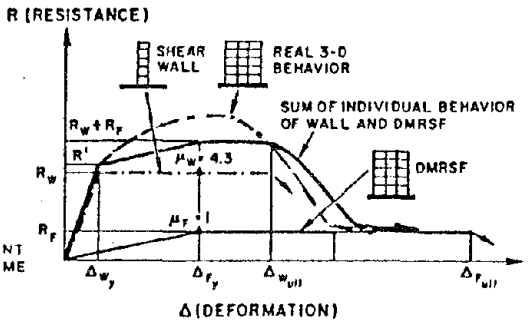

Fig. 4 The Effects of 3-D Interaction on the Strength of an RC Frame-Wall System

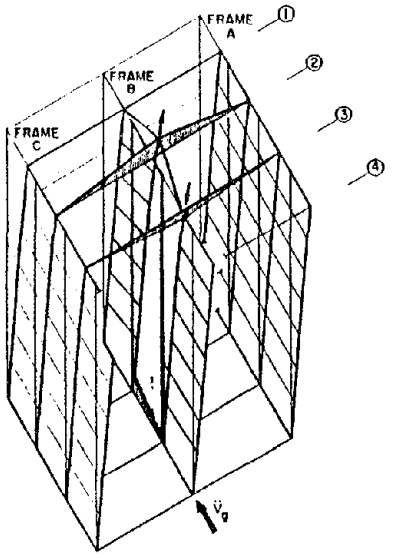

Fig. 5 Isometric View of Wall Rotation illustrating 3-D Outriggering Effect

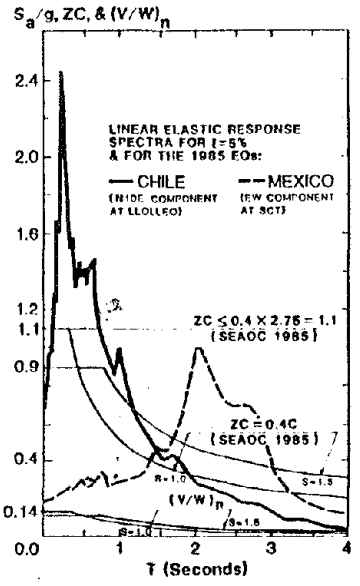

Fig. 7 Comparison of 5% Damped LERS and LEDRS

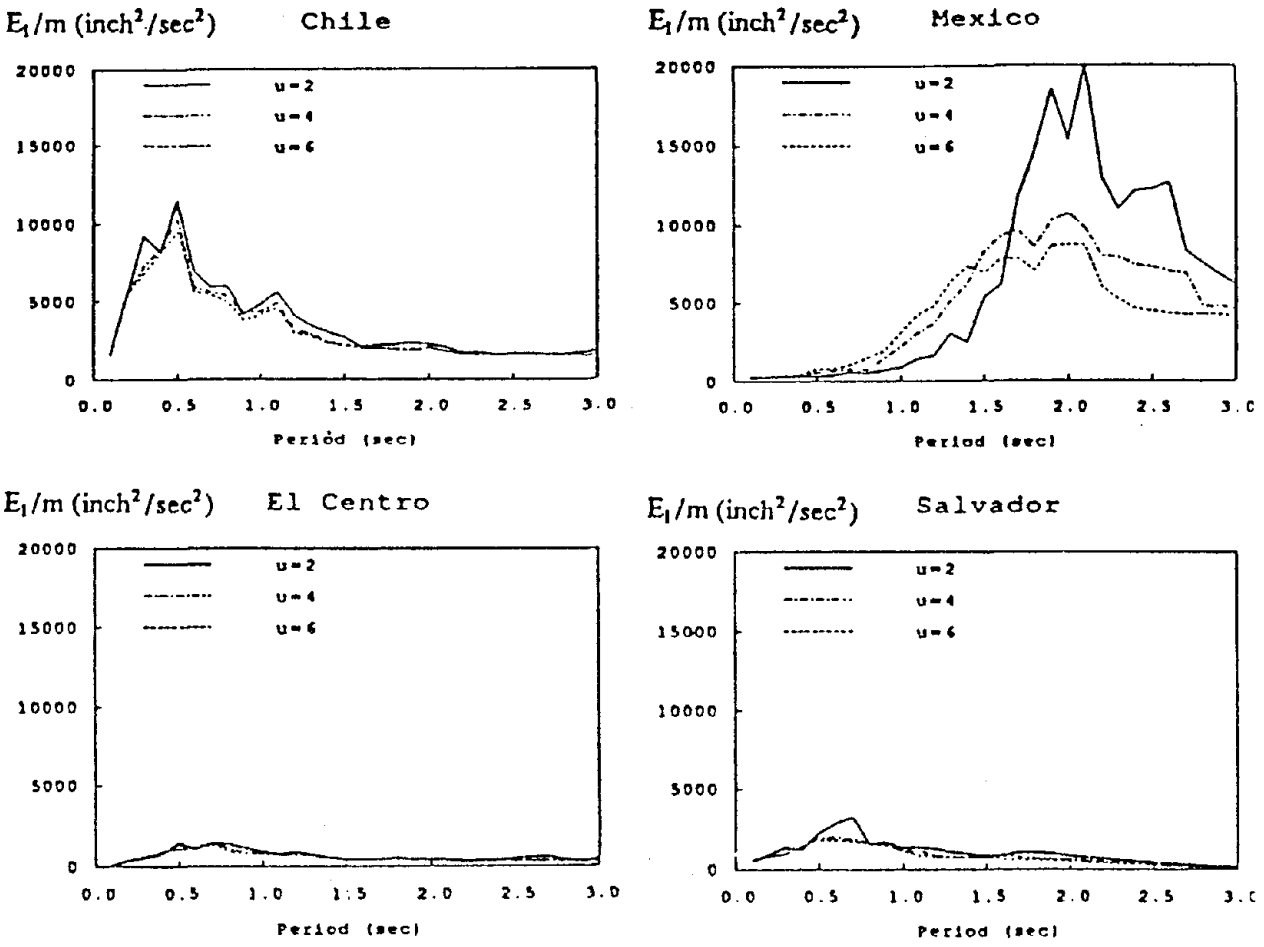

Fig. 6 Input Energy Spectra

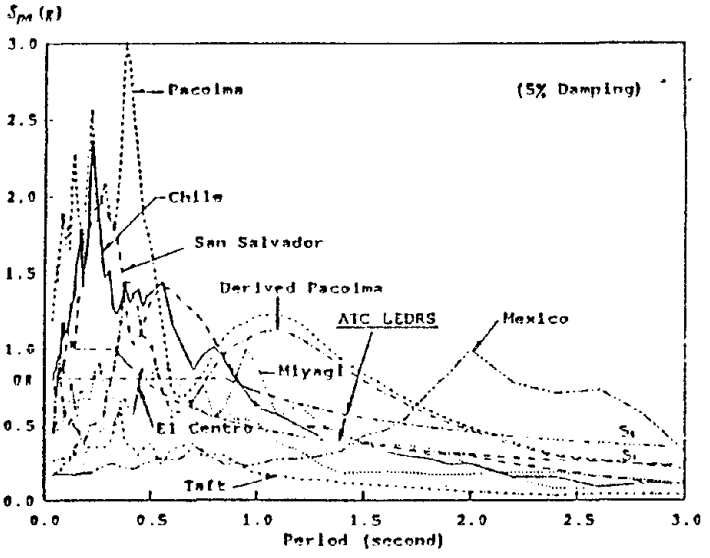

Fig. 8 Comparison of Pseudo-Acceleration Spectra, S_{pa}

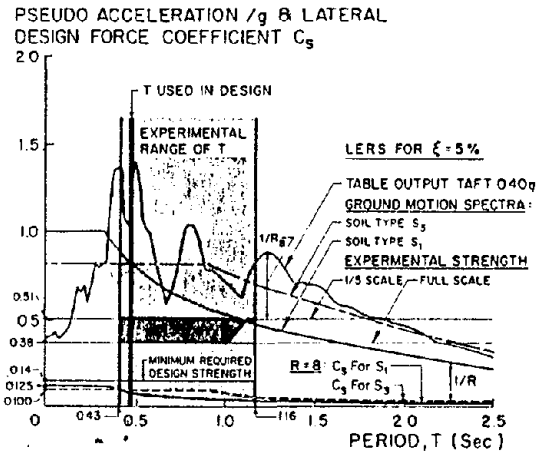

Fig. 9 Strength and Spectral Comparisons - ATC and Experimental

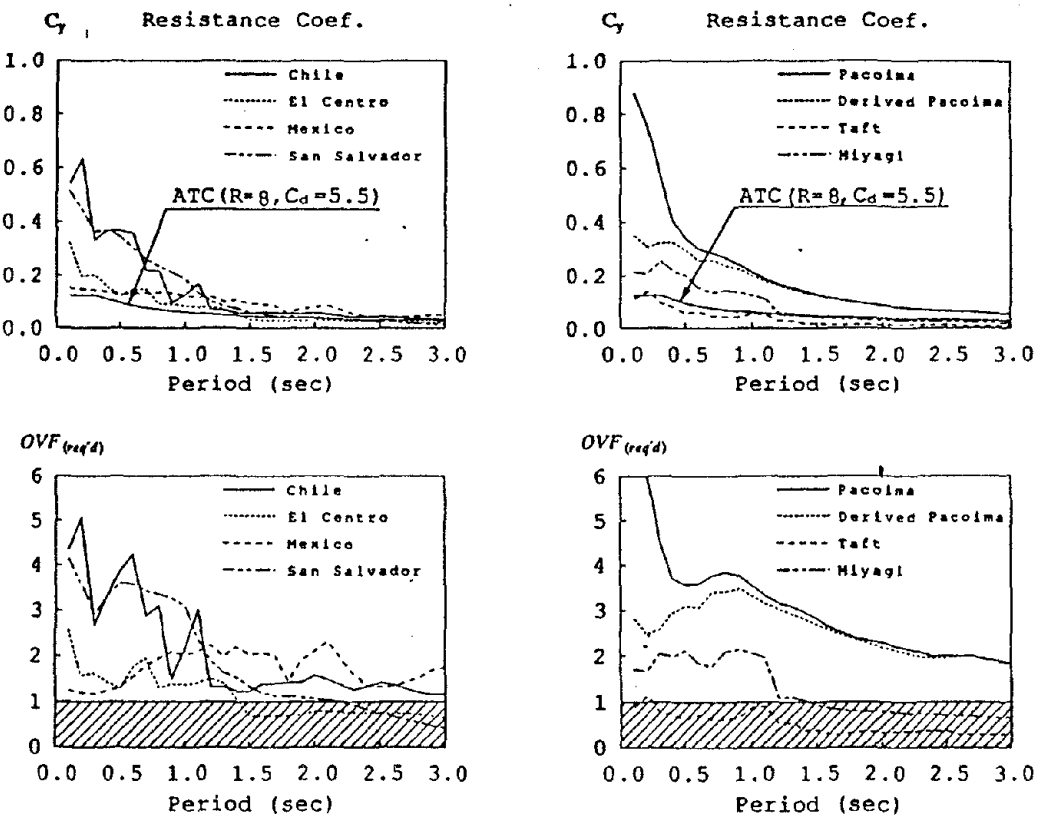

Fig. 10 Required Seismic Resistance Coefficient (C_y), and Over-strength Factor (OVF), for SDOFS designed in accordance with ATC for S_1 and assuming μ=5.5 and ξ=5%

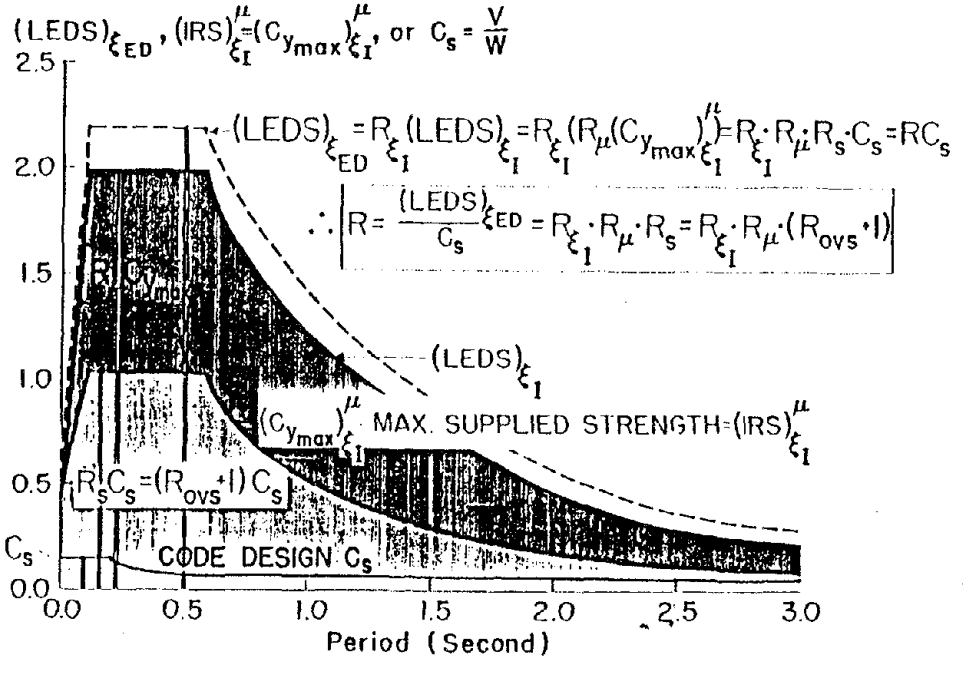

Fig. 11 Definition of the Response Modification Factor ($R = R_\mu \times R_\xi \times R_S$)

EARTHQUAKE SIMULATOR TESTING OF A CONCENTRICALLY BRACED STEEL STRUCTURE

Vitelmo V. Bertero[1] ; Chia-Ming Uang[2] and Andrew S. Whittaker[1]

1) Department of Civil Engineering, University of California at Berkeley, CA, 94720

2) Department of Civil Engineering, Northeastern University, Boston, MA, 02115

SUMMARY

A six-story concentrically braced dual steel system (CBDS) was subjected to a total of twenty earthquake ground motions with effective peak accelerations of up to 0.40g on the earthquake simulator at the University of California at Berkeley. The design of the CBDS complied with the lateral force requirements of the 1985 UBC. The maximum strength of the CBDS was 2.4 times greater than its nominal yielding strength; however, the response modification factor currently adopted by the ATC for CBDSs (=6) was 67% greater than that measured during the testing program.

INTRODUCTION

The Joint Technical Co-ordinating Committee for the U.S.-Japan Cooperative Research Program Utilizing Large Scale Testing Facilities selected a six-story, two bay by two bay, steel framed office building with a composite steel metal deck and a lightweight concrete floor system as the test structure for intensive investigation (Ref. 1), under simulated earthquake loading. A full-scale structure was constructed and pseudo-dynamically tested in the Large Size Structures Laboratory of the Building Research Institute (BRI) in Tsukuba, Japan (Refs. 2,3).

The plan view and braced frame elevation of the full-scale CBDS is shown in Fig. 1. The structure, 49.21 $\times$ 52.49 ft (15.0 $\times$ 16.0 m) in plan and 73.43 ft (21.5 m) high, consisted of three frames parallel to the loading direction; two ductile moment-resisting space frames (DMRSFs) on Grid Lines A and C and an concentrically braced frame on Grid Line B. In the transverse direction there were three frames: two X-braced frames on Grid Lines 1 and 3 and an unbraced frame on Grid Line 2.

Two reduced-scale models were tested at the University of California at Berkeley: concentric bracing (Refs. 4,5) was incorporated into the first model and eccentric bracing (Refs. 6,7) into the second model. Only the test results pertaining to the first model are discussed below due to the length limitations on this paper.

CBDS DESIGN REVIEW

The design of the original full-scale CBDS was based upon the 1979 UBC and the 1981 Japanese Aseismic Design Code (JADC). The design gravity loads for the full-scale CBDS are presented in Table 1. Although the design loads do not represent the minimum quantities specified in the USA or Japan, the total gravity load was appropriate for both countries. The seismic forces were evaluated using the 1981 JADC. The base shear coefficient specified by the JADC for the CBDS was significantly larger than the UBC coefficient. However, by making different assumptions regarding site conditions and assigning twice the UBC designated level of lateral force to the DMRSF (that is, 50% of the design lateral force), a base shear coefficient of 0.197 at the service load level was chosen (Ref. 2). The design reactive weight selected by the design group did not include the floor live loads (currently ignored by the U.S. seismic regulations for office buildings) or the weight of the perimeter walls. If these loads had been included, the resultant lateral load resisting system would have been too strong to be suitably damaged in the BRI testing facility.

The original design satisfied the 1985 UBC (Ref. 8) requirements for a dual system provided that the effective length factor for the braces was taken as 0.7; this assumption was consistent with welded connection used in the full-scale structure. The requirement that the DMRSFs resist 25% of the design base shear was also satisfied.

DESIGN AND CONSTRUCTION OF THE MODEL CBDS

A primary objective of the studies at the University of California was to design, construct and test the largest possible model of the full-scale CBDS that could be accommodated on Berkeley's earthquake simulator. Considering a number of factors that included the weight and size limitations of the earthquake simulator, the most suitable model was determined to be an artificial mass simulation model with a length scale factor of 0.305; this model satisfied similitude with regard to geometric and loading parameters The mass density similitude requirement was satisfied by fastening lead ballast to the roof and floor slabs in such a manner that it did not increase the stiffness of the model CBDS (Refs. 4,5).

EXPERIMENTAL RESULTS

General To compare the experimental results presented below with the provisions of the current U.S. earthquake-resistant design regulations, a number of factors must be noted (Ref. 4), these include :

(1) the design base shear coefficient at working stress levels of 0.197 was significantly larger than that required by the 1985 UBC and the 1984 ATC (Ref. 9); therefore, the design, elastic stiffness, elastic strength and maximum strength of this CBDS cannot be considered as being representative of these seismic regulations;

(2) the as-tested reactive weight (W_{a-t}) of the CBDS was chosen to be 82% of its design reactive weight; as a result the nominal yielding strength of the CBDS was equal $0.3W_{a-t}$ (Refs. 4,5);

(3) the CBDS was a bare steel structure and the important effects of the interaction of structural and non-structural components could not be considered.

Testing Program The model CBDS was subjected to twenty simulated ground motions. The 1978 Miyagi-Ken-Oki (MKO) earthquake record was used as the input displacement signal for the majority of the tests; the MKO command signal was time-scaled in accordance with the similitude laws and the peak acceleration for each test was scaled to different levels to simulate different limit states of response. Only the results of the collapse level test with a peak input acceleration of 65%g (MKO-65) are presented below.

Dynamic Characteristics of the Model Prior to earthquake simulator testing, flexibility tests and free and forced vibration tests were undertaken to measure the dynamic characteristics of the model CBDS. Table 2 presents the natural periods and damping ratios of the first three modes of the model CBDS together with those of the full-scale CBDS.

MKO-65 Test Results The effective peak acceleration (EPA) of the MKO-65 Test was 0.40g and equal to to the maximum EPA adopted by ATC for regions of high seismic risk. During the MKO-65 Test, the braces in the bottom five stories buckled (either in-plane and/or out-of-plane); one brace in the fifth story ruptured at midspan and one in the fourth story ruptured at its lower end. As a result of brace rupture, a maximum inter-story drift index of 1.9%, exceeding the maximum UBC and ATC value of 1.5%, was developed in the fifth story during this test. The lateral displacement, inertia force and story shear profiles over the height of the CBDS at the times of minimum and maximum base shear are shown in Fig. 2; the inertia force profiles reflect the formation of a soft fifth story. The maximum base shear coefficient ($=V_b/W_{a-t}$) of 0.73 was more than six times the UBC base shear coefficient (=0.113) for this collapse limit state earthquake and 2.4 times the nominal yielding strength of the CBDS ($= 0.3W_{a-t}$).

Story Shear and Inter-story Drift The total story shear envelope (V^{TOTAL}), the envelope of the story shear resisted by the concentric braces (V^{BRACE}) and the envelope of the story shear resisted by the DMRSF (V^{DMRSF}) for the first, third and fifth stories of the CBDS are shown in Fig. 3. The DMRSF remained elastic at a fifth inter-story drift index approaching 1.5%; this fact emphasizes the lack of stiffness compatibility between the braced frame and the DMRSF. Of the three stories, only the V^{BRACE} envelope in the fifth story shows signs of strength deterioration; this observation is consistent with the rupture of the concentric braces in the fifth story. However, the total fifth story shear and the inter-story drift relationship clearly shows that as a result of significant strength of the DMRSF, the fifth story shear resistance remain stable, that is, non-decreasing, following brace buckling and rupture. Stable story shear envelopes are mandatory for the sound performance of all structures during severe earthquake shaking.

Response Modification Factors In earthquake-resistant design the structure linear elastic strength demand can be reduced if the ductile behavior of the structural components is provided. ATC (Ref. 9) establishes a linear elastic design response spectrum (LEDRS) for 5% damping and then uses a *response modification factor* (R) to reduce the LEDRS to the minimum required design base shear coefficient. If the increase in damping due to inelastic behavior is neglected, the response modification factor can be considered to be the product of a reduction in the required elastic strength due to ductility ($R_\mu \equiv$ ductility factor) and a strength factor (R_S) defined as (Refs. 6,7) :

$$R_S = \frac{\text{Maximum Strength Ratio}}{C_y} = \frac{(\text{Overstrength} + 1) \times C_y}{C_y} .$$

The actual response modification factor (R) can therefore be represented as :

$$R = R_\mu \times R_S .$$

The total reduction from the MKO-65 LERS to the nominal yielding strength of $0.3W_{a-t}$ was by a factor of 3.6 ($\equiv$ R) with a strength factor equal to 2.4 and a ductility factor equal to 1.5. The ATC response modification factor for a CBDS of 6 exceeds the experimentally measured value of 3.6. As the model CBDS was detailed more conservatively and constructed more stringently than a typical building, the maximum achievable reduction factors for full-scale CBDSs are likely to be significantly less than three, assuming that current analysis and design procedures are used.

Concentric Brace Proportioning The local buckling and rupture of the braces in the CBDS clearly indicated that it is necessary to limit the P_{cr}/P_y and B/t ratios to values significantly less than those maximum values adopted at present (Ref. 10). The ATC requirement that concentric braces have a compressive strength equal to at least 50% of their required tensile strength was insufficient to prevent significant brace strength deterioration under repeated yielding reversals. On the basis of the data provided by these tests; the authors suggest that the following limits apply to the proportioning of tubular concentric braces in regions of seismic risk :

$$\frac{B}{t} \leq 18 \quad \text{and} \quad \frac{P_{cr}}{P_y} \geq 0.8 \quad \text{or} \quad \frac{kl}{r} \leq 0.63\, C_c$$

CONCLUSIONS

(1) The CBDS can provide sufficient elastic stiffness to avoid structural and non-structural damage during minor earthquake shaking. However, the strength and stiffness of a CBDS are

prone to degrade during severe earthquake shaking; this is a direct result of brace buckling and rupture under repeated yielding reversals. Therefore, the ability of a CBDS to respond successfully to long duration, severe earthquake ground motions, such as those measured during the 1985 Chilean earthquake, is extremely questionable.

(2) The measured response modification factor for the model CBDS was 3.6, that is, 60% of that currently adopted by the ATC. There would appear to be an urgent need to reassess the applicability of the empirical ATC 'R' values.

(3) For tubular braces in concentrically braced frames, their compressive strength should be equal to at least 80% of their required tensile strength and their width-to-thickness ratio should be limited to 18.

ACKNOWLEDGEMENTS

The research reported here was supported by the National Science Foundation Grant Numbers ECE 82-08141 and 84-19739. The ongoing encouragement from Drs. M.P. Gaus, S.C. Liu and J.B. Scalzi of the NSF is greatly appreciated. Any opinions, discussions, findings, conclusions and recommendations are those of the authors and do not necessarily reflect the views of the sponsor.

The authors also wish to acknowledge the contributions to this project of Professors R. W. Clough and E. E. Popov, Messrs. P. Quinn, D. Clyde and W. Neighbour and the staff of the Earthquake Engineering Research Center.

REFERENCES

1. U.S.-Japan Planning Group, Cooperative Research Program Utilizing Large-Scale Testing Facilities, "Recommendations for a US-Japan Cooperative Research Program Utilizing Large Scale Facilities," Report No. UCB/EERC-79/26, Earthquake Engineering Research Center, University of California, Berkeley, CA, 1979.
2. Yamanouchi, H. and Midorikawa, M., "Design of the Full-Scale Six-Story Steel Building," The Third Joint Technical Coordinating Committee, U.S.-Japan Cooperative Research Program Utilizing Large Scale Test Facilities, Tsukuba, Japan, July, 1982.
3. Foutch, D.A., Yamanouchi, H., Midorikawa, M., and Nishiyama, I., "Construction of Full-Scale Six-Story Steel Test Structure, "The Fourth Joint Technical Coordinating Committee, U.S.-Japan Cooperative Research Program Utilizing Large Scale Test Facilities, June, 1983, Tsukuba, Japan.
4. Uang C.M. and Bertero V.V., "Earthquake Simulation Tests and Associated Studies of a 0.3-Scale Model of a Six-Story Concentric Braced Steel Structure," Report No. UCB/EERC-86/10, Earthquake Engineering Research Center, University of California, Berkeley, CA, December, 1986.
5. Uang, C.M. and Bertero, V.V., "Earthquake Simulator Testing of a Concentrically Chevron Braced Steel Dual System," Paper submitted for publication in the ASCE Journal of Structural Engineering
6. Whittaker, A.S., Uang, C.M. and Bertero, V.V., "Earthquake Simulation Tests and Associated Studies of a 0.3-Scale Model of a Six-Story Eccentrically Braced Steel Structure," Report No. UCB/EERC-87/02, Earthquake Engineering Research Center, University of California, Berkeley, June 1987.
7. Whittaker, A.S., Uang, C.M. and Bertero, V.V., "Experimental Behavior of a Dual Steel System," Paper to be published in the ASCE Journal of Structural Engineering
8. International Conference of Building Officials., "Uniform Building Code" 1985 Edition, Whittier, California.
9. Applied Technology Council, "Tentative Provisions for the Development of Seismic Regulations for Buildings," ATC 3-06, National Bureau of Standards, U.S. Department of Commerce, Washington, D.C., 1984.

10. American Institute of Steel Construction, "Specification for the Design, Fabrication and Erection of Structural Steel for Buildings," New York, N.Y., 1980.

Load Type	Dead Load		Live Load	
	Floor (psf)	Roof (psf)	Floor (psf)	Roof (psf)
Metal Deck	6	6		
3.5" Lightweight Concrete	39	39		
Ceiling & Floor Finishes	10			
Ceiling & Roofing		20		
Partitions	20			
Structural Steel & Fireproofing	15	10		
Total	90	75	60	20

Exterior Wall Weight = 30 psf

Table 1. Gravity Design Loads

		Free Vibration			Forced Vibration		
	Mode	1st	2nd	3rd	1st	2nd	3rd
Full-scale CBDS	T_i (sec)	0.60	-	-	0.61	0.22	0.13
	ξ_i (%)	0.4	-	-	0.5	0.5	0.5
Model CBDS	T_i (sec)	0.62	0.22	0.12	0.62	0.22	0.12
	ξ_i (%)	1.3	0.7	0.5	1.6	0.7	0.6

Table 2. Dynamic Characteristics of the CBDSs

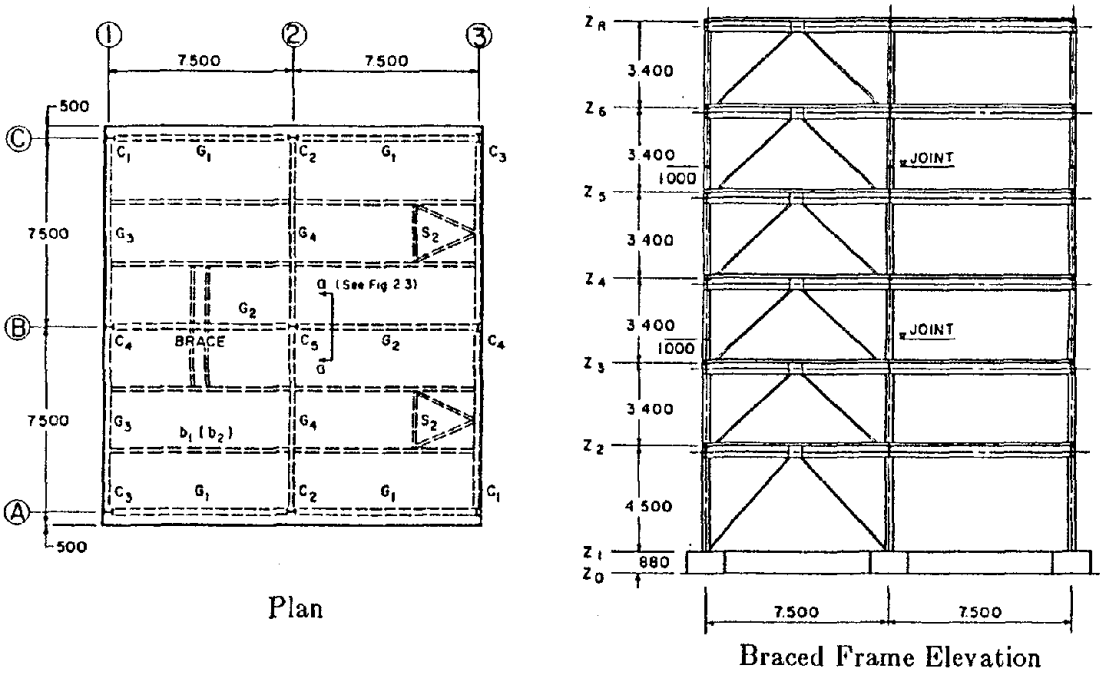

Fig. 1 Full-Scale CBDS Plan and Elevation (mm)

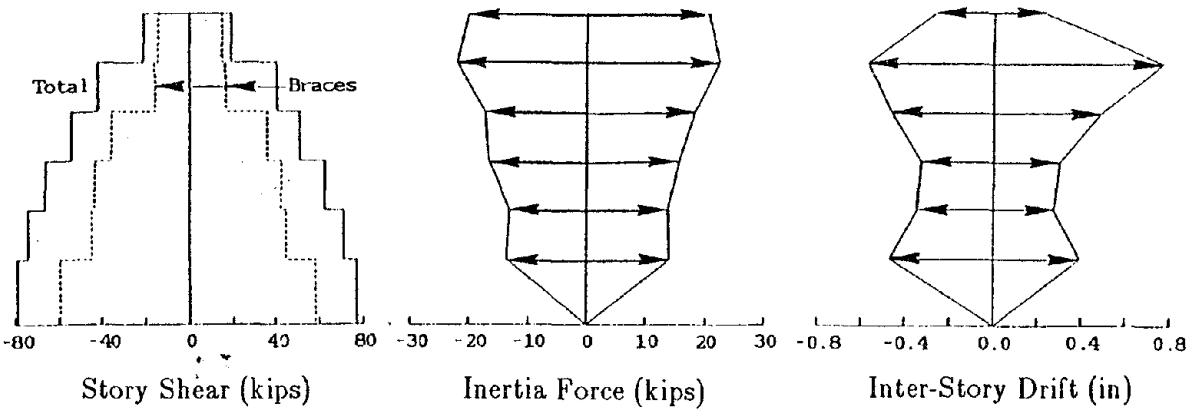

Fig. 2 MKO-65 Response Profiles

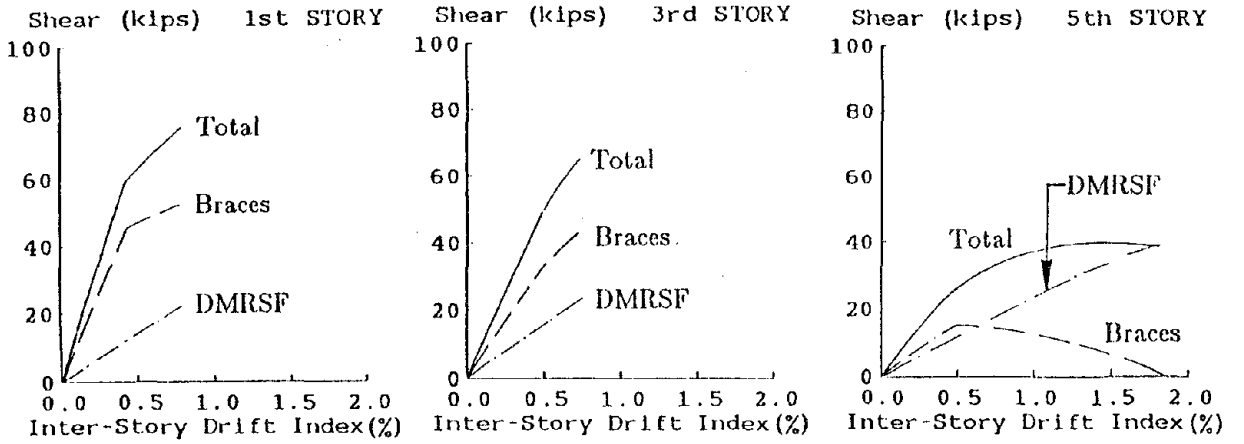

Fig. 3 CBDS Strength - Deformation Envelopes

EFFECT OF INITIAL CONDITIONS AND COMPUTATIONAL ALGORITHM ON LONG PERIOD RESPONSE SPECTRA

Rafael Blázquez[1] and James M. Kelly[2]

[1]Professor of Civil Engineering, Universidad Politécnica de Madrid and Director of Instituto Eduardo Torroja, CSIC, Madrid, SPAIN. Formerly Visiting Lecturer, Dept. of Civil Engineering, University of California, Berkeley, USA
[2]Professor of Civil Engineering, University of California, Berkeley, USA

SUMMARY

The combined effect of initial conditions and numerical integration on the accuracy of velocity and displacement response spectra of earthquake-like signals, with particular emphasis in the long period range is considered. These are important in assessing the seismic response of low frequency systems (e.g., base isolated structures, offshore structures), for which the ground velocity or the ground displacement can be the controlling parameter in the design.

The shock spectra equations are used to investigate the effects of initial conditions in the very long period spectral ordinates. The importance of the duration of the pretriggering event is established by artificially cutting off prefixed segments of the input motion, and comparing the response spectra of the complete and incomplete records. For the moderately long period range a synthetic accelerogram (enriched in low frequencies) that resembles more a real strong motion record is used. This artificial signal is integrable all the way up to the response spectra, thus permitting to calibrate the effectiveness and accuracy of several step-by-step integration algorithms currently employed in spectral analysis.

INTRODUCTION

Response spectrum plots either in natural scales or tripartite log-log form have become a routine design tool to represent the frequency content of the time histories of the earthquake ground motion. Such plots are obtained by maximizing the solution, x(t), of the equation of motion of the 1 d.o.f. system:

$$\ddot{x} + 2\omega\zeta\dot{x} + \omega^2 x = -a(t) \tag{1}$$

as well as the related magnitudes, $\dot{x}(t)$ and $\ddot{y}(t) = \ddot{x}+a(t)$, and are defined as follows:

$SD = |x(t)|_{max}$ = relative displacement response spectrum
$SV = |\dot{x}(t)|_{max}$ = relative velocity response spectrum
$SA = |\ddot{y}(t)|_{max}$ = absolute acceleration response spectrum
$PSV = \omega SD = (2\pi/T)\, SD$ = pseudo-relative velocity spectrum
$PSA = \omega^2 SD = (2\pi/T)^2 SD$ = pseudo-relative acceleration spectrum

In eq. (1), $\omega = 2\pi/T$ is the circular frequency of the oscillator whose spectral ordinate is being computed for the damping ratio ζ and the input motion a(t). To calculate x(t) one has to evaluate for each pair of values (ω,ζ) the expression:

$$x(t) = \left(\frac{1}{\omega_D}\int_0^t a(t)e^{-\omega\zeta(t-\tau)}\sin\omega_D(t-\tau)d\tau\right) + \left(\frac{x(0)+\dot{x}(0)\zeta\omega}{\omega_D}\sin\omega_D t + x(0)\cos\omega_D t\right) \tag{2}$$

where $\omega_D = \omega\sqrt{1-\zeta^2}$ is the damped circular frequency of the oscillator. The first parenthesis in eq. (2) is the Duhamel integral (response of the system to a unit impulse) whereas the second yields the free vibration part of the response due to initial conditions. In practice, errors arise in computing equation (2) from:

(a) uncertainties associated with the initial values x(0) and $\dot{x}(0)$, which are not known beforehand.
(b) numerical evaluation of the Duhamel formula using time integration operators (forced vibration response).

In this paper the above two effects are considered separately, and their implications in the overall accuracy of spectral ordinates at long periods are discussed.

EFFECT OF INITIAL GROUND MOTION ON RESPONSE SPECTRA

After the processing and correction steps of optical accelerograms a set of initial ground motions (displacement, d_o; velocity, v_o; and acceleration, a_o) is arrived at for time zero. Without questioning the representativeness of the above values as true estimates of the actual ones, their existence can be justified on physical grounds. In effect, since the response of the instrument below the prefixed level of sensitivity cannot be recorded, a small portion of the accelerogram is always lost, which translates into some motion at zero time. Clearly, these considerations do not apply to the new digital instruments, whose buffering memory permits the recovery of information at the pretriggering stage.

The initial values which contaminate strong-motion records are obviously unknown (since they emanate from a mechanical shortcoming of the accelerograph), and at most can be estimated for a given instrument and event with great uncertainty. They imply, in turn, that the time histories needed to compute response spectra do depart from "at rest conditions", so that the second parenthesis in the right-hand side of equation (2) is not identically zero, even for t = 0. Thus, to compute accurately the actual response spectra, the initial values of the displacement, x(0), and velocity, $\dot{x}(0)$, of the response of the oscillator must be found first. Such values are again unknown, and will depend on the initial ground motions and on the mechanical properties of the oscillator:

$$x(0) = f(d_o, v_o; T, \zeta) \tag{3-a}$$

$$\dot{x}(0) = g(d_o, v_o; T, \zeta) \tag{3-b}$$

The shape of functions f(•) and g(•) in eq. (3) is portrayed in Fig. 11, which shows the ratios $x(0)/d_o$ and $\dot{x}(0)/v_o$ obtained by numerical simulation of the response of the system (to a sine wave acceleration at a given time). For very long period systems, that is when $T_g/T \to 0$, it can be seen that $x(0) = -d_o$ and $\dot{x}(0) = -v_o$, regardless of the damping level. The same conclusion has been reached by Pecknold and Riddell (Ref. 1), using a different line of reasoning.

At the intermediate range of spectral periods ($0.2 < T_g/T < 1.2$ in Fig. 1), which are the most interesting for design purposes of normal structures, no asymptotic behavior of the initial conditions of the system can be found, leaving the designer with the unpleasant choice of either ignoring or "guessing" them. Since such initial conditions are unavoidable and are always present in the problem, it has become a standard practice in conventional response spectra analysis to assume $x(0) = 0$, $\dot{x}(0) = 0$ for all frequencies. That assumption reduces the calculation of the time history x(t) to computing Duhamel's formula, since the free vibrations of the system are ignored. If such is the case, by extending the calculation for some time (T/2 or until $\dot{x}(t)$ has changed sign three times) after the excitation is over - as is often done in the conventional spectral analysis (Nigam and Jennings; Ref. 2) - only the maxima of undamped resonant oscillators starting from rest can be found, whereas the effect of initial conditions on more general systems remains unknown.

To clarify further this matter a series of computer experiments has been conducted for several acceleration inputs. Since we are only interested in the long period region of the response spectra, the so-called "shock spectra" equations for a short-duration sinusoidal wave are employed first to get an overall picture of the effect of initial conditions at very low frequencies. The input used consists of a single sine wave pulse with period Tg = 1 sec. and amplitude 1 gal. The normalized undamped spectra (with respect to the maximum ground motions) for this excitation are shown in Fig. 2. It can be seen that at $\zeta = 0$ PSA = SA for all frequencies, but PSV ≠ SV. The reason for this discrepancy is that the expression of PSV involves only a sine whereas the SV integral involves a sine and a cosine. Furthermore, beyond a certain critical period, T_c, the SV curve departs clearly from the PSV curve and approaches its asymptotic value, the maximum velocity of the ground, v_m. For the same conditions however $PSV = (2\pi/T)SD \to 0$, since SD approaches its limiting value, d_m, while T increases indefinitely (Hudson, Ref. 3).

Up to this point initial conditions are not involved in the base motions or in the response of the oscillator at t = 0. To bring in these conditions the sine function a(t) with amplitude a_m is substituted in eq. (2),so that x(t) can be computed in closed form for any pair of values x(0) and $\dot{x}(0)$. Fig. 3 shows the results of this calculation for several combinations of the normalization parameters:

$$\alpha = -\left(\frac{2\pi}{T}\right)^2 \frac{x(0)}{a_m} \qquad \beta = -\left(\frac{2\pi}{T}\right) \frac{\dot{x}(0)}{a_m}$$

namely (α, β) = (0,0), (0,1), (1,0) and (1,1). Only the 5% damped velocity and displacement spectra are displayed in the figure, since, as could be anticipated, the variations in shape of either AA or PSA curves for different sets of initial conditions become noticeable at high (rather than low) frequencies (Ventura and Blazquez; Ref. 4). By comparing the Figs. 3-a, 3-b, and 3-c it is concluded that the effect of initial conditions on the response spectra is to introduce spurious noise at low frequencies, which results in a considerable increase in the velocity and displacement ordinates in that region with respect to the case in which such conditions are absent ($\alpha = 0, \beta = 0$ in Fig. 3). This effect is particularly marked for the pseudo velocity spectra, which literally "take off" from the zero condition curve for periods about 1 to 2 sec.

The results just presented are useful inasmuch as they provide the behavioral pattern of the problem. However they are difficult to link to the primary cause of x(0) and/or $\dot{x}(0)$ being nonzero, which is the lost initial part of the accelerogram that leads to $v_o = 0$ and/or $d_o = 0$ at zero time. To cope with this problem the following approach has been implemented: the pretriggering event is established for a given accelerogram by artificially cutting off prefixed segments of the input motion, and comparing the response spectra of the complete and incomplete records. This procedure has been applied to three synthetic accelerograms which are analytically amenable, so that, in principle, a direct comparison between exact and numerical results can be made. Nevertheless such comparison in spectral ordinates becomes very cumbersome when initial conditions are taken into consideration, and for that reason the spectra presented below are computed by the standard Nigam-Jennings method.

Figure 4-a depicts the displacement and pseudo velocity spectra for the sinusoidal acceleration function mentioned before for a triggering time $t_o = T_g/4 = 0.25$ sec. For the incomplete record ($v_o = 0$; $d_o = 0$) the conventional (wrong) at rest initial conditions x(0) = 0 and $\dot{x}(0) = 0$ are used in the response spectrum calculation, with the result of higher spectral content at long periods than the complete record. The justification for that can be found in Pecknold and Riddell (Ref. 1) and is beyond the scope of this work.

Also, Figure 4-a shows the incidence of damping on PSV spectra for both complete and incomplete records. It can be seen that ignoring initial conditions in the computation of response spectra yields psuedo-velocity values which are substantially in error at very low frequencies: the lower the damping the greater the deviation with respect to the asymptotic limit, d_m. The same phenomenon is observed when an amplitude-modulated sine acceleration wave, such as:

$$a(t) = t[e^{-0.3(10-t)} - 1] \sin(2\pi t) \qquad (4)$$

(duration = 10 sec; period = 1 sec) is used (Fig. 4-b).

Finally, Fig. 4-c illustrates the effect of the duration of the pretriggering stage, t_o, on PSV curves of earthquake-like signals, using the same methodology as above. For these purposes the following synthetic accelerogram, enriched in low frequencies, is employed (see Table I):

$$a(t) = t\ e^{-0.333(10-t)} \sum_j \cos(2\pi t/T_{gj} + \Psi j) \qquad (5)$$

The results obtained demonstrate that PSV values are consistently higher for spectra with conventional zero initial conditions; however, if a significant portion of the accelerogram is lost before the instrument is triggered (e.g., $t_o = 2.5$ sec), the opposite effect is found, and the pseudo velocities of the incomplete record fall below the ones for the complete accelerogram within the long period range of the spectra.

ERROR ANALYSIS OF TIME INTEGRATION OPERATORS

For a given digitized accelerogram, the error associated with the forced part of the solution of equation (1) comes as a result of two facts:

(a) the assumption made on the variation of a(t) between the sampling points
(b) the amplitude of the time integration step, $\Delta\tau$, used to evaluate Duhamel's formula.

Frequency domain analysis of time integration operators illustrates their performance at different frequency regions. In general, Nigam-Jennings and Newmark $\beta = 1/4$ methods can be used advantageously in the long spectral range, since they deamplify low frequency noise (Preumont; Ref. 5). However, from a practical viewpoint the errors associated with the size of the integration step are very critical, since there are operators which become unstable as the ratio $\Delta\tau/T$ increases.

In this study a sensitivity analysis of the accuracy of the numerical spectral response has been conducted for the simulated earthquake given in eq. 5 with 10 sec. duration and no initial conditions. Five algorithms have been tested for T = 5 sec and $\zeta = 0\%$, namely: 3rd and 4th order Runge Kutta methods, Newmark -β = 1/4 and $\beta = 1/6$ methods, and Nigam-Jennings method (standard in U.S. processing of strong-motion records). For $\Delta\tau = T/20$ the maximum relative error (in %) of the peak response (forced vibration) computed at integration points of Duhamel's formula is as follows: for the displacement, RK-3 = 1.56; RK-4 = 0.9; N-1/4 = 1.76; N-1/6 = 0.87; N-J = 0.89, whereas for the velocity: RK-3 = 2.99; RK-4 = 2.36; N-1/4 = 1.87; N-1/6 = 2.09; N-J = 2.36. If $\Delta\tau = T/20$, these figures are reduced by a factor of about 4 or 5. Although these results are only preliminary, they seem to indicate that the 4th order Runge Kutta method and the Nigam Jennings method perform similarly and are more accurate than the other computational algorithms at relatively large integration intervals, $\Delta\tau$, where stability problems often arise. Besides, for a given $\Delta\tau$, the velocity response consistently shows more error than the displacement response, regardless of the method used.

CONCLUSIONS

It has been shown that ignoring initial conditions in the computation of response spectra yields pseudo-velocity spectra that can be substantially in error at low frequencies of interest in certain types of structures; the lower the damping the greater the errors become. The assessment of the errors in response spectra, at long periods due to the time integration algorithms indicates that all integration schemes can introduce errors in this frequency range; the greater the integration interval the greater the error.

Both sources of error for long period response spectra appear to be related to ratio of the period of the system to the duration of the input.

REFERENCES

1. Pecknold, D.A. and Riddell, R. (1978), "Effect of Initial Base Motion on Response Spectra," Journal of Engin. Mech., ASCE, Vol 104, No. EM2, April, pp. 485-491. Discussions: Feb 1979, pp. 204-206 and Dec. 1979, pp. 1057-1060.
2. Nigam, N.C. and Jennings, P.C. (1968), "Digital Calculation of Response Spectra from Strong-Motion Earthquake Records," EERL Report, Pasadena, CA, June.
3. Hudson, D.E. (1979), "Reading and Interpreting Strong Motion Accelerograms," EERI Monograph, Berkeley, CA, USA.
4. Ventura, C. and Blazquez, R. (1988), "Sensitivity Analysis of Earthquake Response Spectra to System Initial Conditions" (in press).
5. Preumont, A. (1982), "Frequency Domain Analysis of Time Integration Operators," Journal of Earthq. Engin. and Struct. Dynamics, Vol. 10, pp. 691-697.

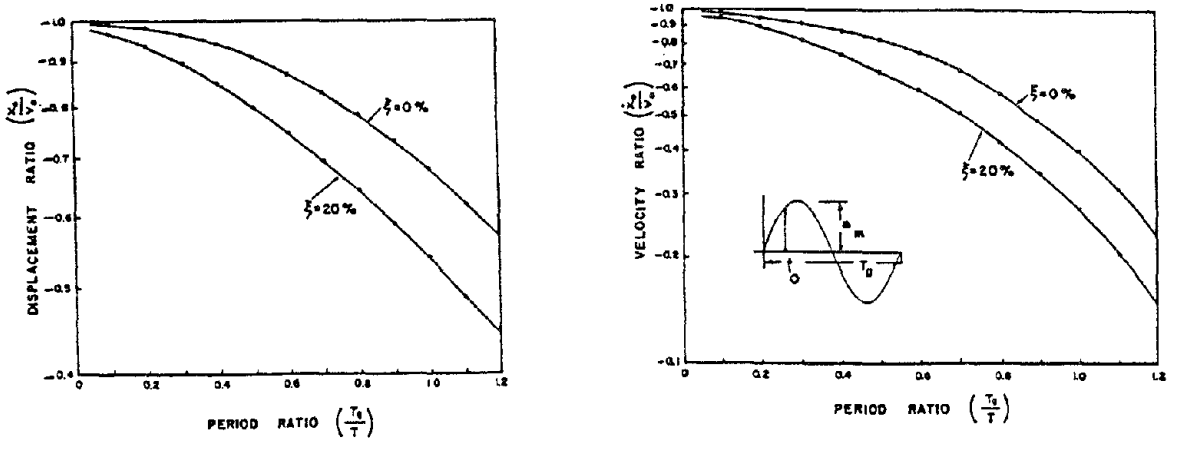

Fig. 1.- Ratio of initial motions of the oscillator to the initial motions of the ground for sinusoidal acceleration wave.

Table I.- Parameters of simulated earthquake

T_g (sec)	10.48	6.28	4.19	2.09	1.40	1.05	0.79	0.63	0.56	0.51	0.47	0.44	0.38	0.36	0.33
Ψ_i (Grad)	2.00	1.00	4.00	3.00	1.00	3.77	1.34	4.88	0.25	4.52	1.88	1.33	1.79	0.15	2.49

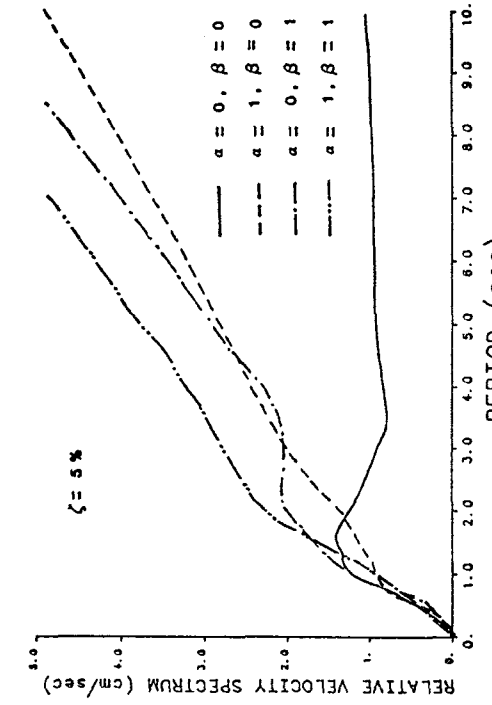

Fig. 2.- Normalized undamped response spectra for sinusoidal acceleration pulse.

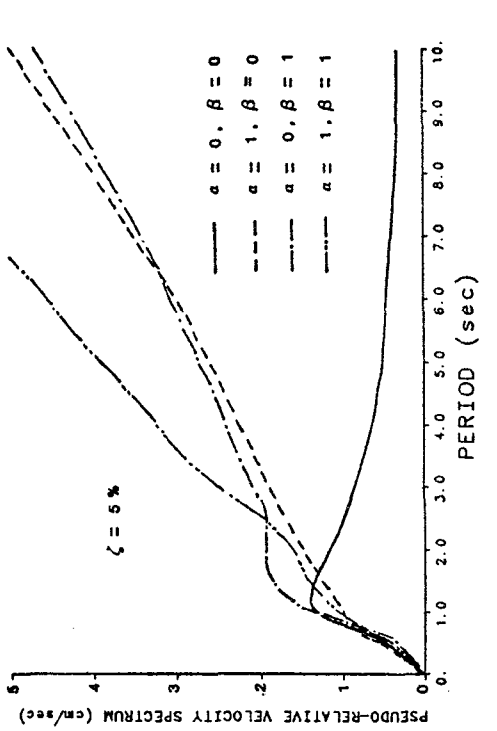

Fig. 3.- Effect of initial conditions on shock spectra for sinusoidal acceleration pulse.

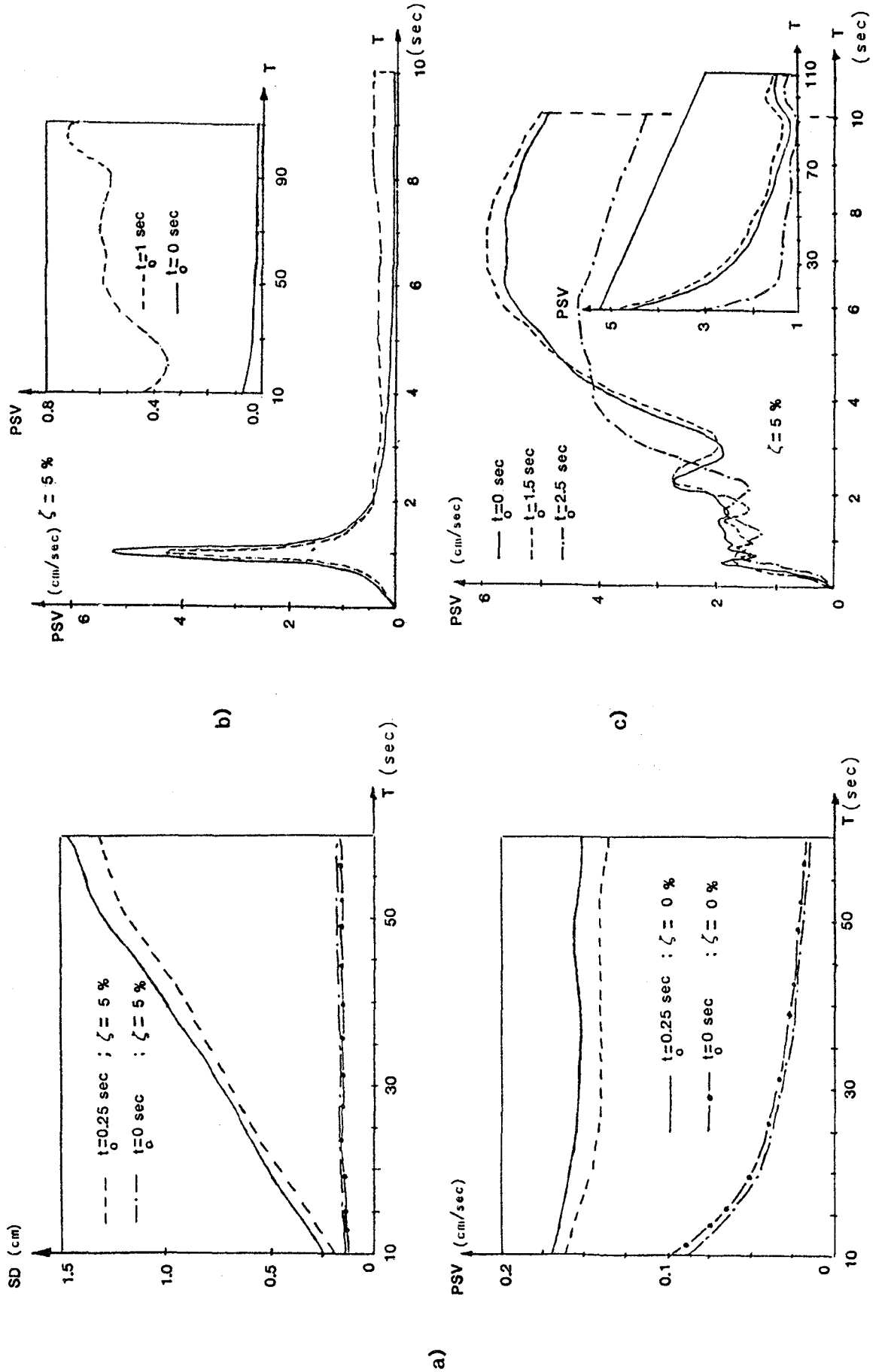

Fig. 4.- Effect of damping and duration of pretriggering stage on response spectra with non-zero initial conditions.

SHAKING TABLE EVALUATION OF STRONG MOTION DATA PROCESSING TECHNIQUES

J. Marcial BLONDET[1] Juan F. YEP[2] and James M. KELLY[3]

[1]Professor, Dept. of Civil Eng., Catholic University of Peru, Lima, Peru, and
Associate Research Engineer, Dept. of Civil Eng., University of California, Berkeley, USA
[2]Assistant Professor, Dept. of Civil Eng., Catholic University of Peru, Lima, Peru
[3]Professor, Dept. of Civil Eng., University of California, Berkeley, USA

SUMMARY

The majority of available earthquake ground motion data has been obtained by processing measurements made with analog accelerographs. Each step of the process to generate information such as ground velocity, displacement, and response spectra introduces errors which can significantly affect the reliability of the results obtained.

Seismic simulation tests were performed to obtain analog acceleration records corresponding to ground motions which were also very accurately measured by other means. The accelerograms were then processed to predict the displacement history and response spectra of the table shaking. The errors introduced at each stage of the process were evaluated and attempts were made to develop procedures to mitigate the effect of these errors in the estimation of ground motion characteristics.

INTRODUCTION

Earthquake resistant design can only be possible if the characteristics of seismic induced ground motions can be reliably determined. Most of the information available to date has been obtained by processing acceleration records registered in photographic film by analog accelerographs. The film must be enlarged and digitized, and the resulting digital record must suffer substantial numerical manipulation to generate information such as ground velocities, displacements and Fourier and response spectra. Each stage induces errors which contribute to pollute the signal with increasing amounts of noise, thus reducing the reliability of the processed data. It is therefore crucial that processing techniques be devised which adequately reduce the noise levels in the seismic signals.

Even though several procedures have been proposed and developed for the "standard" processing of earthquake records (Refs. 1 and 2), there is no definite agreement about which is the most reliable technique for seismic data processing. For instance, Fig. 1 shows displacement response spectra corresponding to the Lima 1970 earthquake (N08E component) computed using the USGS methodology (Ref. 3) and a recently proposed technique (Refs. 4 and 5). Both methods predict similar spectral displacements in the period range of 0 to 4 seconds, but dramatically disagree in the longer period range.

The objective of this investigation was to study the most important error sources in the processing of strong motion records and to determine the impact of each type of error in the quality of the processed information. An attempt was also made to identify procedures capable of producing reliable earthquake data.

SHAKING TABLE TESTING AND SIGNAL PROCESSING

A strong motion analog accelerograph (SMA-1) was mounted on the seismic simulator at the Catholic University of Peru. The imposed table motion is presented in time and frequency domains in Figs. 2 and 3, respectively: it is representative of ground motions recorded on firm soil sites in the Peruvian coast. Horizontal platform acceleration and displacement were also measured with high accuracy with electronic transducers. Peak values of acceleration and displacement were 0.32 g and 30.6 mm, respectively. The frequency bandwidth of the signals was about 0 to 15 Hz.

The acceleration record obtained from the SMA-1 was developed, enlarged, manually digitized, and processed for baseline correction, digital filtering and numerical integration to obtain estimates of the table velocity and displacement. Separate studies of the errors associated with each step of the process were performed. The difference between predicted and measured table displacement was used to evaluate the effectiveness of the techniques employed. Finally, the influence of the processing methods on the computation of response spectra was briefly investigated.

ERRORS DUE TO NUMERICAL PROCESS

The main operation to predict velocity and displacement from an acceleration time history is, of course, numerical integration. It is well known that integration of a signal amplifies its low frequency components and attenuates the high frequency components. Low frequency noise present in the signal is therefore amplified by the integration process, regardless of the numerical algorithm employed. It seems thus reasonable to select a numerical integration scheme with good accuracy in the low frequency band and to high-pass filter the data to remove low frequency noise. (It is hoped that the filtering removes mostly noise: a drastic filtering procedure could also delete important information from the signal with possible disastrous consequences...)

The measured table acceleration time history, assumed to be free of noise, was used to predict table velocity and displacement. All errors were thus due to the numerical algorithms selected.

A constant baseline correction was first made to the acceleration record to remove any offset in the measurements and establish the zero acceleration level. Each integration stage was preceded by high pass filtering of the signal, to remove low frequency noise, and followed by a linear correction to eliminate linear trends in the data.

Numerical integration was performed using the trapezoidal rule, linear baseline correction consisted on a least squares fit, and filtering was performed in the time domain (with an Ormsby filter modified by a Kaiser window). Three high pass bands 0.05-0.07 Hz (USGS), 0.10-0.15 Hz, and 0.25-0.30 Hz were used, since the frequency band dominated by low frequency noise was not known.

Peak and RMS values of the difference between predicted and measured displacements (error signal) are presented in Table 1. The best results were obtained using a 0.10-0.15 Hz high-pass filter. Fig. 4 shows that the errors due to the integration process are relatively small and can be effectively removed by high-pass filtering the signals.

DIGITIZATION ERRORS

The measured acceleration record was accurately plotted to the same size as accelerograms enlarged for digitizing. The resulting graph therefore represented an acceleration trace free of the distorsions produced by film processing and instrumental errors. The acceleration trace was manually digitized by a single operator at a rate of about 100 points per second. Fig 5. shows the measured and digitized acceleration traces for a 1 sec. portion of the signal. The error due to digitization consisted in this case (it depends on the operator skill and the equipment used) of a systematic time shift and a seemingly random but small variation of amplitude. The frequency content of the error signal was found to be quite large, with significant low frequency components.

The digitized acceleration signal was subjected to the procedure described above to predict table velocity and displacement. The error values associated with this process are presented in Table 1. They represent the combined errors of the digitization and numerical processing stages. The best estimation of the table displacement was again obtained with the 0.10-0.15 Hz high-pass filter. The table displacement time histories computed using filtered and unfiltered digitized acceleration records are shown in Fig. 6.

FILM PROCESSING ERRORS

The SMA-1 film was developed and magnified four times in transparent medium. The acceleration trace was then digitized in four segments. This time, digitizing errors were larger than in the case of the plotted measured table acceleration, due to the thicker trace of the accelerogram signal.

Table velocity and acceleration were predicted with the selected procedure, except that a 0.15-0.20 Hz high-pass filter was used instead of the 0.25-0.30 Hz filter, which removed too much information from the signals. Displacement time histories generated with each filter are presented in Fig. 7. It is clear that low frequency noise due to film processing was very important, but could be practically eliminated with a 0.15-0.20 Hz high-pass filter. Except for distortions at both ends of the displacement time history (due to convolution in the filtering process) the table displacement estimated with the 0.15-0.20 high-pass filter was reasonably close to the measured table displacement.

RESPONSE SPECTRA

Acceleration, velocity and displacement response spectra were computed from the digitized accelerogram filtered at different high-pass frequency bands. Results obtained with the 0.05-0.07 "standard" band can be compared in Fig. 8 with those generated with the signal filtered at 0.10-0.15 Hz (which produced the best estimate of table displacement). Spectra obtained from measured acceleration, also shown, were assumed to be correct. All spectra were computed for 5% damping.

The spectra computed with the 0.05-0.07 filter showed relatively small errors in the low period range of 0-3 sec. For longer periods, acceleration spectral values were reasonable, the velocity spectrum showed significant errors and the displacement spectral values were unacceptably large. The spectra computed with the 0.15-0.20 filter gave adequate results in the whole period range considered.

CONCLUSIONS

- The numerical algorithms selected for integration, baseline correction and digital filtering introduced very small error in the process. Errors due to film processing and manual digitization of the accelerogram were responsible for most of the noise in the signal.
- Most of the effects of the low frequency errors within the signals can be removed by filtering with an appropriate high pass frequency band. Adequate selection of the filtering band is therefore a crucial step in the process. Unfortunately, not enough data is currently available to determine the best filtering parameters for "real" earthquakes.
- Low frequency errors in the acceleration record introduced significant distortion in the response spectra for periods longer than approximately 3 seconds. Most "reasonable" signal processing methods will thus produce adequate results in the low period range, but extreme care must be exercised when using seismic information in the long period range.

ACKNOWLEDGMENTS

The research performed at the Catholic University of Peru was funded by the National Council for Science and Technology of Peru (CONCYTEC). Additional funding was provided by the National Science Foundation (NSF, USA) for further studies at the University of California, Berkeley. The support of these institutions is gratefully acknowledged.

REFERENCES

1. Trifunac, M. D. and V. Lee, "Routine Computer Processing of Strong Motion accelerograms", Earthquake Engineering Research Laboratory, California Institute of Technology, California, October 1973.
2. Sunder, S., "On the Standard Processing of Strong-Motion Earthquake Signals", Research Report R80-38, Department of Civil Engineering, Massachussetts Institute of Technology, Massachussetts, September 1980.
3. Brady, A. G. and V. Perez, "Strong Motion Earthquake Accelerograms - Digitization and Analysis - Records from Lima, Peru: 1951 to 1974", Open File Report No. 77-587, Seismic Engineering Data Report, U.S. geological Survey, Menlo Park, California, April 1977.
4. Blondet, J. M., "Studies on Evaluation of Shaking Table Response Analysis Procedures", Earthquake Engineering Research Center Report No. 81-18, Berkeley, California, November 1981.
5. Quiun, D., "Implementation of a System for the Automatic Process of Seismic Signals" (in Spanish), Civil Engineering Thesis, Catholic University of Peru, Faculty of Sciences and Engineering, Lima, Peru, January 1985.

ERROR SOURCE	NUMERICAL FILTER	ERROR (mm) Peak Value	RMS
Numerical Process	No filter	11.49	7.02
	0.05-0.07	6.61	2.75
	0.10-0.15	2.59	1.53
	0.25-0.30	11.18	5.52
Digitization	No filter	39.81	24.30
	0.05-0.07	24.56	12.25
	0.10-0.15	13.70	5.24
	0.25-0.30	11.38	5.48
Film Processing	No filter	688.74	321.37
	0.05-0.07	147.74	69.40
	0.10-0.15	22.52	8.56
	0.15-0.20	17.00	4.97

Table 1: Errors in acceleration record processing
Peak measured displacement: 30.6 mm

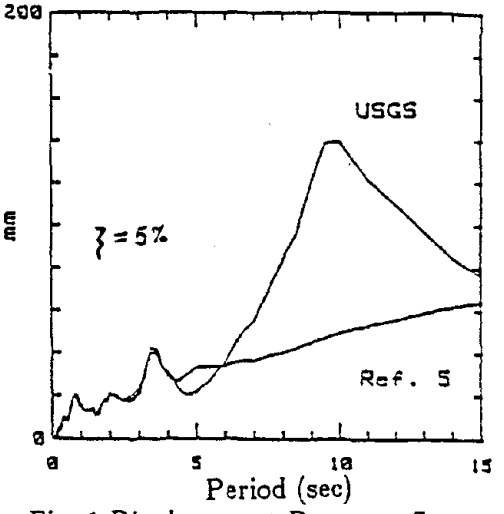

Fig. 1 Displacement Response Spectrum
Lima 05/31/70 T comp.

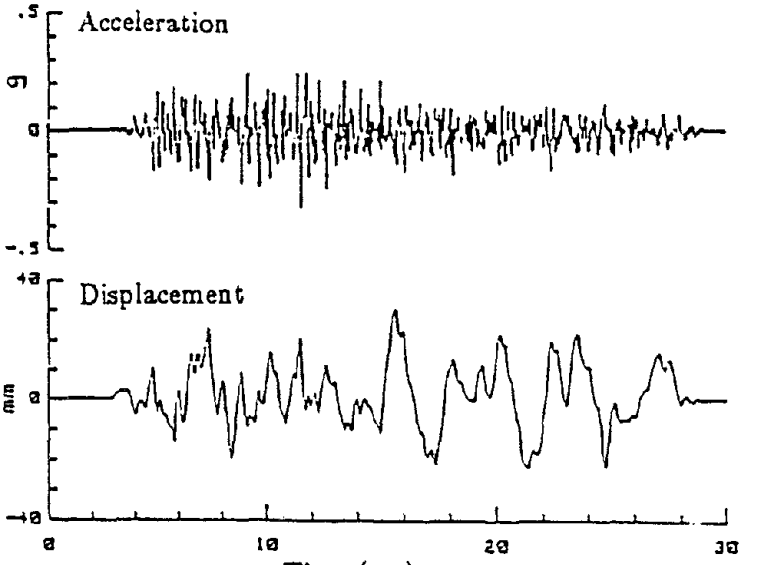

Fig. 2 Shaking Table Motion

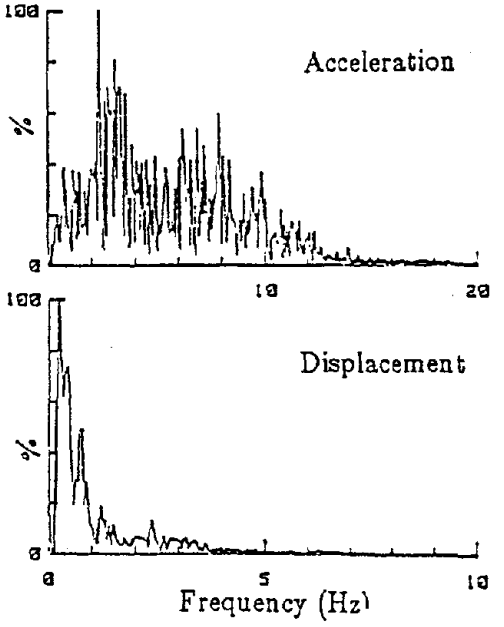

Fig. 3 Fourier Amplitude Spectra

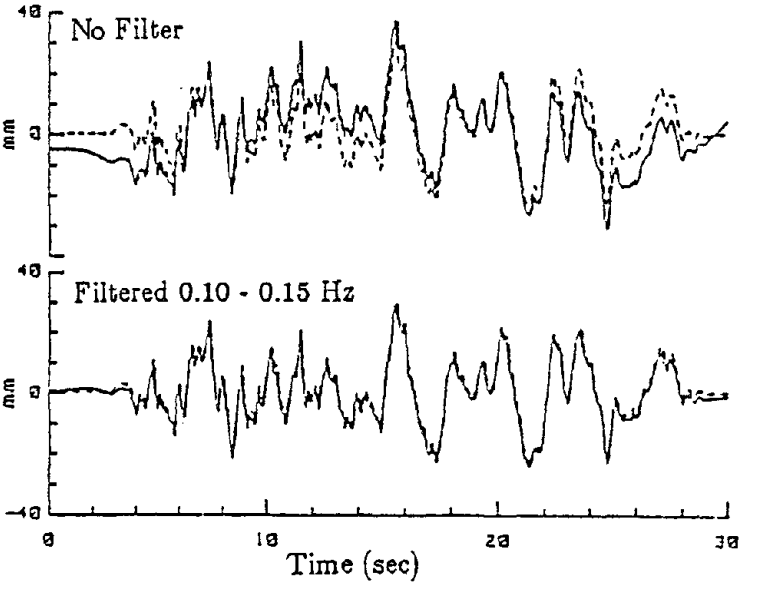

Fig. 4 Displacements Computed from Measured Accel.
(dashed: measured)

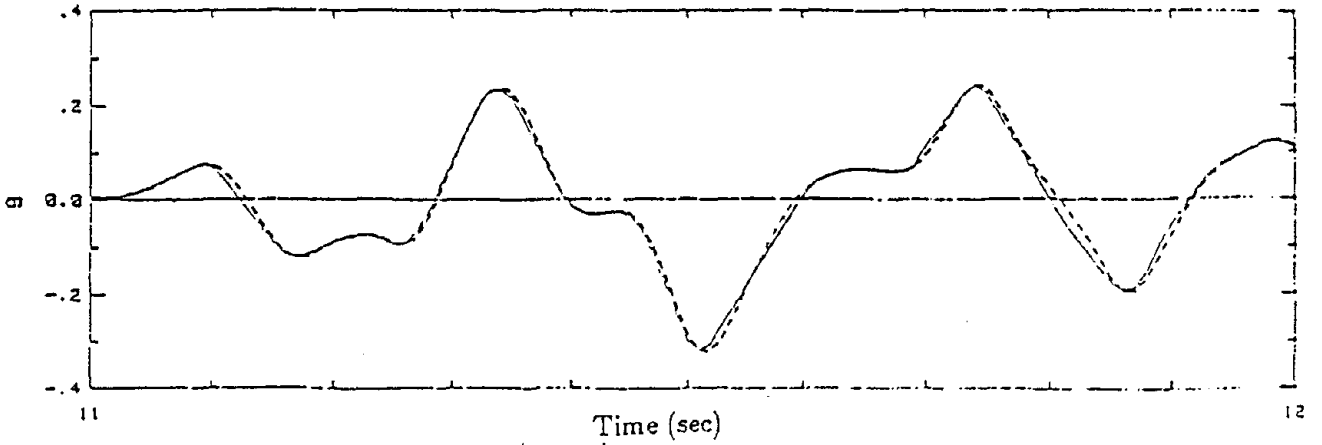

Fig. 5 Acceleration Digitization Error
(dashed: measured)

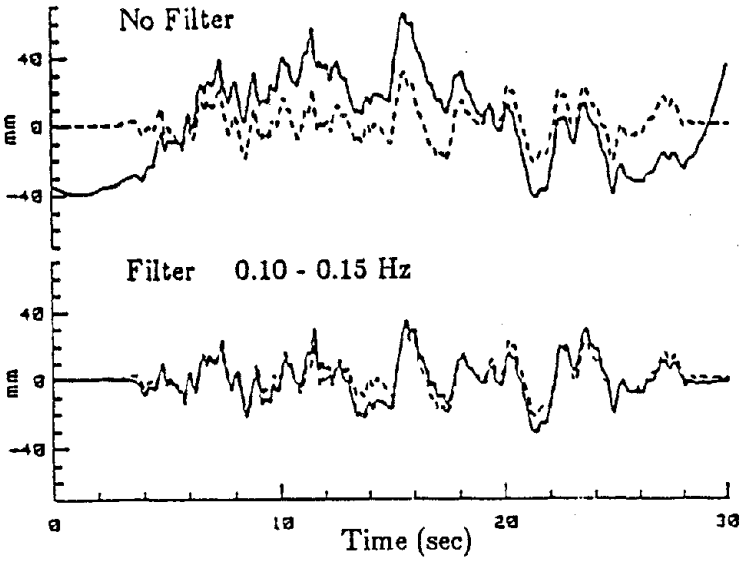

Fig. 6 Displacements Computed from Acceleration Plot (dashed: measured)

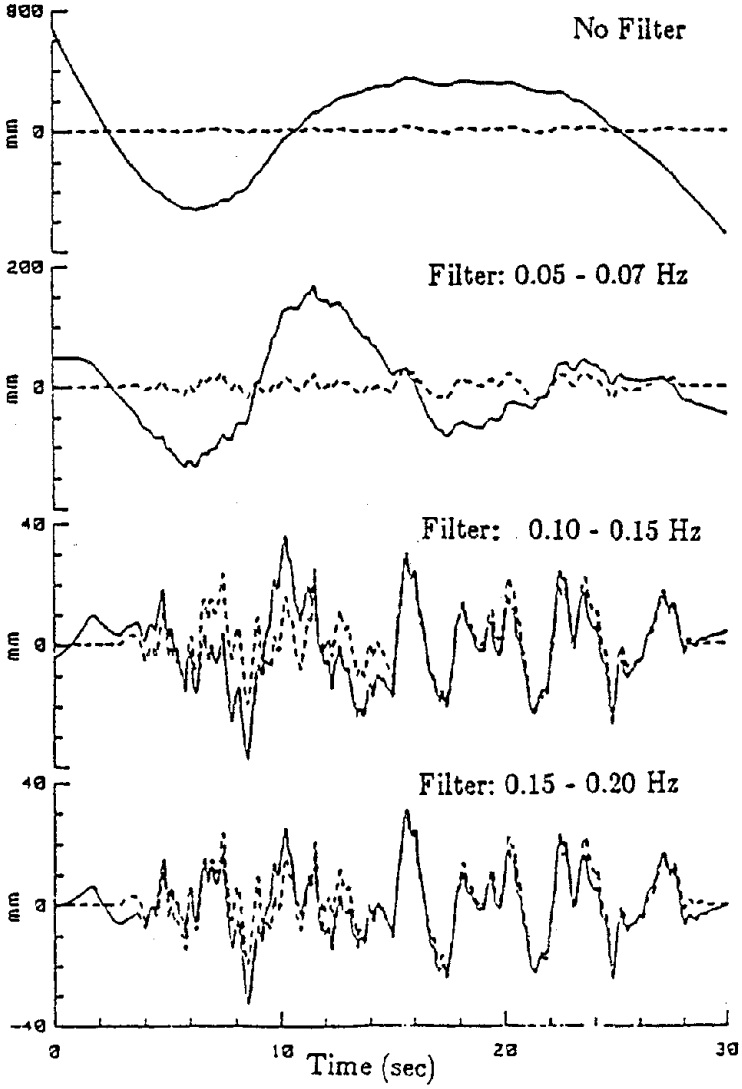

Fig. 7 Displacements Computed from Film Acceleration Record (dashed: measured)

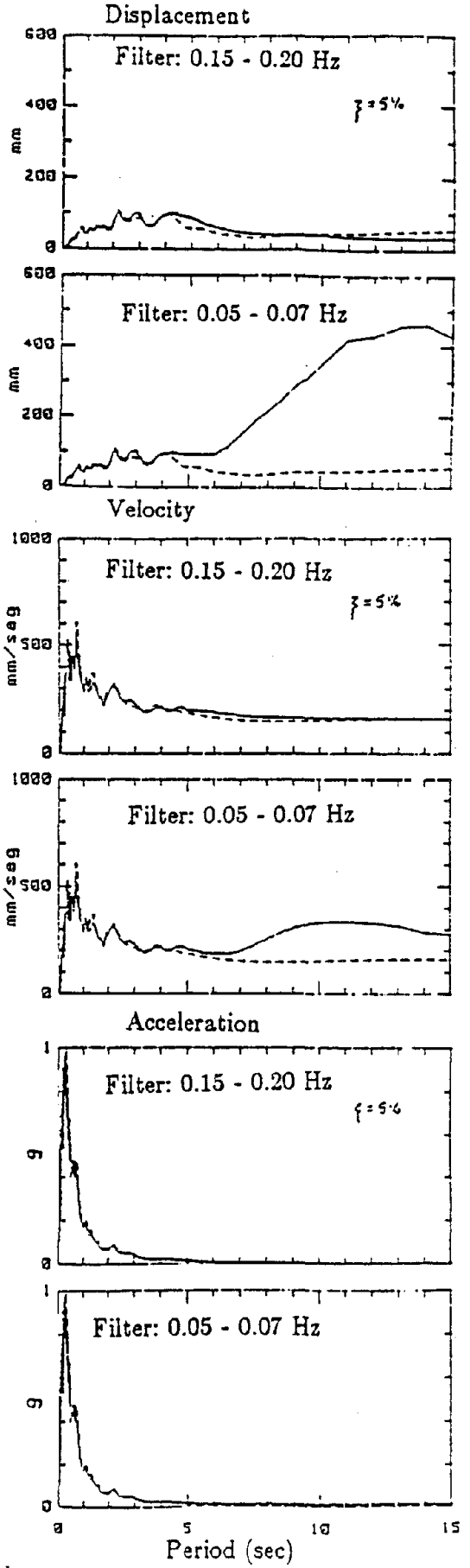

Fig. 8 Response Spectra (dashed: from measured acceleration)

PREDICTION OF THE INELASTIC RESPONSE OF TORSIONALLY COUPLED SYSTEMS SUBJECTED TO EARTHQUAKE EXCITATION

Michel BRUNEAU[1] and Stephen A. MAHIN[2]

[1] Dr., Project Engineer, Morrison Hershfield Limited, North York, Ontario., Canada

[2] Dr., Professor of Civil Engineering, University of California, Berkeley, California, USA.

SUMMARY

A methodology is presented to allow designers to predict the ductility demand of elements in simple torsionally coupled systems by using elastic dynamic analyses and other readily available design tools. The method is validated by numerous non-linear inelastic analyses, and is not affected by variations in the parameters traditionally thought to influence the response of torsionally coupled systems.

INTRODUCTION

Although torsional movements are thought to be responsible for the failure of many structures during major earthquakes, a simple method to estimate the inelastic response of torsionally coupled systems does not yet exist. There is still no consensus on how inelastic response of initially eccentric systems is affected by various parameters. One of the major problems in the study of torsionally coupled systems seems to be the difficulty in finding a reliable comparative torsion-free "benchmark" system whose response would not be sensitive to any of the parameters thought to influence the inelastic torsional response, as well as on the difficulty in setting an unbiased liaison between the true system and its "benchmark". This knowledge is most needed as torsional coupling is practically unavoidable in both new and retrofitted structures: eccentricities can be either initially present, or will develop following non-simultaneous yielding of elements in initially symmetric structures. Although both cases have been studied by the authors, only the results for initially eccentric structures will be presented herein.

EQUATION OF MOTION AND ELEMENT MODEL

For this study, a monosymmetric single-story system with rigid floor-diaphragm is considered (Fig. 1). The equation of motions for this two-degrees-of-freedom system were derived around the center of mass as follow:

$$\begin{pmatrix} m & 0 \\ 0 & mr^2 \end{pmatrix}\begin{pmatrix} \ddot{v}_X \\ \ddot{v}_\theta \end{pmatrix}+\begin{pmatrix} K_X & -K_X e \\ -K_X e & K_\theta \end{pmatrix}\begin{pmatrix} v_X \\ v_\theta \end{pmatrix}=-\begin{pmatrix} m\ddot{v}_{gX} \\ 0 \end{pmatrix} \qquad \text{with} \quad \Omega=\omega_\theta/\omega_X=T_X/T_\theta$$

$$\begin{pmatrix} \ddot{v}_X \\ r\ddot{v}_\theta \end{pmatrix}+\omega_X^2\begin{pmatrix} 1 & -e/r \\ -e/r & \Omega^2 \end{pmatrix}\begin{pmatrix} v_X \\ rv_\theta \end{pmatrix}=\begin{pmatrix} -\ddot{v}_g \\ 0 \end{pmatrix} \qquad \omega_X^2=K_X/m \qquad \omega_\theta^2=K_\theta/mr^2$$

where K_X and K_θ are the system's stiffnesses for the two degrees-of-freedom of interest (translational along X and torsional around θ), ω_X and ω_θ are the

translational and torsional uncoupled frequencies, and Ω is the ratio of those uncoupled frequencies (which varies depending on the reference point around which the equations of motions are derived). The reader not familiar with those equations should refer to Ref. 1 for detailed explanations.

For this study, a bi-linear inelastic element model with strain-hardening was chosen, but the methodology presented hereafter has been found to work equally well with other types of non-linear element models. Strain-hardening was set to 0.5% (E_{SH} = 0.005 E), making the element model practically elasto-perfectly plastic. Elements of the torsionally coupled system were modeled to share the same yield displacements (Fig. 1). The damping was chosen to be of the Rayleigh type, arbitrarily set at 2% of the critical damping for each of the true frequencies of any given system analyzed.

NON-LINEAR ANALYSES OF TORSIONALLY COUPLED SYSTEMS

Parametric Study The intent of this parametric study is to establish the relationship between equivalent single-degree-of-freedom (SDOF) systems' ductility and torsionally coupled systems' element ductilities, more specifically to investigate the effect of various parameters on torsionally coupled elements response when equivalent SDOF systems are calibrated to target ductilities. The study was performed for ten values of uncoupled period T_X, six values of the ratio of uncoupled frequencies Ω, two target ductility levels μ, and two normalized eccentricities (e/r). The particular parametric values selected are shown on Fig. 2 and 3. The liaison between the true systems and the benchmark systems was accomplished as described below:

1) Equivalent SDOF systems were defined to have a period equal to the first period of their corresponding torsionally coupled system when $\Omega \geq 1.0$, and equal to the second period when $\Omega < 1.0$. This decision was dictated by observations on the nature and variations of the true periods, components of the corresponding mode shapes and edge displacement modal participation factors, as a function of Ω, as well as by other considerations. Furthermore, these SDOF systems were designed such that they shared the same inelastic element model and same yield displacement δ_y as the elements of the torsionally coupled systems.

2) Using the program NONSPEC (Ref. 2), the proper strength factors were calculated for each SDOF system in order to attain target ductilities of 4 and 8. For simplicity, the earthquake levels were scaled to produce the necessary strength factors. For this study, ductility demand is defined as the maximum displacement, in absolute value, divided by the yield displacement. These steps were to insure that the SDOF systems were insensitive to variations in ground motion intensity.

3) The program for non-linear structural analysis ANSR-1 (Ref. 3) was used to verify (and improve if needed) the accuracy of the target ductility demands predicted by NONSPEC. All final ductilities for the SDOF systems analyzed were within 10% or less of their targeted ductilities.

4) The same equivalent SDOF systems were then re-analyzed elastically, using the respective earthquake excitation levels that produced the desired target ductilities in item 2 above.

5) The torsionally coupled systems were first analyzed elastically for an arbitrary level of excitation. Then, for each individual parametric case, a new earthquake scaling to be applied to the torsionally coupled systems was calculated such that the torsionally coupled system's weak (more flexible) element maximum elastic response would equal the one of the equivalent SDOF system.

6) Using the new earthquake scalings found in the previous step, the inelastic response of the torsionally coupled systems were calculated, and the ductility demands were calculated for each element.

7) The ductility factors calculated for each individual torsionally coupled case analyzed above were then divided by the ductility factors obtained from their respective equivalent SDOF system, to obtain a ratio of the ductilities (indicated "Ductility Ratios" on Fig. 2 and 3) that is independent of the selected target ductilities.

8) To provide results mostly independent of the particular characteristics of single earthquakes, the above 7 procedures were repeated for 5 different earthquake records (El-Centro 1940, Olympia 1949, Parkfield 1966, Paicoma Dam 1971, and Taft 1952), and the mean (and mean-plus-one-standard-deviation, although not presented here) ductility ratios were calculated.

Observations of the Results By observation of the ductility ratios results (Fig. 2), one may notice that for the Ω=1.0 case, all weak element ductility ratios are equal to 1.0 (i.e. weak element ductility demands are equal to the equivalent SDOF system ductility demands). The analytical demonstration that equal displacements must be observed for the case Ω=1.0, if the above procedure is followed, is presented in Reference 1.

It is apparent from Fig. 2 that the element ductility ratios obtained by the method outlined above are independent of the uncoupled periods (T_X), normalized eccentricities (e/r), target ductility μ, and ratios of uncoupled frequencies (Ω). This means that the method is mainly stable in providing a reliable estimate of the torsionally coupled system's element ductilities based on the concept of an equivalent SDOF system.

The ductility ratios, as measured by the mean of response for five earthquakes, remain mainly close to unity, only exceeding a value of 2.0 for the weak element when T_X = 0.4, Ω=0.8 and (e/r)=0.3. This is a direct consequence of the unique extreme ductility ratio that occurred for the Pacoima Dam earthquake for this particular combination of parameters. Should the Pacoima Dam contribution at this particular point be removed, the mean for the weak element response would drop to 1.39 for target ductility of 4, and 1.05 for target ductility of 8. Other than this particular point of unusually high sensitivity, the mean weak element response exceeds 1.5 only in five occasions (the maximum value being 1.7). Considering the nature of ductility measurements in earthquake engineering, and the accuracy desired in ductility predictions, it can be said that, element ductility ratios of 1.25 or less are not considered significant, ductility ratios from 1.25 to 1.5 are considered of moderate importance, and ratios above 1.5 are judged to be of major importance. Following this arbitrary convention, the predicted increase in ductility from this method are shown to be mostly of moderate importance, which is very satisfying. A conservative strategy would be to plan for a weak element ductility ratio of 1.5, and a strong element ductility ratio of 1.0 (although when Ω=1, a weak element ductility of 1 can be used, of course).

PREDICTION OF TORSIONAL RESPONSE

Obviously, the concept of an equivalent SDOF system can be potentially very useful in design. Although there apparently is no easy way to obtain an EXACT match of the weak element displacement with a meaningful equivalent SDOF system for all values of Ω, it has been shown in the preceding section that the proposed method can provide a relatively accurate prediction of the initially eccentric system's element ductility demand. It will now be illustrated how the equivalent SDOF system procedure can be used, in a design approach, to predict the inelastic response of torsionally coupled system

A design engineer using dynamic elastic analysis tools (like elastic response spectrum method or time history analysis) may easily calculate the elastically predicted response for the weak element. It is supposed, for simplicity, that the calculation is performed for a single ground motion; let this calculated elastic response be called R_W.

The elastic response of the equivalent SDOF system can be read from an SDOF elastic response spectrum (readily available for most earthquake records); let this SDOF response be called R_{SDOF}. In order to match the elastic response of the weak element and of the equivalent SDOF system, the earthquake applied to the equivalent SDOF system should be scaled by R_W/R_{SDOF}.

It is now possible to obtain a prediction of the ductility demand on the equivalent SDOF system subjected to this corrected earthquake level by consulting inelastic response spectra (Ref. 2). These spectra are relatively straight forward to calculate using standard numerical analysis procedures, and need only be constructed once for each combination of earthquake, damping and element model. Single earthquake or multiple earthquake spectra can also be constructed. It is understood that the element model for the SDOF must match the one for the elements of the torsionally coupled system.

It is then straight forward to calculate the strength factor, defined as:

$$\eta = R_Y / m\, a_{MAX}$$

where a_{MAX} is the maximum earthquake ground acceleration, and read the ductility demand for this equivalent SDOF system off the inelastic response spectrum. If Ω=1, this equivalent SDOF system's ductility demand can be assumed equal to both the weak and strong element ductilities of the torsionally coupled system; otherwise, a conservative weak element ductility should be estimated as being possibly 50% larger.

Example An initially eccentric two-element structure having the response parameters T_X=0.2 sec., Ω=2 and e/r=0.1 is analyzed. For this system, the two true periods are T_1=0.20 sec. and T_2=0.10 sec. The element model is bi-linear with 0.5% strain hardening, and damping is 2% of critical. The yield displacement of this system is δy=0.12 inch. The 1940 El Centro earthquake (N-S component) was scaled to a peak acceleration of 0.46g and an elastic dynamic time-history analysis was performed; the resulting edge displacement for the weak element was 0.50 inches.

Then using an elastic response spectrum for this earthquake component (available from the Caltech Strong Motion Database, Volume III) which had an actual recorded peak acceleration of 0.348g, the pseudo-displacement for the equivalent SDOF system (with period T_{SDOF}=0.20 sec.) was found to be Sd=0.36 inch. In order to match the weak element elastic displacement with the equivalent SDOF system, the earthquake used in the equivalent SDOF concept must be scaled as:

$$\frac{\text{Weak element displacement}}{\text{Sd from equivalent SDOF}} = \frac{0.50}{0.36} = 1.39$$

Therefore, the peak acceleration for this equivalent SDOF increases by 1.39 and becomes 0.483g (187 in/s^2), and using the same yield displacement of 0.12 inch for the equivalent SDOF system, the strength level can be estimated by:

$$\eta = \frac{Ry}{m\, a_{MAX}} = \frac{K\ \delta y}{m\, a_{MAX}} = \omega_{SDOF}{}^2\ \frac{\delta y}{a_{MAX}} = 987\ \frac{(0.12)}{187} = 0.64$$

Finally, reading from the constant ductility response spectra of Fig. 4 (which has been derived for two ductility levels, 2% damping and bi-linear model with 0.5% strain hardening), one can see that for a period of 0.20 sec. and a strength ratio of 0.64, the ductility demand on the equivalent SDOF system is

approximately 4. Since Ω is not equal to unity, it is appropriate to increase by 50% the predicted weak element value, and use directly the obtained SDOF ductility as an estimate of the strong element value. The estimated weak element ductility is then 6, and the estimated strong element ductility remains 4. This is adequate, as the calculated strong and weak element ductilities for the initially eccentric system are respectively 5.2 and 3.0 (Fig. 3). In order to illustrate the methodology, only one earthquake excitation has been used. In a true design procedure, it is essential that many earthquake records be included.

CONCLUSIONS

Many initially eccentric systems were analyzed and compared with equivalent SDOF systems in order to investigate the effect of various parameters on their element responses. A methodology has been proposed to perform a meaningful liaison between the equivalent SDOF system and corresponding initially eccentric system, and, for bi-linear inelastic element model, was found to provide a reliable way to predict the inelastic response of structural elements in a two-element system. It was found that the ratio of ductilities obtained using the proposed method were unaffected by changes in the level of excitation (target ductility level), ratio of uncoupled frequencies Ω, uncoupled period T_X, and normalized eccentricities (e/r).

In the case of Ω=1.0, the equivalent SDOF response will perfectly match the weak element response of the torsionally coupled system, provided the inelastic element models are similar, that is, yield displacements, damping and strain hardening values are similar in the case of bi-linear models (the formal analytical proof of this could not be presented because of space limitations).

For other values of Ω, it was shown that the ductility ratios obtained by the proposed equivalent SDOF method, and following the methodology explained in the previous section, are often close to unity in the case of mean response from five earthquake excitations, with a conservative design value to be taken as 1.5. It is understood that response under a single earthquake excitation may strongly differ from the one predicted using the mean response from five earthquake, the same way this can also be expected in the case of symmetric structures.

An easy design procedure, relying mainly on elastic analysis and readily available design tools, has been proposed, and can be used to obtain good estimates of element ductilities for simple torsionally coupled systems.

REFERENCES

1. Bruneau, M., Mahin, S.A., "Inelastic Seismic Response of Structures with Mass and/or Stiffness Eccentricities in Plan", EERC Report No. 87-12, University of California, Berkeley, September 1987.

2. Mahin, S.A., Lin, J., "Construction of Inelastic Response Spectra for Single-Degree-of-Freedom Systems", EERC Report No. 83-17, University of California, Berkeley, June 1983.

3. Mondkar, D.P., Powell, G.H., "ANSR-1 - General Purpose program for analysis of nonlinear structural response:, EERC Report No. 75-37, University of California, Berkeley, December 1975.

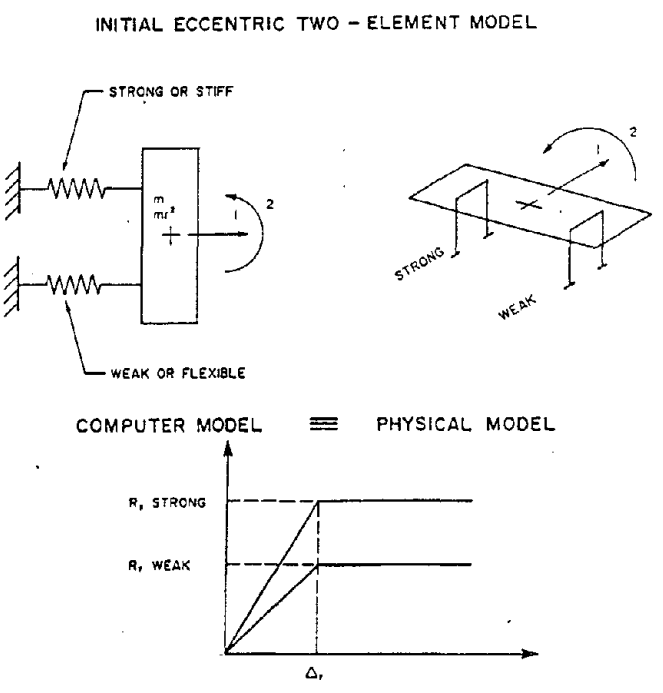

Figure 1 Element Model Used in this Study

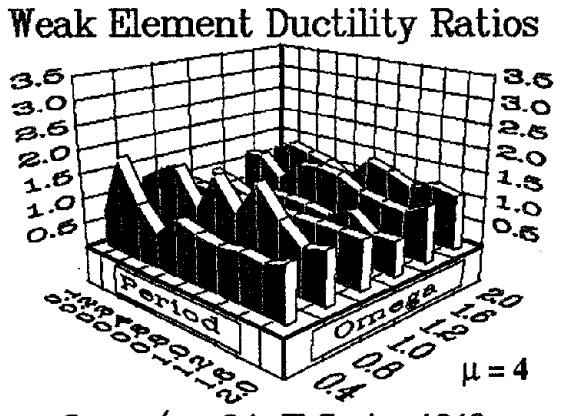

Figure 3 Weak Element Ductility Ratios for Target Ductility of 4 and El Centro Earthquake Record

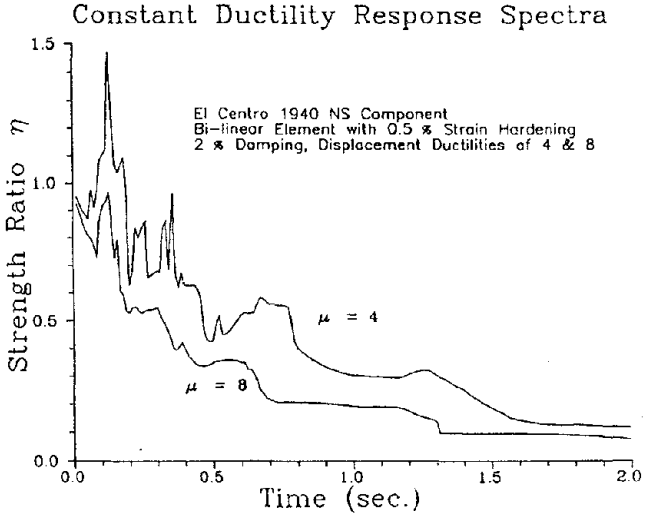

Figure 4

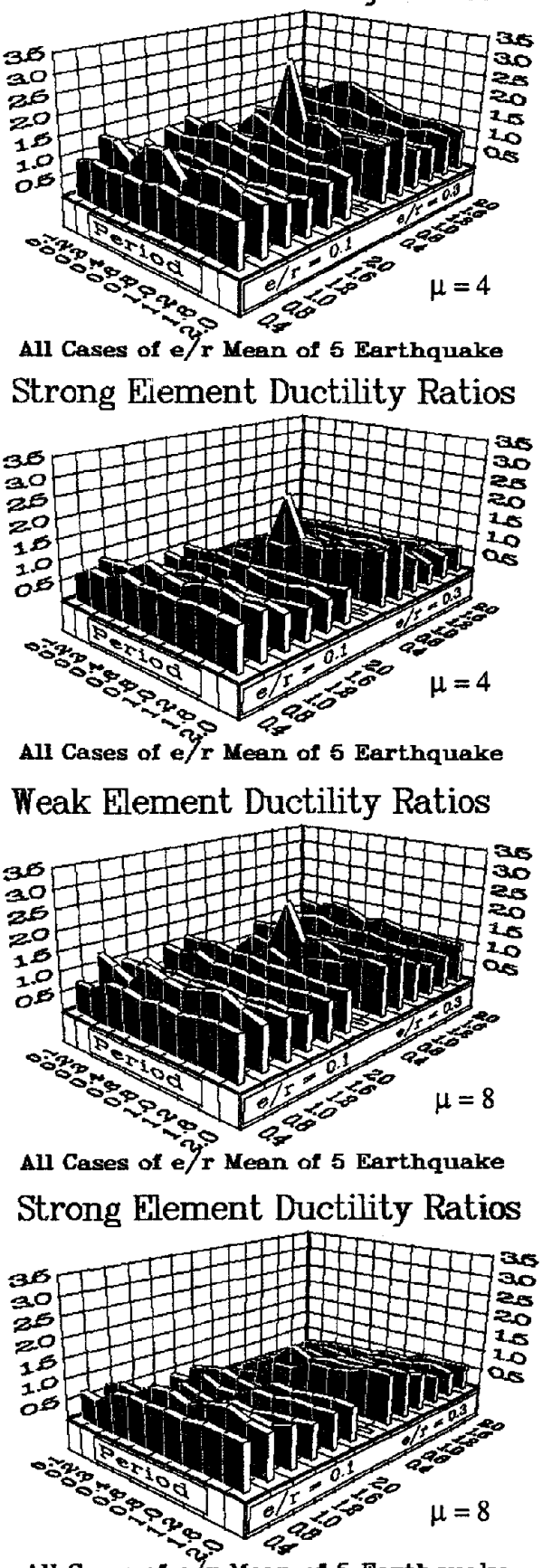

Figure 2 Target Ductility of 4 (Top Two) and 8 (Bottom Two)

EARTHQUAKE SIMULATOR TESTING OF CYLINDRICAL WATER TANKS IN BASE ISOLATED STRUCTURES

Michel S. Chalhoub[1] and James M. Kelly[2]

1 Research Engineer, University of California, Berkeley
2 Professor of Civil Engineering, University of California, Berkeley

SUMMARY

This paper presents the experimental results obtained from the study of two similar cylindrical water tanks, one directly fixed to the earthquake simulator, the other mounted in a scaled model of a nine story steel structure. The model was seismically isolated on eight multilayered elastomeric bearings. Due to the reduction in the ground accelerations, the dynamic pressure was reduced for the tank in the isolated structure. Free surface water elevation was slightly increased due to the lower frequency that characterizes the motion of base isolated structures. This problem can be overcome by appropriate selection of the isolation system or by the addition of dampers at the locations of high particle velocities in the water. For the tank in the isolated structure, the accelerations and displacements at the tank rim were lower than for the tank directly fixed to the shake table. A theoretical solution developed from linear wave theory correlates very well with the experimental results.

INTRODUCTION

Extensive work has been done on the response of internal equipment in structures subjected to ground motion [1], [2]. An important advantage of base isolation is the protection of internal equipment in buildings against high accelerations transmitted from the ground and amplified by the structure. Experimental studies have been made on oscillators simulating the contents of a building, where each oscillator was tuned to a certain frequency [3], [4], and in circumstances where the buildings were both unisolated and isolated.

Fluid containers are an important category of internal equipment for certain buildings and power plants. In the present research, the response of a cylindrical water tank fixed to the shake table is compared to that of a similar one installed in a base isolated nine story steel structure.

Quantities of interest in the response are the dynamic pressure at the tank walls, displacements and accelerations in the shell, and the surface deformation at the free surface of the water. These quantities were measured at different locations. A detailed description of the experimental set-up is presented in reference 5. From a structural view point, it is of primary concern to study the stresses and deformations in the shell. In the present treatment however we were mainly concerned with the loading exerted by the fluid on the container in terms of the dynamic pressure at the wall, and how it is affected by base isolation.

In parallel with this experimental work, a theoretical solution was carried out and expressions for the dynamic pressure and the free surface elevation proposed and compared to experimental results. This solution based on linearized wave theory is presented in detail in [6]. It is commonly accepted that the pressure at the container wall consists of two components: an impulsive pressure and a convective pressure. The first component is due to the container wall accelerating against the fluid, the second component is due to the change in the fluid free surface elevation. The convective pressure is mainly attributed to the sloshing resulting from the formation of forced waves in the tank. Sloshing in tanks is a phenomenon of relatively low frequency (the first mode is predominant) and for this reason base isolation might increase it, causing a slightly higher convective pressure component. However, it was shown that base isolation has more effect on the impulsive component and thus leads to a much lower resultant dynamic pressure.

This study gave some insight on the advantage of mounting large tanks in seismic regions directly on base isolators, in order to reduce the hydrodynamic loading on the shell.

EXPERIMENTAL SET-UP

Structural Model. The structural model used is a one fourth scale nine-story K-braced steel frame described in detail in [6]. The structure was mounted on an isolation system consisting of eight elastomeric bearings provided by the Malaysian Rubber Producers Research Association. Each bearing had a horizontal stiffness of about 1.1

k/in. at 60% shear strain and a vertical stiffness of about 420 k/in. The extremely high vertical stiffness provides a conventional support condition in the vertical direction and the high horizontal flexibility causes the entire structure to move like a rigid body with a very low frequency. This arrangement drastically reduces the ground accelerations transmitted to the structure. Since the total weight of the model was around 91 kips, the natural frequency of the base isolated structure was 0.97 Hz, corresponding to about 0.5 Hz in the prototype.

Tanks. Two similar tanks were used for the purpose of comparison. One of them was directly fixed to the shake table, the other on the lower level of the isolated structure. They were cylindrical steel tanks, 1/25-inch thick, 2 feet in height and 4 feet in diameter. Both tanks were fixed at their bottom by six 2×2×1/4 inch angles; two of the angles were along the diameter of excitation and the four others were installed by pairs at 45° from that diameter. The tank on the structure was mounted on a 1 inch thick steel plate welded to the bottom flanges of the two base beam girders.

For each tank, eight Piezo-electric pressure transducers were used to measure the dynamic water pressure. Six of them were installed along two vertical lines in the plane of excitation at the bottom, at mid-height and near the free surface of the water, while two others were installed at mid-height in a plane perpendicular to the plane of excitation. Two accelerometers were installed at the shell rim, at the north and west sides respectively, to measure horizontal accelerations. Two DCDT's were installed at the north and south sides of the shell rim, respectively, to measure rim displacements relative to the tank base.

The free surface water elevation was measured at the shell wall at the north and south sides, using water level gages. The gages consisted of two parallel conductor wires connected to an electric bridge. The resistance in the circuit varied with the water elevation and thus was converted from mΩ to inches.

EXPERIMENTAL RESULTS

Seven ground motion records were applied to the shake table at various spans ranging from 25 to 100. Five records $\sqrt{4}$ time scaled and applied at a horizontal span of 50 were compared to the theoretical solution. The main concern in this section is the response of the fluid. Due to the size of the tank models, shell deformations were not studied in detail and are not presented here.

In general, the tanks on the model showed more sloshing and less pressure. The input acceleration was more apparent in the response of tank #1 than it was in the response of tank #2. This is due to the filtering provided by the isolation system. The calculated frequencies of free vibrations of the fluid surface were expressed as $\lambda_i = (g\, n_i \tanh n_i h)^{1/2}$, where g is the gravitational constant, h is the fluid height in the tank, and n_i is the i^{th} root of the equation $J_1'(n R_0) = 0$. These frequencies were compared to the experimental ones by using the Fourier transform of the measured water elevation time histories for both tanks under different ground motions.

El Centro. For the El Centro record at 50 horizontal span, the peak table acceleration (PTA) was 0.114 g. The reduction in the accelerations transmitted to the structure's base was of the order of 2.2. The peak base acceleration was around 0.05 g. The peak table displacement was of 0.25 in. while the peak base absolute displacement was 0.37 in. The sloshing was slightly higher in the tank on the structure, and the ratio of the positive peak values in the water surface deformation was about 1.2.

San Francisco. For the San Francisco record at 50 horizontal span, the PTA was 0.331 g. This record is of relatively high frequency and high acceleration. For this reason it did not excite the sloshing for the tank on the table while it yielded higher sloshing for the tank in the structure since the whole system was responding at low frequency. The ratio of the peak sloshing values was around 1.47 for tank #2 to tank #1. The base acceleration was drastically reduced in this case, and the reduction factor was 3.4.

These test results demonstrated a drastic reduction in the dynamic pressure for the tank in the structure. The ratio of the peak values for tank #1 to tank #2 was 4.3. This may be expected since the theoretical solution predicts a high dependence of the dynamic pressure on the tank support acceleration.

Pacoima Dam. For Pacoima Dam, the reduction in the acceleration at the structure base was not noticeable because this signal at a span of 50 caused a very low PTA of 0.076 g, and the isolation system was not quite activated. The lowering of the input frequency caused slightly higher sloshing while the reduction in the pressure was still present, and the ratio of peak pressure in tank #1 to peak pressure in tank #2 was 1.75.

Parkfield. For Parkfield record at 50 horizontal span, conclusions similar to those for Pacoima Dam can be made. The only difference is that the table displacement here consists of a large sway in one direction followed by small cycles and this sway corresponds to a spike in the acceleration. This behavior is changed by base isolation. The displacement and the acceleration are more spread out, equally spaced cycles at lower frequency. This is reflected in the pressure time history but to a lesser extent. The few spikes in the dynamic pressure for tank #1 are reduced and distributed for tank #2. The ratio of the peak water elevation in tank #1 to tank #2 was 0.78 while the ratio peak pressure at z = -16 in. in tank #1 to tank #2 was 1.2.

Taft. For Taft there were no major differences in the response, except a slight reduction in the peak dynamic pressure for the tank on the structure. The reduction factor was around 1.4. The peak values of tank support motions and the fluid response are summarized in Table 1.

COMPARISON WITH THEORETICAL SOLUTION

The dynamic pressure at the tank wall in the plane of excitation and the free fluid surface displacement were expressed as [5]:

$$\frac{P_d}{\rho R_O} = \ddot{v}_g(t)\Big(1 + \sum_{i=1}^{i=\infty} C_i\Big) - \sum_{i=1}^{i=\infty} C_i \lambda_i(t) \tag{1}$$

and

$$\frac{\eta}{R_O/g} = \ddot{v}_g(t)\Big(1 + \sum_{i=1}^{i=\infty} C_i'\Big) - \sum_{i=1}^{i=\infty} C_i' \lambda_i I_i(t) \tag{2}$$

respectively, where

$$C_i = = \int_0^t \sin \lambda_i(t-\tau)\, \ddot{v}_g(\tau)\, d\tau \tag{3}$$

R_0 is the radius of the tank, h is the height of the fluid in the tank, z is the vertical coordinate, the C_i' is C_i at the fluid free surface (z = 0), λ_i are the natural frequencies of vibration of the fluid, and n_i is obtained from $J_1'(nR_0) = 0$. The convolution integrals $I_i(t)$ can be directly used without transforming the oscillating fluid into a mechanical equivalent system, since they each represent the undamped response of a single degree of freedom oscillator of frequency λ_i, subjected to ground acceleration $\ddot{v}_g$.

The measured pressure time histories were compared to those given by equation (1) using the first two modes (i=1,2), for the five table motions and for both tanks. Good agreement was found for the El Centro and San Francisco shake table signals. On the average, there was a difference of about 12% between calculated and measured peak pressures. This level of discrepancy is unavoidable due to the difficulty in achieving perfect measurements on the one hand, and the assumptions made in the theoretical solution on the other. Correlation coefficients between measured and calculated pressure time histories were obtained for most of the table motions and they were 97% for tank #1 and 94 for tank #2 under El Centro record, 97% for tank #2 under San Francisco, 98% for both tanks under Pacoima Dam, and 98% for tank #2 under Parkfield and Taft records.

The water elevation at the tank wall was calculated for El Centro using the first three modes (i=1,2,3) for both tanks. Good correlation (97%) was found for both. Obviously, the higher frequencies in the water surface deformation are absent in the calculated time history but the behavior is extremely well represented and equation (2) using three modes can predict accurately spilling or overtopping.

The preceding comparisons show that the expressions for the dynamic pressure and the water surface deformation can directly be used for a prototype to predict the response of the contained fluid under a given ground motion. Furthermore it gave an insight on the advantages of using the approach to isolate a large tank. The pressure and the acceleration are reduced, and the sloshing is slightly increased. If the isolation system is chosen such that it is not in resonance with the first two sloshing modes, the effects on the water elevation would be small. The present experimental results do not represent the behavior of such a tank because the isolated structural model had a fundamental period very close to the first sloshing mode of the four-foot diameter tank. This was designed to represent the worst possible condition. Also, the scaling would differ greatly if the tanks were to

be tested without the structural model. In other words, the accelerograms were time scaled by a factor of two because the geometric scale was dictated by the structure, while if the four-foot diameter tank is used to represent a prototype of, for example, eighty feet in diameter, the accelerograms should be time scaled by $\sqrt{20}$. This would lead to a ground motion of much higher frequency and thus yield much better behavior for the isolated tank.

Several mechanical analogies have been developed for accelerated fluid containers [7]. The simplicity of the solution here renders the transformation of the problem into a mechanical analog unnecessary for tanks subjected to ground motion. A mechanical analog may be needed for tanks that are part of a more complex system, such as airplane fuel containers [8], where they are incorporated in an overall response analysis of this system.

The equations governing the oscillations of a fluid are similar in nature to those of a spherical pendulum. It was shown however that the motion of a spherical pendulum under an excitation in a vertical plane can become unstable near resonance and deviate from a planar trajectory due to nonlinear coupling [9]. When nonlinear wave theories are used to study forced waves in a fluid container they reveal coupling between the longitudinal modes of oscillation and the transversal modes that linear wave theory ignores. For certain forcing frequencies and certain damping levels in the system, the motion becomes chaotic [10], [11]. These problems are of interest where the tank is subjected to excitations of very long duration, and where it is significant enough to interact with its supporting structure, like tanks in moving vehicles or in aircraft. However, for small tanks in structures or large ground supported tanks subjected to earthquake excitation this problem is of less significance and the present research shows that linear wave theory yields accurate results.

CONCLUSIONS

The dynamic pressure exerted by the fluid on the walls of its container greatly depends on the support acceleration. Since base isolation reduces drastically the amplification of these accelerations, the impulsive component of the fluid pressure is decreased. The low frequency that characterizes the motion of base isolated structures can be close to the sloshing frequencies of the contained fluid and affect the water elevation response. However, the reduction in the impulsive component is much more significant than the increase in the convective component, yielding a lower total dynamic pressure for tanks in isolated structures. The response of fixed base structures is amplified along their height, while for base isolated structures, the base and the higher stories have practically the same response. For this reason, when fluid containers are located in the upper stories of a building, base isolation is very favorable. Since the tanks in the present experiment were designed as internal equipment the scaling of the shake table motions was controlled by the scale of the structural model. Tanks need to be tested separately in order to extend the concept of base isolation to large ground supported fluid containers. A theoretical solution based on linear wave theory was proven to predict accurately the response of the fluid. This solution can now be directly applied to tank prototypes.

REFERENCES

[1] Sackman J. L. and Kelly J. M., "Rational Design Methods for Light Equipment in Structures Subjected to Ground Motion," *Report No. UCB/EERC-78/19*, Earthquake Engineering Research Center, University of California, Berkeley, California, 1978.

[2] Kelly J. M. and Sackman J. L., "Seismic Analysis of Internal Equipment and Components in Structures," *Engineering Structures, Vol. 1*, pp. 179-190, 1979.

[3] Kelly J. M., "The Influence of Base Isolation on the Seismic Response of Light Secondary Equipment," *Report No. UCB/SESM-81/17*, Earthquake Engineering Research Center, University of California, Berkeley, California, 1981.

[4] Kelly J. M. and Tsai H. C., "Seismic Response of Light Internal Equipment in Base Isolated Structures," *Report No. UCB/SESM 84-17*, University of California, Berkeley, September 1984.

[5] Chalhoub M. S. and Kelly J. M., "Cylindrical Fluid Containers in Base Isolated Structures," *Report No. UCB/EERC-88/07*, Earthquake Engineering Research Center, University of California, Berkeley, California, 1988.

[6] Chalhoub M. S., "Theoretical and Experimental Studies of Earthquake Isolation and Fluid Containers," Ph.D. Dissertation, University of California, Berkeley, 1987.

[7] Housner G. W., "Dynamic Pressures on Accelerated Fluid Containers," *Bulletin of the Seismological Society of America*, Vol. 47, No. 1, pp. 15-36, January 1957.

[8] Graham E. W. and Rodriguez A. M., "The Characteristics of Fuel Motion which Affect Airplane Dynamics," *Journal of Applied Mechanics*, ASME Conference, Los Angeles, California, June 26-28, 1952.

[9] Miles J. W., "Resonant Motion of a Spherical Pendulum," *Physica 11D*, pp. 309-323, North-Holland, Amsterdam, 1984.

[10] Miles J. W., "Nonlinear Surface Waves in Closed Basins," *Journal of Fluid Mechanics*, Vol. 75, Part 3, pp. 419-448, 1976.

[11] Miles J. W., "Resonantly Forced Surface Waves in a Circular Cylinder," *Journal of Fluid Mechanics*, Vol. 149, pp. 15-31, 1984.

[12] Wiegel R. L., "Oceanographical Engineering," Prentice Hall, Inc., 1964.

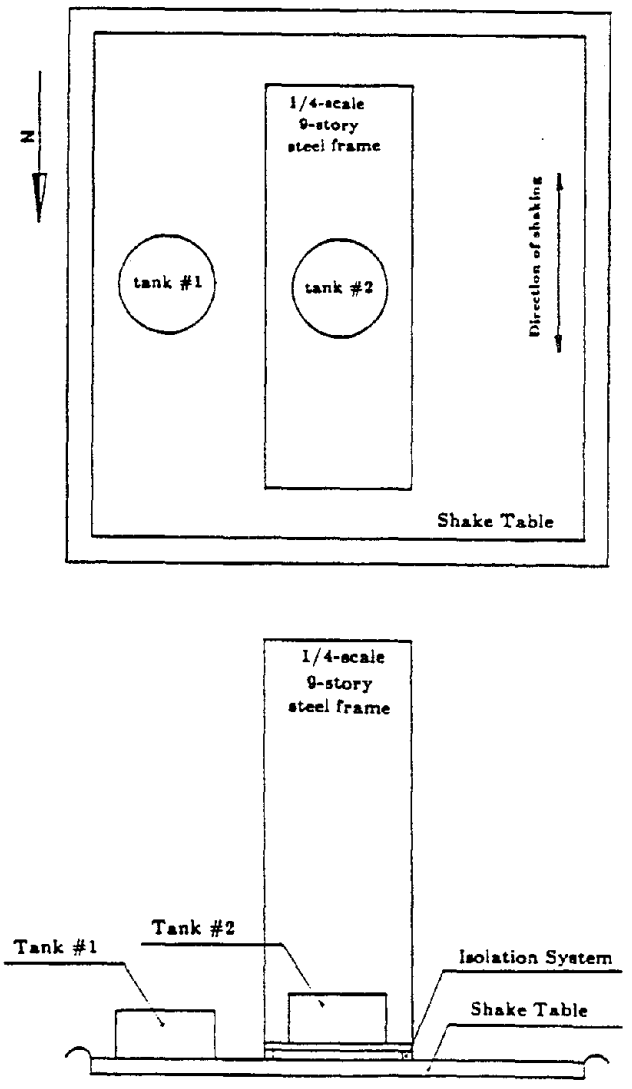

Figure 1 Plan View and Section View of experimental set-up.

SOIL-STRUCTURE INTERACTION
CORRELATION OF FIELD TEST RESULTS WITH ANALYTICAL PREDICTIONS

C. H. CHEN,[1] W. Y. JEAN,[2] Y. J. LEE,[2] J. PENZIEN[3]

[1] Department of Civil Engineering, National Taiwan University, Taipei, Taiwan, R. O. C.
[2] Eastern International Engineers, Inc., Taipei, Taiwan, R. O. C.
[3] Department of Civil Engineering, University of California, Berkeley, California, U. S. A.

SUMMARY

Presented are the results of correlating the measured forced vibration and seismic responses of a 1/4-scale containment model built in Lotung, Taiwan with the corresponding predicted responses using the hybrid method of modelling and the substructure method of analysis as implemented into the HASSI-4 computer program. As demonstrated by the excellent correlations obtained, the methodologies of this program is effective and efficient in solving the three-dimensional dynamic response of a soil-structure system and its associated internal equipment.

INTRODUCTION

The Large Scale Seismic Test program (Ref. 1) at Lotung, Taiwan is a joint research effort sponsored by the U. S. Electric Power Research Institute (EPRI) and the Taiwan Power Company (TPC) to study the effect of soil-structure interaction on the response of a nuclear power plant containment structure. Under the test program, two nuclear power plant containment models (1/4 and 1/12 scales) were built in the seismic active area of Lotung, Taiwan at the site of the well known SMART-1 strong motion array. The two test structures and their near-field soils have been well instrumented to measure seismic responses; thus providing the necessary data base for validating various modelling and analysis methodologies used in predicting soil-structure interaction effects.

The objective of the investigation reported herein is to demonstrate the accuracy of a specific 3-D soil-structure interaction methodology, and associated computer program, through correlation of field test results with analytical predictions. This investigation is one of several such investigations carried out under a joint research program sponsored by EPRI and TPC (Ref. 2).

METHODS

The methodology used for the analytical predictions makes use of the hybrid method of modelling (Ref. 3) and the substructure method of analysis carried out in the frequency domain. The entire soil-structure system is partitioned into a near-field and a far-field by a hemispherical interface passing through the soil region, as shown in Fig. 1(a).

The near-field substructure as shown in Fig. 1(b), consisting of an embedded structure and associated equipment to be analyzed under prescribed load-

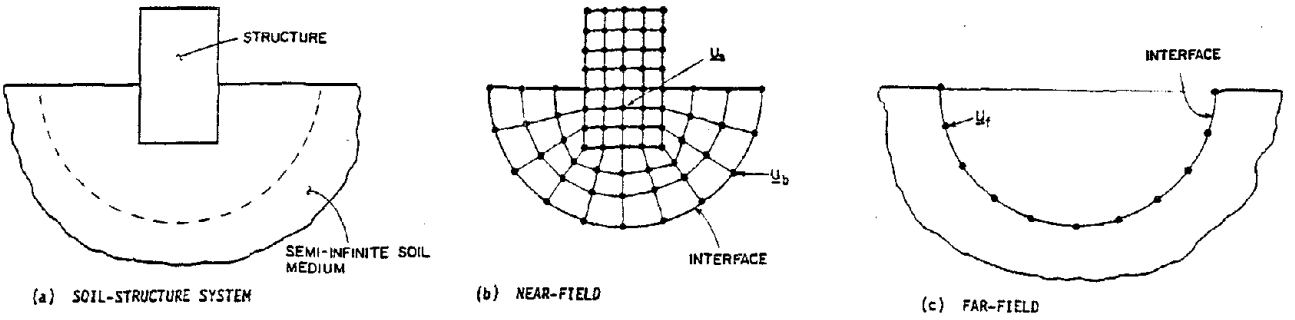

Fig. 1 Hybrid modelling of soil-structure system

ing conditions and a finite portion of soil encompassing its base, which is modelled appropriately using finite elements. The far-field substructure as shown in Fig. 1(c), consisting of a semi-infinite half-space with surface cavity, is modelled as a continuum through the use of an impedance matrix relating the discretized cavity surface forces to their corresponding generalized nodal displacements. The hemispherical interface is chosen judiciously so that it will provide a smooth surface along which mathematical boundary conditions can be easily satisfied. Compatibility of forces and displacements between the two substructures are enforced over this interface in combining the equations of motion of the near- and far-fields. The analysis procedure was implemented into the computer program HASSI-4 suitable for dynamic analysis of the complete soil/structure system under applied harmonic forces or under three simultaneous components of earthquake motion (Ref. 4).

FIELD TESTS AND MODELLINGS

The EPRI/TPC field tests were performed under two types of excitation (1) forced vibration and (2) seismic ground motion. Initially, after excavation to allow for embedment of the 1/4-scale test structure, its basemat was constructed and tested vertically, radially, and tangentially under eccentric forced vibration over the frequency range $0 \sim 30\ Hz$ (Ref. 5). The analytical model using hybrid method is shown in Fig. 2 where the basemat was modelled as a rigid block, the sheet piles were modelled by equivalent beam elements and the soils were modelled by axisymmetric solid elements. Soil properties as shown in Table 1 were chosen after consideration of the low strain level experienced and the effect of excavation.

Next, the full structure, steam generator model, and associated piping were constructed and backfill was placed providing 30 percent embedment. Forced vibration tests were then carried out in the radial and tangential directions with the exciter placed on the structure's roof (Ref. 6). For the correlation study, an analytical model was chosen as shown in Fig. 3 having soil properties as shown in Table 2 which were selected consistent with the results of a geophysical survey (Ref. 7).

Since completion of construction, the entire system has experienced numerous strong earthquakes during which response measurements were recorded. Responses measured during the earthquakes of May 20, and November 14, 1986 of magnitudes 6.5 and 7.0, respectively, were used for correlation purposes. The analytical model shown in Fig. 3 was again used but the soil shear moduli and damping ratios were adjusted to be consistent with the higher soil strains experienced during the earthquakes. These adjusted soil properties are shown in Table 3.

RESULTS

Using the established analytical model shown in Figs. 2 and 3, the equiv-

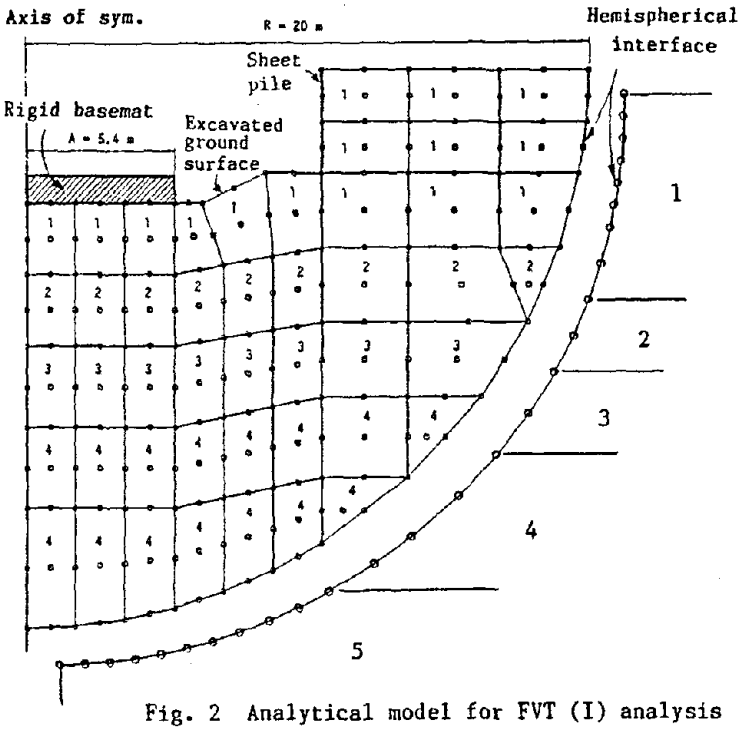

Fig. 2 Analytical model for FVT (I) analysis

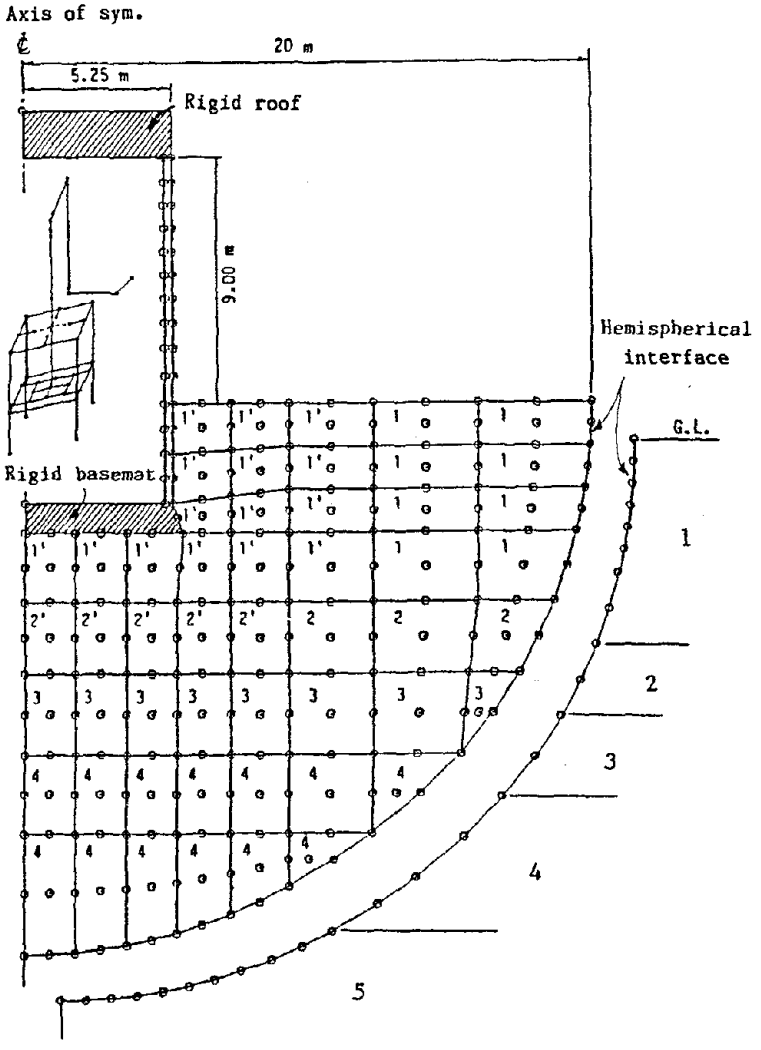

Fig. 3 Analytical model for FVT (II) and seismic analyses

Table 1 Soil properties for FVT(I) analysis

Category	Shear wave velocity C_s (m/sec)	Shear modulus G (kN/m²)	Poisson's ratio ν	Damping ratio β (%)
1	100	18000	0.44	1
2	150	40500	0.48	1
3	180	58320	0.48	1
4	210	79380	0.48	1
5	240	103680	0.48	0

Note: Unit weight $\gamma = 17.7$ kN/m³ for all soils
damping ratio $\beta = 0$ for far-field soils

Table 2 Soil properties for FVT(II) analysis

Category	Shear wave velocity C_s (m/sec)	Shear modulus G (kN/m²)	Poisson's ratio ν	Damping ratio β (%)
1	120	25920	0.44	2
1'	120	25920	0.44	5
2	150	40500	0.48	2
2'	150	40500	0.48	5
3	180	58320	0.48	2
4	210	79380	0.48	2
5	240	103680	0.48	0

Table 3 Soil properties for seismic analysis

Category	Shear wave velocity C_s (m/sec)	Shear modulus G (kN/m²)	Poisson's ratio ν	Damping ratio β (%)
1	93	15550	0.44	4
1'	71	9070	0.44	7
2	116	24300	0.48	4
2'	106	20250	0.48	7
3	161	46660	0.48	4
4	188	63500	0.48	4
5	215	83205	0.48	0

Note: In Tables 2 and 3
unit weight $\gamma = 17.7$ kN/m³ for all soils
damping ratio $\beta = 0$ for far-field soils

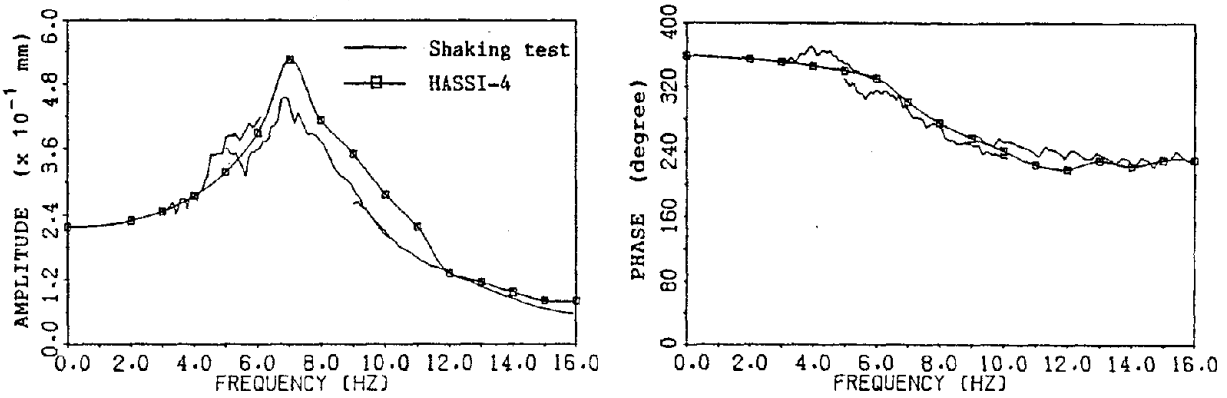

Fig. 4 Tangential displacement responses at shaker location (south edge of the basemat) in tangential test

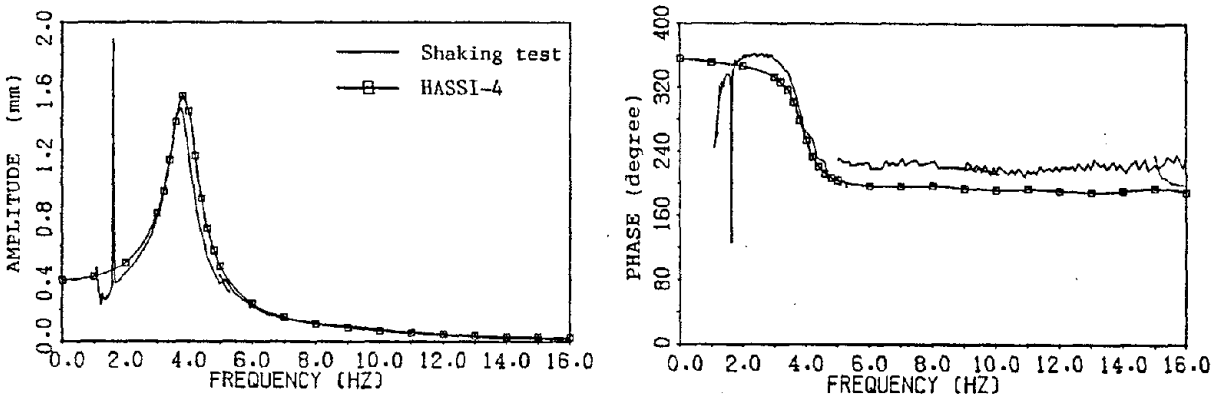

Fig. 5 Radial displacement responses at shaker location (south edge of the roof) in radial test

alent exciting loads were input to find responses under forced vibrations and under the free-field seismic ground motions recorded at a depth of 6 m and at a distance of 49 m from the structure. For the case of forced vibration of the basemat (FVT-I), the measured and predicted tangential displacement responses at the location where the tangential exciting force was applied are shown in Fig. 4 where it is seen that both the amplitude and phase angle distributions are in good agreement. The basemat responded nearly as a rigid body with its peak response occurring at a frequency of 7.0 Hz.

For the case of forced vibration of the full containment model (FVT-II), one analytical prediction using the HASSI model is shown in Fig. 5 where it can be compared with the corresponding measured field test result. Both the corresponding radial and tangential test results, show that the forced vibration response of the 1/4-scale structure is primarily rigid body rocking about a point slightly below its base. Little torsional response was experienced in the tangential test. Resonance was reached at 3.8 Hz where the system's response was magnified only about 3.6 times showing the presence of rather high total damping (material and radiation).

The seismic responses of the containment structure during the May 20, and November 14, 1986 Taiwan earthquakes are shown in Figs. 6 and 7 in the form of 5% damping response spectra. Comparisons show the spectra of the measured and predicted responses to agree very well. The structure experiences primarily rocking type response under seismic excitation which has high amplification at the 2.5 Hz resonant frequency, nearly quasi-static response for those frequencies well under 2.5 Hz, and greatly filtered response for those frequencies well above 2.5 Hz. The steam generator model and associated piping experience complex response under both forced vibration and seismic excitations due to the contribu-

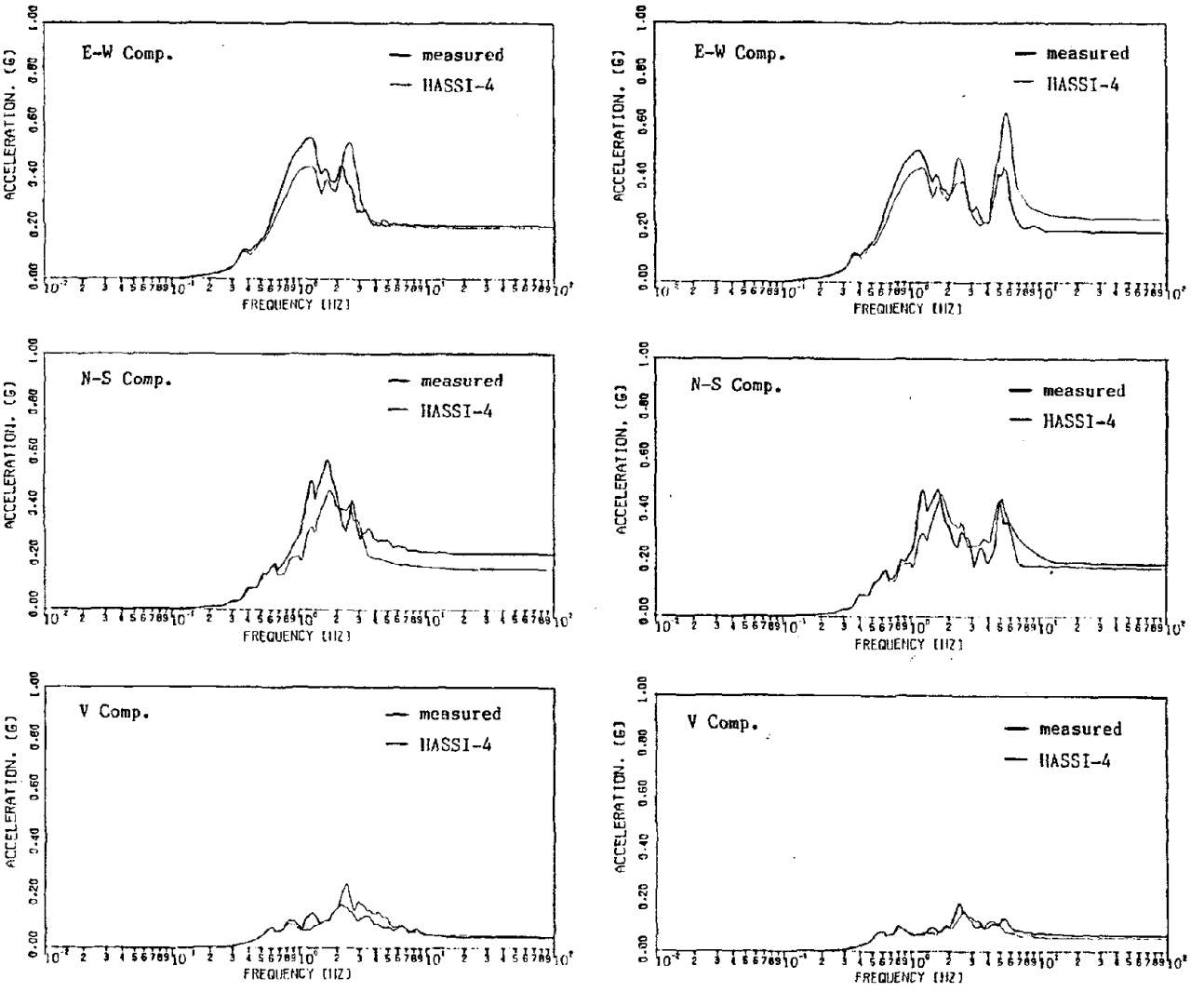

(a) Containment roof (b) Top of steam generator

Fig. 6 Correlation of 5% damping response spectra of May 20, 1986 earthquake

tions of numerous modes having low damping.

CONCLUSIONS

Soil-structure interaction can have considerable influence on the seismic response of a nuclear power plant containment structure and its associated equipment. Analytical modelling for prediction purposes must realistically represent all mass, stiffness, and damping (material and radiation) properties of the system in 3-D form. Through the extensive correlation studies reported herein, the capability of the HASSI-4 computer program in solving the 3-D seismic response of a complete soil-structure-equipment system has been shown to be very effective and efficient.

ACKNOWLEDGEMENT

The authors express their sincere thanks and appreciation to the Tokyo Electric Power Service Company, Ltd. for its financial support and assistance in the development of the HASSI computer programs, and to the Electric Power Research Institute of the U. S. A. and the Taiwan Power Company of the R. O. C. for providing the data obtained at the Lotung, Taiwan test site.

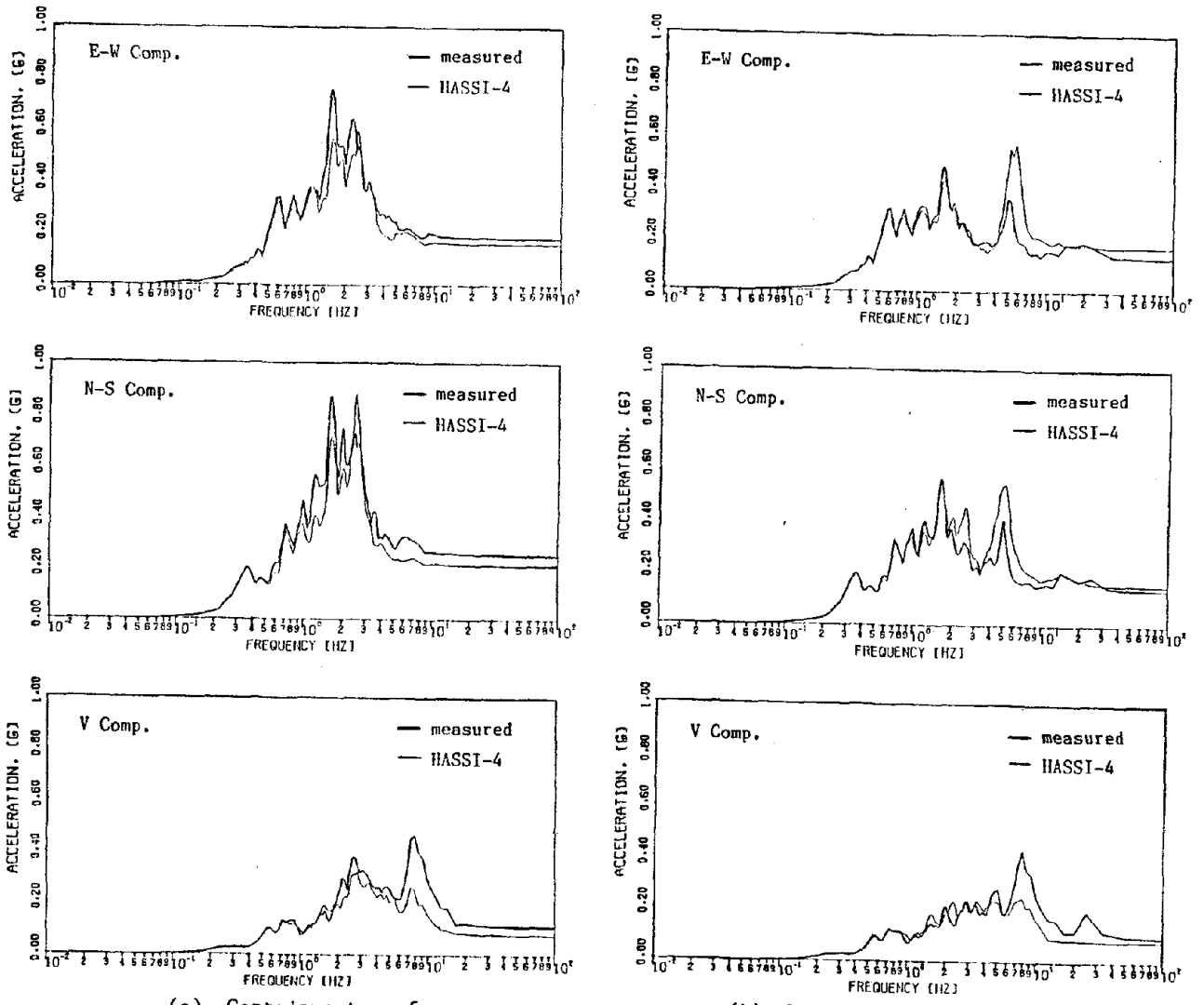

(a) Containment roof (b) Bottom of steam generator

Fig. 7 Correlation of 5% damping response spectra of November 14, 1986 earthquake

REFERENCES

1. "Large Scale Seismic Test Program at Lotung, Taiwan," Distributed by EPRI/TPC.
2. Penzien, J., et. al., "Soil-Structure Interaction Correlations of EPRI/TPC Field Test Results with Analytical Predictions," Workshop on Validation of Seismic SSI Analysis Techniques Using Lotung Experiment Data, Palo-Alto, California, U. S. A., Dec. 1987.
3. Gupta, S., Penzien, J., Lin, T. W., and Yeh, C. S., "Three-Dimensional Hybrid Modelling of Soil-Structure Interaction," Earthquake Engineering and Structural Dynamics, Vol. 10, pp. 69-87, 1982.
4. "Hybrid Analysis of Soil-Structure Interaction - Version 4," by Eastern International Engineers, Inc., May 28, 1984.
5. "Final Report for Forced Vibration Testing of 1/4-Scale Containment Structure Basemat," ANCO Engineers, Inc., July 1985.
6. "Forced Vibration Testing of 1/4-Scale Containment Structure," ANCO Engineering, Inc., April 1986.
7. "Geophysical Survey Report of Lotung Project," HCK Geophysical Company, March 1986.

EARTHQUAKE RESPONSE OF ASYMMETRIC FRAME BUILDINGS

Anil K. CHOPRA[1] and Reem HEJAL[2]

[1]Professor of Civil Engineering, University of California, Berkeley, CA, U.S.A.
[2]Graduate Student, Department of Civil Engineering, University of California, Berkeley, CA, U.S.A.

SUMMARY

The earthquake response of torsionally-coupled buildings is presented for a wide range of the system parameters. By comparing these responses with those of corresponding torsionally-uncoupled systems, the effects of lateral-torsional coupling on building forces, arising from lack of symmetry in building plan, are identified.

INTRODUCTION

Buildings subjected to lateral ground motion simultaneously undergo lateral, as well as torsional, motions if their structural plans do not have two axes of mass and stiffness symmetry. The objective of this paper is to investigate the effects of lateral-torsional coupling on the earthquake response of buildings with asymmetrical plan. Because most of the basic research on this problem has been concerned with shear beam idealization of buildings (e.g. 1, 2, 3), this restriction is relaxed in this investigation. In particular, the influence of the beam-to-column stiffness ratio on the response of asymmetric frame buildings is investigated.

SYSTEMS AND DESIGN SPECTRA

Systems Considered The systems analyzed are five-story buildings with all floors having an identical rectangular plan, symmetrical about the X-axis and consisting of three moment-resisting planar frames (Fig. 1a), connected at each story level by a rigid diaphragm. The properties of each frame are uniform over height: constant story height, h, and one bay of width 2h (Fig. 1b); all beams of a frame have the same flexural stiffness, EI_b, and the column stiffness, EI_c, does not vary with height. The mass at each floor is denoted by m, and r is the radius of gyration of each floor about the vertical axis passing through its center of mass. The static eccentricities of all floors are the same, equal to e, and the centers of rigidity of the floors all lie on a vertical line. The idealized buiding, therefore, belongs to the special class of multi-story buildings, described in (4). The damping ratio, ξ, is assumed to be the same in each mode of vibration.

Frame action is measured by the joint rotation index, ρ, which is defined as the sum of EI/L values for all beams divided by the sum of EI/L values for

all columns at the mid-height story of the frame. By varying the stiffness ratio ρ, the entire range of behavior of a frame can be covered. For $\rho = 0$, the frame behaves as a flexural column with beams imposing no constraint on joint rotations. For $\rho = \infty$, joint rotations are restrained so that the frame behaves as a shear beam. Intermediate values of ρ, therefore, represent frames with both beam and column deformations and joint rotations. The joint rotation index of frame (1) is denoted by ρ_1, and that of frame (2) by ρ_2. In this study it is assumed that $\rho_1 = \rho_2 = \rho$, a condition which implies that frames (1) and (2) have proportional lateral stiffness matrices.

Response Spectra For earthquake response spectra of arbitrary shape the design forces need not be greater than those for either a hyperbolic or a flat spectrum that constitute upper bounds to the design spectrum in the range of periods less than the fundamental period of the structure (Fig. 2). These two idealized spectra are useful since normalized response of the system does not depend on the system vibrational periods, but only on their ratios (3), and because they are representative of the acceleration- and velocity-controlled regions of smooth design spectra.

EFFECTS OF LATERAL-TORSIONAL COUPLING

The effects of lateral-torsional coupling on building response are investigated by comparing the response to ground motion along the Y-axis of the torsionally-coupled, multistory building of Fig. 1 with that of the corresponding torsionally-uncoupled, multistory system--a system with all properties identical to the torsionally-coupled system except that the centers of mass are coincident with the centers of rigidity. This comparison is presented for flat and hyperbolic pseudo-acceleration spectra. The response quantities selected to study the overall behavior of the building are: the base shear V_B and the base torque T_{BR} at the center of rigidity. These quantities, computed by the analysis procedure developed in (4), are normalized, respectively, by V_{Bo} and eV_{Bo}, where V_{Bo} is the base shear of the corresponding torsionally-uncoupled system. The normalized torque T_{BR}/eV_{Bo} can be interpreted as the ratio of the dynamic eccentricity of the system to its static eccentricity, e_d/e, where the dynamic eccentricity $e_d = T_{BR}/V_{Bo}$ is the distance from the center of rigidity at which static application of V_{Bo} results in the dynamic base torque T_{BR}.

The normalized base shear and base torque are presented in Figs. 3 and 4 (and additional responses in Reference (4)). Also shown in these figures are the normalized responses $\bar{V}$ and $\bar{T}_R$ of the associated torsionally-coupled, one-story system which are independent of ρ; see Part I of Reference (4). This one-story system has the following properties: (a) the static eccentricity ratio e/r for the system is the same as for all floors of the torsionally-coupled, N-story building, and (b) the ratio of the uncoupled torsional and lateral vibration frequencies for the system is the same as $\Omega = \omega_{\theta j}/\omega_{yj}$, where $\omega_{\theta j}$ and ω_{yj} are the jth torsional and lateral frequencies of the corresponding torsionally-coupled, N-story building, and their ratio Ω is independent of j.

It is apparent from Figs. 3 and 4 that the effects of lateral-torsional coupling on structural responses are similar for the multistory and the associated one-story systems. For this reason, the general trends of $\bar{V}$ and $\bar{T}_R$ for the one-story system, which are independent of ρ, are described first, and then the differences that occur for the multistory building, in which case ρ influences the normalized responses, are described next. Lateral-torsional coupling has the effect of reducing $\bar{V}$ and increasing e_d/e. These effects increase as the eccentricity ratio e/r increases, and are dependent on the ratio $\Omega = \omega_{\theta j}/\omega_{yj}$. For systems with smaller e/r values the effect is most pronounced, i.e. $\bar{V}$ reaches its minimum value and e_d/e its maximum value, for

values of Ω around unity, i.e. when the uncoupled lateral and torsional frequencies are close to each other. As e/r increases, $\bar{V}$ reaches its minimum values at values of Ω below unity, while e_d/e reaches its maxima for values of Ω above unity. For torsionally-stiff systems (Ω > 1), $\bar{V}$ approaches unity as Ω becomes large, indicating that there is essentially no reduction in the base shear, while e_d/e approaches one, implying no dynamic amplification of eccentricity. For torsionally-flexible systems (Ω < 1) with smaller e/r, there is essentially no reduction in base shear. The dynamic eccentricity ratio, e_d/e, for torsionally-flexible systems approaches zero as Ω tends to zero in the case of a hyperbolic spectrum, implying no torque, but approaches one in the case of a flat spectrum, indicating no dynamic amplification.

These observations on how torsional coupling affects the normalized base shear and torque for the associated torsionally-coupled, one-story system generally carry over to a multistory building. However, unlike the one-story system, the normalized responses of the multistory building depend on ρ, but for e/r up to 0.4 the effects of ρ are generally small. The differences between the normalized responses of the two torsionally-coupled systems--multistory and its associated one-story--are due to the contributions of the terms in the modal combination rule arising from cross-correlation between coupled vibration modes "2j" and "1k" (j = 1 to 4; k = j + 1 to 5) of the multistory building (4). Modes are numbered as "nj" with j = 1, 2, . . . N for an N-story buildilng, and n = 1, 2 for a one-way symmetric building to indicate two DOF per floor. The deviations of the normalized responses of the multistory building from those of the associated one-story system depend on e/r, Ω, ρ, the response quantity, the significance of higher modal-pair contributions, and the response spectrum considered. Since the cross-correlation terms may assume positive or negative values (4), the normalized reponses of the multistory building may be larger or smaller than the corresponding normalized responses of the associated one-story system (Figs. 3 and 4). The deviations between the normalized responses of the two systems are more pronounced in the ranges of Ω where cross-correlation factors $\gamma_{21,12}$ and $\gamma_{21,13}$ are maximum (4). Also, the deviations increase with a decrease in ρ in the case of V_B and T_{BR}, trends which also are related to the importance of the higher modal-pair contributions (4). The deviations increase with increase in e/r and are more significant for the hyperbolic spectrum than the flat spectrum; these trends are related to magnitudes of the cross-correlation terms (4).

HEIGHT-WISE DISTRIBUTION OF FORCES

The effect of lateral-torsional coupling on the height-wise distribution of forces (story shears and story torques at the centers of rigidity) is summarized in Figs. 5 to 8. It is apparent that for a flat spectrum the height-wise variations of forces are insensitive to the values of e/r or Ω and follow the respective variations in the corresponding uncoupled multistory system (e = 0). This can be explained by noting that the response of torsionally-coupled buildings with T_{y1} in the acceleration-controlled region, or the flat portion of the spectrum, is mainly due to the fundamental vibration modal pair--modes "11" and "21"--and the cross-correlation terms are relatively small, thus ensuring small contributions of higher modal-pairs (4). As a result, the responses of the torsionally-coupled building, normalized by the responses of the corresponding torsionally-uncoupled, multistory system, are very close to the normalized responses of the one-story system, resulting in a very little influence of torsional-coupling on the height-wise distribution of responses. The effect of lateral-torsional coupling on the height-wise distribution of forces is more pronounced for the hyperbolic spectrum, or the velocity-controlled region of the spectrum, with the effect increasing as e/r increases and as ρ decreases, primarily because the cross-correlation terms are more significant in this case, and increase with an increase in e/r and a decrease in

ρ (Figs. 3 and 4). For the values of Ω shown in Figs. 5 to 8, the lateral-torsional coupling effects in story shears and story torques are generally most pronounced for systems with closely spaced uncoupled frequencies (Ω close to 1). It appears that the overall effect of lateral-torsional coupling on the height-wise variations of forces is not large.

CONCLUSIONS

This investigation of the effects of lateral-torsional coupling on the earthquake response of multistory buildings has led to the following conclusions:

1. The effects of lateral-torsional coupling on the responses of a multistory building and its associated one-story system are similar. Lateral-torsional coupling causes a decrease in the base shear, the base overturning moment and the top floor lateral displacement at the center of rigidity, but an increase in the base torque; these effects increase as e/r increases and are most pronounced for systems with closely-spaced uncoupled frequencies. However, unlike the one-story system, torsional-coupling effects in the response of multistory buildings depend on ρ, but for e/r up to 0.4 the dependence on ρ is generally small.

2. The differences between the effects of lateral-torsional coupling on the multistory building and its associated one-story system arise due to cross-correlation terms between vibration modes belonging to different modal pairs. These differences increase with an increase in e/r. They are more pronounced for the base shear and base torque than the base overturning moment and the top floor lateral displacement, and are more pronounced for the column moment than the beam moment or column axial force in the base story.

3. The effect of lateral-torsional coupling on the height-wise variations of forces seems not to be very significant (i.e. these force variations are similar for torsionally-coupled and corresponding uncoupled systems), although it is relatively more pronounced for story shears and story torques than story overturning moments. The effect increases as e/r increases and is more pronounced when T_{y1} is in the velocity-controlled region than when it is in the acceleration-controlled region of the spectrum.

ACKNOWLEDGEMENTS

The research reported here was supported by Grant No. CEE-8402271 from the National Science Foundation, for which the writers are grateful.

REFERENCES

1. Tso, W. K. and Meng, V., "Torsional Provisions in Building Codes," Canadian Journal of Civil Engineering, 9, pp. 38-46, 1982.
2. Rutenberg, A., Hsu, T. I., and Tso, W. K., "Response Spectrum Techniques for Asymmetric Buildings, "Earthq. Eng. Struct. Dyn., 6, pp. 427-435, 1978.
3. Kan, C. L., and Chopra, A. K., "Effects of Torsional Coupling on Earthquake Forces in Buildings," ASCE, 103, ST4, pp. 805-820, 1977.
4. Hejal, R. and Chopra, A. K., "Earthquake Response of Torsionally-Coupled Buildings," Report No. UCB/EERC-87/20, Univ. of Calif., Berk., Dec. 1987.

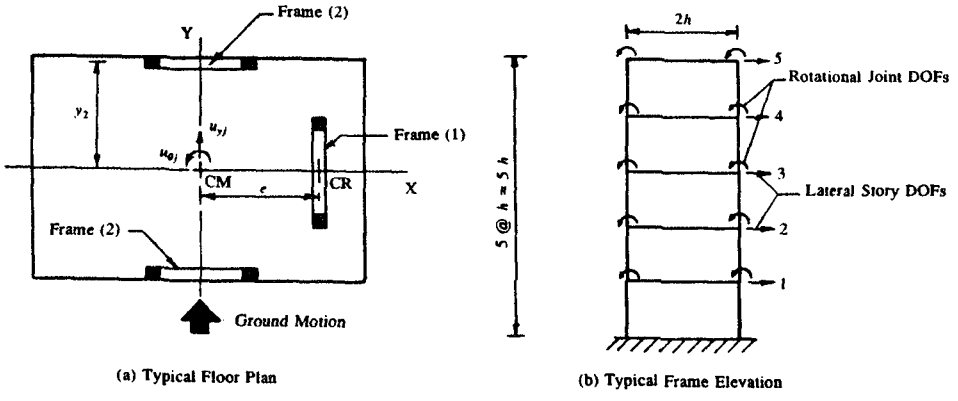

(a) Typical Floor Plan

(b) Typical Frame Elevation

Fig. 1 System Considered

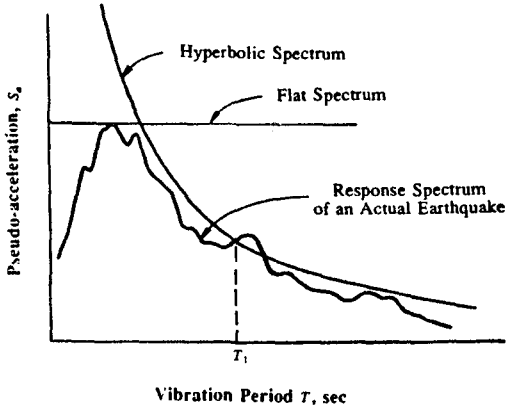

Fig. 2 Flat and Hyperbolic Response Spectra

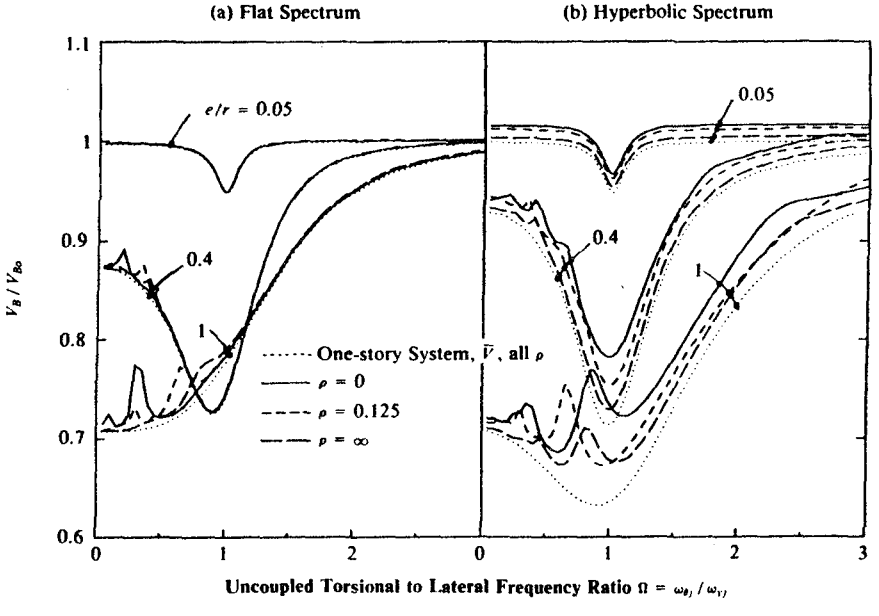

Fig. 3 Normalized Base Shear in Multi-Story Building and Associated One-Story System

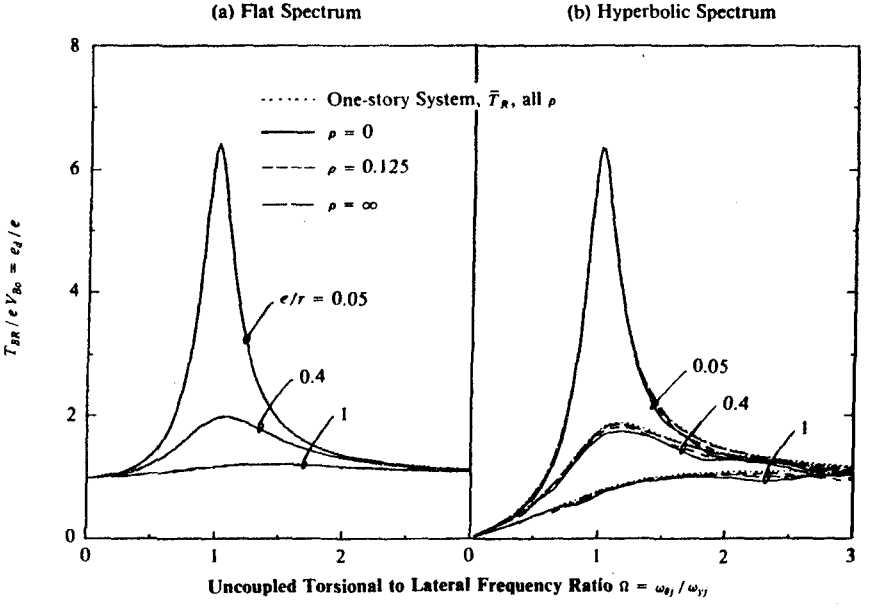

Fig. 4 Normalized Base Torque at C.R. in Multi-Story Building and Associated One-Story System

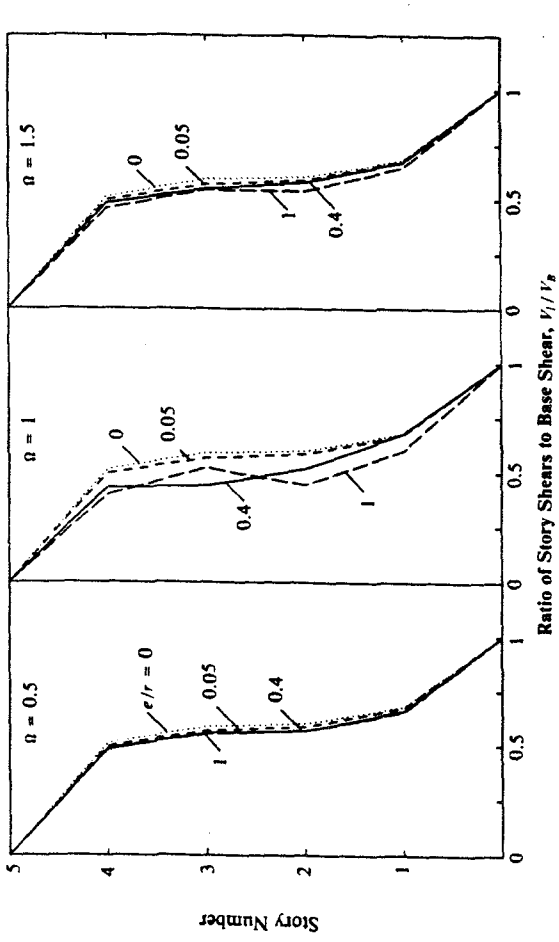

Fig. 5 Comparison of Height-Wise Variation of Story Shears in Torsionally-Uncoupled (e/r = 0) and Torsionally-Coupled (e/r = 0.05, 0.4, and 1) Systems; ρ = 0 for Flat Spectrum

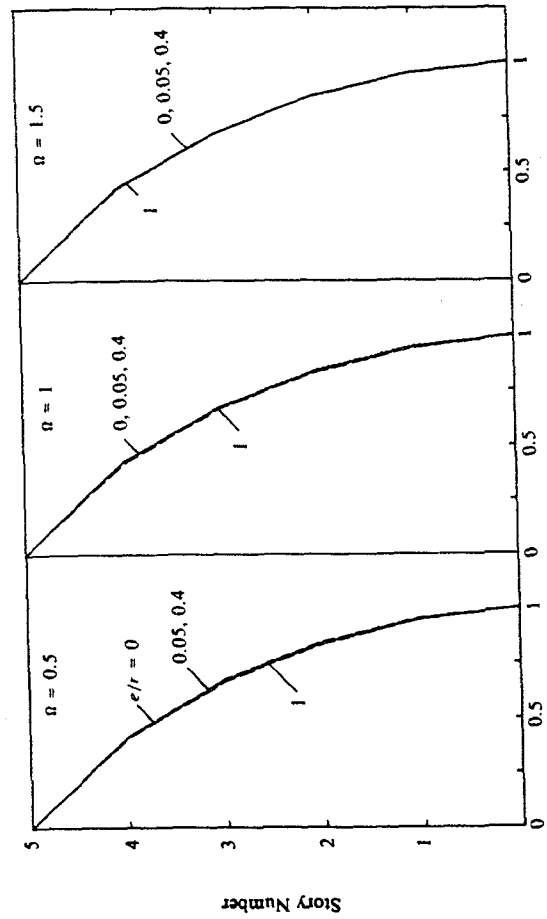

Fig. 7 Comparison of Height-Wise Variation of Story Torques at C.R. in Torsionally-Coupled (e/r = 0.05, 0.4, and 1) Systems and of Story Shears in Torsionally-Uncoupled (e/r = 0) Systems for Flat Spectrum; ρ = 0

Fig. 6 Comparison of Height-Wise Variation of Story Shears in Torsionally-Uncoupled (e/r = 0) and Torsionally-Coupled (e/r = 0.05, 0.4, and 1) Systems for Hyperbolic Spectrum; ρ = 0

Fig. 8 Comparison of Height-Wise Variations of Story Torques at C.R. in Torsionally-Coupled (e/r = 0.05, 0.4, and 1) Systems and of Story Shears in Torsionally-Uncoupled (e/r = 0) Systems for Hyperbolic Spectrum; ρ = 0

EVALUATION OF AN IMPROVED CODE-TYPE PROCEDURE FOR PRELIMINARY DESIGN

Ernesto F. CRUZ[1] and Anil K. CHOPRA[2]

[1]Department of Structural Engineering, Catholic University of Chile, Santiago, Chile.
[2]Department of Civil Engineering, University of California, Berkeley, California, USA.

SUMMARY

An improved code-type procedure for earthquake analysis of buildings is presented. The results obtained from applying the procedure to several building models are compared to response spectrum analysis results. The errors are found to be dependent on overall building characteristics, especially the fundamental period and the beam-to-column stiffness ratio, also to be small enough for the results to be used for preliminary design over a wide range of buildings with different characteristics. This is provided that buildings have distributions of mass and stiffness over the height that do not change abruptly.

INTRODUCTION

The equivalent lateral forces analysis procedures specified in building codes (Refs. 1,2,3) are intended to provide an initial estimate of the earthquake forces without a preliminary design of the building. It was demonstrated (Ref. 4) that earthquake forces are especially affected by two overall building parameters, fundamental vibration period T_1 and beam-to-column stiffness ratio ρ; but the effects of these parameters are not properly recognized in building codes. Based on these results a procedure to estimate the earthquake forces for the preliminary design of buildings, which recognizes the important influence of these parameters on building response was developed (Ref. 5).

An evaluation of the quality of the results obtained from applying the improved code-type procedure to several different model structures is reported here. The ranges of the basic properties of the structures for which the results from the procedure are adequate to be used in preliminary design are identified.

IMPROVED CODE-TYPE ANALYSIS PROCEDURE

The basic idea behind the improved code-type analysis (ICA) procedure is to compute the response of the structure considering the contributions of the first two natural modes of vibration. The total base shear is computed as the product of the first mode effective weight W_1^* and a seismic coefficient C which is obtained from the pseudo-acceleration design spectrum through a simple modification that consists in raising the decaying portion of the spectrum in varying amounts that depend on the overall characteristics of the structure.

The modifications to this spectrum are intended to account for the contributions to the base shear of the modes of vibration higher than the first one. These higher-mode contributions depend on building properties, the most signifi-

cant of which are fundamental vibration period T_1 and stiffness ratio ρ. This parameter was defined (Ref. 6) as the ratio of the sum of the stiffnesses of all the beams at mid-height story of the frame to the summation of the stiffnesses of all the columns at the same story. The design spectrum (Sa/g) is modified as shown in Fig. 1. It is left unchanged in the acceleration-controlled region, but is modified in the velocity and displacement-controlled regions. The exponents β_v and β_d depend on building properties, especially on the stiffness ratio ρ; their values for the 5 different frame models of Fig. 2 can be found in (Ref. 4).

The first mode effective weight W_1^* can be computed from the standard equation (Ref. 7) based on estimates of the height-wise distribution of building weight and of the fundamental mode shape. Alternatively, it can be estimated from Fig. 3, where it is shown as a function of ρ for the 5 frame cases shown in Fig. 2 in terms of W, the total weight of the building.

It has been demonstrated (Ref. 8) that, over a useful range of fundamental vibration periods, the earthquake response of building frames can be satisfactorily estimated by response spectrum analysis considering the contributions of only the first two modes of vibration; even the first mode alone is usually sufficient in the acceleration-controlled region of the spectrum. Thus if we could separate the total base shear into the first mode contribution and ascribe the remainder to the second mode it would be possible to distribute each modal base shear over the building height in accordance with the corresponding mode shape. This is an indirect, approximate way to determine the response in the fundamental and second modes of vibration. The total response can then be obtained by appropriately combining the modal responses.

The first mode base shear V_{01} can be obtained as the product of W_1^* and Sa_1, the ordinate of the pseudo-acceleration design spectrum. The remainder of the base shear, obtained under the assumption that the total base shear is best given by a SRSS combination of modal values, $V_{02}^2 = V_0^2 - V_{01}^2$, is treated as an estimate of the base shear due to the second vibration mode. Having estimated the base shears due to the first two modes of vibration, the equivalent lateral forces in each mode can be determined from standard equations. The remainder of the analysis is the same as the standard response spectrum analysis (Ref. 7).

What remains to be determined are the periods and the shapes of the first two modes of vibration. These vibration properties can not be computed exactly without the building having been designed. An estimate of the fundamental vibration period is required in most of the existing building codes. For this purpose, empirical formulas have been developed (Ref. 1) these are based on only a general description of the building type --e.g. steel or concrete moment frame, shear wall system, braced frame, etc.-- and overall dimensions such as height and plan size. Such formulas may be employed in this ICA procedure, but it should be recognized that they often lead to significantly inaccurate values.

It is recommended that the first two mode shapes be approximated by

$$\phi_{j1} = (h_j/H)^{\delta} \quad \text{and} \quad \phi_{j2} = (h_j/h_0)(1 - h_j/h_0), \; j = 1,2, \ldots N \qquad (1)$$

respectively, where h_j is the height of the jth floor above the base, H is the total height of the building, and h_0 is the height of the node (point of zero displacement) above the base. As shown in Figs. 4 and 5 the exponent δ and the height h_0 depend on the building properties including the number of stories, height-wise variation of mass and stiffness, but perhaps most significantly on the beam-to-column stiffness ratio ρ. Because δ and h_0 vary gradually with ρ they can be estimated to a useful degree of accuracy from the data presented. Although these approximate shapes are not always excellent, they are obviously better than the mode shapes independent of implied in building codes. Similarly, the ratio T_2/T_1, needed to compute displacements in the second mode, can

be obtained from the data shown in Fig. 6.

EVALUATION OF APPROXIMATE RESULTS QUALITY

The analysis procedure used to generate the "exact" results to check the quality of the results obtained from the ICA procedure is the standard response spectrum analysis (RSA) (Ref. 7). The maximum modal responses obtained for the pseudo-acceleration design spectrum in Fig. 1 (Sa/g) are combined using SRSS.

The results obtained using the ICA procedure are compared to the results obtained from standard RSA for the 5 different plane frame building models of Fig. 2. The frames are idealized as single-bay, moment-resisting plane frames with constant story height = h, and bay width = 2h. Only flexural deformations are considered in the members which are assumed to be prismatic. The modulus of elasticity E is the same for all members but the moments of inertia of beams I_b and columns I_c --same for both columns in any story-- may vary over the height, as in cases 3 to 5 (Fig. 2), with the ratio of the two same in all stories. The mass of the structure is assumed to be concentrated at the floor levels and the rotational inertia is neglected. The damping ratio for all the natural modes of vibration is assumed to be 5 percent.

Overall Responses The errors in the ICA results for the base shear V_0 and the base overturning moment M_0 are shown in Figs. 7 and 8 as a percentage of the RSA results for the three ρ cases considered and the 5 frame cases being used. For V_0 errors are seen to be within 10% for all but frame case 5 when T_1 is below 3.75 secs. Errors are larger for the smaller values of ρ and they tend to increase as T_1 increases. For M_0 the errors are much smaller than for V_0 and they do not exceed 10%, except for frame case 5 for T_1 greater than 5 secs. and $\rho = 0$. The errors in the ICA results are negative for most of the cases considered thus indicating that the ICA procedure results tend to slightly underestimate the RSA results for the base shear and for the base overturning moment.

Distributions over the Height The distributions of story shears over the height of the frames obtained from the ICA procedure and the RSA procedure are very close for the 5 frame cases considered and the 3 different values of ρ. Even for the long period cases (T_1 = 4.11 sec.) the ICA distribution closely follows the RSA distribution. In Fig. 9 results are shown for frame case 3, for 4 period cases selected as representative of the different parts of the spectrum and the 3 values of ρ considered. The results for the other frame cases are similar.

The errors in the ICA results are normally within 10% of the RSA results, except for a few cases where the errors are somewhat larger. These larger errors occur mainly in the top stories where the absolute values of the story shears are small. The largest error is smaller than 35%. Equivalent results for the story overturning moments are shown in Fig. 10, where excellent agreement between the results from ICA and RSA is found. This is not unexpected as it has been shown (Ref. 8) that the distribution over the height of story overturning moments is far less sensitive to changes in ρ and the fundamental period T_1 than the story shears distribution because the importance of the contributions of the higher modes to these response quantities is much smaller.

In Figs. 9 and 10 the distributions of story shear and story overturning moments corresponding to the UBC (Ref. 2) lateral forces distribution are also shown. For long period structures the errors in the ICA results are seen to be definitely smaller than those in the UBC distributions.

CONCLUSION

The ICA procedure to estimate the earthquake forces for the initial, preliminary design of buildings presented is able to recognize the important influ-

ence of those building properties and parameters that significantly affect its earthquake response, without requiring the computations inherent in standard dynamic analysis by the response spectrum method. It represents a major conceptual improvement over present building codes with very little increase in computational effort. The errors in the ICA procedure results, for the base shear and the base overturning moment and also for the distribution over the height of story shears and story overturning moments, are such that the procedure can be considered suitable for preliminary design of frame buildings with fundamental period up to about 3 seconds; provided they have distributions of mass and stiffness over the height that do not change abruptly. For all other cases the results should be an improvement over those obtained using actual codes lateral forces but will need refinement before they can be used for design.

ACKNOWLEDGEMENTS

The research reported here was partially supported by the U.S. National Science Foundation and the Research Division of the Catholic University of Chile.

REFERENCES

1. Applied Technology Council, "Tentative Provisions for the Development of Seismic Regulations for Buildings," Report ATC 3-06, NBS Special Publication 510, NSF Publication 78-08, June 1978.
2. International Conference of Building Officials, "Uniform Building Code," Whittier, California, 1982.
3. Rosenblueth, E., "Seismic Design Requirements in a Mexican 1976 Code," Earthquake Engineering and Structural Dynamics, Vol. 7, 1979, 49-61.
4. Chopra, A.K., Cruz, E.F., "Evaluation of Building Code Formulas for Earthquake Forces," Journal of Structural Eng., ASCE, Vol. 112, No. 8, 1881-1899.
5. Cruz, E.F., and Chopra, A.K., "Simplified Methods of Analysis for Earthquake Resistant Design of Buildings," Report UCB/EERC-85/01, Earthquake Engineering Research Center, University of California, Berkeley, Feb. 1985.
6. Blume, J.A., "Dynamic Characteristics of Multi-story Buildings," Journal of the Structural Division, ASCE, Vol. 94, No. ST2, 1968, 337-402.
7. Chopra, A.K., "Dynamics of Structures, A Primer," Earthquake Engineering Research Institute, Berkeley, California, 1982.
8. Cruz, E.F., Chopra A.K., "Elastic Earthquake Response of Building Frames," Journal of Structural Engineering, ASCE, Vol. 112, No. 3, 1986, 443-460.

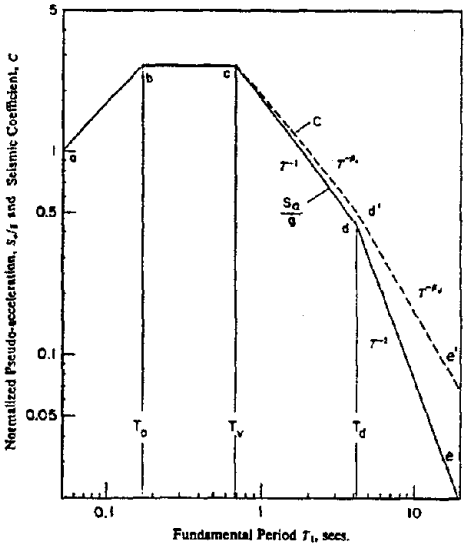

Fig. 1 Construction of C spectrum from Sa/g spectrum.

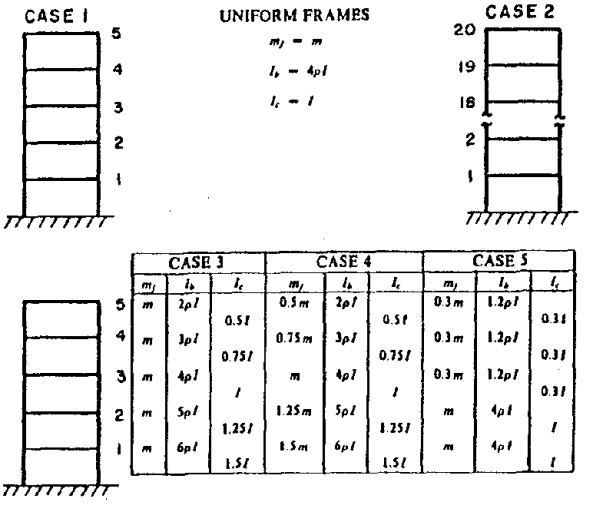

Fig. 2 Idealized building frames

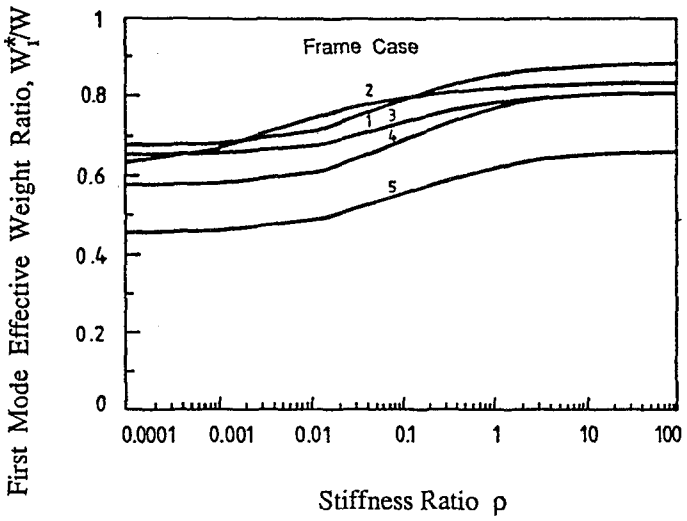

Fig. 3 Variation of first mode effective weight ratio to total weight with stiffness ratio ρ for five frame cases.

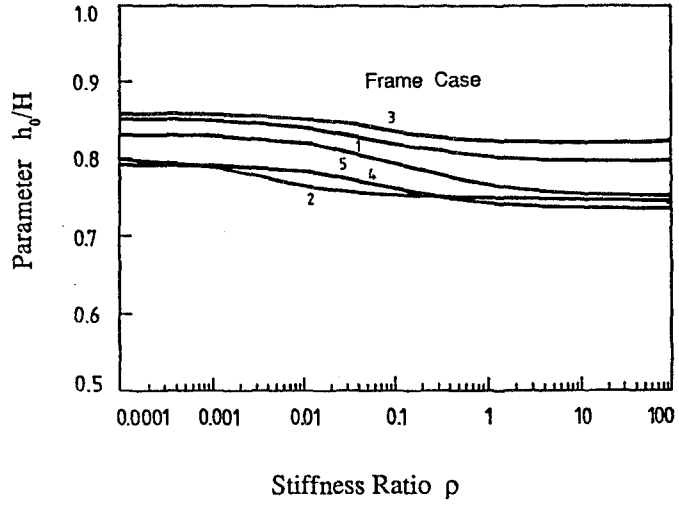

Fig. 5 Variation of parameter h_0 with stiffness ratio ρ for five frame cases.

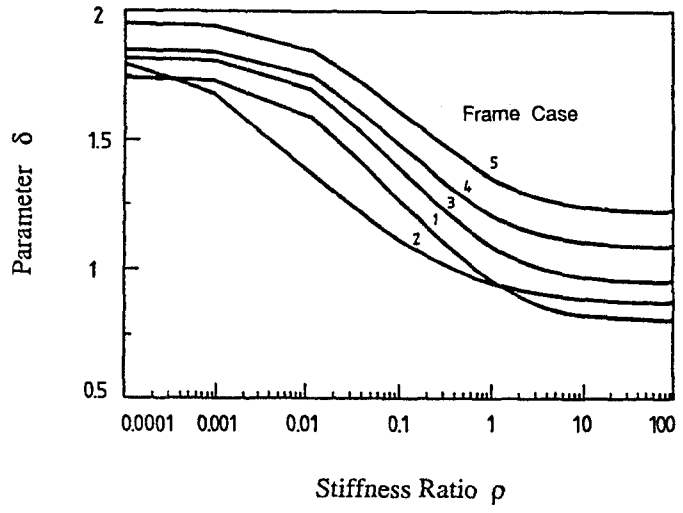

Fig. 4 Variation of parameter δ with stiffness ratio ρ for five frame cases.

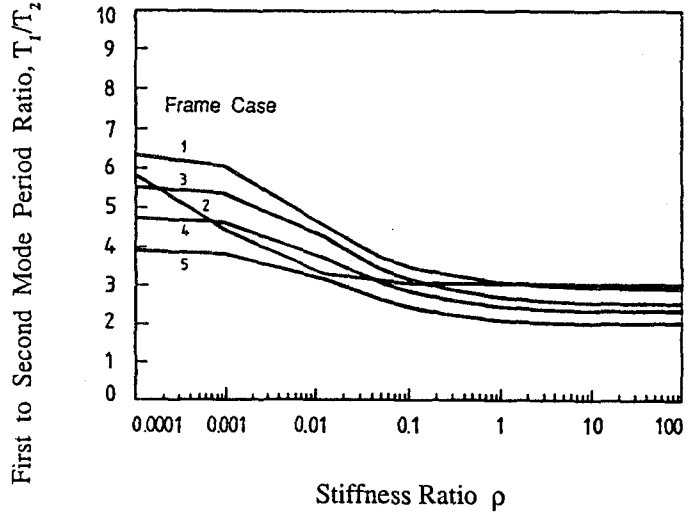

Fig. 6 Variation of the ratio of first mode to second mode period with stiffness ratio ρ for five frame cases.

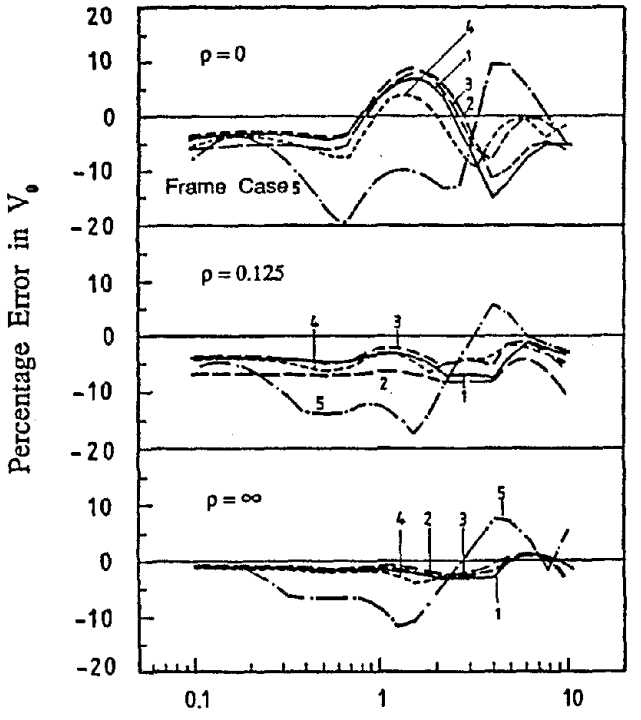

Fig. 7 Percentage error in base shear computed by ICA method, relative to RSA results, 5 frame cases.

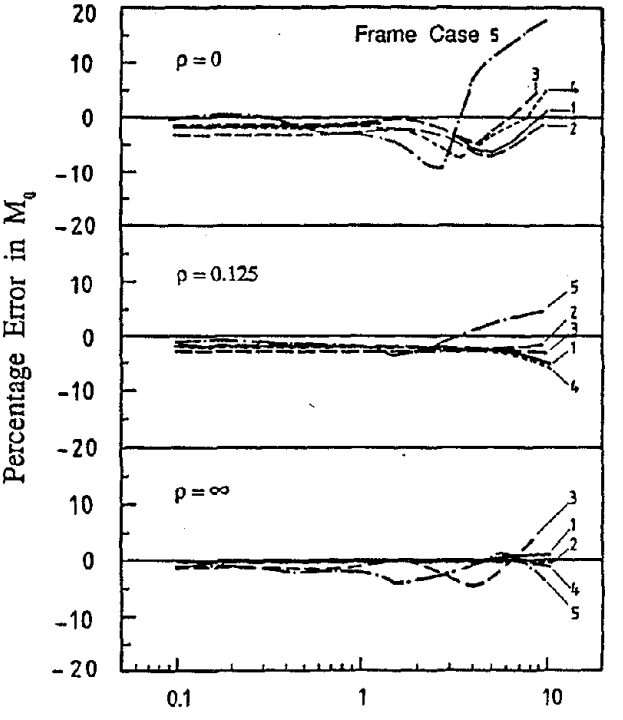

Fig. 8 Percentage error in base over turning moment computed by ICA method, relative to RSA results, 5 frame cases.

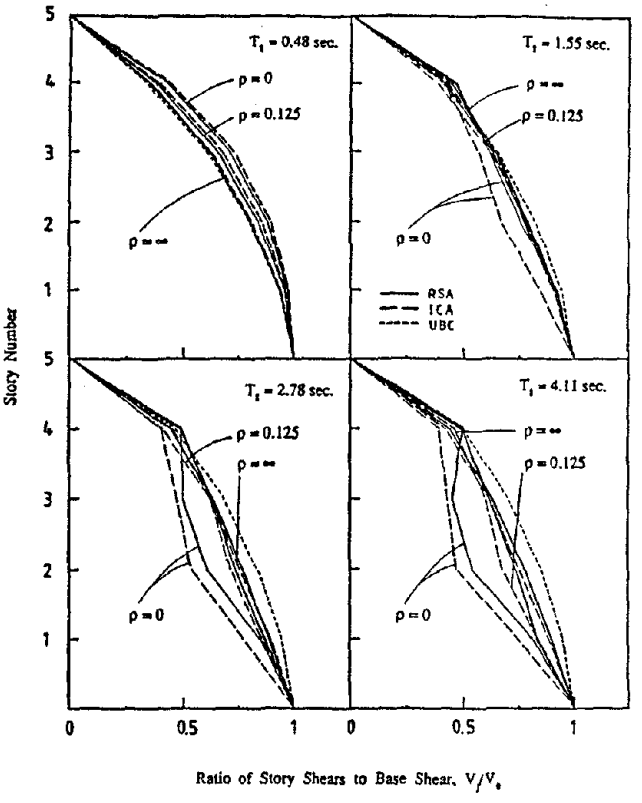

Fig. 9 Comparison of story shears distributions computed by RSA and ICA methods (Case 3).

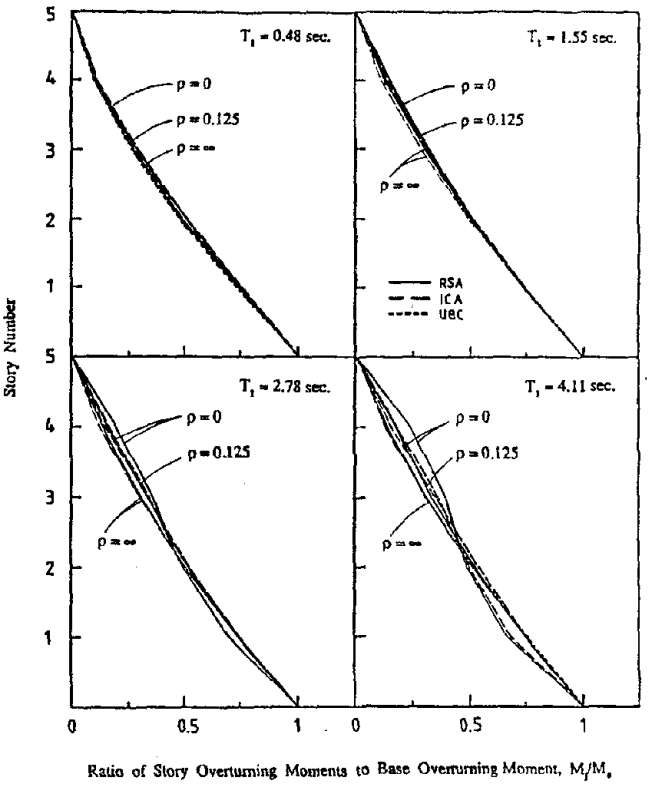

Fig. 10 Comparison of story overturning moment distributions computed by RSA and ICA methods (Case 3).

EFFECT OF MODELING ON SEISMIC RESPONSE OF SECONDARY SYSTEMS

Armen Der Kiureghian

Department of Civil Engineering
University of California
Berkeley, California, U.S.A.

SUMMARY

In the seismic analysis of secondary subsystems, such as equipment and piping in nuclear power plants, highly idealized models are used to represent complex primary structures. Most frequently, a simple lumped-mass, stick model is used and the effect of local vibrations of structural and nonstructural elements are ignored. In this paper, through a parametric study on floor response spectra for two example structures, the influences of various modeling idealizations on the secondary response are examined. It is shown that model idealization can have significant influence on the predicted response of high-frequency secondary subsystems. In particular, the neglect of the local vibration of structural elements may result in an underestimation and the neglect of the local vibrations of nonstructural elements may result in an overestimation of the secondary response. Insight and guidelines for proper modeling of the primary structure are provided throughout the paper.

INTRODUCTION

Secondary subsystems supported on primary structures, such as equipment and piping attached to the containment structure in a nuclear power plant, play important roles in maintaining the safety or operation of industrial facilities, particularly in the event of severe earthquakes. Such subsystems often comprise a large portion of the design and construction cost of facilities. Hence, accurate methods for predicting their responses to earthquake excitations are of great interest.

In recent years, based on methods of random vibrations and perturbation theory, accurate analytical methods for predicting the seismic response of secondary subsystems directly in terms of the ground response spectrum have been developed (Refs. 4,5). These techniques are capable of accounting for such phenomena as tuning (i.e., the coincidence of the frequencies of the two subsystems, which gives rise to resonant responses of the secondary subsystem), interaction, non-classical damping, and cross-modal and cross-support correlations, which are special characteristics of composite primary-secondary systems. Comparisons with "exact" results obtained by time history analyses of the composite system have verified the accuracy of these analytical methods.

The experience with these analytical methods, however, has revealed a curious phenomenon. Namely, theoretically estimated responses for tuned secondary subsystems are much larger than responses observed for similar subsystems in experiments or in real earthquakes. For example, it is not unusual to theoretically predict an amplification of 20 in the peak response of a tuned secondary subsystem, e.g., a peak acceleration of 20g from an earthquake of 1g peak ground acceleration. However, such large amplifications have never been observed or measured for secondary subsystems, even in carefully conducted experiments (Ref. 2). This phenomenon is even more pronounced if one attempts to predict the response of tuned tertiary subsystems, such as a light valve attached to a piping system. In a recent theoretical study, peak tertiary accelerations of order 100g from an earthquake of 0.5g peak ground acceleration were predicted (Ref. 8). Such estimates surely are not in concurrence with our engineering intuition.

It is shown in this paper that a main cause for the overestimation of the response of tuned secondary subsystems lies in the idealization of the primary structure in the theoretical modeling of the system. In the current practice, usually a lumped-mass model of the primary structure describing its global features is used to generate floor response spectra (FRS). (An FRS represents the peak response of an oscillator attached to a specified point in the primary structure, plotted as a function of the frequency and damping of the oscillator.) The peaks of the FRS at tuning frequencies are broadened to account for the effect of uncertainty in the primary modal frequencies; the peak-broadened FRS are then used to estimate the secondary responses (see Ref. 1). Such models neglect the effect of local vibrations of structural elements and of the various nonstructural elements attached to the structure. Whereas the adequacy of such idealized models for predicting the response of primary structures has been established by a long history of experiments and measurements, their validity for predicting the response of secondary subsystems remains to be investigated. This paper demonstrates that the conventional modeling approach which neglects the local vibrations of structural and nonstructural elements may lead to erroneous estimates of the secondary response. In particular, it is shown that neglecting the effect of structural elements may result in underestimation of the response of high-frequency secondary subsystems, and neglecting the effect of nonstructural elements may result in a gross overestimation of the response of tuned secondary subsystems.

EFFECT OF MODELING OF THE PRIMARY STRUCTURE

A visit to a nuclear power plant is an enlightening experience for any structural engineer interested in the dynamic response of structures and secondary subsystems. At each floor of the structure one observes an enormous number of nonstructural attachments, such as equipment items, pipes of all sizes running in all directions, valves, hangers, cabinets, ducts, etc., as well as structural elements, such as beams, columns, walls, and slabs. Although virtually all such elements participate in the dynamic response of the system, for pragmatic reasons it is virtually impossible to account for every detail. In practice, most typically a lumped-mass model (usually a simple stick) is used, where the entire mass of a floor or a segment of a floor together with its attachments is lumped at a nodal point. In this approach no account is made of the local vibrations of structural or nonstructural elements.

Four factors in the modeling of the primary structure are relevant to an accurate prediction of the secondary response: (a) the level of refinement in the model describing the global features of the primary structure, (b) the effect of local vibrations of structural elements, (c) the effect of local vibrations of nonstructural elements, and (d) the effect of uncertainty in the properties of the primary structure. In this paper, the effects of the first three factors are evaluated by examining the floor response spectra for two example structures: a cantilever column representing the containment vessel of a nuclear power plant, and a four-story frame structure representing an auxiliary building. The two structures with their properties are depicted in Fig. 1. In all cases, the floor response spectra are computed with a zero mass of the oscillator (i.e., neglecting the effect of oscillator-structure interaction) and for 2 percent damping of the oscillator. The NRC RG-160 recommended ground response spectra for the horizontal and vertical directions with 1.0g and 0.5g peak ground accelerations, respectively, are employed for this analysis. The effect of the fourth factor is studied elsewhere (6,7).

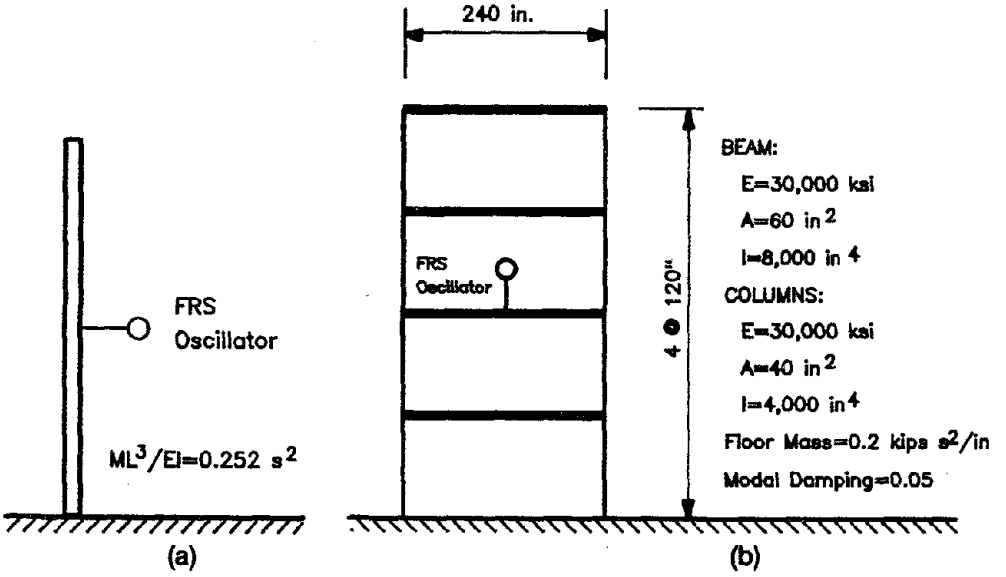

Fig. 1. Example Structures: (a) Cantilever; (b) Frame

Effect of Model Refinement A measure of refinement of the primary structure model is the level of mass discretization. To examine this effect, the cantilever column is represented by a lumped mass stick model with in turn 4, 8, and 16 nodal masses. In each case, the rotational moments of inertia of the nodal masses are ignored. The resulting floor response spectra for an oscillator attached at the midheight of the cantilever are shown in Fig. 2a. The following observations can be made: (a) Refinement in the mass discretization tends to shift the peaks of FRS towards higher frequencies without appreciably changing their amplitudes. This is due to a shift in the modal frequencies of the primary structure as the mass distribution is refined. (b) The shift in the peaks is increasingly more pronounced at higher frequencies and for a coarser mass discretization. (c) For the 4-DOF model, the FRS exhibits a fourth peak which is due to the largely shifted fourth mode of the primary model. Obviously, this model is inadequate for predicting the FRS at high frequencies.

The main conclusion from these observations is that the level of mass discretization in the primary model should be such that all primary modal frequencies that are within the range of FRS frequencies are accurately represented. Otherwise, spurious peaks from shifted modal frequencies may appear in the FRS. Since secondary subsystems often have high-frequency modes, the needed level of model refinement can be greater than that needed for predicting the response of the primary structure itself. From the preceding observations, it is also clear that, provided the proper level of model refinement is used, shifts in the peaks of FRS due to further model refinement would be sufficiently small so as to be absorbed by the peak broadening mentioned above.

Effect of Local Vibration of Structural Elements The FRS for an oscillator attached at the middle of the second-floor beam of the frame structure is considered. Curves 1 in Fig. 2b depict the horizontal and vertical FRS based on a model of the primary structure in which the mass at each floor level is lumped at the two end points (i.e., neglecting the local vibrations of the beam), mass rotational moments of inertia are neglected, and axial deformations of all members are included. Curve 2 depicts the horizontal FRS for the same model but ignoring the effect of axial deformations. Curves 3 depict the horizontal and vertical FRS including the effect of the local vibration of the attachment floor. For this purpose, the floor mass is discretized at eight points along the beam. The following observations can be made: (a) The effect of axial deformations on the horizontal FRS is negligible. (b) The refinement in the mass discretization results in shifts in the peaks of the horizontal FRS similar to those observed in the preceding example. (c) For the vertical FRS, in addition to the shift in the peaks, a new peak is observed at 42.6 Hz. This peak is due to the local vibration mode of the floor beam in the vertical direction.

The main conclusion from the above observations is that the local vibration of an attached structural element can have a significant influence on the FRS if the modal frequency of the structural element is within the frequency range of interest. Since structural elements usually have high-frequency modes, their effect is significant only for secondary subsystems with high-frequency characteristics.

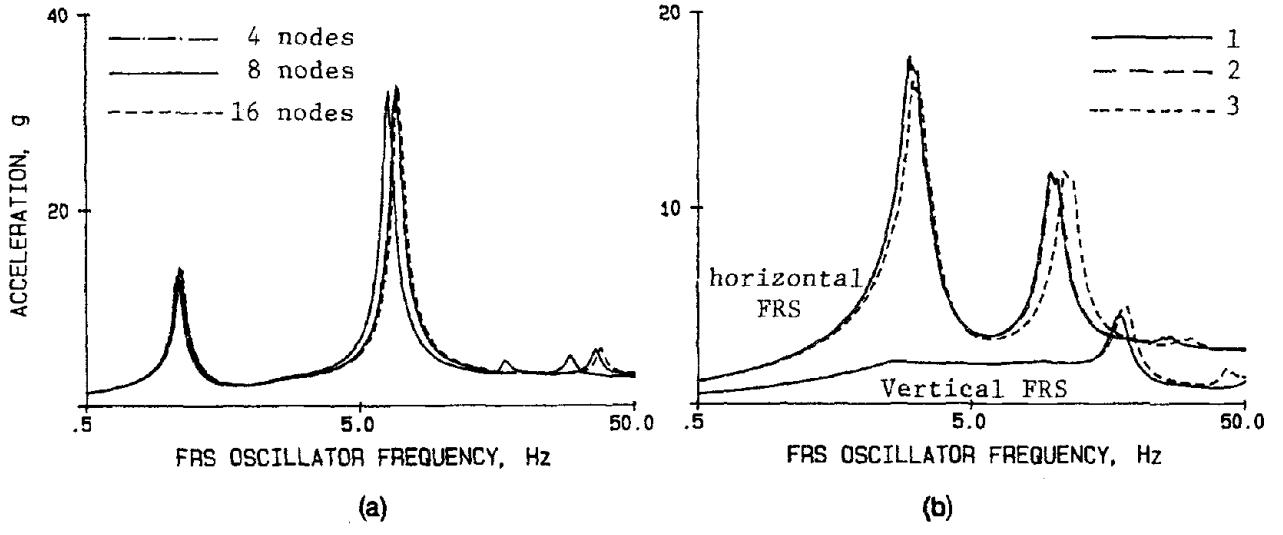

Fig. 2. Effect of Modeling on FRS: (a) cantilever Structure; (b) Frame Structure

Effect of Local Vibration of Nonstructural Elements A nonstructural element attached to the primary structure is modeled herein as an oscillator of frequency ω_0, damping ratio z_0, and mass m_0, the latter being a small fraction of the attached floor mass, m. Each such attached oscillator tends to affect the modes of the primary structure. This influence is greatest when the oscillator mass is large and when its frequency is near

a modal frequency of the primary structure. In that case the modal frequencies of the primary structure are shifted and closely spaced modes appear in the combined oscillator-structure system (Ref. 4). Such closely spaced modes are known to result in a "dispersion" of vibratory energy and, hence, reduced resonance peaks in the FRS (Ref. 3).

To investigate this effect, consider a nonstructural element attached in the second floor (same floor as the FRS oscillator) of the frame structure with a frequency equal to the first mode of the primary structure and a damping ratio $z_0 = 0.05$. The horizontal FRS (excluding the local vibration of the beam element) for three values of the mass ratio $m_0/m = 0., 0.01, 0.05$ are shown in Fig. 3. Observe that the effect of the local vibration of the nonstructural element is to reduce the peak of the FRS corresponding to the first mode of the primary structure. This is due to two effects: dispersion of the vibratory energy in the primary structure and, hence, reduced sharpness in the resonance, and the added energy dissipation due to the damping in the nonstructural element. Also observe that the nonstructural element does not have a significant influence on the FRS at frequencies beyond the immediate neighborhood of its natural frequency.

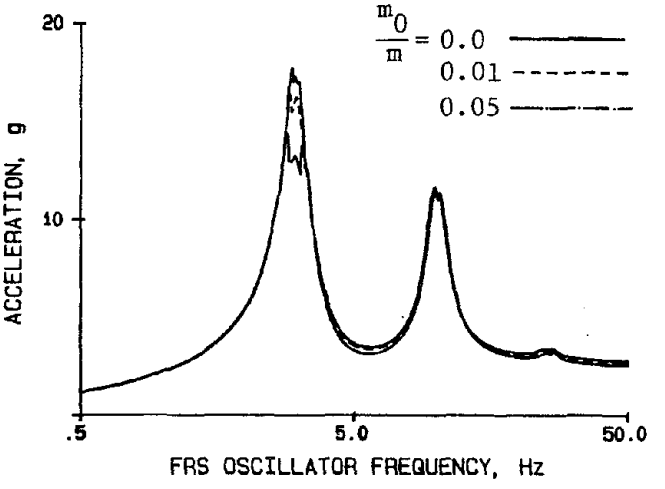

Fig. 3. Effect of a Nonstructural Element on FRS of the Frame Structure

To further investigate the above effect, a parametric study of the FRS of the 8-DOF cantilever column is performed. The results, taken from Ref. 3, are summarized in Fig. 4. These results show the second peak in the FRS in Fig. 2a (shown as a dashed curve in Fig. 4) as affected by the local vibrations of nonstructural elements with varying mass, frequency, and point of attachment. In all cases $z_0 = 0.02$ is assumed. Fig. 4a shows the influence of the mass of the nonstructural element which is attached to the DOF 4 and has a frequency equal to that of the second primary mode. The reduction in the peak is significant even for small values of the oscillator mass. Fig. 4b shows the influence of the frequency of the oscillator for a mass ratio of 0.05. The reduction in the peak becomes less significant with increasing distance between the frequency of the oscillator and the primary modal frequency. Fig. 4c shows the influence of the location of the nonstructural element; it is found that the influence on the FRS is greater when the element is attached at DOF's where the second primary mode has a large displacement.

From the above results, it is clear that a single nonstructural element with the proper frequency, mass, and location of attachment can significantly reduce the peak in the FRS. In reality, a primary structure has numerous nonstructural attachments with varying characteristics. Also, at the time of analysis or design of a secondary subsystem, the characteristics of other attachments to the primary structure are largely unknown. Therefore, a statistical approach to the modeling of nonstructural elements is essential. In this paper, purely as a preliminary investigation, the combined effect of such multiple nonstructural elements is studied by the following means: At each DOF of the primary structure three oscillators of equal mass are attached; the oscillator frequencies are selected by random generation with a uniform distribution between 5 to 10 Hz; each oscillator is assumed to have 2 percent damping; the combined (8 + 3x8 =) 32-DOF system is considered as the primary structure for which the FRS are computed. The resulting FRS for two values of the oscillator/floor mass ratio are depicted in Fig. 4d. This figure shows that in a realistic structure with many attached nonstructural elements the peaks in the FRS can be significantly smaller than those predicted without considering the effect of the nonstructural elements.

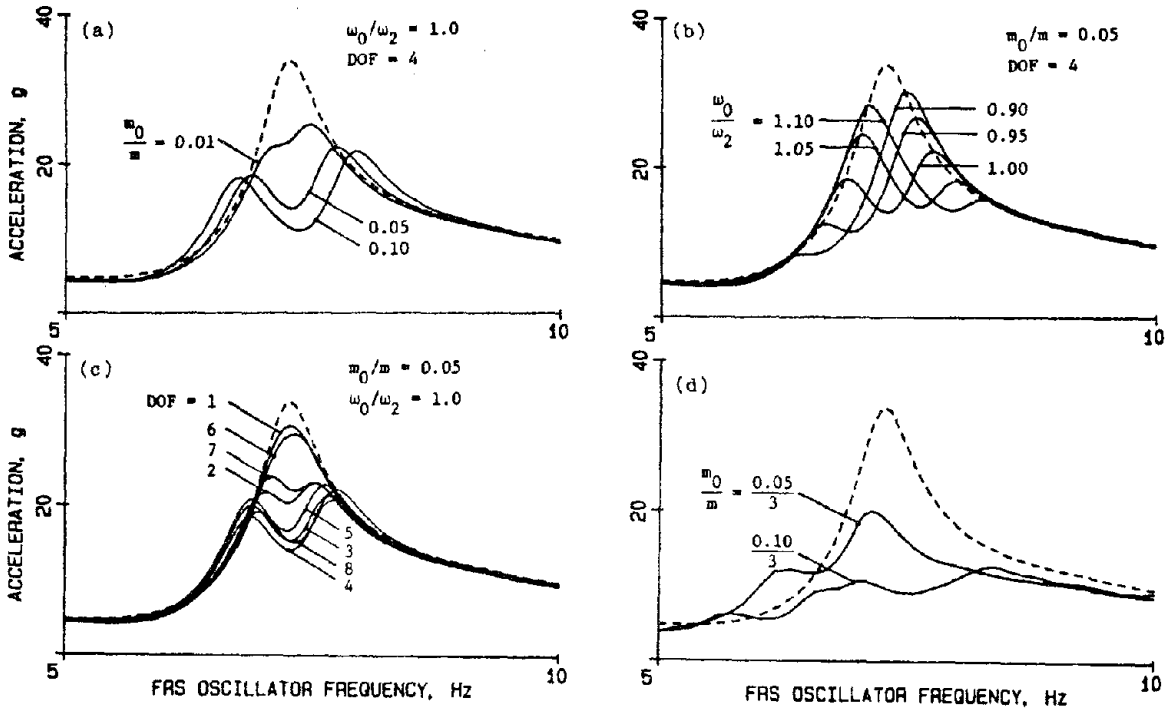

Fig. 4. Effect of Nonstructural Elements on FRS of the Cantilever Structure: (a) Effect of m_0; (b) Effect of ω_0; (c) Effect of Location; (d) Effect of Multiple Elements

Effect of Uncertainty in the Properties of the Primary Structure Uncertainty in the mass and stiffness properties of a primary structure result in uncertainty in its natural frequencies and, hence, in the positions of the peaks in the FRS. On the other hand, uncertainty in the damping characteristics results in uncertainty in the amplitude of FRS. Recent analytical studies using first and second-order reliability methods (Ref. 7) reveal that the uncertainty in the mass and stiffness characteristics can have a dominant influence on the secondary response, even if the associated uncertainty is smaller than that in the damping. This and an earlier study (Ref. 6) also reveal that the conventional peak-broadening procedure is a reasonable and practical approach to account for the effect of the uncertainty in the natural frequencies. More refined methods, such as those described in Ref. 7, are available for more careful investigations of this effect.

CONCLUSIONS

The main conclusions from this study can be summarized as follows: (a) The mass discretization in the primary model should be sufficiently fine such that all global modal frequencies of the primary structure within the frequency range of the FRS are accurately represented; (b) local vibrations of attached structural elements may introduce peaks in the FRS if the natural frequencies are within the range of interest; (c) local vibrations of attached nonstructural elements may significantly reduce the amplitudes of the peaks in the FRS; (d) uncertainties in the mass, stiffness and damping characteristics of the primary structure can have significant influence on the secondary response; (e) in general, a careful modeling of the primary structure is necessary for accurate prediction of the response of attached secondary subsystems. The level of refinement necessary might be greater than that required for predicting the response of the primary structure itself.

REFERENCES

1. American Society of Mechanical Engineers, **ASME Boiler and Pressure Vessel Code**, ANSI/ASME BPV-III-1-A Section III, Rules for Construction of Nuclear Power Plant Components, Div. 1, Appendix N, July 1981.
2. Der Kiureghian, A., and A. Prakash, "Comparison of Measured- Computed Floor Response Spectra for a Test Structure," Draft Report, EPRI Research Project No. RP 964-8, Department of Civil Engineering, University of California, Berkeley, CA, February 1986.

3. Der Kiureghian, A., and T. Igusa, "Effect of Local Modes on Equipment Response," **Transactions**, 9th Int. Conf. on Structural Mechanics in Reactor Technology, **K2**, pp. 1087-1092.
4. Igusa, T. and A. Der Kiureghian, "Dynamic Response of Multiply Supported Secondary Systems," **Journal of Engineering Mechanics**, ASCE, **111**(1), January 1985, pp. 20-41.
5. Igusa, T., and A. Der Kiureghian, "Generation of Floor Response Spectra Including Oscillator-Structure Interaction," **Earthquake Engineering and Structural Dynamics, 13**(5), September-October 1985, pp. 661-676.
6. Igusa, T., and A. Der Kiureghian, "Reliability of Secondary Systems with Uncertain Tuning," **Proceedings**, 4th Int. Conf. on Str. Safety and Reliability, Kobe, Japan, May 1985, pp.
7. Igusa, T., and A. Der Kiureghian, "Response of Uncertain Systems to Stochastic Excitation," **Journal of Engineering Mechanics**, ASCE, **114**(5), May 1988, pp. 812-832.
8. Igusa, T., and A. Der Kiureghian, "Dynamic Response of Tertiary Subsystems," **Journal of Engineering Mechanics**, ASCE, to appear.

A DISPLACEMENT CONTROL AND UPLIFT RESTRAINT DEVICE FOR BASE ISOLATED STRUCTURES

Michael C. Griffith[1], James M. Kelly[2], and Ian D. Aiken[3]

1 Lecturer, Dept. of Civil Engineering, University of Adelaide, Adelaide, South Australia 5001
2 Professor, Dept. of Civil Engineering, Davis Hall, University of California, Berkeley, CA 94720
3 Graduate Student, Dept. of Civil Engineering, University of California, Berkeley, CA 94720

SUMMARY

A displacement control device that can be installed within multilayer elastomeric base isolation bearings is described. The device acts to limit the displacement of the bearings and can also be used to take uplift tension forces if necessary. The device was tested in earthquake simulator tests of a nine-story, 1/4-scale steel frame model, conducted at the Earthquake Simulator Laboratory of the Earthquake Engineering Research Center, University of California, Berkeley. The model was isolated using eight multilayer elastomeric bearings, four of which were located at the corners of the model and contained the displacement control devices. The system was subjected to a large number of simulated earthquakes. In some tests the design acted to control the displacements and in others where uplift forces at the corners were generated the devices simultaneously limited the displacements and carried the uplift forces.

The test results show that the action of the devices is smooth and that there is no sudden jerk when one comes into action. The devices can perform as a fail-safe system for base-isolated buildings and in this role they would be designed to act only when the ground motion is greater than that for which the base isolation system has been designed.

INTRODUCTION

Base isolation is becoming a widely accepted seismic design strategy for low-rise, stiff buildings in seismic regions. However, it has generally been accepted that elastomeric isolators should not be expected to resist tension forces. A medium-rise building, even when isolated, could generate an overturning moment that would cause uplift on some isolators. If a method could be devised to enable the elastomeric isolators to sustain tension then the technique could be extended to a building with a larger number of stories than has so far been contemplated, provided that the superstructure of the building is sufficiently stiff.

Some tension capacity in the isolation bearings would be advantageous for both low-rise and medium-rise buildings for another reason. It would provide a fail-safe system for limiting the maximum displacement of the isolators. This is important since for a fixed-base design, member ductility and design redundancy are counted upon to provide overstrength while isolation systems without fail-safe characteristics appear to have only the one line of defense, namely that of the isolation system.

Fail-safe systems to be used with isolation systems have of course been designed. In some, the building comes against a stop when a certain displacement is exceeded [1]. In others, sliding surfaces come into contact beyond a specified horizontal displacement [2]. In this paper a new fail-safe system will be described and shown that it is effective and practical. The system fits within a standard elastomeric bearing requiring no modification of the foundation or surrounding retaining wall. Its effectiveness has been demonstrated by tests on the earthquake simulator at the Earthquake Engineering Research Center (EERC) of the University of California at Berkeley. It has been used in an isolation system tested under a tall steel frame model which, under moderate earthquake loading, generated uplift forces on the bearings.

PROPERTIES OF THE TEST STRUCTURE

The shaking table experiments were carried out on a nine-story three-bay welded steel frame model (Figure 1) which represents a section in the weak direction of a typical steel frame building at approximately 1/4-scale. The lowest story of the model was 4 feet (1.22 m) high and the others were 3 feet (0.91 m) high. The top of the model was almost 29 feet (8.84 m) above the top of the isolation bearings and the width of the model was 18 feet (5.49 m). The aspect ratio was large enough that the model would

experience uplift in the corner columns with moderate accelerations in the structure. The additional mass necessary for similitude requirements was provided by concrete blocks at each floor level. The total weight of the structure and the concrete blocks was 122 kips (543 kN). The two rows of columns were bolted to stiff wide flange sections (W8x31) which ran the length of the base of the model, and with cross beams these represented the base mat of a prototype structure. The base isolators were placed between these W8x31 beams and the shaking table.

The first two natural frequencies of the model structure in the fixed-base condition were 2.8 Hz and 9.0 Hz. These were determined by taking fast Fourier transforms (FFTs) of the ninth floor horizontal acceleration time history when the model was subjected to a free-vibration pull-back test. In a similar fashion the first three natural frequencies of the base-isolated model were found to be 1.11 Hz, 6.09 Hz, and 13 Hz.

ISOLATION SYSTEM

The isolation system consisted of eight natural rubber bearings of multilaminate construction with a bearing located under each column of the steel frame. The natural rubber compound used in these bearings is designated EDS 39 [3] by the Malaysian Rubber Producers Research Association. It is a high strength lightly filled rubber which has a shear modulus of approximately 100 psi (689 kPa) at 50% shear strain. It is relatively low in damping; the equivalent viscous damping ratio at 50% shear strain is in the range of 5% to 7%.

The bearing design is shown in Figure 2. The bearings are designed with four dowel holes in the top and bottom end plates to provide shear connections between the isolation system and the structure. When the uplift restrainers were not in place the dowel holes contained 3/4-inch (19 mm) long tapered pins. In this configuration the frame was free to uplift and no tension was generated in the rubber.

Each bearing provided a stiffness of 1.6 kips/inch (2.8 kN/cm) at 50% shear strain, or 1.125 inches (28.6 mm) displacement, which provided an isolation frequency for the model of 1.01 Hz. This frequency was too low to generate uplift forces at the corner columns for this model since the isolation system did not permit enough transmission of accceleration to the model to generate tension in the corner columns. In order to increase the likelihood of uplift, lead plugs were inserted in the central holes of the four bearings under the center columns. Lead yields at a stress of approximately 1500 ksi (10,000 MPa) which corresponded to 1.8 kips (8.0 kN) shear load in a lead plug, and at 50% shear strain the effective contribution of each lead plug to the stiffness was 1.6 kips/inch (2.8 kN/cm). With the four bearings filled with lead the isolation frequency at 50% shear strain rose to 1.24 Hz. The increased stiffness and the tendency of the lead plugs to generate response in the higher modes made uplift more probable with moderate table inputs.

UPLIFT RESTRAINT AND DISPLACEMENT CONTROL DEVICE

A device that provides uplift restraint and displacement control was inserted in each of the four corner bearings (Figure 3). It consists of two high-strength bolts contained in a cylindrical sleeve that allows a certain amount of free movement of the bolts. The devices have hemispherical ends held in hemispherical recesses which were machined into the 1 inch (25.4 mm) thick top and bottom plates of the bearings. When the bearing is not displaced the bolt heads are together in the center of the sleeve and when the bearing is displaced through a preselected distance the device becomes taut. Since uplift occurs at maximum displacements the device will also resist the uplift forces in addition to acting as a displacement control device. A further modification necessary to enable the bearing to resist uplift is that the four dowel holes in each end plate be threaded and the bearing firmly connected to the foundation and to the superstructure. If displacement control only is needed it is unnecessary to bolt the bearings to the foundation and the superstructure and dowels can be retained to transfer shear loads. It should be noted that the lead plugs in the center four bearings were used in these tests only for the purpose of producing uplift at the corners at moderate levels of earthquake input. They are not an essential component of the isolation system.

As mentioned above, the uplift restraint and displacement control device can move a certain distance within the cylindrical sleeve before going taut. When the bearing has displaced horizontally through this distance the bolt heads are constrained by the ends of the sleeve and at this displacement the horizontal

stiffness of the bearing is greatly increased. While this results in a sudden increase in stiffness there is not a sudden stop because, although the restraint device is now inextensible, the bearing can continue to deform horizontally by deforming vertically at the same time. Thus, the horizontal stiffness which is normally low becomes comparable with the much higher vertical stiffness.

Tests were performed on individual bearings in a testing device which applied a constant axial load to the bearings while forcing them through several cycles of constant amplitude sinusoidal displacement. Force versus displacement curves were obtained from these tests at several different displacement amplitudes (Figure 4). Possibly because of friction between the device and the surface of the hole in the bearing, the transition from the stiffness at low shear strain to the combined stiffness of the bearing and the restrainer device at high shear strains was smooth. This smooth transition in stiffness at the initial operating displacement (u_d) of the device had the effect of minimal excitation of higher structural frequencies and led to a far better structural response than might have been expected if the stiffness had been sharply bilinear.

A linear elastic analysis of the response of the bearing with the device was carried out taking into account the vertical and horizontal stiffnesses of the natural rubber bearing, the displaced geometry of the bearing (Figure 5), and assuming small strains in the steel restrainer and a constant axial dead load (W) on the bearing. With these assumptions the following relationship for force versus displacement of the uplift restrainer bearing was obtained. The derivation is given in Reference [4].

$$F_x = k_h\, u_x \qquad \text{for } u_x \leq u_d$$

and

$$F_x = k_h\, u_d + \left[k_h + \frac{k_v\, u_d^2}{h^2 + \frac{k_v}{k_d} L^2} \right] e_x \qquad \text{for } u_x \geq u_d$$

$$\text{with } u_d = \left[L^2 - h^2 \right]^{\frac{1}{2}} \text{ and } u_x = u_d + e_x \,;$$

where the terms are defined as

P = axial force in the restrainer device;

F_x = shear force applied to the bearing;

W = axial dead load on bearing;

L = length of restrainer device when $P = 0^+$;

k_v = vertical stiffness of bearing;

k_h = horizontal stiffness of bearing;

k_d = axial stiffness of restrainer device;

u_x = horizontal displacement of bearing;

u_d = horizontal displacement of bearing when $P = 0^+$;

δ_y = decrease in height of bearing due to W; and

h = total height of rubber $- \delta_y$.

The curve predicted by these equations is shown in Figure 4.

TEST PROGRAM

In order to study the effectiveness of the uplift restraint device the model was subjected to three different earthquake signals on the shaking table. The earthquake characteristics ranged from predominantly low frequency ground motion (Mexico City and Bucharest) to moderately high frequency ground motion (El Centro). The earthquake test signals used were digitized records based on the earthquake ground motion data recorded at the sites listed below.

(1) Imperial Valley Earthquake (El Centro) of May 18, 1940 — S00E component, peak ground acceleration (PGA) = 0.35g.

(2) Bucharest Earthquake (Building Research Institute) of March 7, 1977 — EW component, PGA = 0.21g.

(3) Mexico City Earthquake (Mexico City Station SCT) of September 19, 1985 — S60E component, PGA = 0.20g.

The records were time-scaled (compressed) by a factor of two to satisfy similitude requirements for the 1/4-scale model.

Table 1 lists the input signals used in the testing program and the maximum model responses to the input signals for the tests on the model in the free-to-uplift condition. Table 2 lists the maximum responses of the model when it was restrained against uplift.

TEST RESULTS

Each earthquake input signal was run at increasing levels of peak table acceleration until the model lifted off the unrestrained corner bearings. Time histories of column vertical displacement (Figure 6) showed that column uplift of 0.75 inch (19 mm) occurred during the El Centro PGA = 0.842g test. This result for the 1/4-scale model implied 3 inches (76 mm) of column uplift of the corner columns in a corresponding full-scale structure. The Mexico City PGA = 0.217g test caused 0.47 inch (12 mm) column uplift and the Bucharest PGA = 0.348g test caused 0.61 inch (16 mm) column uplift. It should be noted that column uplift occurred at the time of peak horizontal displacement. Also associated with column uplift were large vertical accelerations which were generated in the structure when the structure dropped back to its foundation. Vertical accelerations of approximately 1g occurred in the model when the structure was subjected to the El Centro motion which caused 0.75 inch (19 mm) column uplift.

Although the bearings dissipated little energy axially during the uplift motion they did continue to dissipate energy in shear. The column uplift distorted the shapes of both the shear and axial hysteresis loops (Figure 7). The effect of column uplift on the axial hysteresis loop is clear — the vertical displacement of the column base increased from about 0.1 inch to about 0.75 inch (2.5 - 19 mm) without any change in the axial load on the bearing. Column axial load appears to have more of an effect on the shear hysteresis loop when it comes back into contact with the bearing than when it lifts off the bearing. Keeping in mind the fact that positive horizontal displacement corresponds to tensile axial load on the bearing, the shear hysteresis loop appears to become unstable at the time of maximum compressive load (15 kips (67 kN) due to overturning plus the bearing dead load of 8 kips (36 kN)). This was probably due to the combination of a decrease in the thickness of the rubber layers and a sudden drop in shear stiffness because of the sudden increase in axial load on the bearing. This phenomenon would probably only be observed in cases where the axial loads approach the buckling load. Nevertheless, this behavior is clearly undesirable since any sudden drop in the stiffness of the isolation system could result in significantly larger bearing displacements.

Although significant column uplift occurred during the largest magnitude tests using the three test signals the bearing shear connection did not uncouple as had happened during previous tests performed on a base-isolated reinforced concrete structure [5]. Recognizing the importance of preventing uncoupling of the bearings during extreme uplift events, longer dowels were designed for this test series to overcome the problem. A dowel length of 0.75 inch (19 mm) was used, and this proved to be sufficient to prevent uncoupling.

After the tests on the free-to-uplift structure were completed the unrestrained corner bearings were replaced by bearings containing the uplift restrainer device. The model was then subjected to the same set of earthquake ground motions. The records of corner column vertical displacement (Figure 6) and

horizontal bearing displacement confirm that the restrainer device not only prevented the uplift seen previously but also essentially limited the relative horizontal displacement of the structure to the free displacement of the restrainer device.

The peak story acceleration profiles are plotted for the El Centro tests on the isolated structure with and without the displacement control device (Figure 8). For the shaking table inputs which did not cause the restrainer device to go into tension the profiles are similar in shape to the free-to-uplift profiles. The acceleration profiles for the tests which had peak table accelerations similar to those in the tests on the free-to-uplift model where uplift occurred are different. The magnitude of the peak roof acceleration when the displacement control device was activated was almost double for the El Centro test signal.

The restrainers also reduced the magnitude of the vertical acceleration response from approximately 1g in the free-to-uplift test to approximately 0.3g. The effect of the restrainer on the shape of the axial and shear force hysteresis loops for a restrained bearing is seen in Figure 9. Both hysteresis loops are now stable and the shear loop reflects the bilinear stiffness properties characteristic of the displacement control device.

CONCLUSIONS

Although earthquake simulator tests have been performed previously to evaluate base isolation systems, these studies were all performed on short stiff structures. Base isolation has not been proposed for taller buildings because of the obvious problems of column uplift and longer structure period.

The displacement control device described herein successfully restrains columns from uplift during earthquake motions having magnitudes which previously caused column uplift in the unrestrained nine-story steel frame model. The device was installed within the hollow core of a multilayer elastomeric bearing and was placed under each corner column of the base-isolated structure. The interior columns were supported by the similar bearings but without the displacement control device. The devices were set to allow only 2.25 inches (57.2 mm) of free horizontal displacement before they were fully extended, thereby limiting further horizontal displacement because of the increased horizontal stiffness of the isolation system. The vertical component of force in the device served to restrain the column against uplift.

For earthquake tests during which the device extended fully, the maximum story accelerations were about double those for similar input signal magnitudes where the device had not been installed. The higher frequency responses of the structure were not increased at the times when the device was fully extended because of the smooth transition in the horizontal bearing stiffness.

While column uplift was the primary concern in the isolation tests on the nine-story steel frame, the uplift restrainer devices could clearly also be used for horizontal displacement control. The devices would act in this capacity as a fail-safe mechanism, and would be designed to come into effect only when the bearing displacement exceeded the maximum allowable displacement or the design displacement of the isolation system.

ACKNOWLEDGEMENTS

The research reported herein was supported by the National Science Foundation under Grant No. ECE-8414036, and was conducted at the Earthquake Engineering Research Center of the University of California at Berkeley. The views expressed here are those of the authors and not necessarily those of the National Science Foundation.

REFERENCES

1. A. G. Tarics, "The Implementation of Base Isolation for the Foothill Communities Law and Justice Center," Report the the National Science Foundation and the County of San Bernardino, Reid and Tarics Associates, San Francisco, (1984).

2. J. M. Kelly, K. E. Beucke and M. S. Skinner, "Experimental Testing of a Friction Damped Aseismic Base Isolation System with Fail-Safe Characteristics," Report No. UCB/EERC-80/18, Earthquake Engineering Research Center, University of California, Berkeley, (1980).

3. "Natural Rubber Engineering Data Sheets," Malaysian Rubber Producers Research Association, Hertford, England.

4. J. M. Kelly, M. C. Griffith and I. D. Aiken, "A Displacement Control and Uplift Restraint Device for Base Isolated Structures," Report No. UCB/EERC-87/03, Earthquake Engineering Research Center, University of California, Berkeley, (1987).

5. M. C. Griffith, J. M. Kelly and I. D. Aiken, "Experimental Evaluation of Seismic Isolation of a 9 Story Braced Steel Frame Subject to Uplift," Report No. UCB/EERC-88/05, Earthquake Engineering Research Center, University of California, Berkeley, (1988).

FILE NO.	RUN	SPAN	PK. TABLE ACCEL. (g)	PK. MODEL ACCEL. (g)	REL. BEARING DISPL. (in.)	UPLIFT (Y/N)
860708.03	√4 ec	150	.313	.244	.904	N
860708.04	√4 ec	225	.460	.288	1.712	N
860708.05	√4 ec	300	.604	.453	2.848	Y
860708.06	√4 ec	400	.842	.607	3.784	Y
860709.01	√4 buc	275	.241	.293	1.825	N
860709.02	√4 buc	350	.296	.444	2.729	Y
860709.03	√4 buc	400	.343	.537	3.259	Y
860709.04	√4 mex	175	.146	.254	1.898	N
860709.05	√4 mex	250	.194	.425	3.063	N
860709.06	√4 mex	275	.219	.586	3.372	Y
860709.07	√4 mex	275	.217	.520	3.416	Y

buc = Bucharest signal; ec = El Centro signal; mex = Mexico City signal.

Table 1 Maximum Model Responses on Bearings without Displacement Control Device

FILE NO.	RUN	SPAN	PK. TABLE ACCEL. (g)	PK. MODEL ACCEL. (g)	REL. BEARING DISPL. (in.)	UPLIFT (Y/N)
860711.03	√4 ec	150	.336	.279	.637	N
860711.04	√4 ec	225	.487	.341	1.150	N
860711.05	√4 ec	225	.420	.372	1.313	N
860711.06	√4 ec	300	.627	.503	1.930	N
860711.07	√4 ec	350	.726	.727	2.451	N
860711.08	√4 ec	400	.832	.851	2.958	N
860711.09	√4 buc	400	.351	.620	2.854	N
860711.10	√4 mex	275	.168	1.524	3.635	N

Table 2 Maximum Model Responses on Bearings with Displacement Control Device

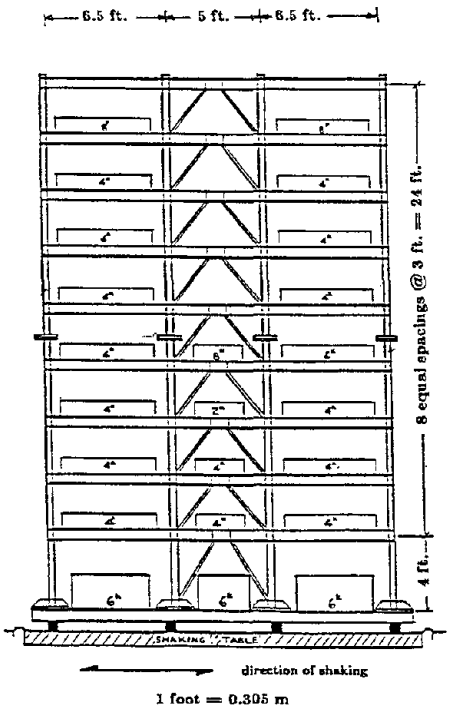

FIGURE 1 NINE STORY STEEL TEST FRAME

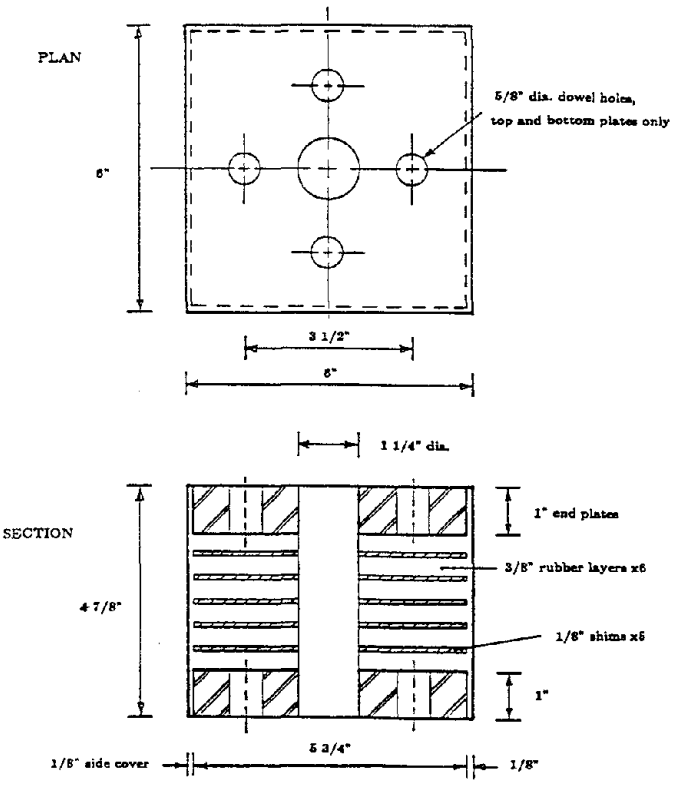

FIGURE 2 LEAD PLUG BEARING DETAILS

1 inch = 25.4 mm

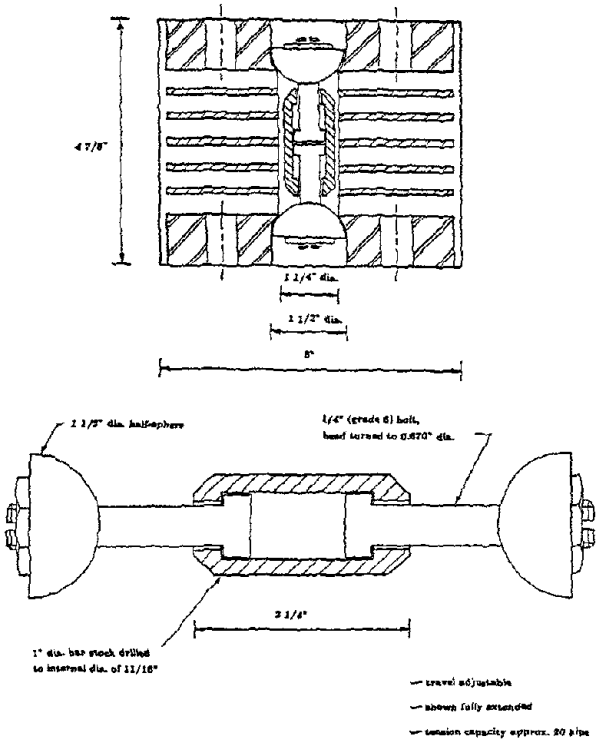

FIGURE 3 BEARING MODIFIED TO ACCEPT DISPLACEMENT CONTROL DEVICE

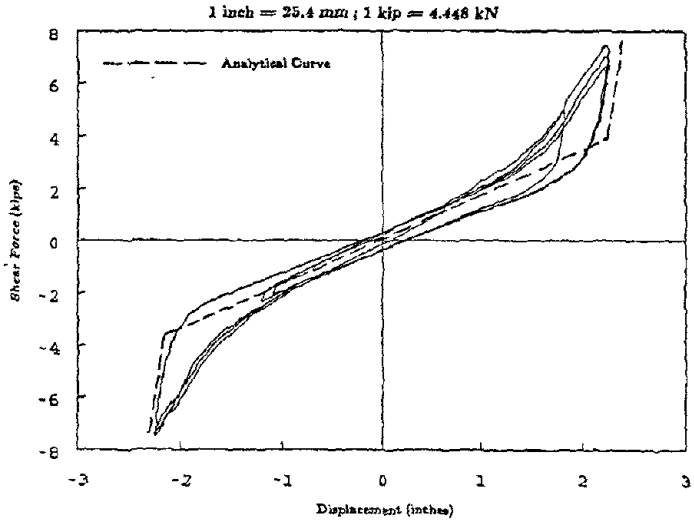

FIGURE 4 EXPERIMENTAL AND PREDICTED FORCE-DISPLACEMENT CURVES FOR RESTRAINED BEARING

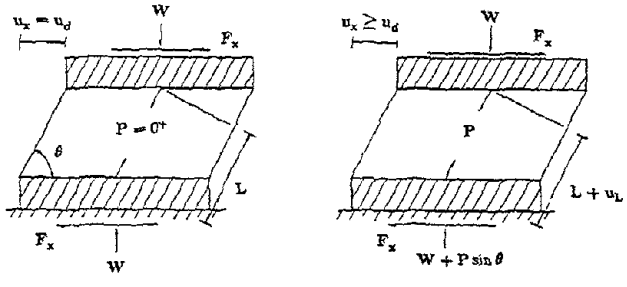

FIGURE 5 RESTRAINER BEARING FORCE DIAGRAM

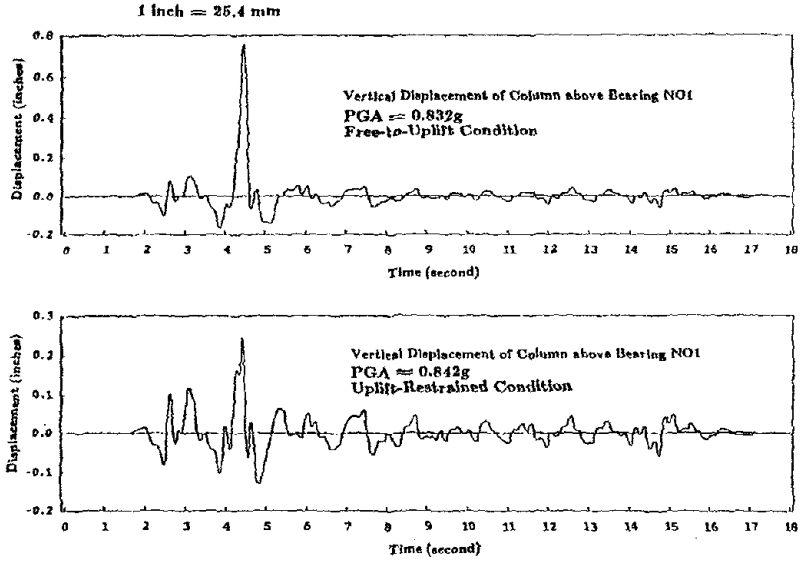

FIGURE 6 COLUMN VERTICAL DISPLACEMENT DURING *EL* CENTRO TESTS

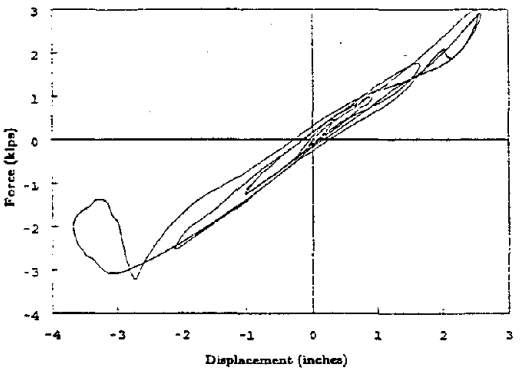

(a) Shear Force vs. Horizontal Displacement

1 inch = 25.4 mm ; 1 kip = 4.448 kN

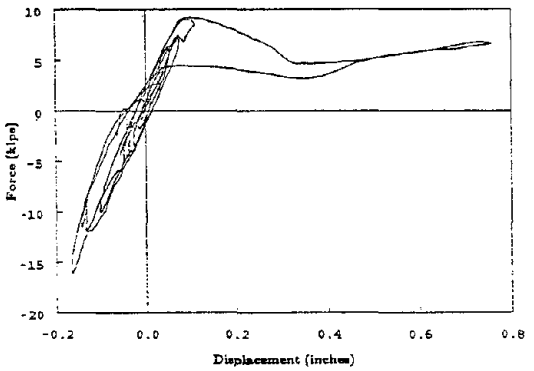

(b) Axial Force vs. Vertical Displacement

FIGURE 7 SHEAR AND AXIAL FORCE BEHAVIOR OF BEARINGS IN FREE-TO-UPLIFT CONDITION DURING EL CENTRO, PGA = 0.842g

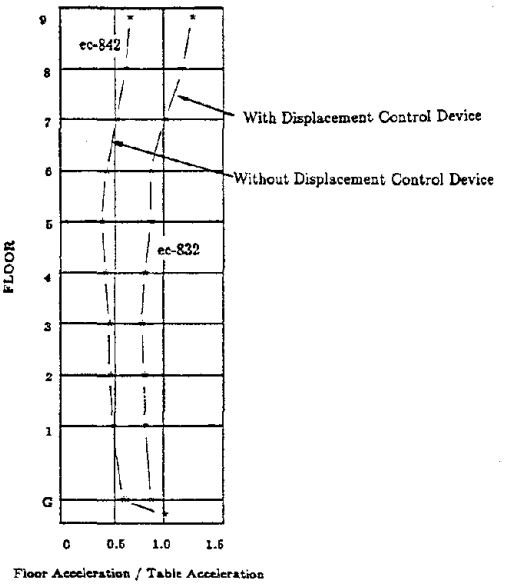

FIGURE 8 PROFILES OF PEAK STORY ACCELERATIONS FOR THE FREE-TO-UPLIFT AND UPLIFT-RESTRAINED ISOLATION CONDITIONS

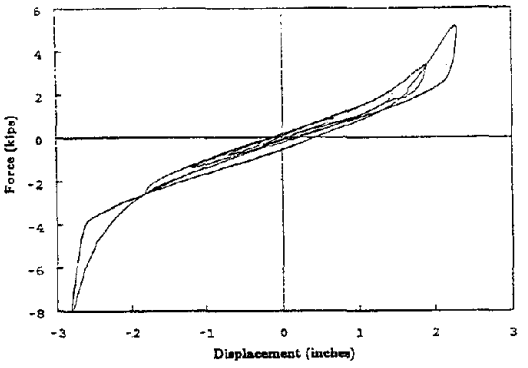

(a) Shear Force vs. Horizontal Displacement

1 inch = 25.4 mm ; 1 kip = 4.448 kN

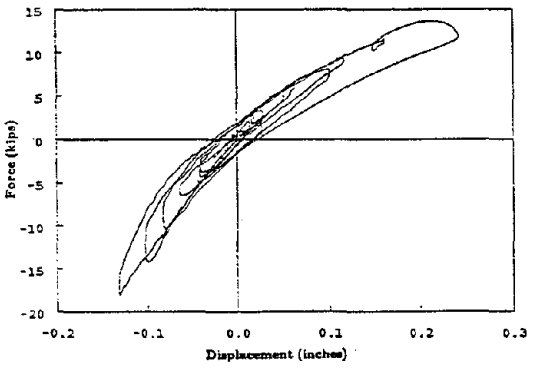

(b) Axial Force vs. Vertical Displacement

FIGURE 9 SHEAR AND AXIAL FORCE BEHAVIOR OF BEARINGS IN UPLIFT-RESTRAINED CONDITION DURING EL CENTRO, PGA = 0.832g

COMBINING SLIDERS AND TENSION CONTROLLED ELASTOMERIC BEARINGS FOR BASE ISOLATION

James M. Kelly[1] and Michel S. Chalhoub[2]

1 Professor of Civil Engineering, University of California, Berkeley
2 Research Engineer, University of California, Berkeley

SUMMARY

Essential requirements of a base isolation system include wind restraint, stability, and fail safe capacity. A new base isolation system combining sliders and rubber bearings inherently satisfies all three requirements, and possesses other advantages. The system was tested on the earthquake simulator at the University of California under the base of a one-fourth scale nine story steel structure. The base behaves as fixed for low magnitude inputs. When sliding starts the rubber bearings provide additional stiffness and recentering. Displacements are better controlled than those for a purely elastomeric isolation system. The fail safe capacity is provided by tension restrainers installed inside the rubber bearings, and by the constant contact of the base with the sliders. Base shear hysteresis loops are drastically enlarged by the addition of the sliders.

INTRODUCTION

Base isolation is a seismic design strategy based on the concept that a structure can be partially protected from earthquakes by uncoupling it from the ground. This can be achieved by mounting the structure on horizontally flexible foundations capable of accommodating large displacements acting as shock absorbers.

The buildings which have been constructed world-wide using the concept have in the main been built using laminated elastomeric bearings of natural or artificial rubber, often with additional elements for the purpose of enhanced energy dissipation and control of displacements under wind loading [1-6].

In the U.S., the first building using laminated elastomeric pads for seismic protection is the Foothill Communities Law and Justice Center in Rancho Cucamonga [7], dedicated on 20 March 1986. In Salt Lake City, the City and County building is in the process of being rehabilitated by the insertion of elastomeric isolators between its base and the ground [8]. Base isolation seems to be the best solution for the rehabilitation of old buildings of historical and architectural importance.

There are several important requirements for base isolation systems. They must provide a low frequency response with high damping in order to limit displacements. The system must incorporate a wind restraint and have a recentering effect. In the case of an unexpectedly severe earthquake, the system must provide a fail safe capacity. Sliding systems have been proposed as aseismic isolation systems due to their inherent simplicity and low cost. However, they present problems such as excessive drift and lack of fail safe constraints. This is due to their force-deflection characteristics which show no resistance once their sliding threshold is overcome. In addition they may produce a very low effective frequency leading to extremely large relative displacements.

The arrangement described and tested in the present research combines sliders with elastomeric bearings and produces a system with the desirable features of base isolation systems with none of the disadvantages of a purely sliding system. The major difference is the drift control due to the stiffness of the rubber springs which includes a recentering effect. The damping needed in a base isolation system is here replaced by friction energy dissipation.

Sliding bearings are used in large reinforced concrete structures to control shrinkage cracking and thermal deformations, but in that application, they include a mechanism that locks up the structure at one end, so that the sliding elements play no role in its seismic response. The present system incorporates the sliding elements into the seismic response. Since this system is but a slight modification of an existing practice, it is possible that the resistance to its use by civil engineers will be less than that which has been manifested against

the rubber bearing isolation system which is a more radical departure from conventional engineering.

TEST STRUCTURE AND ISOLATION SYSTEM

Test Structure. A one-fourth scale nine-story steel frame was used in this experiment. The structure, its dimensions, and the story weights distribution are given in Ref. 10. There is a critical category of medium size structures between 9 and 20 stories, for which isolation can be effective but for which uplift can play a role in the performance of the isolation system. The structure simulated in the present experiment falls into this category. Its fixed base fundamental frequency was of 3.4 Hertz, corresponding to 1.7 Hertz in the prototype and it was well suited to examine the possibility of extending the concept of base isolation further to the category of medium rise buildings.

Elastomeric Bearings. The natural rubber bearings used with the sliders had a 5.75x5.75 inch square cross section and consisted of 6 layers of rubber 3/8 inch thick each, interleaved by 5 steel shims 0.2 inch thick each. The top and bottom limiting plates were 1 inch thick. The bearings had a 1.25 inch diameter central hole. A 1/8 thick protective rubber layer was glued to their lateral surface. Their effective horizontal stiffness was about 1.3 k/in at 50% shear strain. Under the structure, each rubber bearing carried an axial load of 9 kips.

Uplift Restrainers. Since excessive tension could be destructive for multilayered rubber bearings, a device was installed inside each of the outer corner bearings. Its role was to control uplift and horizontal drift. A restrainer consisted of a short steel sleeve and two steel bolts. The bolts were connected to the two limiting plates of the bearing. The assemblage locks when the bolts are pulled a certain distance apart. Its tension capacity was about 18 kips. The horizontal displacement of the bearing at which the restrainer locks up can be adjusted by appropriate tightening of the bolts. At the level of horizontal displacement corresponding to the locking of the restrainers, the stiffness of the unit increases substantially. It should be noted that the restrainer system does not act as a sudden stop. Although the restrainer is effectively rigid when it acts, the bearing can continue to displace horizontally by shortening vertically, thus the normally low horizontal stiffness is replaced by a stiffness that is related to the much higher vertical stiffness. A detailed description of the restrainer design and its performance is given in Ref. 9.

Sliding Bearings. The basic components of a slider consisted of a teflon layer bearing against a stainless steel plate. A separate testing of the sliders showed a coefficient of friction that depended on the sliding velocity and the pressure in the material.

The Combined Isolation System. The system using the combination of the elastomeric bearings, the sliders, and the uplift restrainers was designed to fulfill four important goals:

(1) **Providing Threshold for Base Motion.** The friction of the sliders keeps the structure from moving under wind loading and small earthquakes. The base shear must exceed a certain limit in order to start sliding. This limit is proportional to the friction coefficient, and to the fraction of the weight of the building carried by the sliders. This wind restraint capacity was experimentally verified by applying earthquake signals of small magnitudes. The ability of an isolation system to ensure a certain fixity for low level dynamic loading makes it practical and avoids unnecessary movement of the structure when seismic isolation is not yet needed.

(2) **Additional Stiffness and Restoring Effect.** Once the shear force that activates the sliders is reached, the elastomeric bearings provide an additional stiffness. The force-deflection relationship of the combined system is bilinear with infinite initial stiffness followed by the finite stiffness of the rubber bearings. This arrangement also insures a restoring force that brings the structure to almost its original at rest location.

(3) **Control of Drift and Overturning.** The presence of tension devices inside the bearings, limits the horizontal drift of the base and the uplift of the columns. If a medium rise building were to be base isolated, it would be essential to control its uplift; tension devices would prevent catastrophical overturning in the case of an unexpectedly severe earthquake. Also, they provide stiffening as they come close to locking, this compensates for the softening of the rubber bearings when they are largely deflected.

(4) **Fail Safe.** The horizontal stiffness of rubber bearings decreases with shear strain and axial load, and at a certain level of axial load they become unstable. For this reason systems consisting of solely rubber bearings use other accessories to provide fail safe action on which the structure can depend in case of

bearing buckling or bearing roll out. For the combined rubber-slider system, this problem is non existent since the structure is constantly resting on the sliders and when the base drift is very large some of the axial load that was initially carried by the rubber bearings is transferred to the sliders.

The test structure, the isolation system, and the mechanical properties of its components are described in detail in Ref. 10.

EARTHQUAKE SIMULATOR TEST RESULTS

Displacements. One of the advantages of the combined sliding bearing rubber bearing system over a purely rubber system was the reduction in the relative base displacements. For example, the respective peak base displacements for the rubber system and the combined rubber-sliders system were 2.06 in. and 0.77 in. for the El Centro record at 200 horizontal span (1 in. peak table displacement), and 2.57 in. and 0.94 in. for the Bucharest record at 250 horizontal span (1.25 in. peak table displacement). yielding 2.06 and 0.75 as respective base displacement amplification. Under the Mexico City input, the peak base displacement for the rubber system was of 0.11 in. at 50 horizontal span (0.25 peak table displacement), while it was 0.09 in. for the combined rubber-sliders system at 150 horizontal span (0.75 in. peak table displacement). In sum, the rubber system amplified the base drift about 3 times more than the combined rubber-sliders system did.

Deflected shapes of the structure at the instants where each story individually reached its maximum displacement showed that the presence of the sliders in the proportion used (31 % of the total bearing area, carrying 60% of total weight) did not change the main effect of an elastomeric base isolation system, that is causing the structure to move like a rigid body. For the Mexico City signal at 375 span the story drifts at t=21.9 sec. were 0.13, 0.08, 0.08, and 0.07 in. for the first, second, third and ninth stories respectively while the base drift was 1.91 in. For the San Francisco record at 200 span the story drifts at t=2.4 sec. were 0.07, 0.05, 0.05, and 0.03 in. for the first, second, third and ninth stories with a base drift of 0.84 in. In sum, for most table motions, base displacements were larger than story drifts by a factor of 10 to 15.

The magnitudes for all signals applied to the isolated structure were larger than the ones applied to the fixed base structure by a factor of 2 to 3, yet resulting in story drifts of about the same order of magnitude. For instance, the maximum story drifts for the 3rd, 6th, and 9th stories under the San Francisco signal applied at 100 horizontal span (PTA=0.7 g) were of 0.07, 0.07, and 0.04 in. for the fixed base condition, while they were of 0.06, 0.06, and 0.05 for the isolated structure on the combined system for the same signal at 200 horizontal span (PTA=1.2 g).

Recentering provided by the rubber bearings was demonstrated by the negligible base drift offset at the end of each test run. The largest offset encountered throughout the whole testing program corresponded to a Mexico City input of 1.9 in. peak table displacement and yet the offset was only about 0.2 in. The table displacement time history shows a significant sway of 1.8 in. in one direction followed by small amplitude cycles of less than 0.5 in., the base, however, recentered with an offset of only 0.04 in. Very small cycles were enough to recenter the system even though they were preceded by a strong ground motion in only one direction. Table 1 shows some results.

Previous work has been done on the sliding of rigid blocks under earthquake excitations [12]. Various materials were used between the block and its supporting slab to change the coefficient of friction which varied between 10% and 30%. In Ref. 12, pp. 3.39-3.42, the time histories of the block displacement relative to the table under the Pacoima Dam s74w component of the 1971 earthquake accelerogram showed extremely large end-of-signal offsets that reveal the need for a recentering spring.

Accelerations. By the addition of sliders, the accelerations in the structure were slightly higher than the ones corresponding to a solely rubber system. The peak base acceleration to peak ground acceleration ratio increased from an average of 0.5 for the system using elastomeric pads, under input spans around 150, to an average value of 0.9 for the system that included sliders, for input spans as high as 375. The isolated base acceleration amplification ratio was highest for the Mexico City signal (about 1.7) and lowest for the San Francisco signal (about 0.6), because high frequency signals induced more sliding. Intermediate values were found for most of the other earthquakes that had their input energy spread over a wider range of frequencies. Significant reduction in the accelerations was provided by the combined system since for the fixed base case, the amplification ratios reached 4 or 5 for input spans of about 100.

Effect of Input Magnitude. The amplification of base displacement increased with the magnitude of the input until a certain span level (around 300), after which the ratio started decreasing due to the tension devices. Generally, the displacement amplification ratio for the base was for all spans between 0.5 and 1.0, and for the ninth story, between 0.9 and 1.5. The amplification ratios for the accelerations generally decreased with increased span. However, the lowest value was between 300 and 350 horizontal span, due to the stiffening caused by the tension devices locking.

If a building under consideration is expected to house equipment, sensitive to high frequencies and high accelerations, the proportion of sliders in the isolation system should be reduced. However, if good isolation is required with reduction in displacements, a high proportion of sliders can be used.

Energy Dissipation Efficiency. It is commonly accepted that the total energy transmitted from the ground to a structure is absorbed under two different forms. The first one is due to the elastic strain, the second one is due to the plastic strain. The elastic strain energy is temporarily absorbed by the structure, part of it is transmitted back to the soil through the foundations and the other part released as kinetic energy causing amplification in the response quantities. For this reason, conventional design has tendency to dissipate the major amount of the total energy absorbed by means of inelastic behavior of structural and non-structural elements. It is shown here that the major portion of the total energy absorbed was dissipated by friction, minimizing the amplification in the response, and concentrating the deformations at the isolation interface.

For each test run, the total dissipated energy was calculated by numerical integration of the areas enclosed in the base shear hysteresis loops. The total input energy was obtained by integrating the product of the base shear with the table displacement time histories. The proportion of the total input energy dissipated by hysteresis was above 90% for all eight table motions used.

To evaluate an equivalent viscous damping, the total energy E dissipated for each test run, was divided by an estimated number of significant cycles N, read from the base drift time histories. Thus, $\omega_d = E/N$ provides an average value of energy dissipated per cycle. An equivalent elastic work, was expressed as $\omega_s = F_m \delta_m/2$ where F_m is the maximum base shear and δ_m the maximum base relative displacement. An equivalent viscous damping ratio is then evaluated by $\xi_e = \omega_d/4\pi\omega_s$. The values of ξ_e were consistently clustered around 20% for all signals. A detailed account of the test series results is given in Ref. 11.

CONCLUSIONS

Various base isolation systems have been previously proposed but most of them necessitated separate accessories to provide wind restraint, displacement control, stability, and fail safe capacity. Systems that provide large reduction of ground borne accelerations usually consist of horizontally flexible rubber bearings only. These however might present stability problems in case of accidental excessive base drift, and thus need a support on which the structure can depend in case of bearing buckling or roll-out. On the other hand, a system that is very economical and closest to an existing practice consists of frictional elements currently used for purposes other than earthquake protection. The two above systems were combined yielding a new system that satisfies all requirements for the earthquake isolation of structures. The threshold of sliding provides wind restraint, the friction provides energy dissipation, the reinforced rubber bearings carry part of the vertical load and recenter the structure, and the tension device keeps the structure from uplifting. Furthermore, since the base is constantly resting on the sliders, they act as inherent fail safe.

The earthquake simulator testing showed that the inclusion of teflon sliders in a base isolation system drastically improves the control of displacements on the cost of a slight decrease in its efficiency of reducing accelerations. For the same model, where fixed base tests resulted into acceleration amplification ratios as high as 6, the combined slider-rubber system yielded ratios around 1, while a solely rubber system typically yields ratios around 0.5. However, solely rubber systems resulted into base displacements around 3 times the ones that correspond to the combined slider-rubber system.

The high energy dissipation is characterized by a large area enclosed in the base shear hysteresis loops, and on the average the system provided an equivalent damping of about 20%.

The Alexisismon system uses sliders combined with unreinforced neoprene pads that act as restoring springs [13]. This system has two major differences with the one described herein. The neoprene springs in the Alexisismon system are not allowed to carry any axial load and all the weight of the building is carried by the sliders. This causes the base shear sliding threshold to be totally controlled by the weight of the building

and by the friction coefficient of the sliders which changes with velocity, temperature and pressure. Thus, the above arrangement do not allow the designer to distribute the weight of the building on both sliders and reinforced bearings. Also, excessive drift of the base may cause tension in the neoprene springs and thus make them more vulnerable to external factors, while in the case of the reinforced rubber bearings used here, they are initially under compression by carrying a fraction of the weight of the structure and this risk is eliminated. Also for the present system, in the case of accidental excessive base drift, part of the vertical load that is initially carried by the rubber is transferred to the sliders and prevents the rubber bearings from buckling.

REFERENCES

[1] Kelly J. M., "Aseismic Base Isolation: review and bibliography", *Soil Dynamics and Earthquake Engineering*, Vol. 5, No. 3, 1986.

[2] Kelly J. M., and Tsztoo D. F., "The Development of Energy-Absorbing Devices for Aseismic Base Isolation Systems", *Report No. UCB/EERC-78/01*, Earthquake Engineering Research Center, University of California, Berkeley, California, 1978.

[3] Kelly J. M., and Chitty D. E., "Testing of a Wind Restraint for Aseismic Base Isolation",*Report No. UCB/EERC-78/20*, Earthquake Engineering Research Center, University of California, Berkeley, California, 1978.

[4] Kelly J. M., Beucke K. E., and Skinner M., "Experimental Testing of a Friction Damped Aseismic Base Isolation System with Fail-Safe Characteristics", *Report No. UCB/EERC-80/18*, Earthquake Engineering Research Center, University of California, Berkeley, California, 1980.

[5] Delfosse G. C., "Full Earthquake Protection through Base Isolation System", *7th World Conference on Earthquake Engineering*, Istanbul, Turkey, Vol. 8, p. 61, 1980.

[6] Plichon C., Gueraud R., Richli M. H., and Casagrande J. F., "Protection of Nuclear Power Plants against Seism", *Nuclear Technology*, Vol. 49, pp. 295-306, 1980.

[7] Tarics A. G., "The Implementation of Base Isolation for the Foothill Communities Law and Justice Center", *Report to the National Science Foundation and the County of San Bernardino*, Reids and Tarics Associates, San Francisco, CA, 1984.

[8] Walter M., Elsesser E., and Allen E. W., "Base Isolation of the Existing City and County Building in Salt Lake City",*Proceedings, Seminar on Base Isolation and Passive Energy Dissipation*, ATC-17, Applied Technology Council, San Francisco, pp. 113-122, 1986.

[9] Kelly J. M., Griffith M., and Aiken I.,"A Tension Restraint for Uplift Control", *Report No. EERC-87/08*, Earthquake Engineering Research Center, University of California, Berkeley, 1987.

[10] Kelly J. M., and Chalhoub M. S., "Earthquake Simulator Testing of a Combined Sliding Bearing and Rubber Bearing Isolation System", *Report No. EERC-87/04*, Earthquake Engineering Research Center, University of California, Berkeley, 1988.

[11] Chalhoub M. S., "Theoretical and Experimental Studies on Earthquake Isolation and Fluid Containers", *Ph.D. Dissertation*, University of California, Berkeley, 1987.

[12] Aslam M., Godden W.G., and Scalise D.T., "Sliding Response of Rigid Bodies to Earthquake Motions", *Report to the U.S. Energy Research and Development Administration*, Lawrence Berkeley Laboratory, 1975.

[13] Ikonomou A. S., "Alexisismon Isolation Engineering for Nuclear Power Plants", *Nuclear Engineering and Design*, Vol. 85, 2, pp. 210-216, 1985.

Table Motion	Base Offset (inches)	PTD (inches)	PTA (g)
El Centro 1940 s00e, span 375	-0.061	1.96	0.73
Mexico City 1985 s60e, span 375	0.212	1.97	0.18
Bucharest 1977 s00e, span 300	-0.006	1.56	0.27
Miyagi-Ken-Oki 1978 w00s, span 350	0.119	1.81	0.33
Pacoima Dam 1971 s16e, span 350	-0.025	1.82	0.49
Parkfield 1966 n65e, span 350	-0.041	1.82	0.41
San Francisco 1957 s80e, span 200	0.037	1.01	1.20
Taft 1952 s69e, span 350	0.057	1.83	0.72

Table 1 Base displacement end-of-signal offsets for eight earthquake records with their corresponding peak table displacement (PTD) and peak table acceleration (PTA).

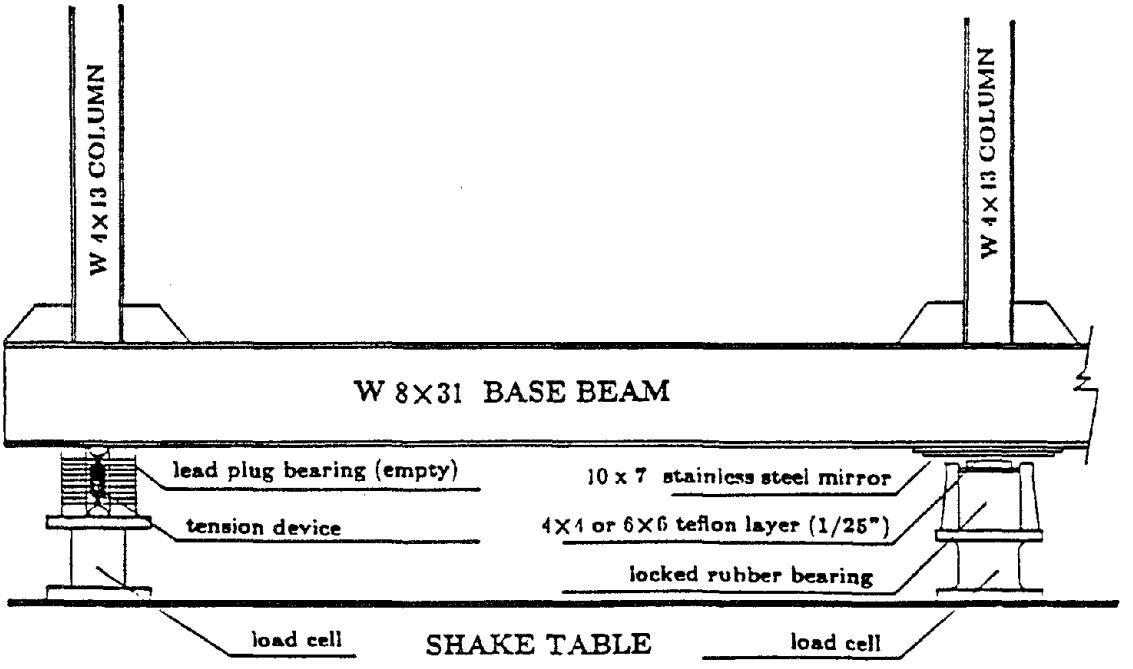

Figure 1 Disposition of tension controlled bearing under corner column and teflon-stainless steel slider under adjacent interior column, repeated 4 times for entire model.

INELASTIC BEHAVIOR AND MODELING OF REINFORCED CONCRETE COLUMNS UNDER MULTIDIRECTIONAL SEISMIC EXCITATIONS

by Stephen A. Mahin[1]

[1] Professor of Civil Engineering, University of California, Berkeley, CA 94720, USA

SUMMARY

During the past two decades considerable research has been performed to assess the performance of reinforced concrete columns subjected to the biaxial flexure and/or varying axial forces associated with multidirectional seismic excitations. These studies are reviewed in this state-of-the-art report. Emphasis is initially placed on experimental studies on column elements and on observed behavioral characteristics. Techniques for modeling this behavior for seismic analysis are then presented. Some examples are shown to illustrate design implications. Recommendations for future experimental and analytical research are offered.

INTRODUCTION

The partial and complete collapse of reinforced concrete buildings during recent earthquakes has demonstrated the need to design columns to be able to withstand the multidirectional nature of seismic excitations and response (1- 3). However, the inelastic flexural behavior of such columns is complicated by the wide variety of physical phenomenon involved. At the section level, such phenomenon include yielding, Baushinger effects and buckling of the reinforcement, cracking and constitutive nonlinearity in the concrete, shear, bond deterioration, and spalling of the concrete cover. Moreover, in the case of beam-columns, the presence of axial load influences the closing of cracks, the location of the neutral axis along and across the member and the plastic hinge length (4, 5). These factors and their interaction complicate structural response and its prediction.

To mitigate such problems, model building codes often stipulate a strong column - weak girder design philosophy. However, it may not be possible to achieve this ideal situation in practice due to the special conditions existing at the base of a structure, the contribution of the slab to the strength of the beams, variations in axial loads (associated with overturning moments developed in the structure as well as with the vertical component of ground motions), the structural system used, the presence of nonstructural elements, and of course, biaxial bending effects. Thus, careful study is required to understand the behavior of individual columns, to assess the effects of this behavior on structural response and to devise appropriate design methods.

The intent of this report is to review current experimental and analytical research related to reinforced concrete columns subjected to bidirectional flexure and/or varying axial loads. Emphasis is placed on the behavior and modeling of individual elements. Implications for design will be highlighted as will future research needs. Additional sources of information may be found in the companion papers and state-of-the-art reports (6-13) as well as in Refs. 2 and 14.

EXPERIMENTAL STUDIES

A variety of experimental research programs have been carried out to assess the flexural response of columns under bidirectional excitations (14- 24). Most of these studies have been performed on simple

cantilever specimens. While a variety of tests have examined the effects of monotonically increasing bilateral loads (e.g. Ref. 25), fewer studies have considered cyclic loading conditions representative of seismic excitations. In these latter tests, square or circular cross sections are generally considered, with relatively few tests of rectangular or more complex shaped sections (24). Predetermined displacement histories (resembling stylized diagonal, elliptical, diamond, square or clover leaf patterns) are generally employed in the tests. Because of the need for loading simplicity, many tests have been performed without axial load (19, 22). Other cases have considered constant axial forces (14, 15, 17, 18). Recently, members with varying axial loads (proportional to lateral forces) have been tested for uniaxial (4, 11, 26) and biaxial bending (12, 24). Only a few investigations have considered axial load variations that are not proportional to lateral displacement, and these have been generally restricted to uniaxial bending (4, 11, 26, 27). To have a better understanding of column behavior under earthquake like excitations, a few on-line control (pseudodynamic) tests have been performed (11, 17). Actual dynamic tests of column elements are few. However, several shaking table tests have been performed on framed structures with bidirectional base excitations (e.g., Refs. 28 and 29).

Experimental results indicate that well confined columns with adequate shear reinforcement subjected to biaxial flexure sustain more damage, suffer more deterioration of stiffness and strength, and exhibit substantially more complex and irregular hysteretic characteristics than comparable columns or beams loaded in uniaxial flexure (Figs. 1 and 2). The responses are very sensitive to the history and pattern of loading applied. In comparison with uniaxial response, stiffness under loading in one direction decreases significantly as a result of previous or concurrent loading in the transverse direction. This is primarily due to the effects of cracking associated with the additional load or of accumulated damage from the prior transverse loading (cracking and spalling of concrete, Baushinger effects in the reinforcement and bond deterioration). Stiffness reductions of 50% or more have been observed within the working load regime. While principles of mechanics indicate that reductions in projected strength would be expected under bilateral loading, the effect of cyclic loading in the transverse direction is generally much greater than would be anticipated on this basis alone (due in part to increased damage). In some cases, strength reductions in one direction have exceeded 80% when loads are applied in the orthogonal direction even though displacements are held constant in the first direction. Damages (concrete cracking and spalling as well as steel strains) are consistently larger than those for uniaxial loading to similar displacement levels. The larger the axial load level the more pronounced are these effects (12).

Some of these characteristics can be observed in the envelopes of cyclic response hysteretic loops (24) shown in Fig. 3. In this figure Curve 1 corresponds to a uniaxially loaded specimen. Curve 2 corresponds to an identical specimen loaded at a 45 degree inclination. As would be expected on the basis of flexural theory, this envelop is lower. Curve 3a corresponds to the point on a clover leaf displacement pattern which is in uniaxial deformation. Comparison of this curve to Curve 1 indicates a significant reduction. Curve 3b corresponds to the point on the clover leaf which is aligned with the points plotted on Curve 2. Thus, prior cracking, straining and damage due to transverse loads does adversely influence inelastic behavior.

Concurrent variation of axial load leads to even more complex hysteretic behavior as a result of the dependence of flexural strength and neutral axis position on axial load. Axial loads that vary in proportion with lateral deformation produce systematically unsymmetrical hysteretic loops for either uniaxial (4, 24, 26) or biaxial (12, 24) flexure. For low compressive mean loads, apparent stiffness and strength increase with increasing axial load and vice versa. For loads near the balanced point hysteretic loops are more symmetrical, but still show complex triaxial interaction effects (12). Results show that columns often suffer a preferred orientation for damage (toward the compression-most load direction) which can reduce the capacity in this direction (24, 26). For axial loading which varies non-proportionately with lateral deformations (4, 26) very irregular hysteretic loops can be obtained which do not match commonly used analytical representations or design approximations.

Results also indicate that a significant proportion of the specimen deformations are associated with slippage of the reinforcement at the end of the specimen (22, 23, 24). Few tests (e.g., Ref. 23) have been instrumented sufficiently to identify quantitatively the contribution of the resulting fixed end rotations to the total lateral displacement and to study the mechanism of bond deterioration.

Most of the specimens considered in the above studies were proportioned so that flexure dominated the behavior. A few test have, however, been made of short columns (effective length to depth < 2.5) in which shear would be expected to control response (22, 23, 30 - 32). These tests indicate that

cycling and increased axial loading accelerates deterioration of the section once the lateral displacement at which maximum resistance occurs is exceeded. Figure 4 compares the cyclic response of a bilaterally loaded short column to an identical unidirectionally loaded one (marked M).

In view of the limited data on bilateral behavior of columns, additional tests would be desired to extend the range of sections considered, axial loads imposed, amounts and detailing of transverse and longitudinal reinforcement used, and loading histories and boundary conditions employed. On-line and shaking table tests are required to assess response under realistic earthquake excitations and to identify any rate effects. Loading histories (proportional and nonproportional variation of axial loads) need to be established to better evaluate analytical models. Tests to assess slenderness and lateral stability issues need to be performed. Specimens need to be instrumented to measure local deformations so that analytical models can be better assessed. In particular, information regarding bond slip and the distribution of flexural, axial and shearing deformations along the length of the member are needed. To facilitate analytical and design related studies data should be put in a form that can be easily exchanged between researchers.

ANALYTICAL MODELS

A variety of analytical techniques have been developed to model the inelastic cyclic behavior of reinforced concrete column sections and elements. The increasing availability of low cost, high performance engineering workstations has lead to the development of interactive, graphically oriented computer programs for the design (33) and analysis (34, 35) of biaxially loaded sections. For example, in the case of Ref. 35, arbitrarily shaped sections can be analyzed considering the section to be discretized into an arbitrary grid of concrete and steel fibers. The program is capable of considering a series of sequentially applied load and/or deformation histories. As such, information can be obtained on three dimensional interaction curves for various limit states (first cracking, yielding, ultimate strength, etc.), biaxial moment- curvature hysteretic loops, axial load-elongation relations, stress state and neutral axial position. The interactive nature of such programs permits rapid assessment of the effects of variations in design parameters and loading conditions.

The techniques used to model complete members depend on the type of information needed, the quality of information available regarding the column to be analyses and the nature of the applied loads. For example, at the preliminary stages of analysis or to assess the effects of overall design changes on global response quantities, relatively simple macroscopic models may be most appropriate (3, 36). If more detailed information is required regarding the damage state in individual elements, more traditional finite element approaches are appropriate. However, due to the level of computational effort required a variety of simplifying assumptions are generally introduced. To achieve computational economy phenomenological idealizations are often utilized which mimic the observed behavior of columns. The applicability of such models is limited to the loading and boundary conditions considered in their formulation. More refined physical and analytical representations are able to account for the spatial and temporal variation of inelasticity. However, they require more precise information regarding the constitutive modeling of materials, distribution of damage, bond slip relations, and so on. In many cases this information must be estimated.

Comprehensive bibliographies of the literature may be found in Refs. 2, 14 and 15. A brief summary is presented here to indicate the approaches used in modeling damage due to material inelasticity. Studies for considering geometric nonlinearities and long term effects are treated elsewhere (e.g., see Ref. 37). Two basic approaches have been used to model the damage at the element's critical regions: one in which inelasticity is averaged (lumped) at the ends, or another in which damage is monitored at various sections along the length. These will be referred to as lumped and distributed plasticity models, respectively. In nearly all of the available models, shear and torsional deformations are disregarded, and plane sections are assumed to remain plane.

Lumped Plasticity Models Emerging from series and parallel element representations for beams (38-40), various unilateral beam-column models have attempted to included axial loading-bending moment interaction by idealizing the critical regions by inelastic rotational springs governed by a series of phenomenological rules (41, 42). The portions of the member between these idealized plastic regions are assumed to remain elastic. Typically, the rules included do not account for the effects of axial load on member stiffness in the elastic range. Only a few of these phenomenological models account for the variations in axial stiffness that result from yielding or axial load fluctuations (42).

It is possible to extend such phenomenological rules into two or three dimensions using plasticity theory. While the basic approach used for elasto- plastic materials may be suitable for steel structures and certain ranges of behavior for reinforced concrete structures (36), this tends to ignore the stiffness degradation and pinching typically associated with reinforced concrete columns. Takizawa and Aoyama developed a modified formulation (14) utilizing a trilinear envelop curve and a set of degradation rules for cycling. Constant axial load is assumed. The plasticity model consists of two similar ellipses, representing "cracking" and "yielding" surfaces in a biaxial moment plane (Fig. 5). Since the "cracking" surface is used to control the stiffness changes on initial flexural cracking as well as on unloading from a yielded state, its shape must be empirically defined. Rules for movement, relative sliding and expansion of these two surfaces are based on plasticity theory. As shown in Fig. 1, results obtained correlated very well with overall nature of experimental data (14, 21). However, discrepancies are noted for local details in the hysteretic loops. This is apparently a consequence of the underlying phenomenological model and the assumptions inherent with the plasticity approach. This approach has been extended to more complex situations including varying axial load (13, 21, 43). In this case, phenomenological rules are established for axial force versus elongation and three dimensional plasticity models are employed. Good correlations (Fig. 1) have been reported in recent studies (13, 43).

Another approach to concentrated plasticity models is to employ a simplified physical representation of the critical cross section(s). Although a detailed fiber representation could be used, in most cases a simpler idealization is employed. The model proposed by Lai, Will and Otani (44) uses a five spring idealization for the critical end region (Fig. 6). The four corner springs represent the effective combined stiffness and strength of the steel rebars and concrete in compression and of the steel reinforcement in tension. The fifth center spring is used to represent the effective compressive properties of the concrete in this region. The effective properties of these springs are based in part on the deformations in a bar over its development length into the beam-column joint core. A bilinear, degrading stiffness, phenomenological model is used to represent the cyclic characteristics of these springs. The concrete contribution is modeled by an estimate of the indentation of the joint core concrete in compression and the strength of the concrete. The areas and locations of the effective concrete springs are assigned such that the moments and axial loads predicted match those for the balanced point based on flexural theory. The element has demonstrated good analytical correlation for members with constant axial loads (44) and incorporates many features not possible with other models, such as variation of elastic stiffness with axial loading.

Refinements have been made to these multi-spring elements based on the use of different methods for estimating the effective properties and locations of the springs (10, 12, 45, 46). Recent studies have considered cases of varying axial loads (12) and unsymmetric hysteretic loops of the type observed experimentally were predicted. The model is, however, unable at this stage to account for deterioration of the capacity and spalling of the concrete which can result in overall softening of the member. Nonetheless, the model provides an economical and realistic method for predicting the response of members which having loading and boundary conditions consistent with the development of the controlling analysis parameters and assumptions.

Distributed Plasticity Models To obtain solutions for more general loading conditions or more severe deformation ranges, a more complex approach is needed which monitors response at the stress or section level. A complete finite element approach would be possible, but is often disregarded as being computationally prohibitive. However, in a recent study of uniaxial column behavior under nonproportional unilateral loading, Saadeghaviri and Foutch (9) have employed isoparametric plane stress elements for the concrete and bar elements of the reinforcement. Post-crushing and cracking are modeled to account for the confinement and tension stiffening of the concrete which are not directly accounted for in previously mentioned models. However, extension to bidirectional excitations and inclusion of bond slip and shear cracking effects would substantially increase computational requirements so that this approach might be impracticable for studies of complete structures.

Because of these computational demands, most finite element studies have idealized behavior around the section. In some cases, this has been on the basis of classical plasticity (43), or as shown in Fig. 7, by explicitly refining the section into fibers (Refs. 2, 15, 37, 47-50). A high degree of refinement is generally necessary to approximate the plastification in the critical regions, making such models computationally intensive, especially if fiber section representations are used. Considerable computational

economy can be achieve by approximating the distribution of section flexibilities, as introduced in Refs. 47 and 52.

Several recent studies have utilized a flexibility approach to formulate the element tangent stiffness matrix (2, 11, 47, 52). Nonetheless, most formulations follow the standard displacement approach to determine the distribution of deformations along the member (53). These are typically approximated by means of cubic Hermitian polynomials. Very good correlations with experimental results have been obtained for unilateral cases with large variations in axial load (11, 47) and for bilateral excitations (Fig. 8) under constant axial loads (2). For improved representations of internal damage and improved computational efficiency, recent models have introduced variable interpolation functions (2, 47, 51). The fiber representations used in these models allows for a wide variety of physical phenomenon to be accounted for with little need for empirically based analysis parameters. Moreover, such models can provide the user with detailed information regarding response.

When the standard displacement approach is adopted to estimate the internal distribution of deformations, numerical problems have been encountered at or near the point of maximum resistance and the member begins to soften. This has been observed for both section and member models (2, 47, 49, 51, 54). For example, the simple cantilever column shown in Fig. 9 exhibits deformation softening as the concrete at the base begins to spall. In a standard displacement approach for estimating internal deformations, the interior sections have no way of detecting the resulting loss of capacity at the end section. Consequently, they continue to load while the end section sheds load. Thus, equilibrium is violated and results are erroneous or unstable. To correct for this, many studies have adopted unrepresentative material properties, especially for the concrete where elasto-perfectly plastic behavior is often assumed. In such cases, the resulting predictions may be unrealistic, especially if large deformations and damage are expected. A detailed study of the reasons for this unsatisfactory numerical behavior has been recently made (51).

An alternative formulation has been proposed to correct for these numerical problems considering unilateral and bilateral excitations with varying axial loads (2, 51). In this formulation, the tangent stiffness matrix for the member is computed using the flexibility interpolation approach (47, 52). To reduce the number of sections required, flexibilities are assumed to vary linearly between monitored sections. The tangent stiffness is obtained by inversion of the member flexibility matrix. Deformations at the critical end sections are based on variable transformation functions based on the current distribution of flexibilities along the member. To obtain the deformations at internal sections a mixed approach is used. Moments and axial loads at the internal sections are determined by equilibrium considerations. The current state of deformations at these sections is then obtained by iteration on the curvatures and axial strains at the section until the target forces are matched. In this way, equilibrium and stability are preserved. Illustrations of this technique indicate good correlation with experimental data and stability under large deformations as shown in Fig. 9.

Experimental results indicate that a considerable portion of the deformations in a column may be associated with anchorage slip (22, 23, 24). Multi-spring models (44) directly incorporate this source of deformation in their phenomenological rules. In the case of distributed plasticity models, fixed end rotations associated with bond slip in the anchorage regions need be treated with special elements devised for this purpose (2). Figure 10 shows a case where such springs are employed at the base of a simple cantilever column. The response is somewhat softer, as expected, when the bond slip is included. Significantly, for this example, the mode of failure is also different since the bond slip is sufficient to prevent crushing of the concrete at the deformation levels considered.

Short Columns The complexities of the inelastic cyclic behavior of short columns dominated by shear makes precise modeling much more difficult. Pinched and degrading hysteretic rules have been proposed on a phenomenological basis. A conceptual model for predicting deformations has been proposed and has led to some success (32). In addition analytical procedures for estimating the behavioral modes of short columns and their shear capacities have been proposed (30-32).

Other Analysis Approaches Little work has been done to assess the effects of initial conditions associated with aging on the behavior of concrete columns. For static loading conditions, several analytical studies have focused on creep and shrinkage effects on performance (e.g., Ref. 37). While this may not have a profound effect on the seismic response of many structures, it may influence dynamic characteristics as well as the distribution and intensity of damage. Similarly, few studies have examined the effect of

slenderness on column behavior. Studies for static loading (e.g., Ref. 55) have not been extended into the dynamic range. Slenderness effects may have a significant effect on the performance of structures in which columns are subjected to high fluctuations in axial loads due to overturning moments or vertical ground accelerations (9). An assessment of realistic boundary conditions for determining slenderness effects in actual structures would be valuable.

While a variety of analysis procedures have been developed, the limitations and capabilities of these models have not been fully assessed. In part, the analytical models are capable of providing the user with detailed information about the local stress/strain state and damage in the members analyzed. Typically, detailed experimental information of this type is not available for correlation with analytical results. Thus, an integrated approach is needed in which more refined information is obtained in experiments and the analysis results are used to give insight into critical loading conditions for use in formulating experimental programs. A systematic study of the various analytical models available is desirable. Clearly, each of the various approaches will have advantages in certain situations. However, the limits of the ranges of applicability of the models have not been established. These types of studies will also suggest improvements in the modeling procedures, and possibly enable substantial simplifications to be made in some circumstances. Models should be able to reflect the softening behavior associated with spalling or disintegration of the concrete cover. Additional work is needed to devise numerically efficient and stable methods for predicting this behavior. The work in Ref. 51, while providing a practicable solution, does not address the larger theoretical problems related to nonproportional deformations, softening and numerical instability. Similarly, theoretical research is needed to improve our capabilities for predicting response as influenced by shear and bond slip as well as the initial conditions associated with creep and shrinkage. As these models are verified, they should be implemented in general purpose computer programs to enable researchers and designers to assess the effects of bidirectional column behavior on the overall performance of structures.

EFFECTS ON STRUCTURAL BEHAVIOR

While the effect of column behavior on structural performance is treated in Ref. 6, it is useful to look at a few implications of the observed and predicted performance of bilaterally loaded columns. The complex hysteretic relations observed are likely to have significant effects on structural response. For example, consider a simple cantilever column with a constant axial load (about 60% of balanced). The section considered is rectangular. If this column is subjected to an imposed displacement which is skewed with respect to the principal axes of the section, the response is initially, as expected, oriented along the direction of deformation. However, as the base of the column begins to yield, the moment paths in the two directions no longer follow the direction of the imposed tip displacement, as shown in the moment plane projection in Fig. 11. As a result of spalling the moment path diverges quickly form the theoretical interaction surface. The deterioration in strength is preferentially oriented toward the nearest principal axis. This is a consequence of the distribution of damage occurring in the base section. While not shown here (2), such behavior has a complex influence on dynamic response. Simple sinusoidal force excitations at the top of such a cantilever, for example, produce complex and offset elliptical orbits. Thus, skewed unidirectional excitations will produce bidirectional response in the inelastic range.

The dynamic response of the roof of a two-story concrete frame is shown in Fig 12 (2). For the Taft record scaled to produce 60%g in the larger component, the orbital motion of the roof to bidirectional excitations is complex. For this structure, the maximum response obtained in each direction is slightly less than that obtained in that direction if only unidirectional excitation is considered. However, the maximums occur bilateral response occurs almost simultaneously in the two principal directions so that the maximum amplitude of response is significantly worse for the bilaterally loaded case. More significantly, the damage to the columns as inferred from the analysis is also considerably worse. For example, Fig. 13 shows for the bidirectionally excited structure the strain history for one of the base steel reinforcing bars in a column as well as the local energy dissipation history for that column's hinge region. For comparison, the maximum values obtained for a comparable unidirectional analysis is shown as well. This comparison indicates that damage and energy dissipation demands can be substantially larger for biaxially loaded structures than for unidirectionally loaded ones. Additional studies of the implications of the biaxial behavior of columns are needed (see Ref. 6). These examples do indicate that current modeling techniques are capable of providing the user with detailed and meaningful information regarding global response and local damage.

CONCLUSIONS

Recent experimental and analytical research has led to substantial improvements in our understanding of the performance of columns subjected to bilateral flexure and constant or varying axial loads. However, the behavior is quite complex, and influenced by a wide variety of parameters, including the loading history, the boundary conditions, the shape, proportioning and detailing of the column. Results indicate that the biaxial response of columns can be substantially different than that observed for uniaxial bending. Variation of axial load leads to even greater differences. In many cases, in comparison with unilaterally loaded columns, bilateral loading results in a lower stiffness and strength, a more rapid deterioration in strength and stiffness, and greater damage. The consequences of this on design must be addressed by integrated analytical and experimental research as indicated above for individual columns as well as for complete structural systems. Analytical models are capable of providing detailed information on global as well as local response. However, the capabilities and limitations of various methods remain to be fully assessed. On-going developments in computer software and hardware will permit these techniques to be utilized in the design of complex structures and in the development of more reliable design procedures.

ACKNOWLEDGMENTS

The author is grateful for the discussions and comments by many individuals. In particular, the assistance of Dr. C. Zeris in preparing the material for this report is greatly appreciated. The research performed by the author was sponsored by the National Science Foundation. The comments and conclusions in this report are, however, those of the author alone.

REFERENCES

1. Okada, T., et al, "Analysis of the Hachinohe Library Damaged by 1968 Tokachi-Oki Earthquake", **Proceedings**, U.S.-Japan Seminar on Earthquake Engineering, Sendai, Sept. 1970.
2. Zeris, C., Three Dimensional Nonlinear Response of Reinforced Concrete Buildings," Thesis presented to the University of California, at Berkeley, Calif., in partial fulfillment of the requirements for the degree of Doctor of Philosophy, 1986.
3. Selna, L.G., Morill, K.B., and Ersoy, O.K., "Earthquake Response Analysis of the Olive View Hospital Psychiatric Day CLinic", **Earthquake Engineering and Structural Dynamics**, Vol. 3, 1974.
4. Abrams, D., "Influence of Axial Force Variations on Flexural Behavior of R/C Columns," ACI Structural Journal, Vol. 84, No. 3, May - June 1987.
5. Otani, S. and Cheung, V., "Behavior of RC Columns under Biaxial Lateral Load Reversals," **Publication 81-02**, Univ. of Toronto, Canada, Feb. 1981.
6. Shibata, A., "State-of-the-Art Report: Inelastic Response of 3-D Frame Structures and Multi-Directional Seismic Forces on Structural Components," **Proceedings**, 9WCEE, Japan, 1988.
7. Paulay, T., "State-of-the-Art Report: Inelastic Behavior of Slab-Beam- Column Connections Under Multi-direction Reversal Loading," **Proceedings**, 9WCEE, Japan, 1988.
8. Shen, J. and Weng, Y., "Inelastic Behavior of Reinforced Concrete Columns Under Biaxial Reversal Lateral Load," **Proceedings**, 9WCEE, Japan, 1988.
9. Foutch, Douglas A. and Saadeghaviri, M. A., "Inelastic Behavior of RC Columns under Cyclic Vertical and Lateral Loads," **Abstract Volume**, 9WCEE, Japan, 1988.
10. Jiang, Y. and Saiidi, M., "Simulating Combined Axial Load/Biaxial Bending Response Using a Five-spring Hysteretic Element," **Abstract Volume**, 9WCEE, Japan, 1988.
11. Ristic, D., Yamada, Y., and Iemura, H., "Inelastic Stress-Strain Based Seismic Response Prediction of RC Structures Considering Dynamically varying Axial Forces," **Proceedings**, 9WCEE, Japan, 1988.
12. Li, K. and Aoyama, H., "Reinforced Concrete Columns Under Varying Axial Load and Bi-directional Lateral Load Reversals," **Proceedings**, 9WCEE, Japan, 1988.
13. Fukuzawa, E., Isozaki, Y. and Fujisaki, K., "Elastic-plastic Earthquake Response Analysis of RC Frame in Consideration Fluctuation of Axial Forces on Columns," **Proceedings**, 9WCEE, Japan, 1988.
14. Takizawa, H., and Aoyama, H., "Biaxial Effects in Modeling Earthquake Response of R/C Structures." **Earthquake Eng. and Struct. Dyn.**, V. 4, No. 6, 1976.
15. Aktan, A.E., Pecknold, D.A.W. and Sozen, M.A., "Effect of Two-Dimensional Earthquake Motion on a Reinforced Concrete Column", **Structural Research Series No. 399**, University of Illinois, Urbana, May 1973.

16. Takiguchi, K., Kokusho, S., and Okada, K., "Experiments on RC Columns Subjected to Biaxial Bending Moments, **Transactions**, AIJ, No. 229, March 1975.
17. Okada, T., Seki, M. and Asai, S., "Response of Reinforced Concrete Columns to Bi-Directional Horizontal Force and Constant Axial Force", **Bulletin**, Earthquake Resistant Structure Research Center, The Institute of Industrial Science, University of Tokyo, No. 10, Dec. 1976.
18. Takiguchi, K. and Kokusho, S., "Hysteretic Behaviors of Reinforced Concrete Members Subjected to Bi-Axial Bending Moments", **Proceedings**, 6WCEE, New Delhi, India, 1977.
19. Otani, S. and Tang, C.S., "Behavior of Reinforced Concrete Columns Under Biaxial Lateral Load Reversals - (I) Pilot Test," **Publication 78-03**, University of Toronto, Toronto, Feb. 1978.
20. "A List of Experimental Results on Deformation Ability of RC Columns under Large Deflection" (No. 3), Building Research Institute, Tsukuba, Japan, Feb. 1978.
21. Otani, S., Cheung, V.W.-T. and Lai, S.S., "Behavior and Analytical Models of Reinforced Concrete Columns under Biaxial Earthquake Loads", **Proceedings**, Third Canadian Conference on Earthquake Engineering, Vol. 2, Montreal, June 1979.
22. Otani, S. and Cheung, V., "Behavior of RC Columns under Biaxial Lateral Load Reversals," **Publication 81-02**, University of Toronto, Canada, Feb. 1981.
23. Saatcioglu, M. and Ozcebe, G., "Effect of Bar Slip on Hysteretic Behavior of Concrete Columns," **Proceedings**, Fifth Canadian Conference on Earthquake Engineering, Ottawa, Canada,1987.
24. Low, S. and Moehle, J., Experimental Study of Reinforced Concrete Columns subjected to Multiaxial Cyclic Loading," **Report No. UCB/EERC - 87/14**, University of California, Berkeley, Sept. 1987.
25. Hsu, C., "Biaxially Loaded L-shaped Reinforced Concrete Columns," **Journal of Structural Engineering**, ASCE, V.III, No. 12, Dec. 1985.
26. Kreger, M. and Linbeck, L., "Behavior of RC Columns Subjected to Lateral and Axial Load Reversals," **Proceedings**, 3USNCEE, South Carolina, 1986.
27. Gilbertsen, N. and Moehle, J., "Experimental Study of Small Scale RC Columns Subjected to Axial and Shear Force Reversals," **Structural Research Series No. 481**, University of Illinois, July 1980.
28. Shahrooz, B. and Moehle, J., "Experimental Study of Seismic Response of RC Setback Buildings," **Report No. UCB /EERC - 87/16**, University of California, Berkeley, Oct. 1987.
29. Oliva, M. and Clough, R., "Shaking Table Testing of a RC Frame with Biaxial Response," **Report No. UCB/EERC- 80/28**, University of California, Berkeley, 1980.
30. Ramirez, H. and Jirsa, J., "Effect of axial Load on Shear Behavior of Short RC Columns under Cyclic Lateral Deformations," **PMFSEL Report No. 80-1**, University of Texas, Austin, TX, June 1980.
31. Maruyama, K., Ramirez, H., and Jirsa, J., " Short RC Columns under Bilateral Load Histories," **Journal of Structural Engineering**, ASCE, V.110, No. 1, Jan. 1984.
32. Umehara, H. and Jirsa, J. "Short Rectangular RC Columns Under Bidirectional Loading," **Journal of Structural Engineering**, V. 110, No. 3 March 1984.
33. "PCACOL: Program for the Analysis of Columns in Biaxial Bending," Portland Cement Assoc., Skokie, IL, 1987.
34. Kaba, S., and Mahin, S., "Interactive Computer Analysis Methods for Predicting the Inelastic Cyclic Behavior of Structural Sections," **Report No. EERC 83-18**, University of California, Berkeley, CA 1983.
35. Zeris, C. and Mahin, S., "Interactive Biaxial Column Analysis Program: Bicola," Department of Civil Engineering, University of California, Berkeley, 1987.
36. Nigam, N.C., "Yielding of Framed Structures Under Dynamic Loads", **Journal of the Engineering Mechanics Division**, ASCE, Vol. 96, No. EMS, Oct. 1970.
37. Kang, Y., and Scordelis, A., "Nonlinear Geometric, Material and Time Dependent Analysis of Reinforced and Prestressed Concrete Frames." **Rep. UC-SESM No. 77-1**, University of California, Berkeley, Calif, 1977.
38. Clough, R., and Johnston, S., "Effect of Stiffness Degradation on Earthquake Ductility Requirements," **Proceedings**, Second Japan Earthquake Engrg. Symp., Tokyo, Japan, 1966.
39. Takeda, T., Sozen, M.A. and Nielsen, N.N., "Reinforced Concrete Response to Simulated Earthquakes", **Journal of the Structural Division**, ASCE, Vol. 96, No.ST12, Dec. 1970.
40. Golafshani, A., and Powell, G. H., "Drain-2D2: A Computer Program for Inelastic Seismic Response of Structures," Thesis presented to the University of California, at Berkeley, Calif., in partial fulfillment of the requirements for the degree of Doctor of Philosophy, 1986.
41. Saatcioglo, M., Derecho, A. and Corley, W., "Modeling Hysteretic Behavior of Coupled Walls for Dynamic Analysis," **Earthquake Engineering and Structural Dynamics**, V.11, No. 5, Sept. - Oct. 1985.

42. Takayanagi, T., and Schnobrich, W., "Non linear analysis of coupled wall systems." **Earthquake Eng. and Struct. Dyn.**, 7(1), 1979.
43. Chen, P. "Generalized plastic hinge concepts for 3D beam column elements." **Rep. No. UCB/EERC-82/20**, University of California, Berkeley, CA 1982.
44. Lai, S., Will, G., and Otani, S., "Model for inelastic biaxial bending of concrete members." **J. Struct. Engrg.**, ASCE, V. 110, No. ST 11, Nov. 1984.
45. Lai, S., "Post-Yield Hysteretic Biaxial Models for Reinforced Concrete Members," **ACI Structural Journal**, Vol. 84, No. 3, May - June 1987.
46. Ghusn, G. E., Jr., and Saiidi, M. (1986). "A hysteresis model for biaxial bending of reinforced concrete columns," **Proceedings** , 3USNCEE, Charleston, S.C., Aug. 1986.
47. Kaba, S., and Mahin, S. A., "Refined modeling of reinforced concrete columns for seismic analysis," **Rep. No. UCB/EERC-84/03**, University of California, Berkeley, Calif, 1984.
48. Kent, D., "Inelastic behavior of reinforced concrete members with cyclic loading," thesis presented to the University of Canterbury, at Christchurch, New Zealand, in partial fulfillment of the requirements for the degree of Doctor of Philosophy, 1969.
49. Mark, K., and Roesst, J., "Nonlinear dynamic response of reinforced concrete frames." **Rep. R76-38**, Massachusetts Institute of Technology, Cambridge, Mass, 1976.
50. Suharwardy, M., and Pecknold, D., "Inelastic response of reinforced concrete columns subjected to two-dimensional earthquake response." **Rep. No. UILU-ENG 78-2022**, University of Illinois, Urbana, Ill, 1978.
51 Zeris, C. and Mahin, "Analysis of Reinforced Concrete Beam-Columns Under Uniaxial Excitation," **Journal of Structural Engineering**, ASCE, Vol. 113, No. 4, April 1987.
52. Mahasurevachai, M., "Inelastic analysis of piping and tubular structures." **Rep. No. UCB/EERC-82/27**, University of California, Berkeley, Calif., 1984.
53. Zienkiewicz, O. C., **The finite element method**, McGraw Hill, London, 1979.
54. Maekawa, K., Yamazaki, J., and Higai, T., "Numerical problems in non- linear finite element analysis of the post-failure behavior of structural systems." **Finite element analysis of reinforced concrete structures**, H. Okamura and C. Meyer, eds., ASCE, 1985.
55. Menegotto, M., and Pinto, P., "Slender RC compressed members in biaxial bending." **J. Struct. Div.**, ASCE, V. 103, No. ST 3, March 1977.

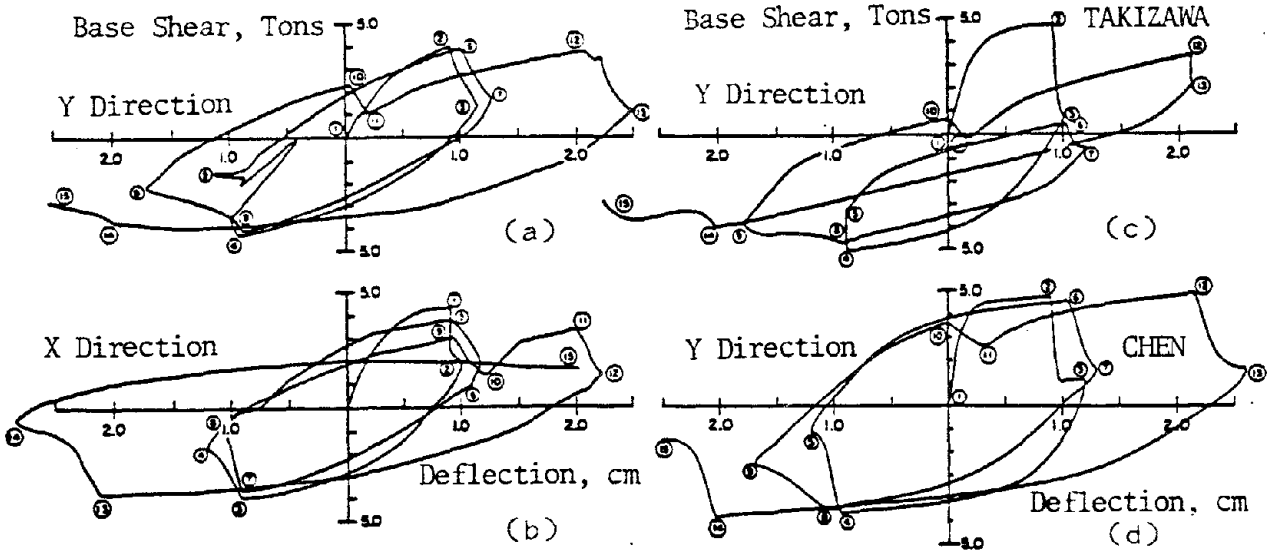

Fig. 1 Comparison of Results for a Bilateral Square Loading Pattern: (a and b) Experimental Results (14) and (c and d) Analytical Results (14, 43).

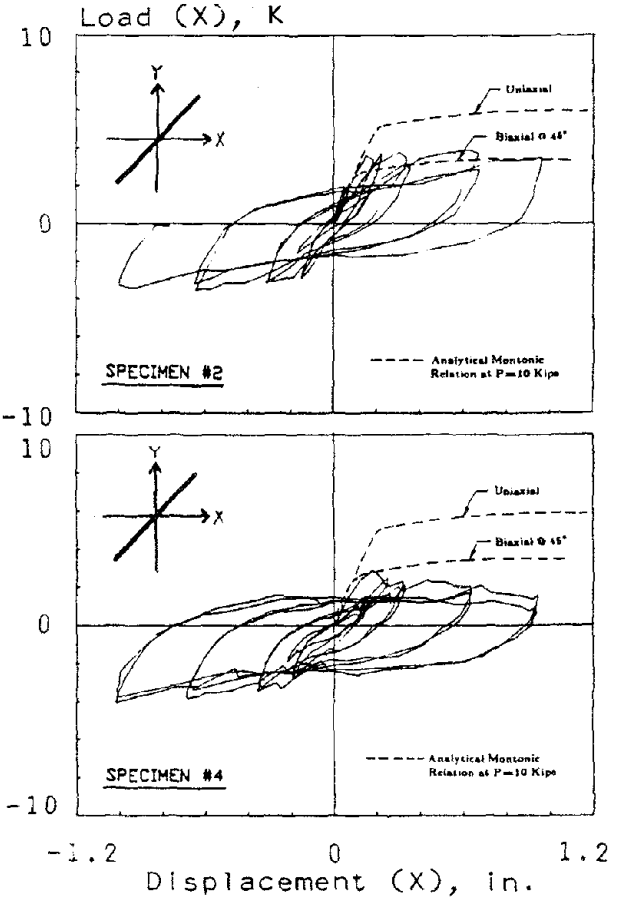

Fig.2 Effect of Skewed Loading (24): (a) Load equals 10 kips, and (b) Load averages 10 kips.

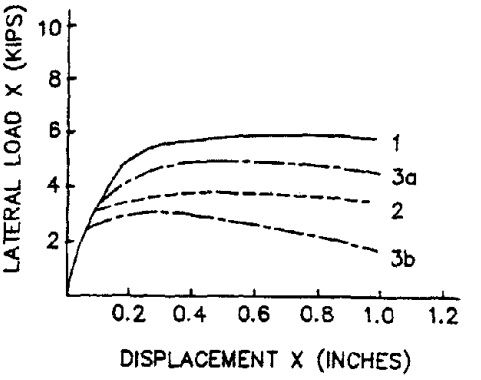

Fig.3 Comparison of Loading Envelopes (24).

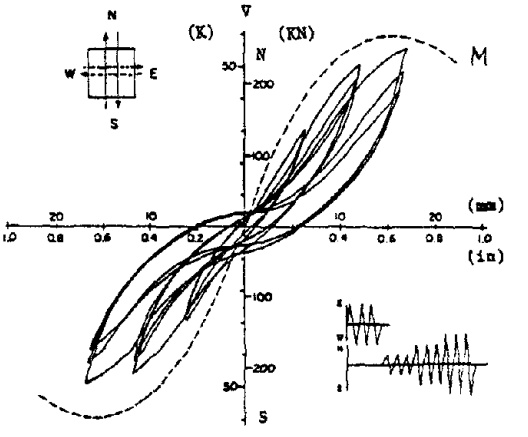

Fig.4 Behavior of Short Columns (30).

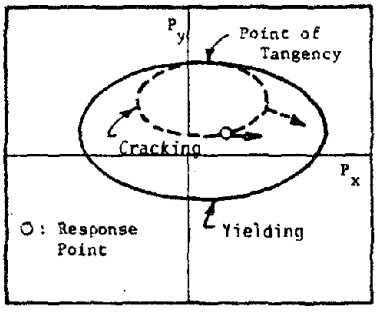

Fig.5 Sliding of Cracking Ellipse along Yielding Ellipse in Plasticity Model (14, 21).

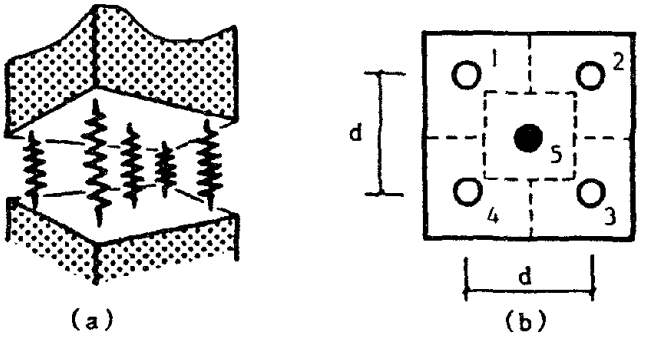

Fig.6 Multi-Spring Model (44,12)

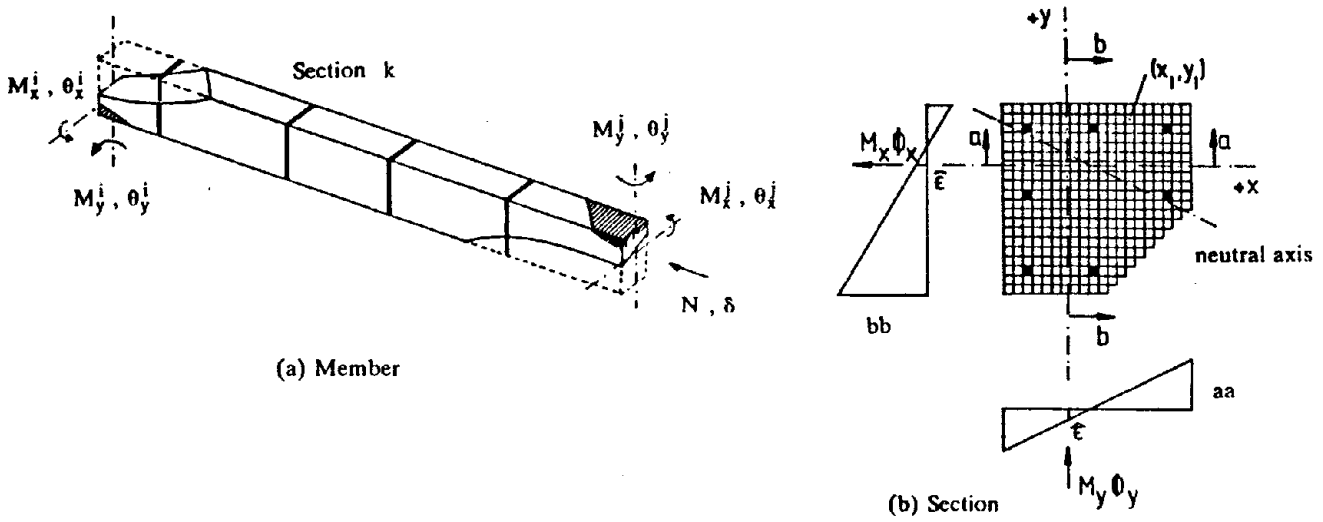

Fig. 7 Stress-Strain Based Fiber Model (2,47,51)

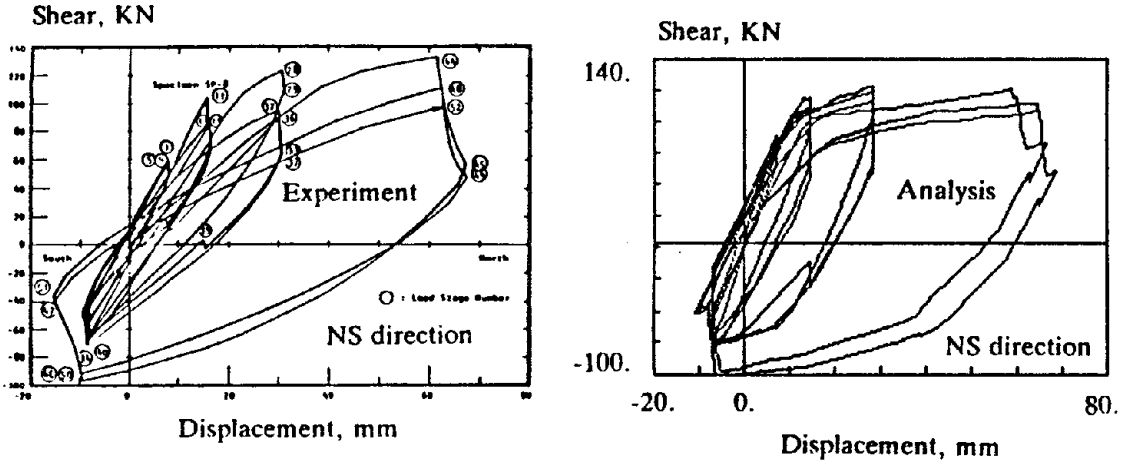

Fig.8 Comparison of Experimental (22) and Analytical (2) Results.

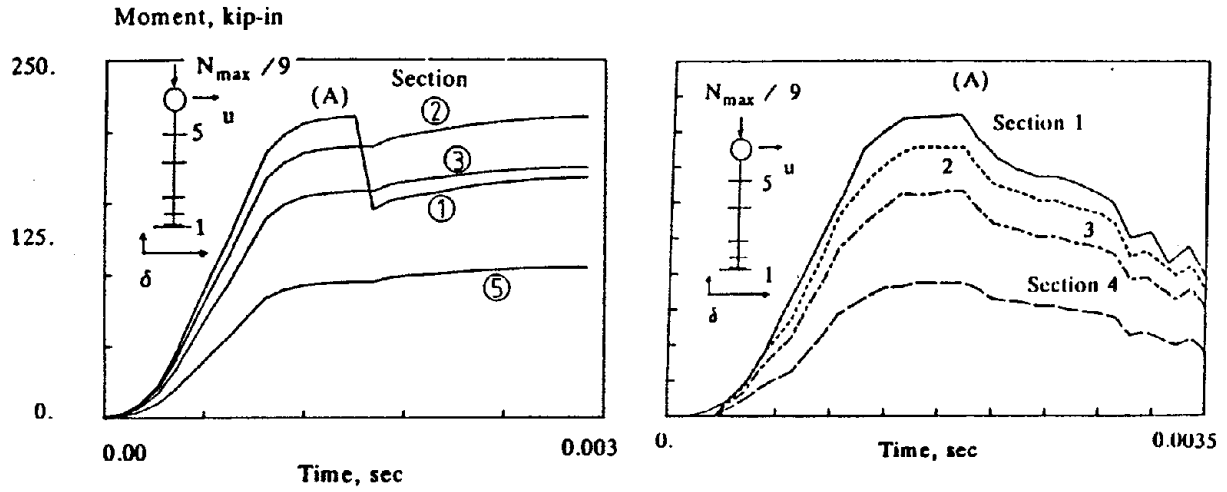

Fig.9 Numerical Problems with FE Models Under Softening Response: (a) Standard Displacement Approach and (b) Improved Mixed Force/Displacement Approach (51).

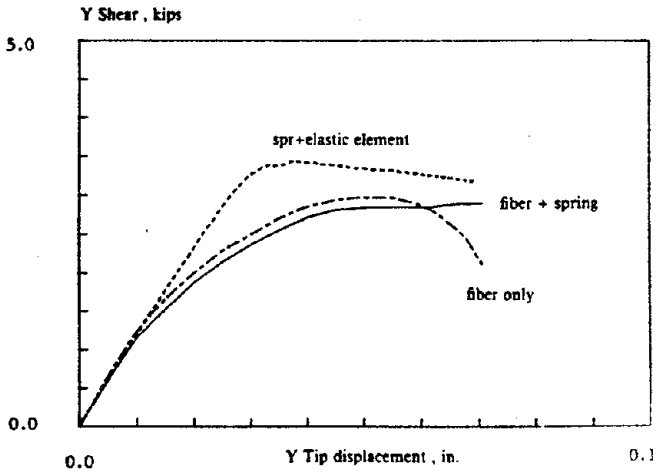

Fig.10 Effect of Fixed End Rotation Spring on Fiber Model Results (2).

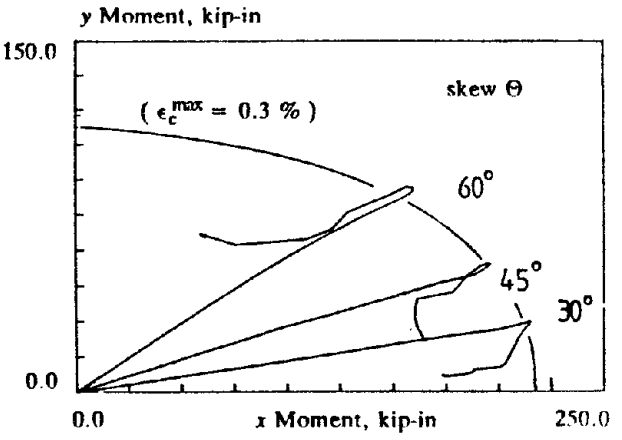

Fig.11 Biaxial Moment Paths For Constant Displacement Inclination Angle (2).

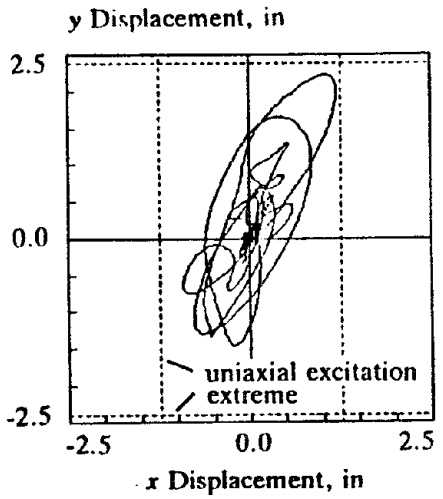

Fig.12 Predicted Particle Motion at Roof of Two Story RC Frame -- Centroid (2)

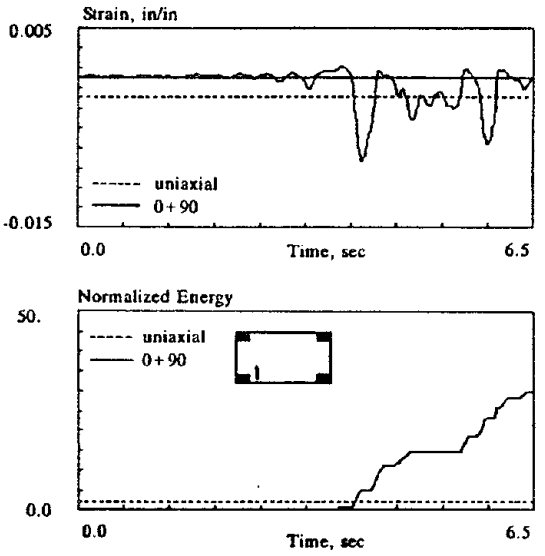

Fig.13 Predicted Steel Strain and Local Energy Dissipation Demands for a Column (2).

AN UPDATE OVERVIEW OF THE UNIVERSITY OF CALIFORNIA SEISMIC SAFETY PROGRAM

Frank E. McCLURE[1]

[1]Senior Structural Engineer, Lawrence Berkeley Laboratory, Berkeley, California, U.S.A.

(Presented at the Ninth World Conference on Earthquake Engineering, August 2-9, 1988, Tokyo-Kyoto, JAPAN)

SUMMARY

The September 1985 Mexico earthquakes and coincidental release of the report "A Campus at Risk," dated September 1985, prepared by the University of California at Los Angeles Earthquake Safety Committee, renewed The Regents' and State Officials' 1971 concerns about the seismic safety of University buildings. Long-held State funds were then released. Funding of earthquake safety programs almost always follows and does not precede major earthquakes. Unfortunately, the usual approach is to prepare a seismic safety program, seek its funding, keep it current and wait for funds to implement the program after the next damaging earthquake.

INTRODUCTION

Since 1887, the University of California has been active in research and instruction regarding all aspects of seismology, including recording of seismic events with regard to intensity and location and the probability of future occurrences. As a result, the University for many years has been concerned about the adequacy of its structures with regard to seismic resistance.

Following the 1971 San Fernando Valley earthquake, the University undertook a survey of existing buildings to identify those which warranted engineering analysis to assess their relative ability to withstand seismic forces. The engineering analyses conducted during the period 1971-1975 disclosed serious and extensive seismic resistance deficiencies in many University structures, both old and relatively new. About one-third of the existing University of California buildings were designed and constructed prior to 1955. Although they were designed to be in compliance with building codes when constructed, many are no longer considered to be adequate with regard to seismic safety.

In January of 1975, The Regents of the University of California adopted a policy regarding seismic safety in University structures with the expressed intent of providing an acceptable level of seismic safety for students, employees and the public who occupy and utilize University buildings and facilities. This University Policy on Seismic Safety was reaffirmed in a May 17, 1988, letter from the President of the University to the Chancellors and appropriate chief administrative officers and Directors of the Lawrence Berkeley Laboratory, Lawrence Livermore National Laboratory, and the Los Alamos Scientific Laboratory. The background and history of the development and implementation of the University Seismic Safety Policy is presented in a 1984 paper by the author entitled, "Development

and Implementation of the University of California Seismic Safety Policy" (Ref.1).

This current paper is an update overview of this Policy since 1984 to 1988. It is presented to provide a continuing documentation of the success of the University's program in seismic hazard abatement to aid others involved in the development and implementation of similar seismic programs.

BACKGROUND

In 1976, the State of California Legislative Analyst, after being alerted to the seismic problems of the University, recommended that the California Seismic Safety Commission (CSSC) undertake a study to determine the need for a State-wide seismic safety rehabilitation program and to report to the Legislature by January 1977. The recommended study concluded in 1979 with a report from the Commission to the Legislature (Ref.2). This CSSC report established a methodology for rating buildings with regard to seismic safety and was intended to serve as a budget tool for allocating funds on a "benefit-cost" priority basis among State buildings most urgently requiring correction of seismic deficiencies (Ref.3).

The University utilized the methodology developed in the CSSC Report (Ref.3) and the results of the University's building survey to establish a priority list of University facilities based on the life-saving potential of each project. In addition, the University engaged a consultant to investigate the possibility of a phased approach to the correction work so that the maximum value could be obtained for the construction dollars invested. In spite of the University's effort to develop a rational program, the State was reluctant to proceed with a program on a State-wide basis because of the magnitude of the problem and limited availability of funds.

In 1982, the State Public Works Board provided $175,000 to the University to study the seven highest priority University buildings included in the CSSC priority report. The following information was developed for each of these buildings:

1. Detailed information on specific seismic resistance deficiencies which exist in the particular buildings.

2. Details of structural improvements required for increased seismic resistance capabilities to provide and improve seismic resistance ratings.

3. Construction costs for each individual building's structural improvements.

4. Investigation of the possibility of phased construction to provide for correction of the most serious deficiencies. This was intended to maximize the reduction of seismic risks through the implementation of limited rather than comprehensive correction. Development of the cost of each phase if phased construction is feasible.

5. The buildings for which detailed studies have been completed are: 1) Los Angeles Campus - Powell Library and Moore Hall, 2) Berkeley Campus - South Hall, Wheeler Hall and California Hall, 3) San Diego Campus - Undergraduate Science Building, and 4) Riverside Campus - Soils and Plant Nutrition Building.

In September 1982, the President recommended to The Regents in the 1983-86 Capital Improvement Program that 56 University buildings be carried as approved by the University for authorization of funding, pending availability of State funds.

In September 1983, The Regents approved an authorization for the President to include projects in the "Program for Correction of Seismic Deficiencies" and to request appropriate State funding, should the State indicate a willingness to provide funds for seismic safety projects.

In September 1984, the Regents' 1985-1986 Budget for Capital Improvements requested State funds for the planning and design of seismic corrections of Wheeler Hall and South Hall and for additional studies of the Doe and Moffitt Libraries, all on the Berkeley campus. Funds totalling $721,000 were appropriated for the preparation of the design drawings and specifications for the South Hall project and for the studies (only) of the Berkeley Libraries.

In September 1985, prior to the September 19, 1985 Mexico earthquake, The Regents' 1986-87 Budget for Capital Improvements requested State funds for construction of the South Hall seismic structural corrections project at Berkeley, planning and design of the Wheeler Hall seismic structural correction project at Berkeley, and study funds to determine the solution for correction of seismic structural problems of the Powell Library at Los Angeles.

Concurrently, there were continuing seismic investigation studies being conducted at the Berkeley campus and the Los Angeles campus. The events described in the following section of this paper were important in getting funds totalling $3.7 million appropriated, in late 1985, for the above two Berkeley projects, and $693,000 in design funds appropriated for a project at the San Diego Medical Center that includes seismic structural correction of the main hospital building. The University provided study funds for Powell Library.

"A CAMPUS AT RISK"

The UCLA Ad-Hoc Joint Senate-Administration Earthquake Safety Committee was appointed on June 15, 1983, by the Administrative Vice-Chancellor and the Chair, Academic Senate, Los Angeles Campus. This Committee was asked to specifically undertake the following: 1) review the current information about the seismic safety at UCLA; 2) consider and make recommendations for up-dating the current priority and safety ratings for seismic rehabilitation; 3) review and, as necessary, make recommendations for the amplification and updating of the Campus Emergency Plan; 4) monitor and make recommendations for improving measures to reduce the impact of the physical damage and personal injury resulting from earthquakes and other catastrophes; 5) devise methods for the improvement of communications about the existence of the Emergency Plan for the entire campus; and 6) report at least annually to the Chancellor and the Chair of the Academic Senate on the above matters and such others as the Committee believes should be brought to their attention.

The Committee held fifteen meetings, and on June 7, 1984, made an initial presentation to Chancellor Young and his senior staff. It was the strong and unanimous opinion of this Committee that UCLA was "a campus at risk," and faced a potentially devastating catastrophe as a result of the next great earthquake in Southern California (Ref.4).

The Committee was completing its written Report, dated September 1985, when the September 19, 1985 Mexico earthquake occurred. Their Report, "A Campus at Risk," was "leaked" and the October 19, 1985, Los Angeles Times quoted from the

Report that "When the next great earthquake rumbles through Southern California, UCLA will be left in a shambles.....The number of deaths on campus could approach 2,000 and serious injuries could exceed 4,000" (Ref.5).

The tenured professors on the Committee had nothing to lose by "calling a spade a spade" and included the number of deaths and injuries projected at UCLA in their Report. The large number of casualties in Mexico City added credibility to the Report because many of the buildings on the UCLA campus, which had been rated "Very Poor", were similar to buildings that had collapsed in Mexico City.

Two investigative reporters from the Los Angeles Times who were looking into the seismic safety of University buildings picked up on "A Campus at Risk" Report and kept it alive for several weeks (Ref.5). They reported in the Sunday, December 8, 1985, Los Angeles Times an excellent summary of the University Seismic Program and its problems in getting funding from the State of California (Ref.6).

Despite the longstanding concern about the seismic hazards on the University campuses, the 1985-1986 fiscal year was the first in which the Legislature has appropriated large sums of money to strengthen the University buildings. The September 19, 1985 Mexico earthquake got The Regents and the State Legislature thinking again about seismic safety.

It is the author's considered opinion that the coincidence of the release of "A Campus at Risk" Report (Ref.4) immediately following the September 19, 1985 Mexico earthquake and the follow-up articles in the Los Angeles Times renewed concerns by The Regents and underscored their wisdom in adopting a 1975 University Seismic Safety Policy and their annual request for State funds to carry out this Policy.

Immediately upon the release of "A Campus at Risk" Report, the UCLA Chancellor authorized a detailed seismic study of thirty-seven structures including buildings for teaching and research, libraries, residence halls, parking structures, and student and sports facilities. A 1987 report, "The Seismic Correction Program at UCLA" (Ref.7), outlined a conceptual master plan for seismic corrections projecting total costs for the above thirty-seven structures falling between $110 and $150 millions. Approximately $75 to $100 million would be needed from State funds, while the remainder would have to come from the residence halls, student union, and parking revenues or non-State funds. Among the top seven State building priorities set forth by the CSSC Report (Ref.3), was Powell Library, built in 1929 before any seismic building codes were in place. Seismic improvements in other State-funded buildings, such as Moore, Royce and Kinsey Halls, are further down the priority list. Other non-State-funded buildings include Ackerman Union, Kerckhoff Hall, student residence halls - Hedrick, Rieber, Sproul, and Dykstra.

It is important to note that the UCLA Ad-Hoc Joint Senate-Administration Earthquake Safety Committee (ESC), whose report "A Campus At Risk" led to the extensive structural analysis of the UCLA buildings in 1986, has also helped to shape the comprehensive earthquake preparedness program at UCLA (Ref.7).

CONCLUSIONS

In the 1985-88 University Capital Improvement Program, it is estimated that $319.8 million will be needed from the State Legislature to strengthen the top priority 56 State-owned buildings and $35.0 million from other sources to upgrade 36 top priority campus housing, sports and recreation facilities and other non-State-funded buildings (Ref.2).

The Los Angeles, Berkeley, Davis, Riverside, San Diego and Santa Barbara campuses have immediate 1987 funding needs of $150.0 million, $90.0 million, $30.0 million, $1.6 million, $6.0 million and $21.0 million, respectively. At least $500.0 million would be needed to mitigate all of the University seismic hazards in 1987 dollars, based on an Engineering News Record 20 Cities ENR Cost Index of 4440 (Ref.2).

In November 1986, an $800 million State capital improvement bond issue provided the first major funding of the University Seismic Program. It includes the funding of the first phase of the Berkeley campus and Mt. Lick Observatory reconstruction programs which includes 1873 South Hall ($2.5 million), 1905 California Hall ($1.7 million) and 1915 Wheeler Hall ($1.6 million) and the 1888 Mt. Lick Observatory ($1.5 million). This first phase is to be completed by 1991 - twenty years after the 1971 San Fernando earthquake that initiated the University Seismic Safety Program.

On October 1, 1987, an earthquake of 6.1 on the Richter scale occurred in the Whittier area of the Los Angeles basin. No serious damage occurred to University of California facilities. One student fatality and severe architectural and structural damage were experienced at the California State University at Los Angeles, which is part of the California State University System, not the University of California System.

Although progress made to date on seismic correction work has been limited because of lack of funding, there is a November 1988 State bond issue bill being considered in the California State Legislature. This $500 million bond issue program would provide the funding for a start on the seismic correction work with $150 million to be used for seismic retrofitting of local government buildings and facilities, and $350 million for seismic strengthening of buildings owned by the State, University of California and the California State University systems. This legislation, "State Earthquake Bond Act of 1988", if passed by the Legislature and approved by the Governor, would provide for the submission of the above Bond Act at the November 1988 General Election and would become operative upon adoption by the voters at this election. Unfortunately, as of late July 1988, this bond issue is being held in a powerful Legislative Assembly Committee on Ways and Means. If this important legislation is not passed by the Legislature, the California Seismic Safety Commission will sponsor this bill again next year.

Approval of the above bond issue would provide the necessary funding for substantial progress on the seismic correction program for University facilities. The University has continued to work on seismic correction problems in its non-State-funded facilities over the years and has taken it upon itself the responsibility to correct non-structural seismic problems, such as falling hazards, with its facilities utilizing the ongoing operational budget provided for departments and for maintenance and operation of plants (Ref.8).

The logical assumption is made that there is an urgent need for earlier completion of the stated goal called for in the "Earthquake Hazards Reduction Act", enacted by the State Legislature in 1986. The stated goal is to significantly reduce seismic life safety hazards by the end of the century. Furthermore, the University of California, owner of approximately one-half of the high occupancy State facilities identified as potentially unsafe, must be a leading force in the efforts to secure funding, to develop appropriate and reasonable seismic rehabilitation programs, and to ensure, to the extent possible, that the lives and safety of the persons using University buildings are protected.

REFERENCES

1. McClure, F. E., "Development and Implementation of the University of California Seismic Safety Policy," Proceedings of the Eighth World Conference on Earthquake Engineering, (1984).

2. 1985-1986 Budget for Capital Improvements, Office of the President, University of California, (September 1984).

3. Wyllie, L. A., Jr. and Olson, R. A., "Establishing Priorities and Financing for Seismic Strengthening of Existing Buildings in California," Proceedings of the Eighth World Conference on Earthquake Engineering, (1984).

4. "A Campus at Risk," Report of the UCLA Ad-Hoc Joint Senate-Administration Earthquake Safety Committee, (September 1985).

5. Harris, S. and Smollar, D., "2,000 at UCLA Could Perish in Quake, Study Shows," Los Angeles Times, (October 19, 1985).

6. Harris, S. and Smollar, D., "Safety Experts Fear State Isn't Ready for Big Quake," Los Angeles Times, (December 8, 1985).

7. The Seismic Correction Program at UCLA - A Conceptual Master Plan, Office of Capital Programs, Planning & Space Management, University of California at Los Angeles, (October 1987).

8. Burnett, J. A., Director of Facilities Construction, University of California Systemwide Administration, "Managing the University of California Seismic Hazard Problem," talk given at the meeting of the Western Council of Construction Consumers, (November 4, 1987).

APPROXIMATE DYNAMIC RESPONSE FOR ARBITRARILY-SHAPED FOUNDATIONS

Francisco Medina[†]

Facultad de Ciencias Físicas y Matemáticas
Universidad de Chile
Casilla 2777, Santiago

ABSTRACT

A semi-analytical technique based upon a discretization by Fourier series and, by finite and infinite elements is presented to numerically compute the dynamic response of soil-foundation systems. The theory is developed for non-axisymmetric, three-dimensional linear systems subjected to arbitrary loading conditions. By using semi-analytical axisymmetric elements, the non-axisymmetric, three-dimensional foundation is approximately modeled. By using axisymmetric finite and infinite elements, the mostly axisymmetric near and far fields are modeled with finite element accuracy. Numerical examples on a square foundation clearly show the substantial savings in mesh preparation and, computing time and storage, yet yielding reasonable accuracy.

INTRODUCTION

In the presence of dynamic excitations, foundations and the surrounding soil interact. Due to the difficulties involved in the analysis of the interaction process, there is not a unique procedure to deal with this problem. Furthermore, when foundations cannot be modeled but three-dimensionally, the problem becomes very complex. It is then possible to differentiate two main sources of difficulty, one coming from the three-dimensional nature of the problem, and the other coming from the existence of an infinite far field. There have been proposed several approaches to model the three-dimensional far field. These approaches present different degrees of generality and efficiency. Among these approaches it is possible to mention the generalized Winkler's medium approach,[1] the consistent boundary approach,[2] the integral equation approach,[3] the cloning algorithm,[4] the boundary integral method,[5] and the finite/infinite element technique.[6] In fact, there is not a general procedure to treat a nonhomogeneous, inelastic, anisotropic, soil-foundation interaction problem in three dimensions, assuming finite, semi-infinite and/or layered soil conditions. There are several analytical and approximate procedures available to treat many cases of soil-foundation interaction.[7] Nevertheless, there are only few approaches dealing with general cases of three-dimensional soil-foundation interaction. For example, using integral equation methods, it is possible to find the harmonic response of square rigid foundations on layered media.[8] On the other hand, the dynamic, time-dependent, response of rigid and flexible surface foundations can be found using boundary integral approaches.[9,10]

What follows outlines an approximate, semi-analytical finite/infinite element technique developed to treat the problem of three-dimensional, linear soil-foundation interaction. The three-dimensional foundation and surrounding media are modeled with semi-analytical finite elements, represented by axisymmetric torus. These torus, of plane section on the (r,z) plane, have properties which vary along the tangential direction, as illustrated in

---

[†]Currently Visiting Research Engineer, Department of Civil Engineering, University of California, Berkeley, California 94720.

Fig.1. The mostly axisymmetric near field and far fields are modeled with axisymmetric elements. The near field is modeled with finite elements, and the far field is modeled with infinite elements. The infinite elements simultaneously transmit Rayleigh, shear and compressional elastic waves. Theoretical considerations on the infinite elements applied to elastic multi-wave propagation may be found elsewhere.[11] The soil in the near field as well as in the far field may be nonhomogeneous, anisotropic and/or viscoelastic, but linear.

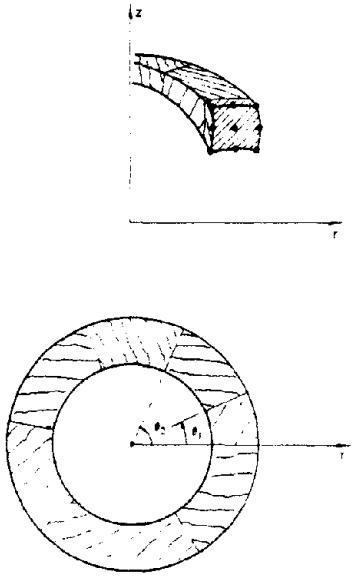

Figure 1.- Semi-analytical axisymmetric finite element.

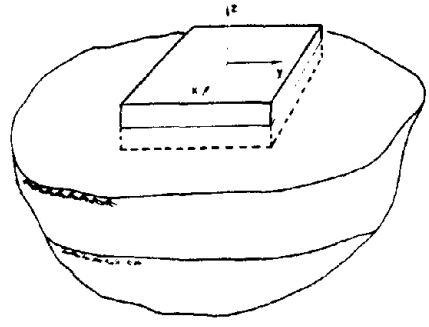

Figure 2.- Three-dimensional foundation embedded in a semi-infinite medium.

AXISYMMETRIC APPROXIMATION TO THE THREE-DIMENSIONAL PROBLEM

The problem of considering non-axisymmetric excitations acting on axisymmetric solids has been already presented in the literature.[12] Furthermore, the discretization of a non-axisymmetric, three-dimensional solid using semi-analytical axisymmetric finite elements has also been reported.[13] Following these approaches, the total energy of an elastic linear solid system, as the one shown in Fig.2, subjected to harmonic excitations of the type $e^{i\omega t}$ is expressed by

$$L = -\tfrac{1}{2}\omega^2 \int \mathbf{u}^T \rho \mathbf{u}\, dV - \tfrac{1}{2}\int \boldsymbol{\varepsilon}^T \boldsymbol{\sigma}\, dV + \int \mathbf{u}^T \mathbf{f}\, dV \qquad (1)$$

where the spatially dependent variables under the integrals are defined as

$\boldsymbol{\varepsilon} = \mathbf{B}\mathbf{u}$, is the strain component vector ($\mathbf{B}$: differential operator matrix);
$\boldsymbol{\sigma} = \mathbf{D}\boldsymbol{\varepsilon}$, is the stress component vector ($\mathbf{D}$: solid constitutive matrix);
$\mathbf{u}$ contains the displacement field components;
$\mathbf{f}$ contains the applied force components; and
ρ is the solid density per unit volume.

In general, the solid elastic ($\mathbf{D}$) and inertia (ρ) properties are of three-dimensional nature. However, if the behavior of the solid is linear, it is possible to assume that these properties are composed by an axisymmetric averaged part and a deviatoric (from the axisymmetric) part, i.e.,

$$\begin{aligned} \mathbf{D}(r,\theta,z) &= \bar{\mathbf{D}}(r,z) + \tilde{\mathbf{D}}(r,\theta,z) \\ \rho(r,\theta,z) &= \bar{\rho}(r,z) + \tilde{\rho}(r,\theta,z) \end{aligned} \qquad (2)$$

Upon replacing in Eq.(1),

$$L = -\tfrac{1}{2}\omega^2 \int \mathbf{u}^T(\bar{\rho}+\tilde{\rho})\mathbf{u}\, dV - \tfrac{1}{2}\int [\mathbf{B}\mathbf{u}]^T[\bar{\mathbf{D}}+\tilde{\mathbf{D}}][\mathbf{B}\mathbf{u}]\, dV + \int \mathbf{u}^T\mathbf{f}\, dV \tag{3}$$

The excitations and responses are decomposed in harmonics of the angle θ. For example,

$$\mathbf{f}(r,\theta,z) = \mathbf{f}_0(r,z) + \sum_{m=1}^{m=N_F} [\mathbf{f}_m(r,z)\cos(m\theta) + \mathbf{f}_{-m}(r,z)\sin(m\theta)] \tag{4}$$

where N_F is the highest Fourier harmonic to be considered. Seeking a finite element approximation to the displacement field,

$$\mathbf{u}^e \approx \hat{\mathbf{u}}^e(r,\theta,z) = \mathbf{N}^e(r,z)\left[\hat{\mathbf{u}}_0^e + \sum_{m=1}^{m=N_F} [\hat{\mathbf{u}}_m^e\cos(m\theta) + \hat{\mathbf{u}}_{-m}^e\sin(m\theta)]\right] \tag{5}$$

for each element e; and then using Hamilton's principle, upon minimizing the energy, Eq.(3) yields

$$\bar{\mathbf{K}}_{mm}^*\hat{\mathbf{u}}_m = \mathbf{f}_m - \sum_{n=-N_F}^{n=N_F} \tilde{\mathbf{K}}_{mn}^*\hat{\mathbf{u}}_n \tag{6}$$

($m=0,\pm1,\pm2,...,\pm N_F$), where $\bar{\mathbf{K}}_{mm}^*$ is the uncoupled, axisymmetrically averaged dynamic stiffness matrix, $\hat{\mathbf{u}}_m$ contains the finite element discretized displacement components, and $\mathbf{f}_m$ contains the discretized applied forces; m is the m^{th} Fourier harmonic of the angle θ. The non-axisymmetric deviatoric dynamic stiffness matrix $\tilde{\mathbf{K}}_{mn}^*$ is the coupled term between harmonics m and n, and can be expressed as

$$\tilde{\mathbf{K}}_{mn}^* = \int \mathbf{B}^T{}_m\tilde{\mathbf{D}}_{mn}\mathbf{B}_n\, dA - \omega^2\int \mathbf{N}^T\tilde{\rho}_{mn}\mathbf{N}\, dA \tag{7}$$

where $\tilde{\mathbf{D}}_{mn}$ and $\tilde{\rho}_{mn}$ are the integrals with respect to the angle θ of the deviatoric material properties. In general, these integrals are non-zero, but when the model presents planes of symmetry passing through the z axis, as the case of rectangular foundations (two symmetry planes), or the case of square foundations (three symmetry planes), some of the terms $\tilde{\mathbf{D}}_{mn}$, $\tilde{\rho}_{mn}$ become zero. In the limit, as the planes of symmetry tend to infinity (axisymmetry), as in most of the near and far fields, $\tilde{\mathbf{D}}_{mn}$ and $\tilde{\rho}_{mn}$ vanish for all m and n. Hence, most of these terms can be neglected, and those to be considered are those coming from the foundation.

By assuming the terms $\mathbf{K}_{mn}^*\hat{\mathbf{u}}_n$ known, Eq.(6) may be solved iteratively. These terms represent the unbalanced force in the m^{th} harmonic due to the n^{th} harmonic. Taking this into consideration, Eq.(6) may be expressed as

$$\bar{\mathbf{K}}_{mm}^*\hat{\mathbf{u}}_m^1 = \mathbf{f}_m - \sum_{n=-N_F}^{n=N_F} \tilde{\mathbf{K}}_{mn}^*\hat{\mathbf{u}}_n^{1-1}\ ; \qquad \hat{\mathbf{u}}_n^0=\mathbf{0},\ \text{all } n \tag{8}$$

($m=0,\pm1,\pm2,...,\pm N_F$). Convergence is achieved when the difference in the response of two successive iterations become negligible in some norm. In this presentation the unbalanced deviatoric force is neglected.

NUMERICAL EXAMPLE: COMPLIANCE FUNCTIONS FOR A SQUARE FOUNDATION

As shown schematically in Fig.3, the foundation and surrounding media are modeled with semi-analytical axisymmetric finite elements. The near field is modeled with a reasonably small number of four- to nine-node axisymmetric finite elements, and the far field is modeled with even fewer six-node infinite elements.[14] It may be mentioned that the rigidity of the foundation is not a limitation of the method, it was simply selected to make comparisons with available solutions.

Rigid square plate resting on a half-space. The foundation is modeled by four regular finite elements and three semi-analytical finite elements. The near field is modeled by forty-one finite elements and the far field by five infinite elements, as shown in Fig.4. The compliance functions obtained are shown in Figs.5a-d, where other available solutions[5,15] are also shown for comparison. The compliance functions have been normalized with respect to the zero frequency value. For this relatively small mesh, the computed approximate numerical solutions are in good agreement with the solutions shown. Discrepancies are below 15%, for an accuracy of seven digits. The total elapsed CPU time spent in all of the computations for this example was 71 seconds, using a non-vectorized code on an IBM-3090.

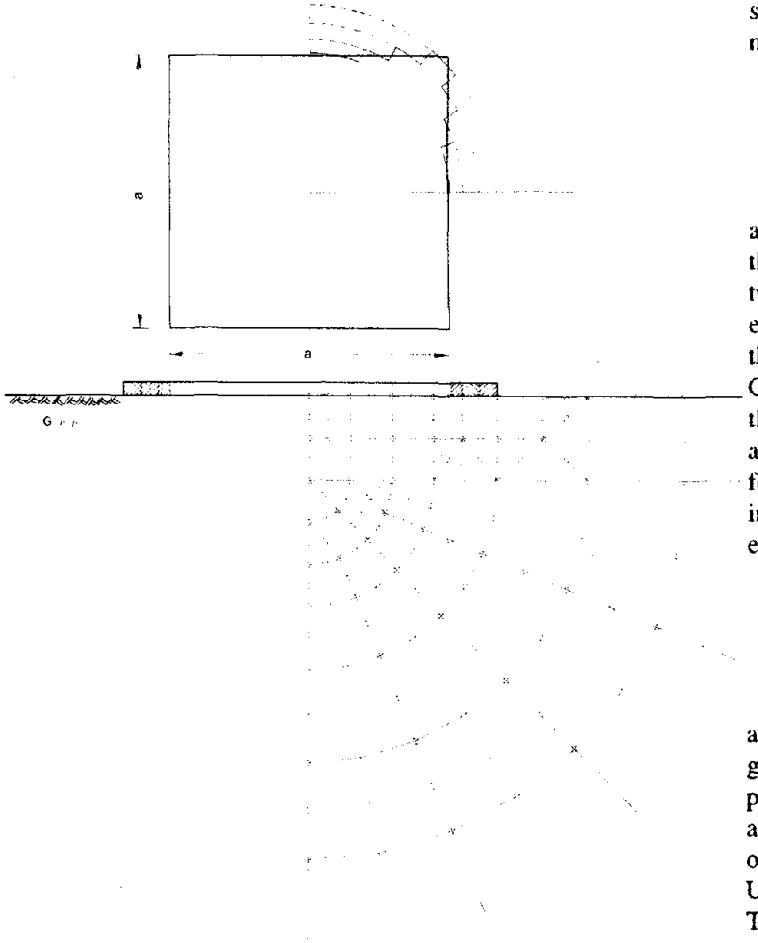

Figure 4.- Semi-analytical finite element discretization for a rigid square plate resting on a homogeneous, isotropic half-space.

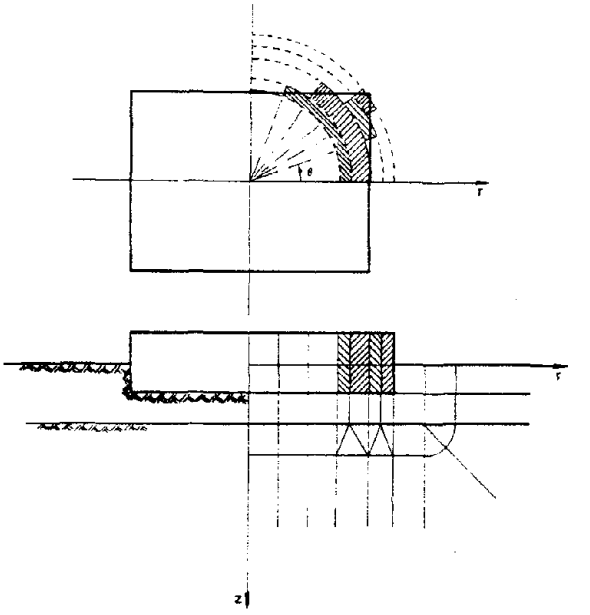

Figure 3.- Three-dimensional soil-foundation system discretized two-dimensionally with axisymmetric semi-analytical finite elements and regular axisymmetric finite and infinite elements.

CONCLUSIONS

By using semi-analytical axisymmetric finite and infinite elements to model non-axisymmetric, three-dimensional foundations, a moderately sized two-dimensional mesh of axisymmetric elements generates a reasonably accurate solution for the dynamic three-dimensional soil-foundation interaction problem. Compared to a conventional three-dimensional analysis the savings in mesh preparation and, computer time and storage are considerable. As the shape of the foundation deviates from being non-axisymmetric (as in the case of the rectangular foundations), it is expected that the procedure looses accuracy.

ACKNOWLEDGEMENTS

For the development of the semi-analytical axisymmetric finite element, the help of Jorge Estay is gratefully acknowledged. This development was supported by the Chilean National Council for Science and Technology (CONICYT) and the Computer Center of the Facultad de Ciencias Físicas y Matemáticas, Universidad de Chile through a grant by IBM (Chile). The actual work presented herein was supported by The Tinker Foundation and the Computer Center of the University of California, Berkeley.

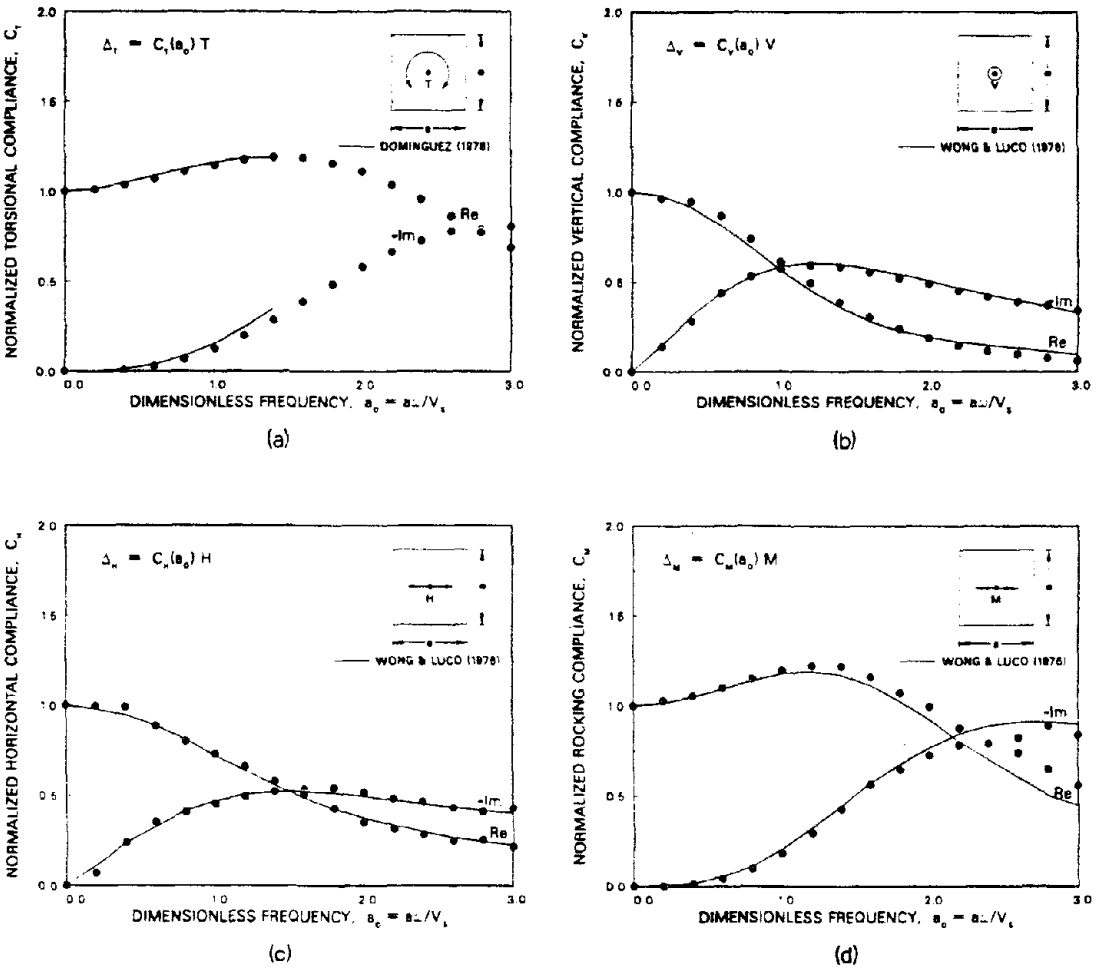

Figure 5.- Normalized compliance functions for a rigid square plate resting on a homogeneous, isotropic half-space (ν=1/3), and subjected to harmonic loadings. (a) Torsional compliance function. (b) Vertical compliance function. (c) Horizontal compliance function. (d) Rocking compliance function.

REFERENCES

1. M. Novak, 'Dynamic Stiffness and Damping of Piles,' *Can.Geotech.J.*, **11**,574-598(1974).
2. E. Kausel, 'Forced Vibrations of Circular Foundations on Layered Media,' *Sc.D. thesis*, MIT (1974).
3. J.E. Luco, 'Linear Soil-Structure Interaction,' *Seismic Safety Margins Research Program (Phase I)*, UCRL-15272, PSA#7249809, Lawrence Livermore Lab., California (1980).
4. G. Dasgupta, 'A Finite Element Formulation for Unbounded Homogeneous Continua,' *trans.ASME: J.Appl. Mech.*, **49**,136-140(1982).
5. J. Domínguez, 'Dynamic Stiffness of Rectangular Foundations,' *res.rep.R78-20*, Dep.Civ.Engng., MIT (1978).
6. F. Medina, 'Modelling of Soil-Structure Interaction by Finite and Infinite Elements,' *rep.UCB/EERC-80/43*, U. California, Berkeley (1980).
7. G. Gazetas, 'Analysis of Machine Foundation Vibrations: State of the Art,' *Soil Dyn.&Earthq.Engng.*, **2**,2-42 (1983) & **6**,186-187(1987).
8. H.L. Wong and J.E. Luco, 'Tables of Impedance Functions for Square Foundations on Layered Media,' *Soil Dyn.&Earthq.Engng.*, **4**,64-81(1985).
9. D.L. Karabalis and B.E. Beskos, 'Dynamic Response of 3-D Rigid Surface Foundations by Time Domain

Boundary Element Method,' *Earthq.Engng.Struct.Dyn.*, **12**,73-93(1984).

10. D.L. Karabalis and B.E. Beskos, 'Dynamic Response of 3-D Flexible Foundations by Time Domain BEM and FEM,' *Soil Dyn.&Earthq.Engng.*, **4**,91-101(1985).
11. S. Ghosh and E. Wilson, 'Dynamic Stress Analysis of Axisymmetric Structures under Arbitrary Loading,' *rep. UCB/EERC-69/10*, U. California, Berkeley (1969).
12. F. Medina and R.L. Taylor, 'Finite Element Techniques for Problems of Unbounded Domains,' *Int.J.num. Meth.Engng.*, **19**,1209-1226(1983).
13. M. Sedaghat, 'Non-Linear Analysis of Nearly Axisymmetric Solids,' *Ph.D. thesis*, U. California, Davis (1981).
14. F. Medina, 'Direct Finite Element Method for Layered Soil-Foundation Interaction,' in *Numerical Methods for Transient and Coupled Problems* (R.W.Lewis, E.Hinton, P.Bettess & B.A.Schrefler, eds.), Pineridge Press, Swansea, U.K., 960-970(1984).
15. H.L. Wong and J.E. Luco, 'Dynamic Response of Rigid Foundations of Arbitrary Shape,' *Int.J.Earthq.Engng. Struct.Dyn.*, **4**,579-587(1976).

ECCENTRICALLY BRACED FRAMES: U.S. PRACTICE

Egor P. Popov[1], Michael D. Engelhardt[2], and James M. Ricles[3]

SUMMARY

Current status of research and U.S. codes on Eccentrically Braced Frames (EBFs) is briefly discussed. Excerpts from the just completed tentative American Institute of Steel Construction (AISC) code pertaining to EBFs are given in detail. Comments on these provisions attempt to interpret them in the light of research and design practice. Based on these provisions a 6-story building employing EBFs in end walls is analyzed for seismic response under the action of several severe earthquakes. For these time-history analyses it is assumed that steel behaves as an elasto-plastic material with strain hardening. The behavior of the frames is found to be satisfactory. Several recommended details for EBFs are illustrated.

INTRODUCTION

EBFs can be considered a hybrid structural system, combining the stiffness of conventional concentrically braced frames with the ductility and energy dissipation capacity of conventional Moment Resisting Frames (MRFs). Common and recommended arrangements of EBFs are illustrated in Fig. 1. The preferred type is shown in Fig. 1(b). The distinguishing feature of an EBF is that at least one end of every brace is connected so as to isolate a beam segment called a *link*. Link lengths are identified by the letter *e* in the above figure. In a well designed EBF, inelastic activity under severe cyclic loading is restricted primarily to the links. These links must be capable of sustaining large inelastic deformations without loss of strength.

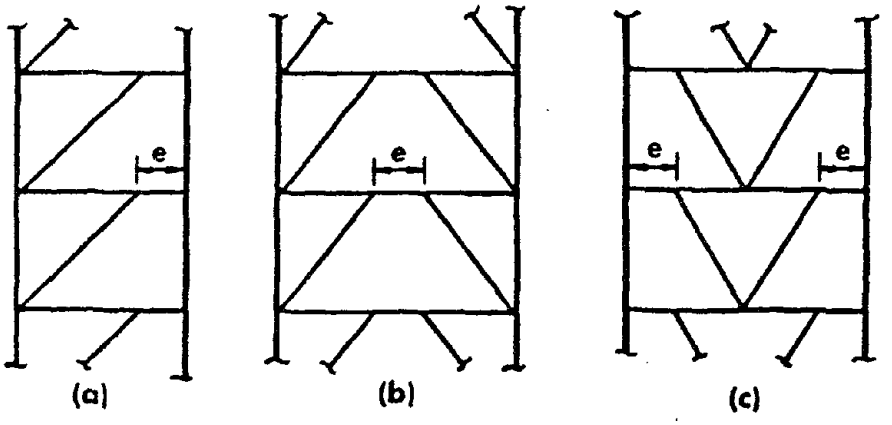

Fig. 1. Typical EBFs

1 Department of Civil Engineering, University of California, Berkeley, CA 94720, U.S.A.
2 Department of Civil Engineering, University of California, Berkeley, CA 94720, U.S.A.
3 Department of AMES, University of California at San Diego, La Jolla, CA 92093, U.S.A.

It is convenient to examine the extent and the nature of inelastic deformation by constructing an energy dissipating mechanism for a frame as shown in Fig. 2(b). (In plastic static analyses such mechanisms are called collapse mechanisms, an inappropriate terminology for seismic design). From this diagram it can be noted that for the same story sway, a link experiences a substantially larger demand than the "links" in a MRF, Fig. 2(a). It can be noted that EBFs with the braces arranged as in Fig. 1(c) for the same θ require only one half the link rotation of that shown in Fig. 2(b).

During the early stages of research on EBFs, often the links were placed at both ends of a brace as shown in Fig. 3. A detailed study of such mechanisms showed [1] that typically, a link at one end of a brace contributes very little to the energy dissipation. Therefore, unless dictated by the architectural requirements, it is less expensive to make concentric or nearly concentric brace connections at one end of braces as in Fig. 1.

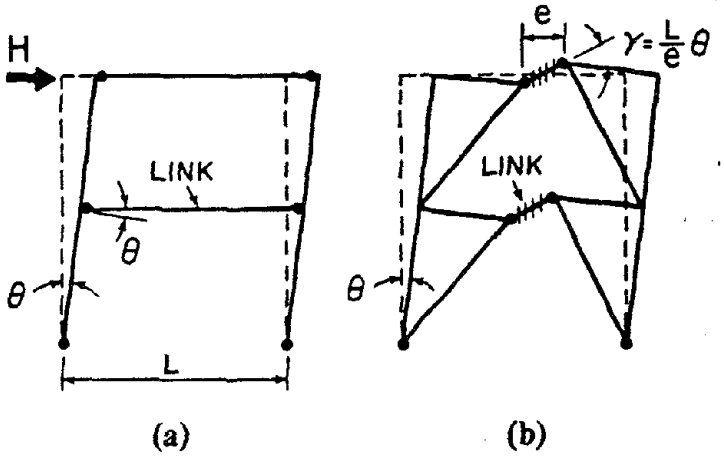

Fig. 2. Comparison of energy dissipating mechanisms for (a) MRF and (b) EBF

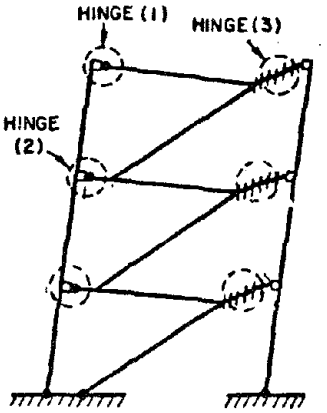

Fig. 3. Hinges 1 and 2 dissipate less energy than hinges 3.

The development of the EBF system for resisting seismic loads required a considerable amount of experimental and analytical work. The principal results of this research carried out at the University of California, Berkeley are summarized below.

EXPERIMENTAL AND ANALYTICAL RESEARCH ON EBFs

After experimentally verifying the concept of eccentric bracing for seismic applications on small frames in 1977 [2] and 1980 [3], the next phase of research was directed to determining cyclic behavior of individual *short* links [4,5]. This effort culminated in accurate criteria for web link buckling control under cyclic loads [1,6]. An experimental study of cyclic behavior of short links in EBFs with a composite floor followed [7,8,9]. This study, conducted on two-thirds scale models based on the full-size EBF tested at Tsukuba [10], is described below.

In the simplified model opposing vertical forces at link ends were used to simulate the brace effects on the beam. This gave good simulation for the composite link, avoiding the problems that may arise outside the link. Six different links were tested in this manner. Three of these links corresponded to links framing into columns as in Fig. 1(a); three other links corresponded to the interior links as in Fig. 1(b). These experiments clearly demonstrated that during the first application of large opposing vertical forces, the link strengths were significantly larger than those for the bare steel links. However, on the application of additional severe cycles, as local floor damage

develops, the shear strengths of composite links became comparable to strain-hardened bare steel links. As shown in Fig. 4, this held true for both the interior and the exterior links. Therefore, in the computer simulation of the link behavior under severe cyclic-loads, no distinction was made between the composite and the bare steel links [7]. A computer program based on these and earlier findings was developed for the analysis of EBFs [7,12].

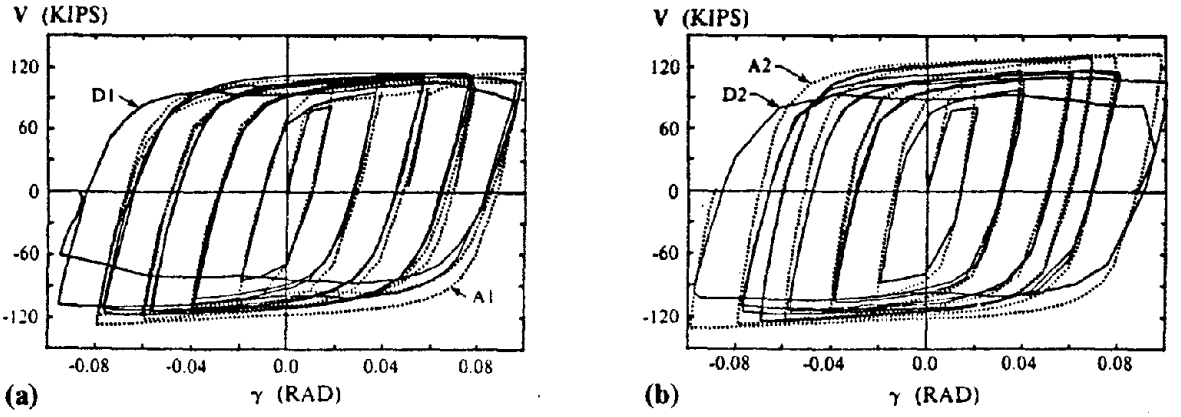

Fig. 4. Comparison of hysteretic loops for shear capacity vs. rotation angle for composite (dotted) and bare (solid lines) links. (a) Interior and (b) exterior link.

In the above experiments a study of the effectiveness of a composite deck on lateral restraint at links was also investigated, Fig. 5. The link twist for a link laterally braced at both ends is shown in Fig. 5(b), and that for an unbraced link in Fig. 5(c). These results definitely indicate the need for lateral bracing at link ends. This conclusion was corroborated by a recent series of tests [13].

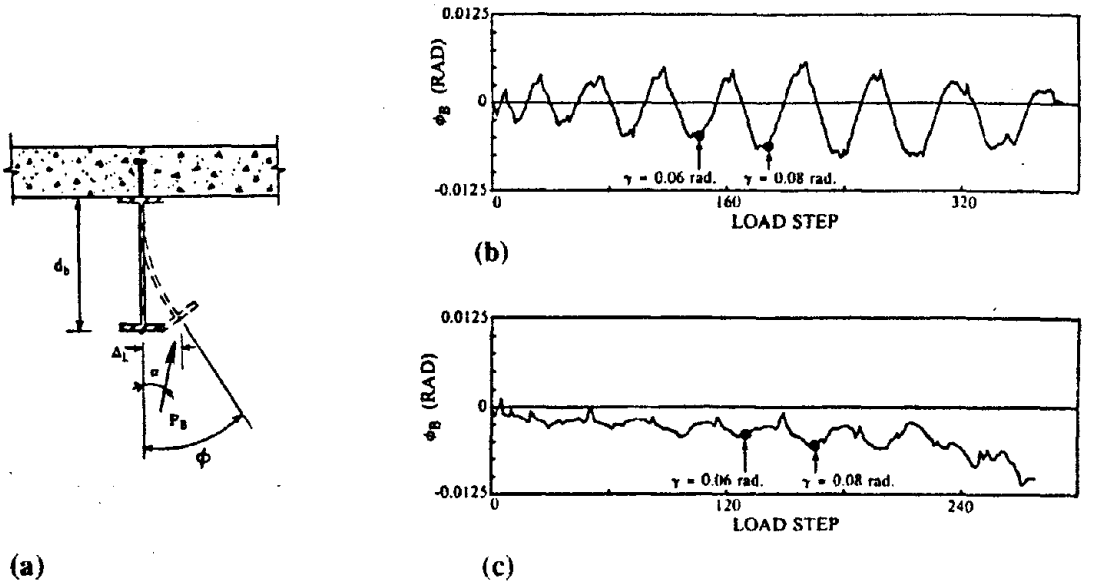

Fig. 5. (a) Lateral-torsional buckling of links (b) cyclic twist of bare link laterally braced at both ends, (c) progressively increasing twist of composite link laterally braced at one end.

The experiments described above were largely performed on individual links with the exception of the Tsukuba tests [10] and the subsequent tests on a one-third scale model on the Berkeley shaking table [14]. In the recent series of tests noted above [13], fourteen complete two-third scale subassemblages, such as those shown in Fig. 6, were investigated. These experiments provided a large data base on moderate length links, and on the behavior of the beam outside the link. A number of different brace-to-beam connections were also studied.

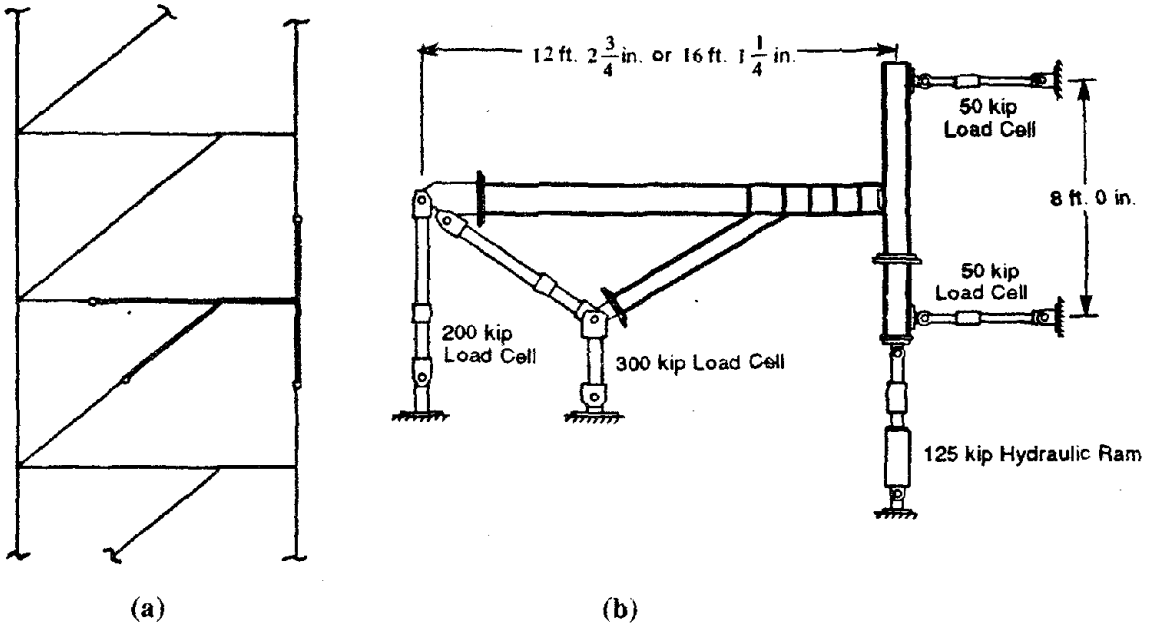

Fig. 6. (a) Location of subassemblage in frame, and (b) experimental set-up for EBF subassemblage.

These experiments showed that links of moderate length connected to column flanges behaved reasonably well as shown in Fig. 7(a), although the maximum inelastic rotation, γ_p, was only half of that provided by a well stiffened short link [6]. Long links in similar applications behaved poorly, Fig. 7(b); most of the inelastic action is concentrated at the ends, placing large demands on the flexural capacity of a connection.

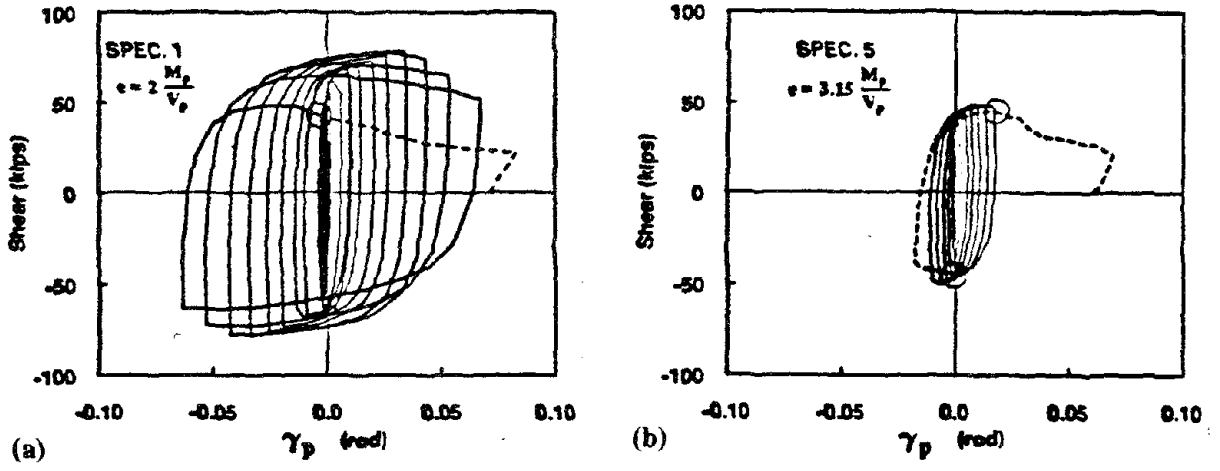

Fig. 7. Hysteretic loops of link shear vs. inelastic rotation for (a) moderately long link, and (b) long link.

Poor behavior of subassemblages was also observed where a brace forms a small angle on the order of 30° or less with the floor beam, Fig. 8. The beam outside the link and the brace in such arrangements provide inadequate stiffness for forming a hinge in the link.

These experiments also have shown that large forces can develop in lateral bracing, Fig. 9. This is particularly likely to occur when beam flanges distort, giving rise to lateral torsional buckling at the link ends.

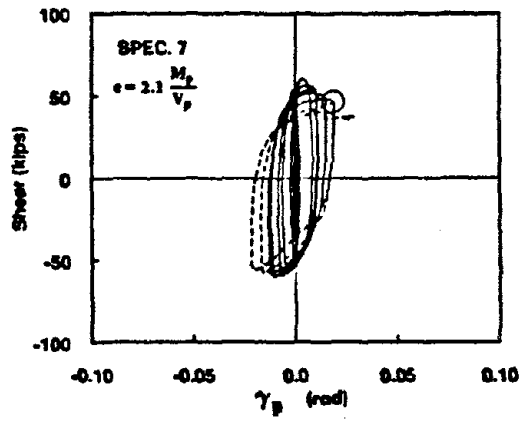

Fig. 8. Hysteretic loops of link shear vs. inelastic rotation for moderately long link in subassemblage with brace forming small angle with beam.

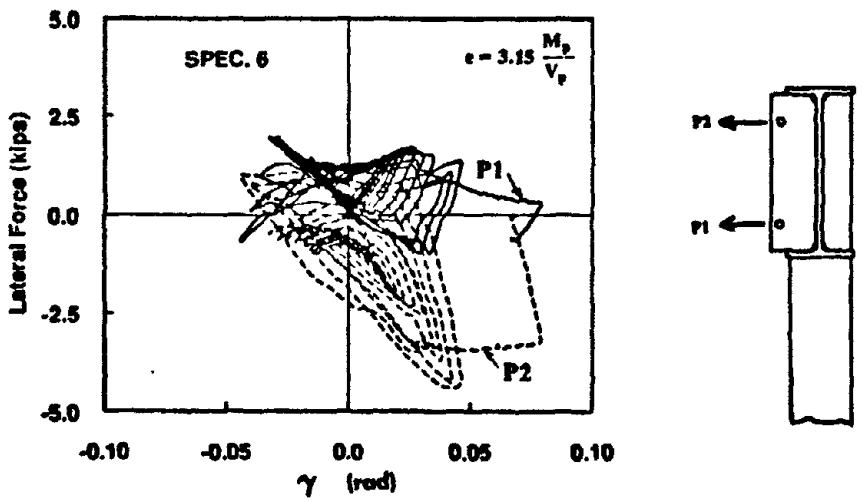

Fig. 9. Forces at link end lateral support in advanced stages of loading of a W12 x 16 link.

The last series of tests also provided considerable insight into the behavior of various brace to beam connections. A full report on this research is in preparation [13].

The above experimental and analytical research provided the bases for practical applications, and together served in the development of code provisions for EBFs.

CODE DEVELOPMENT

Almost immediately upon publication of the first research report [2] on EBFs, several important applications of this concept were made for major buildings. It is interesting to note that the reasons for adopting this system of framing were entirely different in each of the three cases. In one, a forty-seven story building, it was determined that the originally designed frame was too flexible under high winds. In a sense, EBFs were adopted as a retrofit for this project. On another project a municipality was unwilling to accept concentric bracing for a nineteen story building for the lack of ductility in such systems. In the third case, for a four story hospital, it was determined that EBFs provided a rational solution for poor foundation conditions. By means of links, the column loads could be brought within acceptable bounds. These projects were widely scattered throughout California.

The versatility of EBFs shown by the above applications provided the driving motivation for further research in this area. Because of the research noted in the previous section, and considerable competence acquired by the professionals in the design of EBFs, the need for developing a code for such systems became clearly evident. Therefore the *Structural Engineers Association of California* (SEAOC) embarked on the development of recommended seismic provisions for EBFs.

After several years of work, the formidable task of updating the recommended seismic provisions for buildings was completed by SEAOC in January 1988 [15]. These provisions contain a section on EBFs. With minor revisions these recommendations were accepted for inclusion in the 1988 *Uniform Building Code* (UBC) [16]. Paralleling this development the *Building Seismic Safety Council* (BSSC) included in its 1985 edition of the *National Earthquake Hazards Reduction Program* (NEHRP) *Recommended Provisions for the Development of Seismic Regulations for New Buildings* tentative provisions for the design of EBFs [17]. This document is an update on the *Applied Technology Council*, report ATC3-06 [18]. In the forthcoming BSSC publication EBF design recommendations are no longer tentative. Based on the same database, these recommendations are comparable to those given by SEAOC and UBC. *The American Institute of Steel Construction* (AISC), as a supplement to its new *Load and Resistance Factor Design* (LRFD) *Specification* [19] is in the process of finalizing provisions for EBFs. These provisions, taking advantage of the latest findings, represent the most up-to-date and comprehensive requirements for EBFs, and although tentative, are followed in the remainder of this paper.

It is to be noted that the SEAOC and UBC provisions, which are essentially identical, are based on the allowable stress design approach, whereas the BSSC and AISC provisions are based on the strength design approach.

EXCERPTS FROM AISC TENTATIVE PROVISIONS FOR EBFs
(Reproduced with permission of AISC)

EQ3. DEFINITIONS (Only those definitions directly applicable to EBFs are listed)

Eccentrically Braced Frames (EBF).
That form of a diagonally braced frame where at least one end of each brace frames into a beam a short distance from a column-to-girder connection or from another beam-to-brace connection. The EBF shall meet the requirements of Section EQ9.

Link.
The segment of beam located between the end of a diagonal brace and a column or between the ends of two diagonal braces. The length of the link is defined as the clear distance between the ends of two diagonal braces or between the diagonal brace and the column face.

Link Rotation Angle.
The angle between the beam outside of the link and the link that occurs at a total story drift of E'/E times the elastic drift at the Prescribed Design Forces. The rotation angle is computed assuming the EBF bay as a rigid-ideally plastic mechanism.

Prescribed Design Forces.
Forces derived from the nominal earthquake loads per Section EQ2 multiplied by the load factors specified in Section A4.1 of the AISC LRFD Specification.

Link Design Shear Strength.
The lesser of ϕV_n or $2\phi M_p/e$, where $V_n = 0.60 F_y d t_w$, e is the link length, and $\phi = 0.9$; except as modified in sect. EQ9.2e.

Link Intermediate Web Stiffeners.
Vertical web stiffeners placed within the link.

EQ9. REQUIREMENTS FOR ECCENTRICALLY BRACED FRAMES

1. Scope:
Eccentrically braced frames shall be designed so that under earthquake loading, yielding will occur primarily in the links. The diagonal braces, the columns, and the beam segments outside of the links shall be designed to remain essentially elastic under the maximum forces that can be generated by the fully yielded and strain hardened links.

2. Links:

a. Links shall comply with the width-thickness ratios of Table A-EQ7-1. The specified minimum yield strength of steel used for links shall not exceed F_y = 50 ksi.

b. The shear force in the link produced by the prescribed design forces shall not exceed the design shear strength of the link.

c. The web of a link shall be single thickness without doubler plate reinforcement and without openings.

d. If the required axial strength, P_u, in the link at the prescribed design forces is equal to or less than $0.15 P_y$, where $P_y = AF_y$, the effect of axial force on the link design shear strength may be neglected.

e. If the required axial strength, P_u, in the link at the prescribed design forces exceeds $0.15 P_y$, the following additional requirements shall be met:

   (1) The link design shear strength shall be computed as the lesser of ϕV_{na} or $2\phi M_{pa}/e$ where $V_{na} = V_n[\,1 - (P_u/P_y)^2\,]^{1/2}$, $M_{pa} = 1.18\, M_p\,[1 - (P_u/P_y)]$, and $\phi = 0.9$.

   (2) The length of the link shall not exceed:

$$[1.15 - 0.5\,\rho\,(A_w/A)]\,1.6 M_p/V_n \quad \text{for} \quad \rho\,(A_w/A) \geq 0.3$$

$$1.6 M_p/V_n \quad \text{for} \quad \rho\,(A_w/A) < 0.3$$

   where $A_w = d t_w$, $\rho = P_u/V_u$, P_u is the required axial strength of the link, V_u is the required

shear strength of the link at the prescribed design forces.

f. The link rotation angle shall not exceed the following values (except as noted in sect. EQ9.2g):

(1) 0.08 rad. for links of length $1.6\,M_p/V_n$ or less,

(2) 0.02 rad. for links of length $2.6\,M_p/V_n$ or greater.

(3) Interpolation shall be used for links of length between $1.6\,M_p/V_n$ and $2.6M_p/V_n$.

g. Where a link is connected to a column, these additional requirements shall be met:

(1) Links connected to columns shall not exceed the length of $1.6\,M_p/V_n$. This requirement may be waived if it can be demonstrated that the link to column connection is adequate to develop the required inelastic rotation of the link.

(2) The link flanges shall have full penetration welds to the column. The connection of the link web to the column shall be welded to have a design strength to develop the design strength of the link web.

(3) Where the link is connected to the column web, the link flanges shall have full penetration welds to the connection plates and the web connection shall be welded to have a design strength to develop the design strength of the link web. The link rotation angle shall not exceed 0.015 rad. for any link length.

3. Link Stiffeners:

a. Full depth web stiffeners shall be provided on both sides of the beam web at the diagonal brace ends of the link. These stiffeners shall have a combined width not less than $(b_f - 2t_w)$ and a thickness not less than $0.75\,t_w$ nor 3/8 inches, whichever is larger, where b_f and t_w are the width of the link flange and link web thickness, respectively.

b. Links shall be provided with intermediate web stiffeners as follows:

(1) Links of length $1.6\,M_p/V_n$ or less shall be provided with intermediate web stiffeners spaced at intervals not exceeding $32\,t_w - d/5$ for a link rotation angle of 0.08 rad. or $56\,t_w - d/5$ for link rotation angles of 0.03 rad. or less. Interpolation shall be used for values between 0.03 and 0.08 rad.

(2) Links of length greater than $2.6\,M_p/V_n$ and less than $5\,M_p/V_n$ shall be provided with intermediate web stiffeners placed at a distance of b_f from each end of the link, where b_f is the link flange width.

(3) Links of length between $1.6\,M_p/V_n$ and $2.6\,M_p/V_n$ shall be provided with intermediate web stiffeners meeting the requirements of both sections (1) and (2) above.

(4) No intermediate web stiffeners are required in links of length greater than $5\,M_p/V_n$.

(5) Intermediate link web stiffeners shall be full depth. For beams less than 24 inches in depth, stiffeners are required on only one side of the beam web. The thickness of one-sided stiffeners shall not be less than t_w or 3/8 inch, whichever is larger, and the width shall not be less than $(b_f/2) - t_w$. For beams 24 inches in depth or greater, intermediate stiffeners are required on both sides of the web.

c. Fillet welds connecting the link web stiffeners to the beam web shall develop a force of at least $A_{st}\,F_y$, and those connecting the stiffener to the flanges shall develop a force of at least $A_{st}\,F_y/4$, where $A_{st} = bt$ of stiffener, b = width of stiffener plate, and t = thickness of stiffener plate.

d. Lateral supports shall be provided at both the top and bottom flanges of the link at the ends of the links. End lateral supports of links shall have a design strength of at least 4 percent of the

link flange nominal strength computed as $F_y\, b_f\, t_f$.

4. Diagonal Brace and Beam Outside Link:

a. The nominal strength of each diagonal brace shall be adequate to resist the forces generated by at least 1.5 times the design shear strength of the link.

b. The sum of the nominal flexural strength of the diagonal brace and of the beam segment outside of the link shall exceed the link end moment occurring at 1.5 times the design shear strength of the link. The nominal flexural strength of these members shall be determined using interaction equations for combined axial force and bending moment, using the axial force in the member generated by 1.5 times the design shear strength of the link.

c. Diagonal brace to link connections shall develop the nominal strength of the diagonal brace and transfer this force to the beam. No part of the diagonal brace to link connection shall extend over the link length. If the diagonal brace is assumed to resist a portion of the link end moment for satisfying sect. EQ9.4b then the diagonal brace to link connection shall be designed as fully restrained (Type FR).

d. The beam outside of the link shall be provided with sufficient lateral support to maintain the stability of the beam under the forces generated by at least 1.5 times the design shear strength of the link. Lateral supports shall be provided at both the top and bottom flanges of the beam and shall have a strength to resist at least 1.5 percent of the beam flange nominal strength computed as $F_y\, b_f\, t_f$.

5. Beam to Column Connections: Beam to column connections away from links may be designed as partially restrained, Type PR, (simple) connections. The connection shall have a strength to resist rotation about the longitudinal axis of the beam based on two equal and opposite rotation forces of at least $0.015\, F_y\, b_f\, t_f$ acting laterally on the beam flanges.

COMMENTS ON AISC EBF TENTATIVE PROVISIONS

Design Basis and Loads

The AISC seismic provisions are intended for use with the AISC LRFD Specification [19] and much of the nomenclature used in the seismic provisions are defined in the LRFD Specification. Unlike SEAOC, UBC or BSSC, neither the LRFD Specification nor the AISC seismic provisions specify design earthquake loads. Rather, these documents specify that the nominal design loads, including earthquake load E, load factors and load combinations be taken from the applicable local code. In the absence of such a code, loads and load combinations are referred to the American National Standard, *Minimum Design Loads for Buildings and Other Structures*, ANSI A58.1 [20]. The ANSI load factors and combinations for earthquake loads are: $1.2\,D + 1.5\,E + (.5\,L \text{ or } .2\,S)$ and $.9\,D - (1.3\,W \text{ or } 1.5\,E)$, where D, L, E, W and S are dead, live, earthquake, wind and snow loads, respectively. ANSI A58.1 earthquake loads are similar to those specified in the 1985 UBC, using the familiar formula for total base shear: $V = ZIKCSW$, where the various factors are as defined in ANSI A58.1. For EBFs, the AISC seismic provisions specify $K = .8$, unless used as part of a dual system, for which $K = .67$. The 1988 UBC uses a completely different formula for design base shear. However, for EBFs, the nominal unfactored earthquake loads from ANSI A58.1 are comparable to those from the 1988 UBC. In the 1988 UBC, the earthquake loads are not factored, and the design is based on the conventional allowable stress design approach. In the AISC seismic provisions, earthquake loads are factored by 1.5 and the design is based on the LRFD strength approach.

EQ3 - Definitions - Link Rotation Angle

The relationship between link rotation angle γ and story drift θ can be approximated from a rigid plastic mechanism as noted earlier. For example, for the EBF type illustrated in Fig. 1(b), this relationship is $\gamma=(L/e)\,\theta$. The value of θ used in this expression is computed as $(E'/E)\theta_e$, where θ_e is the elastic story drift occurring under factored loads. The quantity E' is defined as $3ZICSW$, where the factors in this equation are as defined in ANSI A58.1. If E is based on ANSI A58.1, then the values of E'/E are 3.75 for an EBF or 4.5 for a dual EBF-MRF system. In the 1988 UBC, the multiplier on θ_e for computing link rotation is $3R_w/8$, which is again 3.75 for an EBF or 4.5 for a dual EBF-MRF system. However, in the 1988 UBC, θ_e is taken as the elastic story drift occurring at unfactored earthquake loads. Thus, for the same frame, the AISC procedure will result in a larger computed link rotation angle as compared with the 1988 UBC.

EQ3 - Definitions - Link Design Shear Strength

The formulas given in this section provide the shear force required to produce significant yielding of the link. These formulas are based on perfect plasticity and assume no shear-moment interaction, a reasonable assumption for links [1,6,22]. Significant yielding of short links occurs when the shear force reaches the fully plastic shear capacity of the W section, which has generally been taken as $V_p=.55F_ydt_w$. The value of $V_n=.6F_ydt_w$ was adopted to be consistent with the LRFD Specification. Using the specified resistance factor of $\phi=0.9$, the value of ϕV_n is nearly identical to the value of V_p. Significant yielding of long links does not occur until flexural hinges form at both ends of the link, corresponding to a shear force of $2M_p/e$.

EQ9.1

The scope statement represents the overall design philosophy for EBFs. That is, under severe earthquake loading, yielding must be restricted to the links, which are designed and detailed to be the most ductile element of the frame. Accordingly, all other frame members must be "stronger" than the link. This design philosophy is implemented through the application of "Capacity Design" concepts. With this approach, the links of an EBF are sized according to the code specified lateral forces. The braces, columns, and beam segments outside of the links, however, are not designed for code specified lateral forces, but rather for the maximum forces generated by the fully yielded and strain hardened links. That is, all other frame members are designed for the *capacity* of the links to assure that the links are the weakest element of the frame, thereby forcing the yielding to occur in the links and preventing non-ductile failure modes such as brace buckling.

EQ9.2.a

The limiting width-thickness ratios specified in Table A-EQ7-1 of the AISC seismic provisions are taken from Table C-B5.1 of the LRFD Specification, with minor modifications.

EQ9.2.b

Links are sized so that their design shear strength (as defined above) exceeds the shear force produced in the link by the factored earthquake loads. When links are attached to columns, an elastic frame analysis will typically show large bending moments at the column end of the link. The links should not, however, be sized on the basis of these large elastic moments. The initially large elastic moment redistributes to the other end of the link, and significant yielding of the link does not occur until the shear force reaches the design shear strength. Links should be sized on the basis of their design shear strength and not on the basis of elastic bending moments.

EQ9.2.c

Tests on links with doubler plates [2], as well as tests on the related problem of column panel zones [21], have shown that doubler plates do not carry their proportional share of shear based on plate thickness under large inelastic shear deformations.

EQ9.2.e

Large axial forces in links affect both the link strength and inelastic rotation capacity. Accordingly, EBF framing arrangements that minimize axial forces in the links are preferred. In cases where significant axial forces are transferred through the links, the reduction in strength can be estimated by the given shear-axial and moment-axial interaction formulas. Further, link length should be limited as indicated in EQ9.2.e(2) to minimize the loss of inelastic rotation capacity. These equations are derived in Ref. 22. Note that these provisions effectively prohibit the use of link lengths exceeding $1.6M_p/V_n$ for links with axial forces exceeding $.15P_y$.

EQ9.2.f

Numerous tests on shear yielding links of length $e \leq 1.6M_p/V_n$ show that with proper stiffening, these links can sustain cyclic inelastic rotations of $\gamma = \pm .10\, rad$. The 1988 UBC limits link rotation for $e \leq 1.6M_p/V_p$ to $\gamma = \pm .06\, rad$. This limit was intended to provide some design conservatism and to account for uncertainties in predicting actual link rotation demand. In AISC, the rotation limit for short links has been tentatively set at $\gamma = \pm .08\, rad$. This limit reflects the difference in the link rotation calculation procedure between UBC and AISC noted earlier. Further, dynamic analyses of an EBF designed according to the draft AISC seismic provisions using an allowable link rotation of *.08 rad* demonstrate that the actual link rotation demands under real earthquake loads are at an acceptable level. These analyses are described later in this paper.

Links of length $e \geq 2.6M_p/V_n$ yield primarily in flexure and provide significantly less inelastic rotation than short shear yielding links. Recently completed tests on long links [13] indicate that $\gamma = \pm .02\, rad$ is a reasonable estimate of inelastic rotation capacity of long, flexural yielding links not attached to columns. Within the length range $1.6M_p/V_n \leq e \leq 2.6M_p/V_n$, the rotation limits reflect the transition from shear yielding to flexural yielding as the factor controlling inelastic link behavior.

EQ9.2.g

Recent tests on EBF subassemblages with long links attached to columns [13] showed failure at relatively low inelastic rotations by fracture of the link flange near the flange to column weld. These premature failures resulted from the very highly concentrated bending strains developed at the ends of long links. To prevent this very undesirable failure mode, the use of links of length $e \geq 1.6M_p/V_n$ attached to columns is prohibited. Further, for any link connected to the column web, the link rotation angle is limited to $\gamma = \pm 0.15\, rad$, reflecting the uncertain reliability of link to column web connections.

EQ9.3.b

Equally spaced web stiffeners for links of length $e \leq 1.6M_p/V_n$ are intended to delay the onset of inelastic shear buckling of the web. The specified stiffener spacing is based on Ref. 6, with slight modifications to simplify design calculations. For links of length $e \geq 2.6M_p/V_n$, inelastic shear buckling of the web is not anticipated and therefore web stiffening is not required. Rather, severe flange buckling and/or lateral torsional buckling are the dominant failure modes. Locating a stiffener at about b_f from each end of the link is intended to delay flange buckling and to torsionally stiffen the link. In the length range $1.6M_p/V_n \leq e \leq 2.6M_p/V_n$, both shear and flexural failure modes are anticipated, and therefore both web and flange stiffening is required. The behavior of very long links of length $e \geq 5M_p/V_n$ is expected to be similar to that of beams in moment resisting frames, and therefore intermediate link stiffeners are not required.

EQ9.4

This section contains the "capacity design" requirements for the diagonal brace and for the beam segment outside of the link. These provisions are intended to permit the full development of

link strength and ductility without the occurrence of significant yielding or instability in the beam or brace. Accordingly, these members must be designed for the maximum forces that can be generated by the link, accounting for all possible sources of link overstrength. Link overstrength can be attributed primarily to i) strain hardening, ii) effects of composite floor systems, and iii) the actual yield strength of steel exceeding the nominal specified yield strength. For design purposes, the AISC seismic provisions specify ultimate link strength to be taken as 1.5 times the design strength. Thus, the ultimate shear force is taken as 1.5 times the design shear force as defined earlier. The corresponding ultimate link end moments can then be computed from statics (link length times link shear equals the sum of the link end moments), and by assuming end moments are equal when the link achieves its ultimate strength. For links of length $e \leq 1.3 M_p / V_p$ attached to columns, experiments [22] have shown that end moment equalization does not occur. For this case, ultimate link end moments can be taken as M_p at the column face and $1.5 V_p e - M_p$ at the brace end of the link [23].

The ultimate link shear force will generate a large axial force in the brace. The horizontal component of the brace force, in turn, must be balanced by a large axial force in the beam. For many EBF configurations, very large axial forces, often in excess of $.5 P_y$, are generated in the beam when link ultimate strength is developed. Axial force levels in the beam can generally be limited by avoiding very shallow braces, say with a brace-beam angle less than about 35 degrees.

At the brace end of the link, the ultimate link end moment will be transferred to the beam and to the brace. If no significant yielding or instability occur in the beam or brace, the distribution of link end moment to the beam and brace can be estimated from an elastic analysis. Such an analysis will typically show that the beam carries 80 to 95 percent of the link end moment. However, since the beam also typically carries very large axial forces, yielding of the beam may occur well before link strength is fully developed. This early yielding, due to moment-axial force interaction in the beam, may result in a redistribution of bending moment to the brace.

When checking the requirements of EQ9.4, both the beam and the brace must be treated as beam-columns in strength and stability calculations. Unlike concentrically braced frames, the brace of an EBF may carry significant bending moments, particularly if an inelastic redistribution of moment occurs between the beam and the brace. These moments must be considered when checking EQ9.4.a. For the beam, adequate lateral bracing must be provided to maintain its stability under the combination of large axial force and large bending moment, as required in EQ9.4.d. For certain EBF configurations, limited yielding of the beam outside of the link may be unavoidable. However, the combined flexural strength of the beam and brace must exceed the ultimate link end moment, to assure that the link end moment can be fully developed. This is the requirement stated in EQ9.4.b. Further, per EQ9.4.c, if the brace is considered to carry a portion of the link end moment, then a rigid brace to beam connection is required.

For EBF geometries involving very flat braces and/or long links, satisfying EQ9.4 may require very heavy braces or cover plates on the beams. Such measures can often be avoided through careful choice of frame geometry at the preliminary design stages. EBFs with relatively steep braces, e.g., brace-beam angles in the range of 40 to 50 degrees, combined with short links are preferable for avoiding design problems with the beam and brace.

Columns in EBFs

Following the capacity design principles noted in the Scope statement of EQ9.1, the strength and stability of the columns must be maintained under the maximum forces generated by the links. One approach for satisfying this requirement is to assume that all links above a column achieve their ultimate strengths (1.5 times the design strength) simultaneously. This may be reasonable procedure for low to medium rise buildings, but is probably too conservative for taller buildings, since all of the links are unlikely to yield simultaneously or uniformly over the height of the frame. Additional research, particularly additional dynamic analyses of EBFs subject to real earthquake

records, is needed before detailed capacity design procedures can be established for columns in EBFs. A useful model for capacity design of columns is the procedure presented in the commentary to the New Zealand Standard on the Design of Concrete Structures [24] for columns in ductile concrete frames. Development of a similar procedure is needed for columns in EBFs.

Even though the AISC seismic provisions do not include specific requirements for EBF columns, there is a provision covering columns in all types of steel frames. With certain limitations and exclusions, this provision states that columns must satisfy the following equations:

$$1.2D + .5L + 1.0E' \leq P_n \quad \textit{for axial compression}$$

$$.9D + 1.0E' \leq P_n \quad \textit{for axial tension}$$

where D and L are dead and live load, E' is the amplified earthquake load defined earlier, and P_n is the nominal axial strength of the column in tension or compression as defined in the LRFD Specification. These equations recognize that columns will experience larger forces than those produced by the basic code specified lateral loads. However, sufficient analyses have not yet been conducted to determine if satisfying these equations will assure frame stability under real earthquake loads.

For EBFs, a more rational sizing of columns can likely be achieved by applying capacity design principles, combined with judgement on the probable distribution of link yielding over the height of the frame. Judgement in column design in EBFs can be guided by the available dynamic analyses of EBFs [11,14] as well as by studying the New Zealand approach for concrete frames noted above.

An additional concern in column design is when a single column forms part of two lateral resisting frames. These "orthogonal effects" are covered by both the 1988 UBC and by ANSI A58.1 by requiring that such columns be designed for 100 percent of the specified earthquake forces in one direction plus 30 percent of the specified earthquake forces in the orthogonal direction.

SEISMIC DESIGN OF 6-STORY EBF

A small six-story office building is considered as a design example using AISC tentative seismic provisions for EBFs. The elevation of one of the two end frames for this rectangular building is shown in Fig. 10. It is assumed that three 24 ft. moment resisting bays are connected to each of the columns of the end EBFs. Therefore, using column centerline dimensions, the building is 72 by 70 ft. in plan. The webs of the corner columns are in the plane of the EBFs. The webs of the inside columns are perpendicular to the plane of the end EBFs.

The lateral force acting on each of the end frames is calculated using the ANSI A58.1 formula for the base shear V defining the LRFD earthquake load E, i.e.,

$$E = V = ZIKCSW$$

It is assumed that this building is located in seismic zone 4, and the EBFs are a part of a dual system. Hence Z = 1, and K = 0.67. In the above equation the response factor $C = 1/\left(15\sqrt{T}\right) = 0.0996$, where $T = 0.05h_n/\sqrt{D_S} = 0.448$ sec., h_n is the height of the frame, and D_S is its width. Further, assume the importance factor I = 1, and the soil factor S = 1.2, and the half-weight of the building W = 2,270 kips. Hence E = V = 182 kips. Therefore, since according to AISC LRFD code the load factor for earthquake loads is 1.5, the base shear for each of the two EBFs is 1.5 x 182 = 273 kips.

For the preliminary design the above base shear was distributed in a triangular manner as shown in Fig. 11. For the dual system considered here, Fig. 10, it was assumed that in the upper three stories 80% of the lateral load is carried by the braced bay, and 20% by the two adjoining moment resisting bays. All lateral load was assigned to the outside two braced bays in the lower three stories.

Using the above lateral force distribution for the braced frames, the link forces were determined by statics applying the procedure shown in Fig. 11. In this approach the member moments at the cut sections are neglected. The links were then selected to satisfy the code requirements for V_n given in EQ3. Preliminary link lengths were then assigned bearing in mind the link rotation angle criteria given in EQ9.2f. As noted previously the use of short links is preferable both for performance and economy. In this design rotation angles $\gamma = .08$ were desired.

All remaining members were sized using the "capacity approach." This means that since the links strain-harden under cyclic loading, the braces are designed for 1.5 times the force that is generated by the link shear ϕV_n. The beams outside the links developing axial forces and bending moments associated with the increased brace forces were checked for code compliance. If it is found that a beam outside the link yields, the beam-brace joint must be moment resistant. Moreover, enough capacity must be developed by the joint such that the brace would not yield. Often this problem can be avoided with short links and steep braces. No such difficulties arose in this design.

The columns for the preliminary design were sized including dead, live, and earthquake loads; applying $1.5\phi V_n$ shear from the links, and including the 30% orthogonality effect in corner columns. Therefore, these columns were designed for bi-axial bending caused by the links and beams in the moment frames.

An elastic analysis for factored loads was then performed giving the elastic story drift θ_e. According to AISC tentative provisions this story drift must be multiplied by the ratio E'/E, where $E' = 3\ ZICSW$, for determining γ assuming an EBF bay as a rigid ideally-plastic mechanism. After carrying out this check the initially assumed link lengths were increased by 10%, and the necessary adjustments in member sizes were made.

The revised frame conformed to the AISC LRFD specifications including the limitation on the maximum link rotations of 0.08 rad. Inelastic time-history responses were obtained for this frame for several well known recorded earthquakes. The selected records were for the 1940 El Centro, 1966 Parkfield, 1952 Taft, 1978 Miyagi-Ken-Oki, and the 1985 Mexico City earthquakes. Of these quakes, the El Centro and the Taft earthquakes were also magnified to 0.50 g for additional computer runs. This was also done with the Miagi earthquake after magnifying the available record by a factor of 1.5.

The principal results of the inelastic dynamic analyses are assembled in the two tables. The maximum link deformations during EBF responses to the above earthquakes are displayed in Table 1. It can be observed from this table that the simple static procedure prescribed by the code based on rigid-ideally plastic mechanisms is remarkably good for the design of links for a large variety of severe earthquakes. Only for a near fault location of a building, exemplified by the Parkfield earthquake, do the rotations of the links exceed the desired limit, but since this occurs only during a single pulse, this condition is tolerable. The Miagi earthquake *per se* presented no problem for link rotations. The behavior of a frame for a magnified Miagi quake, however, indicates some difficulties. Therefore, for Japanese designs a somewhat more conservative criteria may be appropriate than in the U.S. The frame was taxed extremely little by the 1985 Mexico City earthquake designed to the AISC code. This may, however, be attributed to the three to four fold larger dominant period of the earthquake to that of the analysed frame.

It is instructive to examine the normalized link shear forces given in Table 2 for the same earthquake input data as for Table 1. These results show that the braces must indeed be designed for at least 1.5 times the nominal shear strength of the links. For this reason, it may be prudent to be conservative in selecting the braces in the lower two of three stories of a building.

It is interesting to note that using the triangular lateral load distribution both tables show that the upper stories are overdesigned. For buildings of the height considered a uniform lateral load distribution may lead to a more balanced design. Further studies of the type presented in this paper are needed for taller buildings to achieve more economical design of EBFs.

	Earthquake Record							
Floor [1]	El Centro (0.33g) [2]	El Centro (0.50g) [3]	Parkfield (0.50g) [4]	Miyagi (0.26g) [5]	Miyagi (0.39g) [6]	Taft (0.30)g [7]	Taft (0.50g) [8]	Mexico EW (0.17g) [9]
1	0.048	0.081	0.105	0.062	0.133	0.029	0.077	0.014
2	0.035	0.070	0.129	0.060	0.107	0.024	0.069	0.011
3	0.015	0.043	0.105	0.046	0.069	0.016	0.042	0.007
4	0.010	0.013	0.031	0.012	0.015	0.003	0.009	0.002
5	0.012	0.028	0.034	0.031	0.048	0.005	0.022	0.002
R	0.002	0.003	0.002	0.002	0.004	0.002	0.003	0.001

Table 1. Maximum Link Deformation During EBF Response to Selected Earthquakes Records.

	Earthquake Record							
Floor [1]	El Centro (0.33g) [2]	El Centro (0.50g) [3]	Parkfield (0.50g) [4]	Miyagi (0.26g) [5]	Miyagi (0.39g) [6]	Taft (0.30)g [7]	Taft (0.50g) [8]	Mexico EW (0.17g) [9]
1	1.51	1.55	1.58	1.55	1.64	1.53	1.51	1.40
2	1.45	1.52	1.59	1.53	1.59	1.39	1.53	1.21
3	1.33	1.45	1.52	1.40	1.49	1.31	1.47	1.11
4	1.16	1.24	1.40	1.20	1.28	1.03	1.21	0.94
5	1.24	1.39	1.42	1.37	1.49	1.07	1.34	0.98
R	0.82	1.02	0.98	0.84	1.04	0.74	1.03	0.53

Table 2. Maximum Normalized Link Shear Force, V_{max} / V_p, During Response to Selected Earthquake Records.

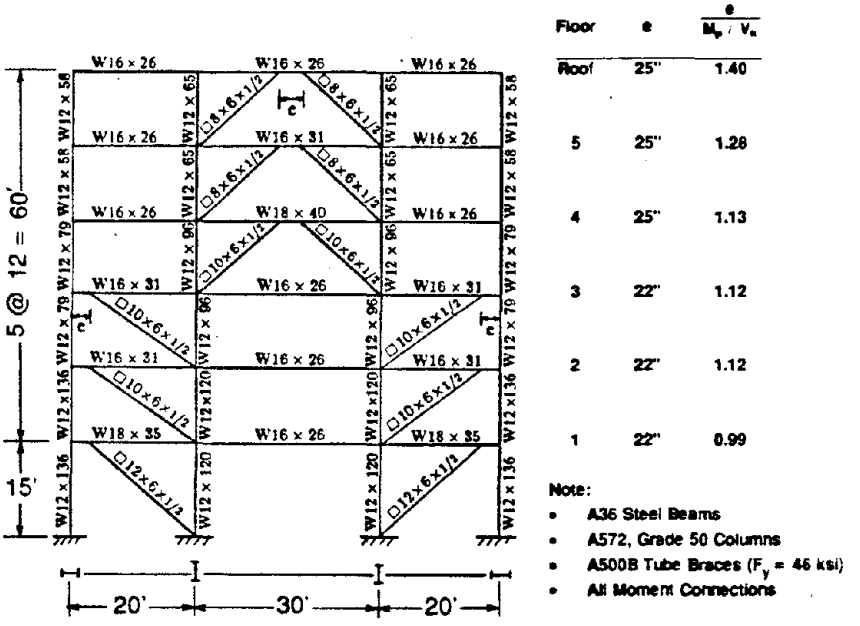

Fig. 10 Elevation of six story EBF

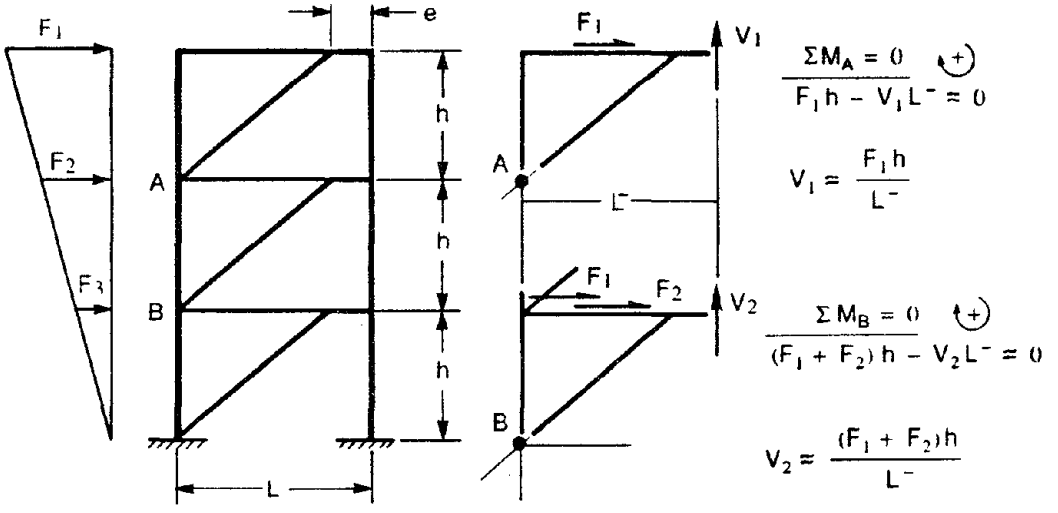

Fig. 11. Simplified Static Analysis of an EBF

EBF DETAILS

In any structure designed to resist seismic forces it is imperative to have joints with good ductile connections. For EBFs there are three kinds of joints that require special detailing. One of these is for connecting the braces to beams, another for connecting the links to a column, and the third, connecting the braces and beams to a column at a joint. All three joints are illustrated below.

The detail shown in Fig. 12 and used in Tsukuba full-size tests [10] proved to be not entirely satisfactory. At extreme cyclic loads beyond the initially planned test, the gusset plate attaching the brace to the beam at the second floor buckled. In extreme cases, a negative bending moment reaching as much as 1.5 M_p may develop at link ends because of strain-hardening. Gusset buckling can be avoided by employing the detail shown in Fig. 13. Here two edges of the gusset plate are stiffened. Note also that the tubular brace comes close to the beam flange. Experiments have shown that such connections behave well under cyclic loads and the tube gusset connection can develop a substantial moment capacity [13].

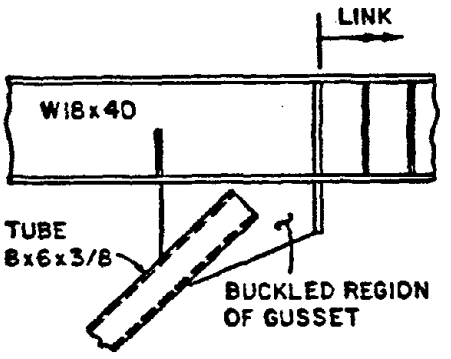

Fig. 12. Detail of failed brace connection.

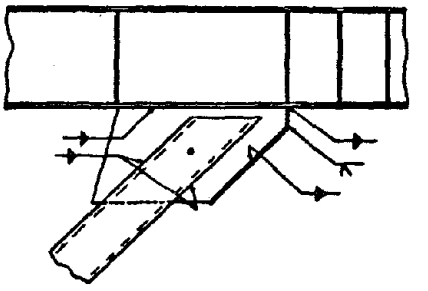

Fig. 13. Detail of improved tube brace-gusset plate connection.

Two other types of satisfactory brace-to-beam connections are shown in Figs. 14 and 15. For field erection both of these details require overhead welds. Horizontal stiffeners placed at beam edges spanning between the vertical stiffeners are required for the detail shown in Fig. 15. Both connections behaved well under severe cyclic loading [13].

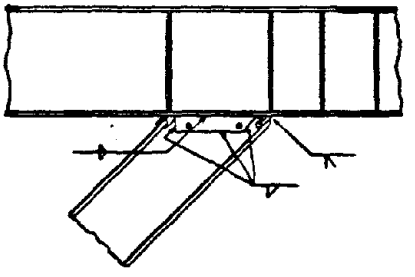

Fig. 14. Detail of WF brace-beam connection.

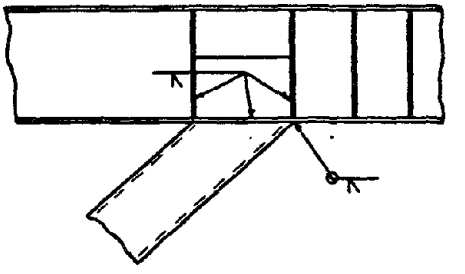

Fig. 15. Detail of tube brace-beam connection.

The link-to-column connection in Fig. 16 is similar to the conventional detail used in MRFs. The shear tab, however, must be welded to the web of the beam. The bolts shown in the figure are erection bolts. Conventional link-to-column web connections, Fig. 17, should be avoided as experiments have repeatedly demonstrated that such connections sustain only very limited cyclic loads.

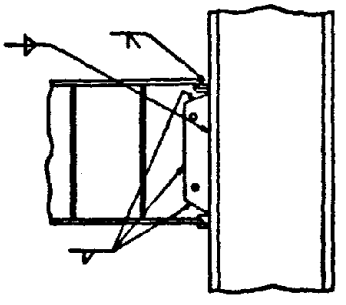

Fig. 16. Typical link-to-column flange connection detail.

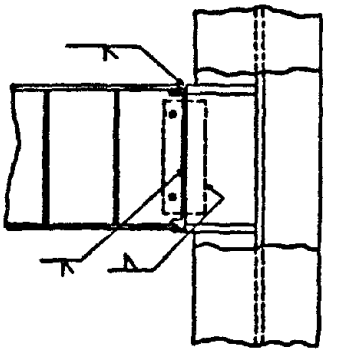

Fig. 17. Link-to-column web connection detail shown has limited cyclic capacity at severe loads.

Nominally concentric joints for beam-column-brace connections are shown in Figs. 18 and 19. The connections shown in Fig. 18 involves field welding, and may be easily modified to make use of a welded detail in connecting the shear tab to the beam web. The detail shown in Fig. 19 is for field bolting. Note that in either detail the centerlines for the three members do not need to intersect at a point permitting design of a compact joint.

Analyses have shown that very little penalty on cyclic frame performance is paid by assuming the connection of the type shown in Fig. 19 as pinned [11].

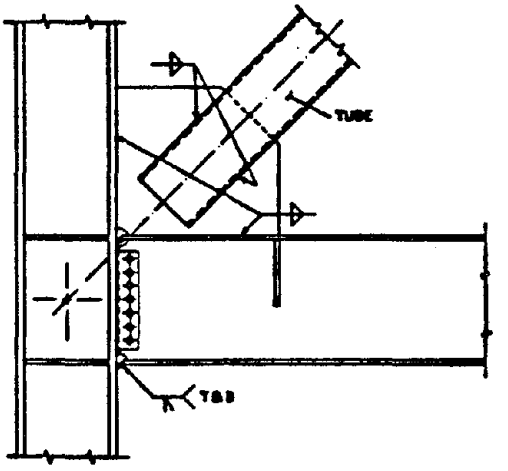

Fig. 18. Detail for brace at beam-column moment connection.

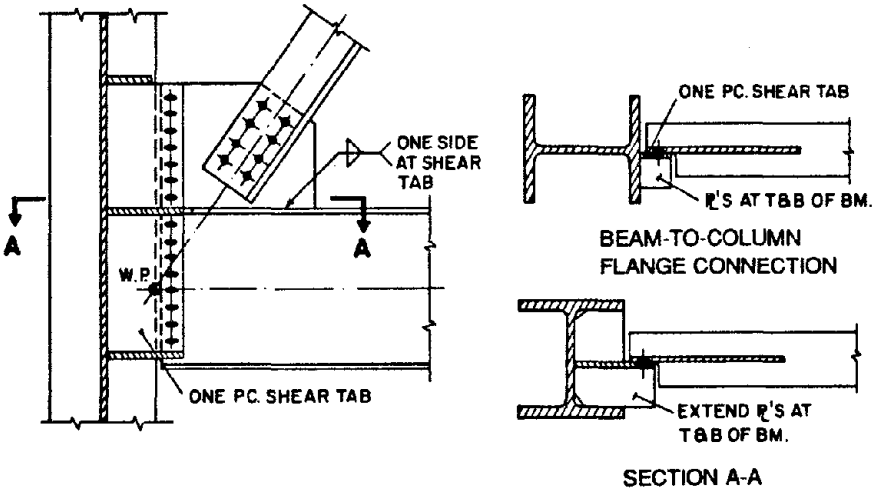

Fig. 19. Bolted detail for beam-column-brace connection.

CONCLUSIONS

Eccentrically braced frames have become a well established structural steel system for seismic resistant construction. Sustained research since the mid-1970's combined with experience from numerous field applications has provided a database for the proper design of EBFs and has lead to the development of code provisions for EBF design and detailing. Selected research findings have been highlighted and the development of code provisions for EBFs in the U.S. has been briefly discussed in this paper.

The most recent EBF code provisions are contained in the just completed tentative AISC seismic provisions for steel buildings. This document represents the most up-to-date and comprehensive code requirements for EBFs currently available in the U.S. Excerpts from the tentative AISC seismic provisions pertaining to EBFs have been reproduced in this paper and comments have been provided on the background of selected provisions.

A six story steel building with EBFs was designed using the tentative AISC provisions. A number of inelastic dynamic time history analyses were performed for this building, using several severe ground motion records. The behavior of the EBFs in these analyses was satisfactory, with acceptable levels of link inelastic rotation demands.

Proper detailing is critical for fully developing the ductility of an EBF. Many of the detailing requirements for EBFs, including link stiffener requirements, are provided in the AISC code provisions. To supplement these provisions, a number of suggested connection details for EBFs have been illustrated in this paper.

Based on research and design experiences with EBFs to date, some of the most important design issues are summarized below.

1. Some desirable EBF bracing arrangements are shown in Fig. 1. The EBF type shown in Fig. 1(b) is particularly advantageous because any potential problems with link to column connections are avoided.
2. The use of short, shear yielding links are preferred, as these provide for the maximum strength, stiffness and energy dissipation capacity of the frame. Links in the length range of about M_p/V_p to $1.2\,M_p/V_p$ appear to be particularly effective.
3. Link lengths exceeding about $1.6\,M_p/V_p$ should only be used when links are not attached to columns, as in Fig. 1(b).
4. The use of link to column weak axis connections should be avoided.
5. The use of very flat braces should be avoided in order to limit axial force levels in the beam segment outside of the link. Design problems with the beam and brace can often be avoided by using relatively steep braces, say with a brace-beam angle of 40° to 50°, together with very short links. The use of short links limits the bending moment transferred to the beam and brace from the link.
6. Strong and stiff lateral bracing should be provided at both ends of the link.
7. The braces, columns, and beam segments outside of the links should be designed for the forces generated by the fully yielded and strain hardened links. That is, "capacity design" principles should be used as an overall design basis for these frame elements.
8. Both the braces and beam segments outside of the link should be treated as beam-columns, considering both axial force and bending moment in strength and stability computations.
9. If the brace is considered to carry a portion of the ultimate link end moment, a rigid brace to beam connection should be used.

ACKNOWLEDGEMENTS

The authors are grateful to the National Science Foundation under grant ECE-8603320, and the American Iron and Steel Institute, for support of this research program over a number of years. Dr. S.-C. Liu of NSF, and A. Kuentz of AISI were particularly helpful. The second two authors also acknowledge the continued financial support of the American Institute of Steel Construction Fellowship Program. The opinions expressed in this paper are those of the authors and do not necessarily reflect the views of the sponsors.

REFERENCES

1. Kasai, K. and E.P. Popov, "A Study of Seismically Resistant Eccentrically Braced Frames," *Report No. UCB/EERC-86/01*, Earthquake Engineering Research Center, University of California, Berkeley, CA, 1986.
2. Roeder, C.W. and E.P. Popov, "Eccentrically Braced Frames for Earthquakes," *Journal of the Structural Division*, ASCE, Vol. 104, No. 3, March 1978, pp. 391-412.
3. Manheim, D.N., "On the Design of Eccentrically Braced Frames," *Thesis*, D.Eng., Department of Civil Engineering, University of California, Berkeley, February 1982.
4. Hjelmstad, K.D. and E.P. Popov, "Cyclic Behavior and Design of Link Beams," *Journal of the Structural Division*, ASCE, Vol. 109, No. 10, October 1983.
5. Malley, J.O. and E.P. Popov, "Shear Links in Eccentrically Braced Frames," *Journal of the Structural Division*, ASCE, Vol. 110, No. 9, September 1984, pp. 2275-2295.
6. Kasai, K. and E.P. Popov, "Cyclic Web Buckling Control for Shear Link Beams," *Journal of the Structural Division*, ASCE, Vol. 112, No. 3, March 1986, pp. 505-523.
7. Ricles, J.M., and E.P. Popov, "Experiments on EBFs with Composite Floors," *Report No. UCB/EERC-87/06*, Earthquake Engineering Research Center, University of California, Berkeley, CA, 1987.
8. Ricles, J.M., and E.P. Popov, "Composite Action in EBFs," *Journal of the Structural Division*, ASCE, (in review).
9. Popov, E.P., and J.M. Ricles, "An Experimental Study of Seismic Resistant EBFs with Composite Floors," *9WCEE Paper*, No. E05-05, August 1988.
10. Roeder, C.W. D.A.Foutch, and S.C. Goel, "Seismic Testing of Full-Size Steel Building - Part II," *Journal of the Structural Division*, ASCE, Vol. 113, No. 11, Nov. 1987, pp. 2130-2145.
11. Ricles, J.M., and E.P. Popov, "Dynamic Analysis of Seismically Resistant EBFs," *Report No. UCB/EERC-87/07*, Earthquake Engineering Research Center, University of California, Berkeley, CA, 1987.
12. Ricles, J.M., and E.P. Popov, "An Analytical Study of Seismic Resistant EBFs," *9WCEE Paper*, No. E05-06, August 1988.
13. Engelhardt, M.D., "Behavior of Long Links in EBFs," *Ph.D. Dissertation*, Department of Civil Engineering, University of California, Berkeley, CA, (to be published in 1988).
14. Whittaker, A.S., C.M. Uang, and V.V. Bertero, "Earthquake Simulation Tests and Associated Studies of a 0.3 Scale Model of a Six-Story Eccentrically Braced Steel Structure," *Report No. UCB/EERC-87/02*, Earthquake Engineering Research Center, University of California, Berkeley, CA, 1987.
15. SEAOC, *Recommended Lateral Force Requirements*, Seismology Committee, Structural Engineers Association of California, Sacramento/San Francisco/Los Angeles, January 1988.
16. ICBO, *Uniform Building Code*, International Conference of Building Officials, Whittier, CA, 1988.
17. NEHRP, *Recommended Provisions for the Development of Seismic Regulations for New Buildings*, National Earthquake Hazards Reduction Program, Building Seismic Safety Council, Federal Emergency Management Agency, Washington, D.C., 1985.
18. ATC 3-06, *Technical Provisions for the Development of Seismic Regulations for Buildings*, Applied Technology Council, U.S. Department of Commerce, 1978.
19. AISC, *Load and Resistance Factor Design Specification for Buildings*, American Institute of Steel Construction, Chicago, IL, 1986.
20. ANSI A58-1, *Minimum Design Loads for Buildings and Other Structures*, American National Standards Institute, 1987.
21. Krawinkler, H., V.V. Bertero, and E.P. Popov, "Inelastic Behavior of Steel Beam-to-Subassemblages," *Report No. UCB/EERC-71/07*, Earthquake Engineering Research Center, University of California, Berkeley, CA, 1971.

22. Kasai, K., and E.P. Popov, "General Behavior of WF Steel Shear Link Beams," *Journal of the Structural Division*, ASCE, Vol. 112, No. 2, February 1986, pp. 362-382.

23. Popov, E.P. and M.D. Engelhardt, "Seismic Eccentrically Braced Frames," *Journal of Constructional Steel Research (U.K.)*, Vol. 10, 1988.

24. NZS 3101, *Commentary on the Design of Concrete Structures*, Standards Association of New Zealand, Part 2, 1982.

AN EXPERIMENTAL STUDY OF SEISMICALLY RESISTANT ECCENTRICALLY BRACED FRAMES WITH COMPOSITE FLOORS

Egor P. POPOV[1] and James M. RICLES[2]

[1]Department of Civil Engineering,
University of California, Berkeley, California 94720, USA
[2]Department of Applied Mechanics and Engineering Science,
University of California at San Diego, La Jolla, California 92093, USA

SUMMARY

Described are the results of an experimental study on the effects of composite action in seismically resistant eccentrically braced steel frames having a concrete floor slab. The objectives of this study were to assess the cyclic strength and ductility of short composite links, the effectiveness of the floor slab in providing restraint to the links against lateral-torsional buckling, and the participation of the floor beam outside the link.

INTRODUCTION

An eccentrically braced steel frame, EBF, is a structural system in which at least one end of every brace is connected so as to isolate a beam segment called a *link*. During overloading of an EBF the links are designed to act as fuses by yielding and dissipating energy, thereby limiting the amount of force that the adjacent columns and braces must resist. When properly detailed, these links provide a stable source of energy dissipation. Brace buckling is inhibited by designing the brace members to resist the forces associated with the strength of the links. This feature, coupled with the property of large elastic stiffness, make EBFs a very suitable structural system for seismically active regions.

Past research in the U.S. has been devoted to studying the hysteretic properties of bare steel links in order to establish criteria for their design. The first experiments dealing with the seismic response of EBFs with composite floors was that of Phase II of the U.S./Japan cooperative research program conducted in Tsukuba, Japan (Ref.1). The test specimen consisted of a full scale K-braced EBF where the links were located at midspan of the floor beams in the braced bay. Test results indicated that links with composite floors would likely perform well during extreme seismic events. Because of a local failure in a brace-beam connection at extreme cyclic load in the Tsukuba test, and a lack of data on link behavior next to columns, a research program on cyclic behavior of composite links was conducted at Berkeley on an NSF sponsored project (Ref.2). The Tsukuba EBF was used as a prototype structure, where the first floor link where failure occurred was a W18 x 40.

EXPERIMENTAL PROGRAM

Links were tested for K-braced and V-braced EBF configurations using two-thirds scale subassemblies simulating the floor beams shown in Figs. 1(a) and (b). In both frames the plastic link rotation γ_p is related to the plastic story drift angle θ_p, bay width L, and link length e by:

$$\gamma_p = \theta_p L / e \tag{1}$$

The kinematics of the K-braced EBF mechanism in Fig. 1(a) requires that the corresponding subassembly be subjected to equal but opposite displacements δ at the ends of the link, while the V-braced EBF

subassembly requires that the imposed link end displacements result in an equal slope of θ in both beam segments outside the link. The link rotations γ in the subassemblies, neglecting small amount of elastic deformation, correspond reasonably well to γ_p of the EBFs. To account for the exterior column rotational constraint in the V-braced EBF, the beam moment of inertia was increased on one side of the link. The link end displacements δ were imposed by cyclic jack forces P_A and P_B. These forces simulated the vertical components of axial brace force in the K-braced subassembly, and the exterior column axial force and the vertical component of axial force of one of the braces in the V-braced subassembly. The experimental simulation did not consider axial force effects in the link. It is believed, however, that the floor beam moment and shear forces developed in the vicinity of the link corresponded reasonably well to conditions in an EBF.

Tests were performed on six composite and two bare steel link specimens. The composite links were a part of a composite lightweight concrete floor slab of 16 ft. width and 18 ft. length, which was cast on formed metal deck and supported from below by three parallel W12 x 19 steel floor beams, Beams A, B, and C as shown in plan in Fig. 2(a). In this figure the locations of the six composite links are identified. The two bare steel links D1 and D2 are shown on an isolated beam. Eight specimens are identified and described in the first and second columns of Table 1. An elevation of the test setup for a composite link in a K-braced subassembly is shown in Fig. 2(b). By moving the test end frame from location 1 to 6, the pinned column support from location 4 to 2, and the hydraulic jacks from locations 2 to 4 and 3 to 5, a V-braced subassembly was obtained for the same beam. The extent of floor slab damage was expected to be small based on observations during the Tsukuba tests, thereby justifying the use of one floor slab and three floor beams for constructing the six composite specimens.

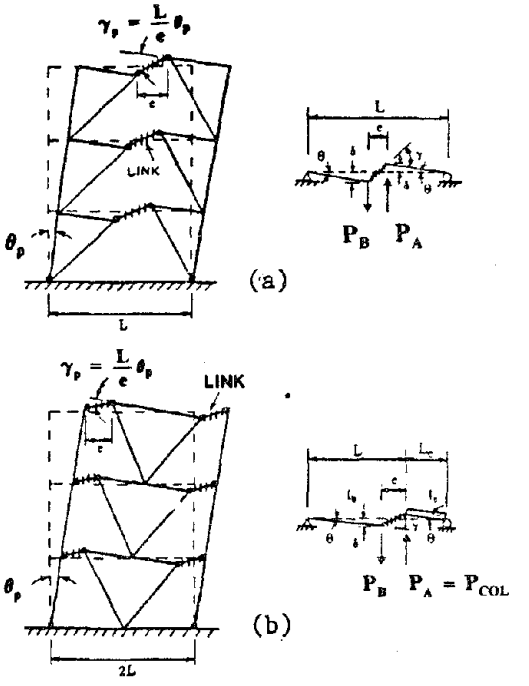

Fig.1 (a)K-Braced, and (b)V-Braced EBFs with Experimental Subassemblies.

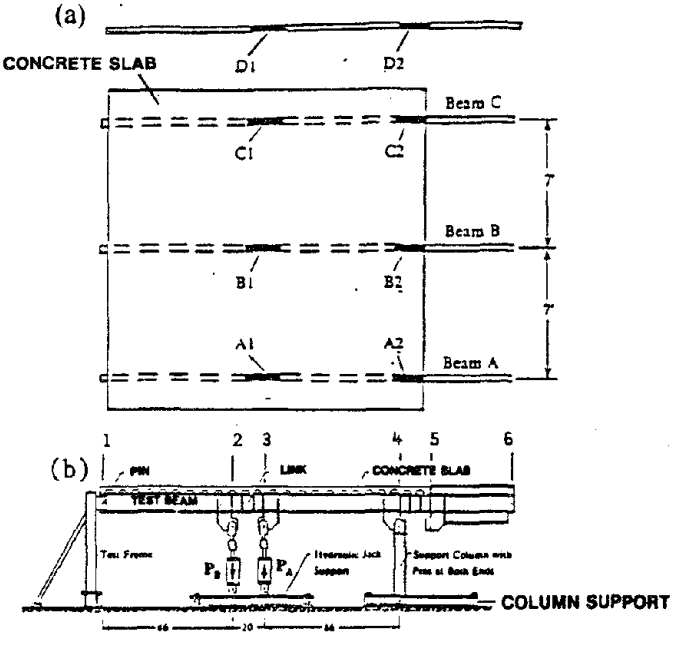

Fig.2 (a)Plan of Specimen Location, and (b)Elevation of K-Braced EBF Subassembly.

The details of the composite floor slab consisted of a standard 20 gage cold formed metal deck with two inch high ribs. The lightweight concrete slab was 4.5 in. thick. The ribs were placed perpendicular to the floor beams. Pairs of shear connectors of 3.5 in. length and 0.5 in. diameter were welded directly through the deck in each rib to the floor beam top flange at a six inch spacing, except along a 12 ft. length centered above Specimen B1, where the metal decking was removed allowing the shear connectors to be placed at a 4 in. spacing. This detail was similar to that in the Tsukuba EBF. The average compressive strength of the lightweight concrete slab during testing was 4200psi. The links were designed to yield in shear based on bare steel criteria and were 19 in. long. One sided web stiffeners were welded to the web and flanges in the link. A stiffener spacing to web thickness ratio, a/t_w, of 25 was used for all composite links, except for Specimen A2 where the stiffener spacing was reduced by one-half resulting in the ratio a/t_w being equal to 12.5. The average yield strength of the W12 x 19 floor beam determined by tension coupon tests was 49.7 ksi, with an average ultimate strength of 64.3 ksi. In all tests except for Specimen

C2, at both ends of the link and at intermediate points outside the link lateral bracing was provided from one side by W10 x 15 beams with simple connections. Specimen C2 was not laterally braced at either end of the link.

Specimen [1]	EBF Type [2]	K^* (kips/in) [3]	V_y (kips) [4]	M_y (kip-in) [5]	$\frac{V_y}{V_{yD1}}$ [6]	$\frac{V_y}{V_{yD2}}$ [7]	$\frac{V_y}{V_p}$ [8]	$\frac{M_y}{M_p}$ [9]
A1	Composite Exterior K-Braced	706	88.1	975	1.03	–	0.95	0.82
B1	Composite Interior K-Braced	859	100.1	1154	1.17	–	1.07	0.97
C1	Composite Exterior K-Braced	707	86.9	965	1.02	–	0.92	0.81
D1	Bare Steel K-Braced	569	85.3	1170	1.00	–	0.92	0.98
A2	Composite Exterior V-Braced	747	87.0	1021	–	1.08	0.93	0.86
B2	Composite Interior V-Braced	812	94.7	1182	–	1.16	1.02	0.99
C2	Composite Exterior V-Braced	744	85.9	914	–	1.06	0.92	0.77
D2	Bare Steel V-Braced	698	81.4	1111	–	1.00	0.87	0.93

Table 1 Link Identification, Initial Elastic Stiffness and Force at Initial Yielding of Specimens.

All test specimens were subjected to quasi-static cyclic forces P_A and P_B (see Fig. 1) causing progressively increasing link rotation angles $\pm \gamma$. The maximum magnitudes of these angles were comparable to those that may occur during a major earthquake. The history of γ for all specimens, excluding C1, consisted of a sequence in which the magnitudes of successive pairs of rotation cycles were 0.02, 0.04, 0.06, 0.08, and 0.10 rad. Prior to this sequence of cyclic deformation in Specimens A1 and C2, random pulses of large γ were applied. The history for γ applied to Specimen C1 was based on the measured first floor inter-story drift of the Tsukuba EBF subjected to the Taft earthquake with a peak ground acceleration of 0.5g. In the subassemblies the link displacements were monitored by linear potentiometers at the link ends to measure both the vertical movement and twist of the beam. Rotation at the link ends and the slip between the floor beam and concrete slab were measured using appropriately placed linear variable differential transformers (LVDTs). Hydraulic jack forces and reactions at the ends of the floor beams were monitored using calibrated load cells. The links were whitewashed to aid in observing the pattern and progress of yielding.

EXPERIMENTAL RESULTS

The initial elastic response of each specimen provided data for determining the elastic link stiffness. This pseudo-elastic link stiffness K^* was computed for each specimen by dividing the elastic shear force V by the relative vertical displacement v between the link ends (e.g. $K^* = V/v$). The computed values for K^* are given in the third column of Table 1. These results indicate that all composite links had a greater initial elastic stiffness than the corresponding bare steel links (Specimens D1 and D2), with the interior composite links (Specimens B1 and B2) showing the largest increase. Specimen B1 of the K-braced subassembly has a K^* equal to 1.51 times that of Specimen D1. Since the elastic lateral stiffness of an EBF is influenced by its link stiffnesses, this implies that EBFs with composite floors will have an increased elastic lateral stiffness. In Fig. 3 the shear-deformation, $V - \gamma$, hysteretic loops for the composite link, Specimen B1, have been superimposed onto those of the bare link, Specimen D1 showing the increased initial elastic stiffness of the composite link. However, in subsequent cycles the elastic stiffness of Specimen B1 appears to deteriorate towards that of the bare steel link, Specimen D1. This is a consequence of floor slab damage above the link during the subsequent cycles of link deformation.

In both the bare steel and composite specimens yielding originated in the link webs. Following this yielding, the stiffness of the links decreased dramatically with continued deformation, as shown in Fig. 3. The link shear force V_y at initial yield for all specimens are summarized in column four of Table 1, and are normalized with respect to the bare steel specimens in columns six and seven. Like K^*, V_y are larger for the composite links, particularly for the interior Specimens B1 and B2; their shear strength is also greater than the plastic shear strength $V_p = 0.55\, F_y d t_w$ of the bare steel links (column 8). In column 9 of Table 1 the largest link end moments M_y at initial yield are normalized by the flexural capacity

$M_p = ZF_y$ of a bare steel link. Unlike the shear force, the moment M_y in the composite links is either approximately equal to or less than that of the bare steel links. This is possible because the shear is related to the sum of link end moments, and the sum of the link end moments at initial yield in the composite links exceeded that of the bare steel links. Note that for the composite links M_y does not exceed M_p.

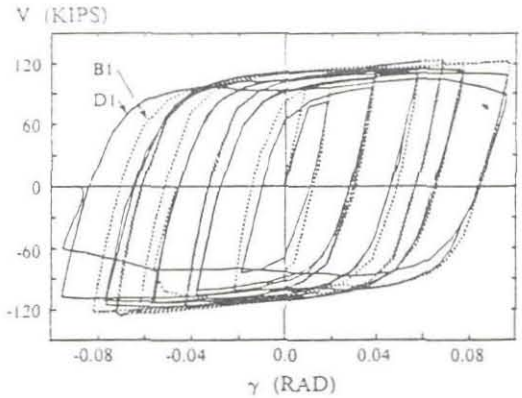

Fig.3 Shear-Deformation Relationship for Composite Specimen B1 and Bare Steel Specimen D1.

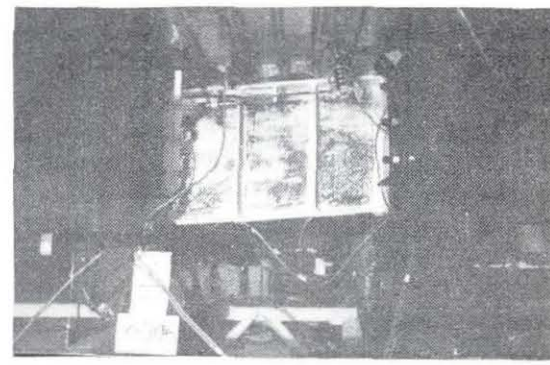

Fig.4 Link of Specimen B1 Prior to Web Buckling with Extensive Web Yielding.

With continued cyclic deformation both the bare steel and the composite links developed extensive web yielding. Furthermore, as shown by the hysteretic loops in Fig. 3, a larger shear force developed in the links in successive cycles is due to combined isotropic and kinematic hardening. However, the discrepancy between their strengths diminishes with the increased number of cycles. Fig. 4 shows the link of Specimen B1 with significant web yielding, evident by the flaked whitewash, and deformed into the shape of a parallelogram at $\gamma = 0.06$ rad. The bare steel links yielded and deformed in a similar manner.

Due to strain hardening the link shear forces increased in successive cycles, until web buckling occurred in the link. Following web buckling the link strength would gradually deteriorate; this effect was more pronounced for the bare steel links. The web stiffeners delayed web buckling and provided a means of developing tension field action in buckled web panels. The deformation of the web stiffeners and flange around the buckled panel shown in Fig. 5 was typical of both the composite and bare steel links following web buckling. The maximum magnitude of link deformation γ_u for bare steel links given in Ref. 3 is

$$a/t_w + d/(5t_w) = C_B \qquad (a \le d) \tag{2}$$

where a, t_w, and d are the stiffener spacing, web thickness, and beam depth, respectively, and the constant C_B = 56, 38, and 29, respectively, for γ_u = 0.03, 0.06, and 0.09 rad. A calculated value of γ_u = 0.072 rad. for the specimens (excluding Specimen A2) agrees reasonably well with measured values of γ_u summarized in column 2 of Table 2. Specimen A2 did not develop web buckling because of the small web stiffener spacing.

A summary of the maximum shear force V_{max} and moment M_{max} developed in the links is given in the third and fourth columns of Table 2. V_{max} of the composite links exceeds that of the bare steel links, where Specimens B1 and B2 developed a V_{max} that was 10 and 11 percent greater than that of Specimens D1 and D2, respectively. Column five of Table 2 gives and indication of the amount of strain hardening, where it is shown that the composite links with web buckling developed a V_{max} ranging from 1.29 V_y to 1.44 V_y and the bare steel links developing similar values, where V_{max} = 1.38 V_y and 1.44 V_y. Since Specimen A2 did not suffer link web buckling, it was able to achieve V_{max} = 1.53 V_y. M_{max} of the composite links was either approximately equal or greater than M_{max} of the corresponding bare steel links. All specimens developed magnitudes of M_{max} exceeding M_p, as shown in column six of Table 2. Specimen C1 developed the largest magnitude of M_{max}, however, as shown in the seventh column of Table 2 this represents only 0.75 M_{ult}, where M_{ult} is the AISC (Ref.4) flexural capacity based on full composite action.

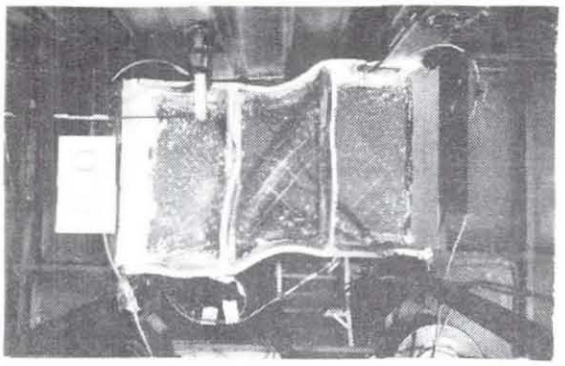

Fig.5 Link of Specimen B1 After Developing Web Buckling in Center Panel.

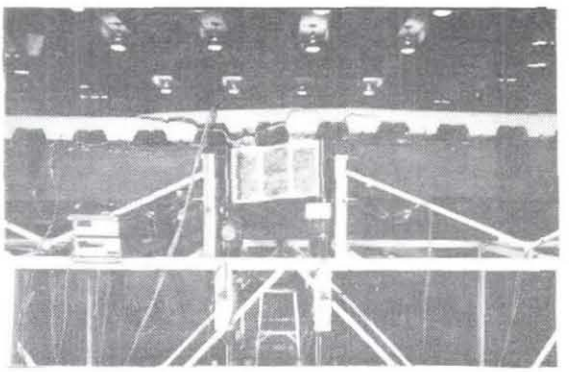

Fig. 6 Floor Slab Damage, Specimen C1.

Specimen [1]	γ_u (rad) [2]	V_{max} (kips) [3]	M_{max} (kip-in.) [4]	$\frac{V_{max}}{V_y}$ [5]	$\frac{M_{max}}{M_p}$ [6]	$\frac{M_{max}}{M_{ult}}$ [7]
A1	0.079	127.2	1534	1.44	1.29	0.70
B1	0.069	129.2	1369	1.29	1.15	0.61
C1	0.070	118.0	1644	1.36	1.38	0.75
D1	0.073	117.5	1323	1.38	1.11	0.61
A2	–	133.2	1609	1.53	1.35	0.74
B2	0.071	130.7	1500	1.38	1.26	0.66
C2	0.069	120.0	1358	1.40	1.14	0.62
D2	0.076	117.7	1377	1.44	1.16	0.64

Table 2 Maximum Link Forces for Specimens in the (a) K-Braced and, (b) V-Braced Subassemblies.

M_{ult} is not achieved in the links because of the loss of composite action resulting from slab damage. Most of the floor slab damage occurred in the vicinity of the link and consisted primarily of rib cracking, deck separation from the concrete, and slip δ_f between the steel beam and concrete slab due to deformation of the shear connectors. The rib cracking and deck separation is shown in Fig. 6, and the slip δ_f inside the link is compared to δ_f 18 in. outside the link in Fig. 7. The moment-rotation relationship of the floor beam outside the link remained essentially linear, with a change in stiffness under moment reversal, as shown in Fig. 8, where the rotation θ_{ch} of the beam is plotted against moment M. Based on a regression analysis of the experimental data it was determined that for positive moment the effective moment of inertia I_{eff} of the composite floor beam was 2.59I and 1.75I for the interior and exterior floor beams, respectively, where I is the moment of inertia of only the bare steel beam. Under negative moment it was found for all composite beams that I_{eff} = 1.28I. To assess whether the floor slab provided adequate restraint against lateral-torsional buckling of the link, measured histories of the angle of twist ϕ of the steel cross-section at the end of the link were examined. Fig. 9(a) shows a measured history of ϕ at the end of a link with W10 x 15 lateral bracing, and Fig. 9(b) the response of a composite link without lateral bracing. It is apparent from Fig. 9 that the slab does not effectively restrain the steel section against lateral movement, for in Fig. 9(b) the specimen cross-section shows drift from its initial configuration while in Fig. 9(a) the specimen cross-section returns to its initial position.

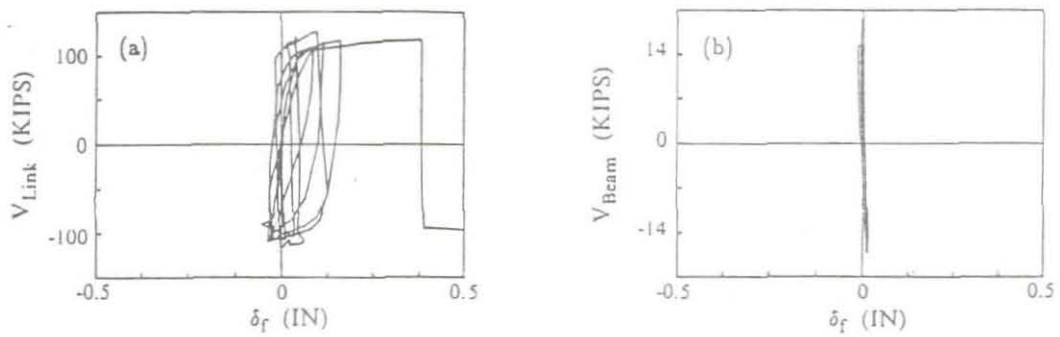

Fig.7 Slip δ_f between Floor Beam and Concrete Slab (a) In the Link, and (b) 18 in. Outside the Link.

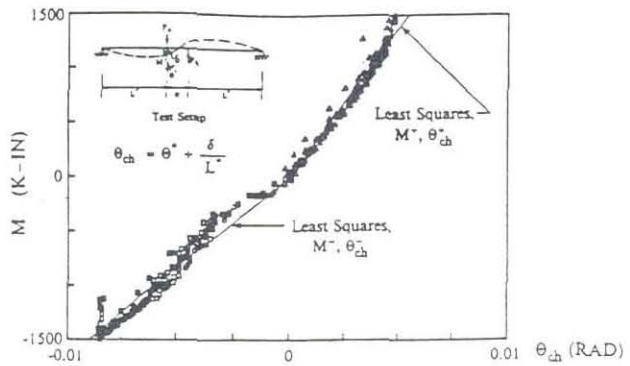

Fig.8 Moment-Rotation Relationship of Composite Floor Beam Outside the Link.

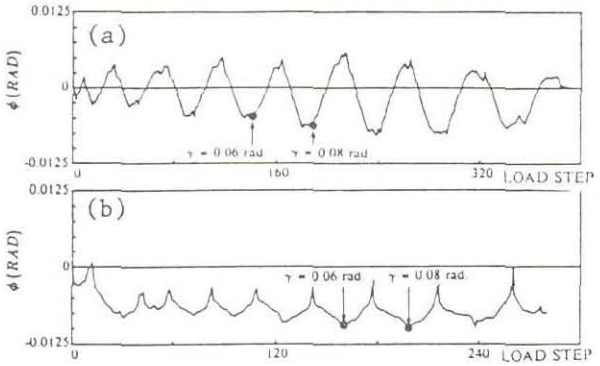

Fig.9 Twist at End of Link for (a) Laterally Braced, and (b) Unbraced Link.

CONCLUSIONS

Based on this limited experimental investigation of the effects of composite action in floors of EBFs, the following tentative conclusions can be reached:

1. Links with composite action have a greater initial elastic stiffness, yield and ultimate strength. Composite links can be designed to yield in shear using current bare steel criteria. The increase in strength should be considered when designing braces and columns adjacent to composite links.
2. Full composite action in the composite links is not maintained during severe cycling due to slab damage. The behavior of the composite floor beam outside the link is essentially linear, for the slab damage is concentrated primarily above the link.
3. Link web buckling occurred in both the bare steel and composite specimens, and can be predicted and controlled using current bare steel link criteria.
4. To maintain ductility of composite links, lateral bracing at the ends of a link must be provided in order to avoid lateral-torsional buckling of the steel beams.

REFERENCES

1. Goel, S.C., and Foutch, D.A., "Preliminary Studies and Test Results of Eccentrically Braced Full-Sized Steel Structure," *U.S.-Japan Cooperative Earthquake Research Program 16th Joint Meeting*, May 15-18, Washington, D.C., 1984.
2. Ricles, J.M., and Popov, E.P., "Experiments on Eccentrically Braced Frames with Composite Floors," *EERC Report No. 87-06*, Earthquake Engineering Research Center, University of California, Berkeley, California, June 1987.
3. *Uniform Building Code*, International Conference of Building Officials, Whittier, California, 1988.
4. *Specification for the Design*, Fabrication and Erection of Structural Steel for Buildings, 8th ed., American Institute of Steel Construction, Chicago, 1980.

AN ANALYTICAL STUDY OF SEISMICALLY RESISTANT ECCENTRICALLY BRACED STEEL FRAMES

James M. RICLES[1] and Egor P. POPOV[2]

[1]Assistant Professor of Structural Engineering,
Department of Applied Mechanics and Engineering Science,
University of California at San Diego, La Jolla, California, USA
[2]Professor Emeritus of Civil Engineering,
University of California at Berkeley, Berkeley, California, USA

SUMMARY

Presented are results of an analytical study of seismic resistant eccentrically braced frames, EBFs, subjected to severe earthquakes. The purpose of this study was to assess current EBF seismic design criteria involving short links designed to yield in shear. Two EBFs were designed and analyzed for response to different earthquake accelerograms using inelastic time history procedures. Parameters which were investigated included the effects of strain hardening and composite action. In order to assure accurate results, link and composite beam-column elements were developed based on experimental data to model floor beams in EBFs.

INTRODUCTION

An EBF is a braced frame in which the braces are offset from adjacent braces, thereby creating an eccentricity in the floor beams. For some EBF configurations the eccentricity in the floor beams is created by offsetting the braces from columns. The part of a floor beam which defines the eccentricity is referred to as a link. The design of an EBF is based on the principle that during overloading the links yield and act as ductile members, thereby inhibiting brace and column buckling, for these member forces are therefore limited by the ultimate forces developed in the links. The members outside the links are designed to resist the ultimate capacity of the link in an elastic manner, thereby assuring a ductile structural system. This form of design is known as capacity design. Current design criteria for short links bases the ultimate link strength on a shear force of $1.5V_p$, where $V_p = 0.55\ F_y dt_w$ and is the plastic shear strength of the steel floor beam. Link deformation is limited in order to prevent link failure due to excessive web buckling which may lead to link web tearing and strength deterioration. The above criteria are based on test data obtained using EBF subassemblies under pseudo-static cyclic loading conditions. To assess these provisions for more realistic conditions, inelastic dynamic time history analysis of EBFs were performed (Ref. 1). Specially developed elements were used to model the links and composite floor beams outside the links for random cyclic loading.

Link Element Formulation The link element was based on a stress resultant formulation and consisted of an elastic beam with rigid-plastic hinges at each end (Ref. 1), as shown in Fig. 1(a). The EBFs were analyzed as planar frames, therefore only the effect of in plane forces had to be considered in the link

element. Each hinge consisted of a set of three subhinges of zero length, see Fig. 1(b), with each subhinge having a yield surface in moment-shear force space. The yield surfaces were concentric in order that the three subhinges of a hinge would sequentially yield at specific force levels. The behavior of the combined elastic beam element and two hinges consisted of elastic shear, flexural and axial deformations developing in the elastic beam, with inelastic shear and flexural deformations developing in yielded subhinges. This produced a force-deformation response consisting of an initial elastic curve followed by a reduction in stiffness in three steps under increased load which resulted in sequential yielding of all subhinges. A tangent stiffness matrix, $\underline{K}_T$, was calculated for the element by forming the tangent flexibility matrix, $\underline{F}_T$, and then equating $\underline{K}_T$ to the inverse of $\underline{F}_T$. $\underline{F}_T$ is equal to the combined flexibility of the elastic beam, $\underline{F}$, and yielded subhinges $\underline{f}_p$: Since each subhinge had rigid-plastic behavior only yielded subhinges contribute to $\underline{f}_p$. The forces resulting in element deformations θ_i, θ_j, and γ are the moments at the element's ends, M_i and M_j, and shear V, where θ_i and θ_j are flexural deformations at end i and j, respectively, and γ shear deformation. Based on experimental data (Ref. 2), a series of rectangular yield surfaces was selected for each subhinge. Experimental data also indicated that both isotropic and kinematic hardening occurred in links yielding predominantly in shear. Therefore, an anisotropic hardening rule was devised for each subhinge where isotropic and kinematic hardening occurred in shear, with moment yielding following only a kinematic hardening rule.

Composite Beam-Column Element Formulation To effectively model the floor beam in a braced EBF bay outside the link, the change in stiffness of this member under moment reversal observed during experiments (Ref. 2) had to be accounted for. Although these experiments on EBFs with composite floors indicated that the floor beam outside the link remained elastic, an element was developed which allowed for yielding considering axial load-moment interaction (Ref. 1). A typical cyclic force-deformation curve for moment causing load reversal and yielding for the element is shown in Fig. 2. The element was based on in plane forces and consisted of the well known parallel component beam-column model in series with a zero length rigid-plastic rotational hinge at each end, as shown in Fig. 2. The purpose of the hinges was to add flexibility to the parallel component model upon moment reversal in order to obtain the change in stiffness depicted in Fig. 2. Inelastic deformations resulting in a reduced stiffness due to yielding of the composite beam-column element were assumed to occur only in the parallel component model.

Both the link and composite beam-column elements were implemented into a computer program for the nonlinear static and dynamic analysis of structures (Ref. 1). Before analyzing EBFs for inelastic dynamic response, the elements' formulations were verified. This involved modeling several test specimens of bare and composite links in EBF subassemblies (Ref. 2) and a three story EBF, all of which were subjected to severe static cyclic loading. The response predicted by an analysis of a bare steel EBF subassembly consisting of a link and floor beam is shown in Fig. 3. The results show excellent agreement with the experimental data. Similar agreement was also achieved for the analysis of the other test specimens.

EBF ANALYSIS

EBF Design Using the capacity design concept described previously, and equivalent static lateral seismic loads per NEHRP (Ref.3), the two EBFs shown in Fig. 4 were designed, where both designs (Designs 1 and 2) had all moment connections. NEHRP provisions are based on ultimate loads with an inverted triangular distribution for the equivalent lateral loads. The EBFs, with all moment connections, were considered as dual systems. The links were designed as

short members where $e < 1.6M_p/V_p$, in which e and M_p are the link length and plastic moment capacity. The exterior columns adjacent to the links at the lower three floors were designed based on magnified moments, $M_{col}=\omega M_{code}$, where ω is an amplification factor applied to column moments M_{code} from an elastic static analysis to account for dynamic amplification and movement of the point of inflection in the columns during an extreme seismic event. A value of 1.8 for ω was used. The EBF designs were checked for compliance with the NEHRP code by means of elastic analysis. This included checking whether the total link deformation γ exceeded the maximum permissible value of ± 0.06 rad. The plastic deformations for determining the maximum γ were estimated by magnifying the elastic deformations by the factor $(C_d - 1)$, as suggested in the NEHRP code. C_d is equal to five for an EBF. Under the lateral loads, the link shears were restricted to be less than or equal to V_p in order to comply with the NEHRP provisions.

Program of Investigation The two EBF designs were subjected to the NS component of the 1940 El Centro earthquake record which had been scaled by a factor of 1.5, and the NE component of the 1966 Parkfield earthquake record. As a result, both of these records had a peak ground acceleration of 0.5g. These particular earthquakes were selected and scaled as noted in order to study the EBF response involving several significant cycles of yielding (1.5*El Centro) and large excursions of plastic deformation due to large pulses (Parkfield). The information to define the force-deformation relationships for the elements was based on experimental data (Ref.2). Design 1 was analyzed assuming bare steel behavior, both with and without strain hardening. Design 2 was analyzed assuming bare steel and composite behavior, respectively, with strain hardening. Both an interior and exterior composite EBF were considered. The composite links were modeled using the link element with a 5 and 17 percent greater initial shear yield strength, respectively, for the exterior and interior composite EBFs relative to the bare steel EBF model.

Results The envelopes of the story shear forces representing maximum and minimum values for Design 1 are shown in Fig. 5 for the response of EBF models with straining hardening to the Parkfield and scaled El Centro records. Included are results of EBF analysis assuming elastic-perfectly plastic behavior (EPP), as well as the design story shear forces per NEHRP. The effects of strain hardening are shown to be pronounced, where the base shears for the El Centro and Parkfield analysis were, respectively, 1.31 and 1.46 times greater than that of the corresponding EPP analysis. The response envelopes exceed the design envelope because larger beam sections with greater capacity were used in order to limit γ in the links per the elastic design check, and the fact that the design envelope does not include strain hardening. The corresponding maximum link shear forces, V_{max}, for each floor have been normalized by their respective values of V_p, and are plotted in Fig. 6. The analyses with strain hardening had all of the links in the bottom five floors yield, with the largest values of V_{max} developing in the first floor ($1.55V_p$) for both earthquakes. The Parkfield record caused more strain hardening in the upper floors than the scaled El Centro record, however for both analyses the first and second floor links developed a V_{max} equal to or greater than $1.5V_p$. The envelopes of maximum link deformation γ_{max} are shown in Fig. 7 where it is apparent that the lower floors developed larger values of γ_{max} than the upper floors. The Parkfield record caused larger link deformation, and resulted in γ_{max} exceeding the NEHRP design limit of 0.06 rad. in the lower three floors. The scaled El Centro record caused γ_{max} to exceed 0.06 rad. only in the first floor. Consideration should be given to increasing the bottom floor link sizes in order to reduce γ. The envelope of axial brace force for the analyses involving strain hardening are compared in Fig. 8 to the design envelop for compression based on $1.5V_p$ and to the EPP analysis. With strain hardening, greater axial brace forces developed, particularly in the lower floors where the Parkfield earthquake caused compressive axial brace forces in floors 1 and 2 to exceed the design envelope based on $1.5V_p$. The scaled El Centro record is shown

to have resulted in the first floor brace achieving an axial force equal to a value corresponding to a shear of $1.5V_p$ in the link. The effect of strain hardening resulted in a maximum increase of 41 and 29 percent, respectively, in the first floor bracing during the Parkfield and scaled El Centro earthquakes compared to the EPP analysis.

The columns in the EBFs were designed on the basis of all of the links simultaneously developing a shear force of $1.5V_p$. A comparison of the resulting design envelope for compressive axial column force with the response of the EBF models with strain hardening, shown in Fig. 9, indicates this to be a conservative assumption for the interior columns. The exterior columns show a much closer agreement with the design envelope, particularly the Parkfield earthquake where larger link shear forces developed in each of the bottom three floors. The significance of applying the amplification factor ω to the column moments M_{code} is demonstrated by the behavior of the bending moments in the exterior columns in Fig. 10, where it is shown at time t=5.0 sec. that the column moments above and below the first floor are not equal, as well as at the second floor. Furthermore, the point of inflection in the columns above the first three floors have shifted away from the column midheights. At time t=4.5 sec. these phenomena are also evident at the first floor. The above phenomena are a consequence of link yielding, where at t=4.5 sec. the first floor link was yielding, and at t=5.0 sec. all three bottom floor links were yielding. The columns of the bottom three floors would have yielded if it had not been for the application of the ω factor to the moments M_{code}.

The envelopes of story shear forces for Design 2 subjected to the Parkfield earthquake record are shown in Fig. 11, where results for analyses assuming bare steel and composite floor slab behavior are plotted. Composite action is shown to have increased the story shear forces, with the exterior composite EBF having a 3 percent increase in base shear and the interior composite EBF a 10 percent increase. Similar results were found for the response to the scaled El Centro earthquake. Envelopes of maximum link shear force, V_{max}, are compared in Fig. 12 for the Parkfield earthquake. In the lower four floors, composite action in the interior and exterior EBFs resulted in an increase of 10 and 4 percent in V_{max} relative to the bare steel EBF model. At the first floor the maximum shear force in the link of the bare steel EBF model was $1.5V_p$, while the interior and exterior composite EBFs, respectively, had values of 1.65 and $1.55V_p$. Similar results were found for the second and third floor links, with smaller increases occurring in the remaining upper floor links of the composite EBFs. The effect of larger link forces in the composite EBFs is evident in the axial brace force envelopes given in Fig. 13 for the bare steel and interior composite EBF, where the bottom four floors show an average of 12 percent increase in axial brace force relative to the bare steel EBF. The design envelope appears to be satisfactory in the upper floors for the bare steel results, although the first floor exceeded this envelope by 5 percent. The interior composite EBF exceeded the design envelope by an average of 11 percent in the lower three floors.

An examination of the inelastic action in Designs 1 and 2 indicated that only a minute amount of yielding occurred outside the links, where some of the floor beams in the unbraced bays and outside the links in braced bays yielded. The ductility demand placed on these members however was small. The links accounted for over 98 percent of the energy dissipated by the EBF models.

CONCLUSIONS

Based on the analytical investigation of the inelastic response of the 6 story, 3 bay EBF involving short links, the following conclusions are noted:

1) Capacity design can successfully be applied to EBFs in order to confine the inelastic action primarily to the links. To apply this concept, a designer

must know the ultimate link capacity. For short bare links in these analyses this capacity was found to be as large as $1.55V_p$ at the first floor. A maximum shear equal to $1.65V_p$ was found for the interior composite EBF. This phenomenon should be carefully considered when designing the braces and columns of EBFs with composite floors systems where significant link strain hardening is expected.

2) The column moments were found to be nonuniformly distributed above and below yielded links, resulting in the movement of the column's point of inflection. In view of this fact, great care must be taken when designing columns and column splices.
3) The assumption of all links simultaneously yielding for establishing column design axial forces was found to be satisfactory for the lower three floors. In the remaining upper three floors this assumption was more conservative.

REFERENCES

1) Ricles,J.M., and Popov,E.P.,"Dynamic Analysis of Seismically Resistant Eccentrically Braced Frames," Earthquake Engineering Research Center Report No. 87-07, Univ. of Calif., Berkeley, Calif. June 1987.
2) Ricles,J.M., and Popov,E.P.,"Experiments on Eccentrically Braced Frames with Composite Floors," Earthquake Engineering Research Center Report No. 87-06, Univ. of Calif., Berkeley, Calif. June 1987.
3) National Earthquake Hazards Reduction Program, Recommended Provisions for the Development of Seismic Regulations for New Buildings, Seismic Safety Council, Fed. Emergency Management Agency, Wash. D.C., 1985.

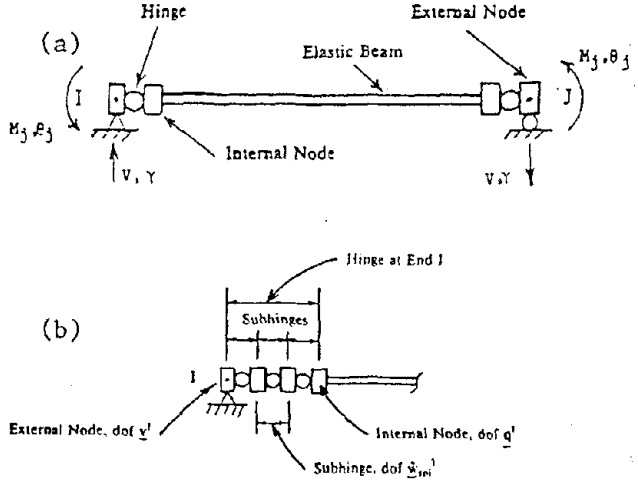

Fig.1 (a) Link element with (b) subhinges.

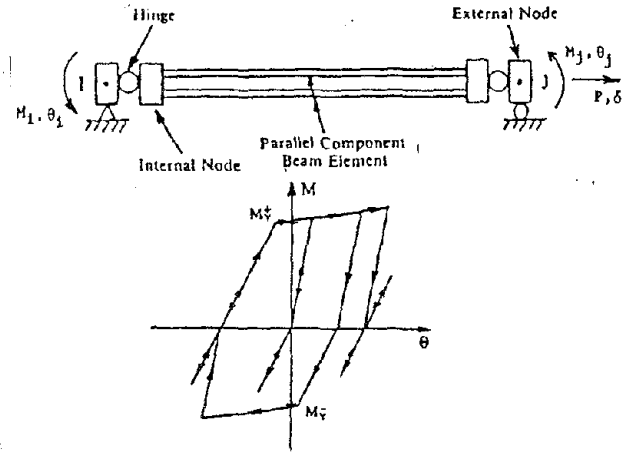

Fig.2 Composite beam-column element.

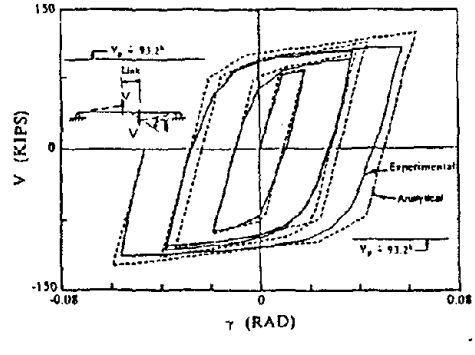

Fig.3 Analytical and experimental comparison.

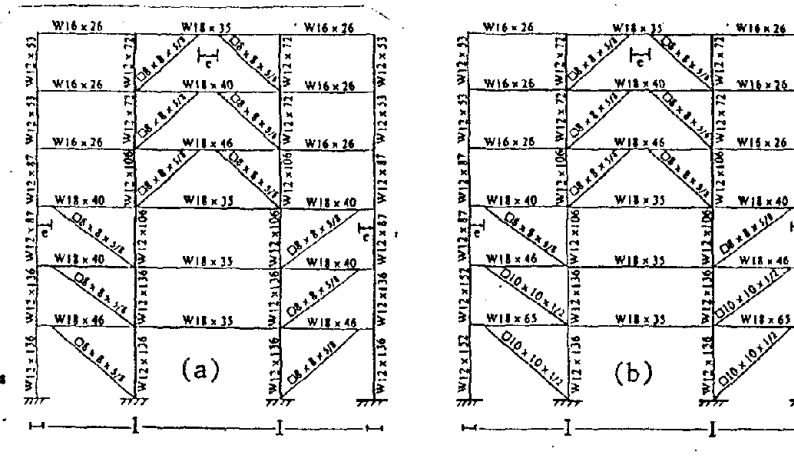

Fig.4 EBF (a) Design 1 and (b) Design for analysis

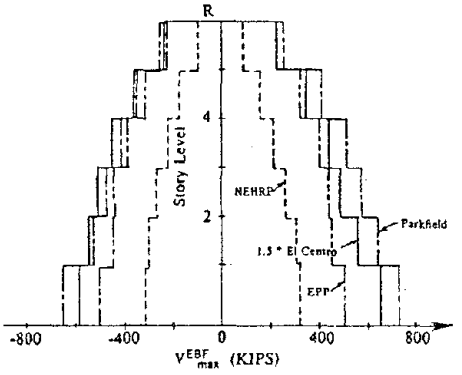

Fig.5 Story Shear envelopes for Design 1.

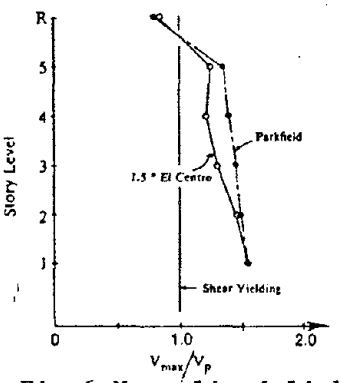

Fig.6 Normalized link shear envelopes, Design 1.

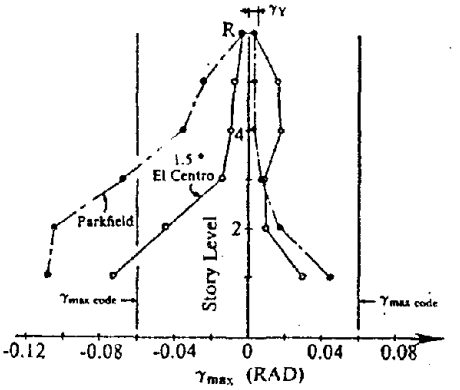

Fig.7 Link deformation envelopes, Design 1.

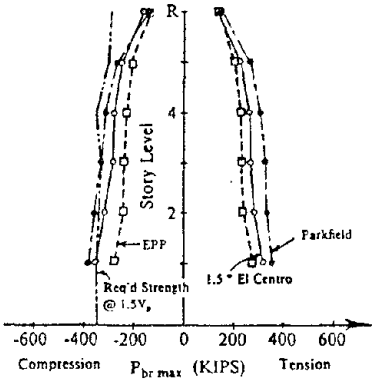

Fig.8 Axial brace force envelopes, Design 1.

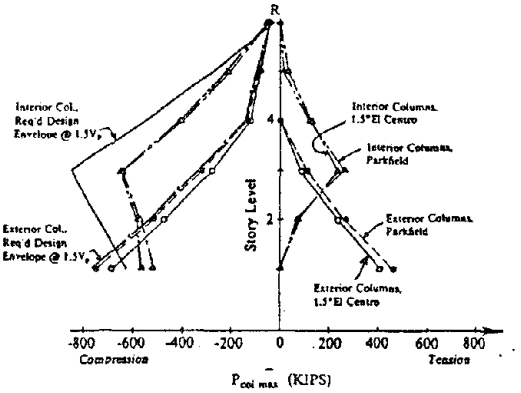

Fig.9 Axial column force envelopes, Design 1.

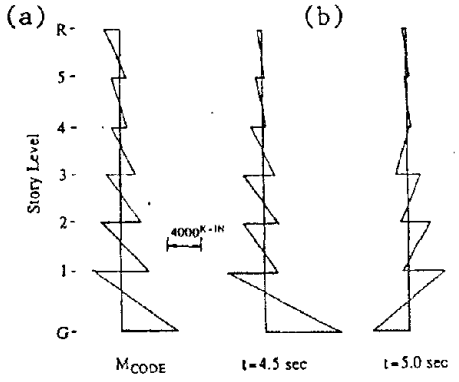

Fig.10 Exterior column (a) design moments with no amplification, and (b) moments at selected times, Design 1.

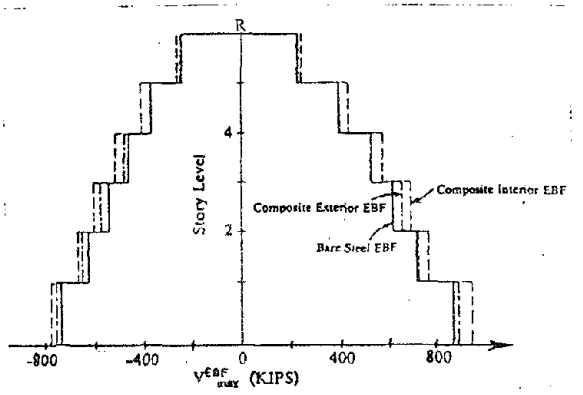

Fig.11 Story shear envelopes, Design 2.

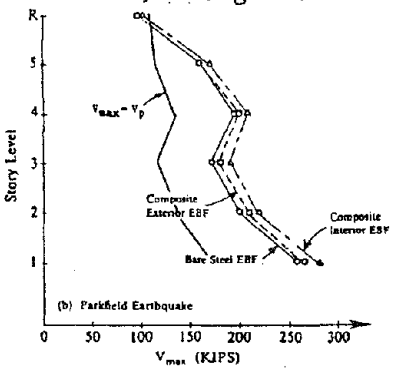

Fig.12 Link shear force envelopes, Design 2.

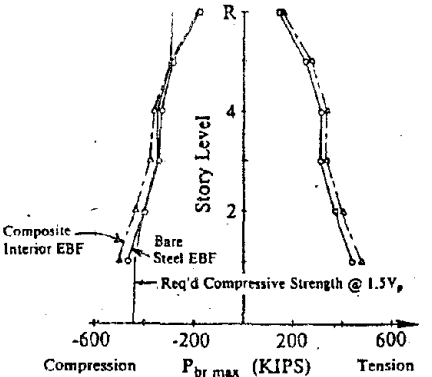

Fig.13 Axial brace force envelopes, Design 2.

PITCHING AND INTERACTION EFFECTS IN THE EERC EARTHQUAKE SIMULATOR

Abdulkarim M. RINAWI[1] Ray W. CLOUGH[2] and J. Marcial BLONDET[3]

[1]Graduate Student, Dept. of Civil Eng., University of California, Berkeley, USA
[2]Professor, Dept. of Civil Eng., University of California, Berkeley, USA
[3]Associate Research Eng., Dept. of Civil Eng., University of California, Berkeley, USA

SUMMARY

Recent tests at the multi-degree of freedom shaking table at the University of California, Berkeley, showed an undesired pitching motion. The objective of this paper is to study the pitch effect on the response of test structures. The effect of pitching and interaction are investigated through transfer function measurements and through actual earthquake motions applied to a SDOF steel test structure with high overturning moment capacity. Although the effective motion was quite different from the earthquake record, the response of the structure can still be predicted from the earthquake record using the coupled structure properties.

INTRODUCTION

It was observed during the tests of heavy and tall structures on EERC shaking table that significant pitching, rolling and twisting can occur (Ref. 1). The objective of this research is to study the shaking table-structure interaction effects, and evaluate shaking table performance. In this paper the interaction effects are studied by transfer function measurements and actual earthquake records applied to a test structure, a test mass and to the bare table system.

EXPERIMENTAL PROGRAM

The interaction and performance of the table were studied under three different loading cases:

- The bare table was subjected to both random signals and earthquake signals. The random signals test was performed in order to establish the transfer functions between the table motions and the command displacement. Transfer functions can give a measure of system reproduction of the command signal, the frequency bandwidth and the stability of the table motion. In order to evaluate the interaction effects during normal test operation, two earthquake records were used: the 1952 Taft and the 1978 Miyagi-Ken-Oki.
- The table was then loaded with three concrete blocks (WxHxL=48x21.5x240 inches) having a total weight of 70.5 kips. Each block was anchored by three post tensioned steel rods to the table. Only random signals were applied to the table-mass system.
- A steel structure was then constructed so as to have similar dynamic characteristics to that of the US-JAPAN reinforced concrete model (Ref. 1) for which significant pitching was observed. The steel structure had a mass of 62.5 kips placed on the top. The center of mass was 200 inches from the table level. A sketch of the test structure is shown in Fig. 1. The structure was subjected to both random and earthquake signals.

IDENTIFICATION OF STRUCTURE PROPERTIES

Two separate tests were performed to identify the structure's vibration characteristics. First, the fixed base case was handled by placing a small shaker at the top of the structure, a random signal was applied to the small shaker mass and the induced inertia forces were adequate to estimate the frequency (2.87 Hz) and damping (0.3 %). Second, the coupled structure properties were evaluated by subjecting the structure to random command displacement. The transfer function of the relative mass acceleration with respect to the command was evaluated and circle fitting (Ref. 2) was performed to evaluate the frequency (2.54 HZ) and damping (3.33 %). These properties reflect the coupling due to both the horizontal and pitching degrees of freedom. In order to evaluate the coupled parameters in the pitching degrees of freedom only, another transfer function, the relative mass acceleration with respect to the horizontal table acceleration was used. During the second test, an independent estimate of the fixed base characteristics was also made by considering the rigid body movement of mass at the top of the structure $\ddot{x}_t+\ddot{\theta}h$ (effective acceleration). The transfer function between this input and the relative mass acceleration was estimated. Surprisingly a completely different estimate was obtained for the damping (0.8 %). This significant change in damping can be attributed to the fact that the mass was not rigidly attached to the structure. The movement of this mass can lead to friction and hence energy dissipation. It also was possible to estimate the fixed structure's frequency and damping from its response to the earthquake signals. The results are shown in Figs. 2a and 2b which clearly show the damping dependence on the response amplitude.

The frequency and damping of the SDOF test structure for the two earthquake signals used are listed in Table 1 for the fixed base case, for the pitch coupling case, and for the pitch and horizontal coupling case.

SHAKING TABLE PROPERTIES FROM MEASURED TRANSFER FUNCTIONS

In order to understand the table behavior, transfer functions between the command displacement and the actual table horizontal and pitch displacements were determined. The results, in Figs. 3a and 3b, show the transfer functions for the displacement and pitch respectively.

- For the bare table, the transfer function of the horizontal table displacement with respect to the command is shown by the long dash line. The system behaves as low pass filter with little attenuation for frequencies less than 10 Hz but almost completely attenuating frequencies over 25 Hz. The phase curve of the transfer function shows that table displacement frequencies above 12.6 Hz are out of phase with the command displacement. The bare table pitch consists mainly of high frequency response. It is out of phase with the command displacement at about 11.5 Hz and peaks around 12.5 Hz.
- The addition of the mass of 70.5 kips to the table caused a decrease in the frequency bandwidth as shown by the short dash line. The table displacement is out of phase with the command at about 8.5 Hz. The pitch transfer function had two prominent peaks at about 8 and 15 Hz. The pitch displacement is out of phase with the command at about 8 Hz.
- Adding the structure to the table had two clear effects on the horizontal transfer function as shown by the solid line. It decreased the frequency bandwidth and had a prominent peak (amplitude=2.2) and notch (amplitude=0.7) near the coupled table structure frequency. The table displacement was out of phase with the command at 9.6 Hz. Table pitch (Fig. 3b) occurs mainly at a frequency close to the coupled table-structure frequency.

TIME HISTORY COMPARISONS

In order to predict the response of the SDOF test structure to the command acceleration, to the measured horizontal table acceleration or to the measured effective table acceleration, it is essential to use the frequency and damping values which properly represent the coupling effects between the table and the structure.

Recognizing the dependence of the damping on the response amplitude it was necessary to identify the coupled properties from the measured responses. Transfer functions were evaluated for the relative mass acceleration with respect to the command signal, to the measured horizontal table

acceleration and to the effective table acceleration. Damping values and frequencies obtained from transfer functions of the relative mass acceleration versus the command signal reflect the coupling effects due to the flexibility of the table in the rotational and translational degrees of freedom; those versus the horizontal acceleration reflect the coupling due to pitching only; while those versus the effective table acceleration reflect the fixed base properties of the structure (i.e. no coupling). The two earthquake signals used have some energy near test structure resonance. Transfer functions evaluated had no spikes corresponding to dividing by small input amplitudes. Circle fitting was performed near the peak amplitudes and corresponding damping and frequency estimates were obtained. The frequencies were 2.59, 2.71 and 2.86 Hz and the damping ratios were 1.8, 2.5 and 1.4 % respectively.

Fig. 4 shows plots of the measured mass acceleration together with those predicted from the three motions using the respective coupled properties. It is clear that the correlation is very good between the analytical and experimental results for the three cases.

RESPONSE SPECTRA COMPARISONS

The effective acceleration spectrum represent the peak response of a SDOF test structure with no coupling effects (i.e. with fixed base properties). The original spectrum in this case represent the maximum response of a SDOF test structure taking into account coupling in both the horizontal and pitching degrees of freedom. Response spectrum of the horizontal table acceleration represent the SDOF structure with pitch coupling.

Fig. 5a shows the response spectra of the original Taft acceleration record and the measured table acceleration record. It is clear that the spectrum of the table acceleration is slightly higher near the coupled table-structure period. The spectrum evaluated from the effective table acceleration $\ddot{x}_t+h\ddot{\theta}$ can be compared with the original Taft spectrum in Fig. 5b. Clearly the effective acceleration has a much higher response at periods greater than the fixed base structure period.

CONCLUSIONS

1) The response of the system for the bare table and rigid load conditions is acceptable within the operating frequency bandwidth.

2) In the case of the table loaded with a test structure, the horizontal table acceleration versus command signal transfer function shows a prominent peak and notch distortion near the resonant frequency of the structure. The table pitch response is mainly concentrated near the coupled frequency of the structure.

3) Time history responses of the structure can be predicted from either the command, horizontal table or effective table acceleration as long as the appropriate properties are considered. Structural frequency and damping should adequately represent the coupling between the table and structure.

4) Response spectrum of the horizontal table acceleration is reasonably similar to the spectrum of the command signal whereas the spectrum of the effective acceleration is quite different. However, in order to use these response spectra, adequate structural properties must be specified; appropriate coupled frequencies and damping need to be used for the command and the horizontal table acceleration spectra and fixed base values for the effective table acceleration spectrum.

5) As long as the frequency content of the input motion is not negligible near the frequency of interest, coupled frequencies and fixed base characteristics for the structure may be derived from transfer function measurements.

ACKNOWLEDGMENTS

The shaking table experiments reported here were funded by the National Science Foundation by grant No. ECE-8316662 and additional research support was provided by the Nishkian Professorship in Structural Engineering; both of these are gratefully acknowledged.

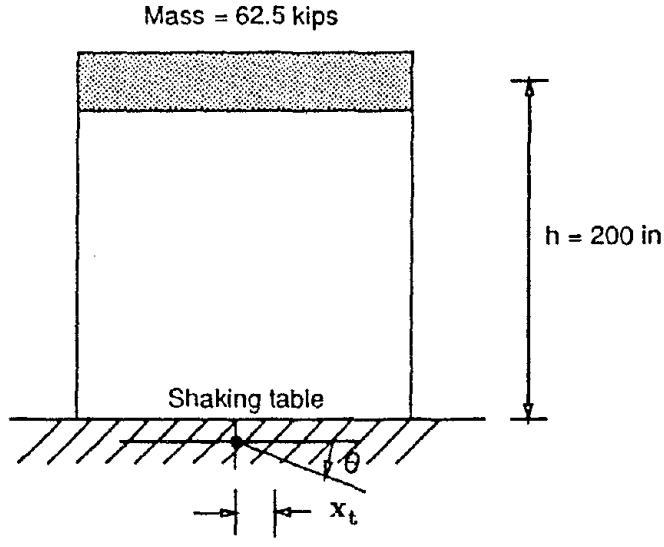

Fig. 1 Steel structure mounted on
EERC shaking table

Fig. 2: Variation of Frequency and Damping with Response Amplitude

a) Frequency

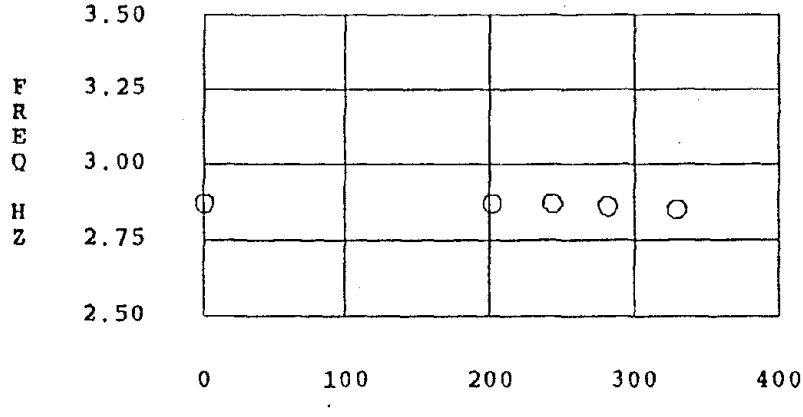

b) Damping

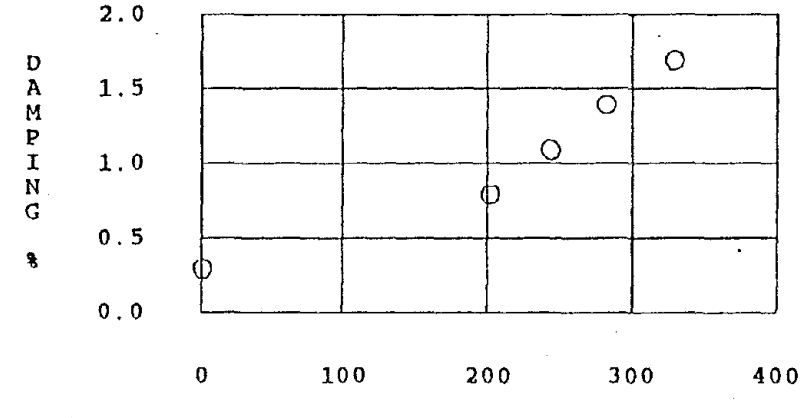

Fig. 3: Transfer Function w.r.t. Command Displacement

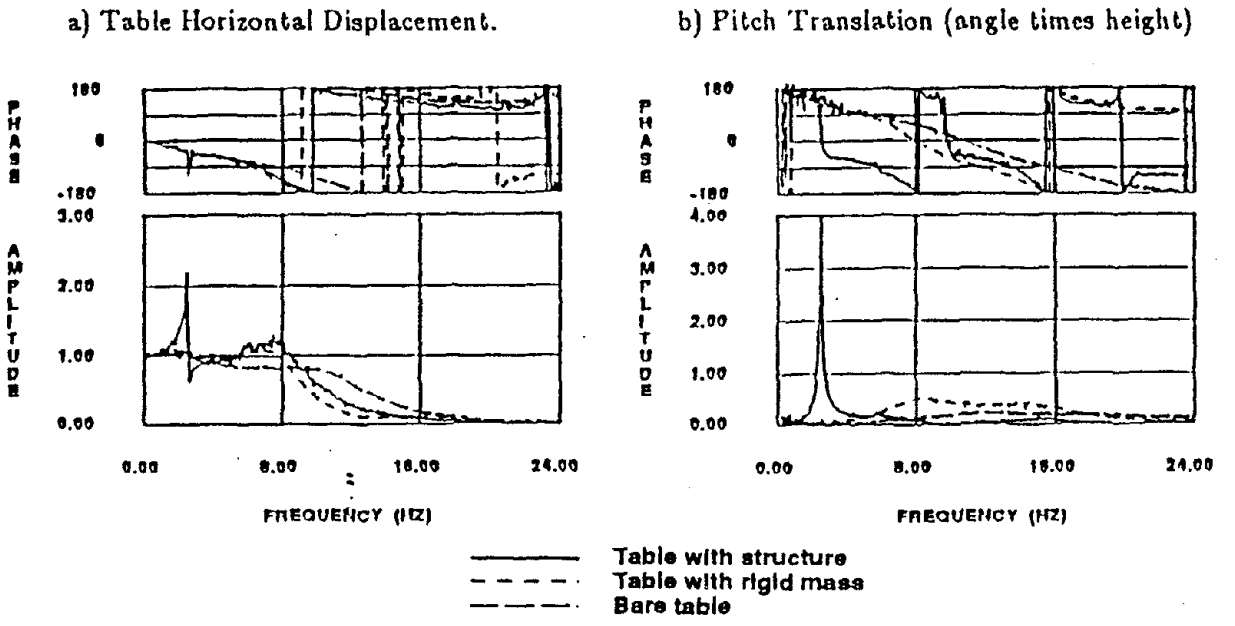

Fig. 4: Comparisons of Measured and predicted Mass Acceleration (in/sec2). (measured: solid, predicted: dotted)

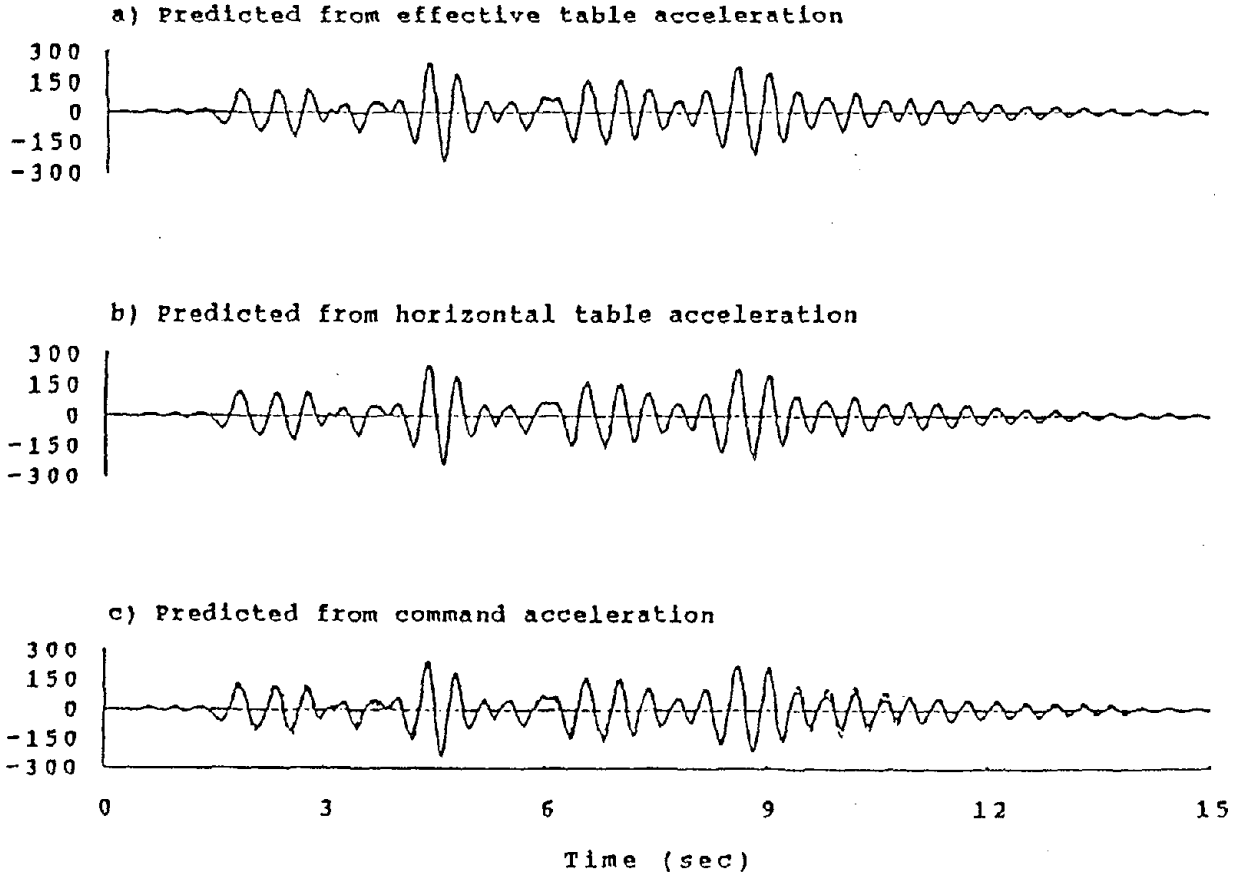

Fig. 5: Comparisons of Pseudo Velocity Spectra (5% Damping)

a) Original Earthquake Record vs. Measured Table Acceleration.

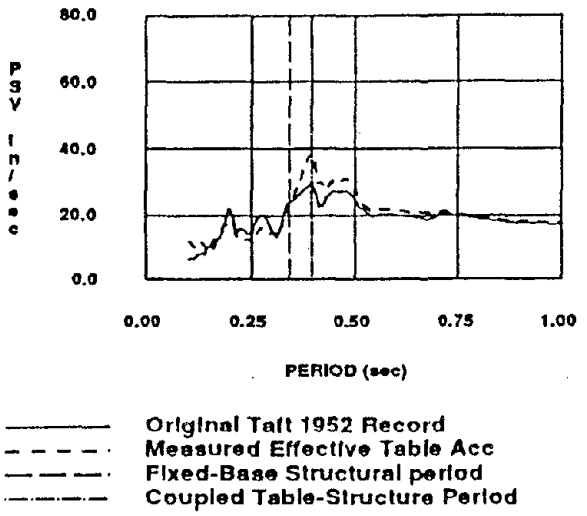

b) Original Earthquake Record vs. Measured Effective Table Acceleration.

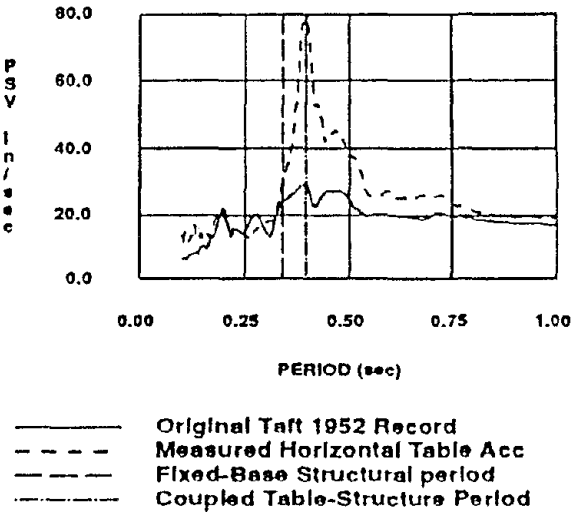

EARTHQUAKE RECORD	Fixed base		Base rotation coupling		Transl. and rot. coupling	
	FREQ (Hz)	DAMP (%)	FREQ (Hz)	DAMP (%)	FREQ (Hz)	DAMP (%)
Miyagi span 270	2.87	1.2	2.71	2.3	2.62	2.0
Miyagi span 350	2.86	1.4	2.71	2.5	2.59	1.8
Taft span 200	2.86	1.7	2.70	1.0	2.58	2.4

Table 1: Vibration characteristics of the structure for three boundary conditions and three different records.

REFERENCES

1. Bertero, V. V., Aktan, A. E., Charney, F. A., Sause R. "US-JAPAN Cooperative Earthquake Research Program: Earthquake Simulation Tests And Associated Studies of a 1/5 scale Model of a 7 Story R.C. Test Structure" EERC Report No. 84/05, University of California, Berkeley, 1984.
2. Ewins D. J., "Modal Testing: Theory and Practice". Research Studies Press LTD. John Wiley and Sons Inc. 1984 (pp 158-168)

HYBRID ANALYSIS TECHNIQUES FOR SEISMIC PERFORMANCE TESTING

Christopher R. THEWALT[1] and Stephen A. MAHIN[2]

[1]Assistant Professor of Civil Engineering, Carnegie Mellon University, Pittsburgh, PA 15213 USA
[1]Professor of Civil Engineering, University of California at Berkeley, Berkeley, CA 94720 USA

SUMMARY

Reliable prediction of inelastic structural performance during a severe seismic event is an extremely difficult task, due to the complex nonlinear behavior exhibited by members and connectors. Therefore, experimental testing remains the most reliable means of assessing seismic performance and devising improved design and analysis methods. An on-line computer controlled experimental procedure has been developed which appears to combine the simplicity of quasi-static testing with the realism of shaking table tests. The method has been under investigation for more than ten years now, and this paper will examine recent research and extensions to the applicability of the pseudodynamic test method.

INTRODUCTION

The inelastic behavior of structures is generally quite sensitive to the imposed histories of displacement. Therefore, the nature of a testing technique has a significant effect on the observed data. Quasistatic tests are simple to perform, but due to the preselection of force or displacement histories, it is difficult to relate specimen response to expected seismic performance. Shake table tests provide realistic assessment of the specimen's response to an earthquake, but such tests limit the size, mass and strength of the specimens to be tested. Furthermore, most available shaking tables can only excite the specimen in one lateral direction and on some tables also in the vertical direction. A new technique, called on-line or pseudodynamic testing has recently been proposed (Ref. 9) as a means for overcoming many of these difficulties.

A coordinated series of investigations has been performed to evaluate the pseudodynamic technique as part of the U.S. - Japan Cooperative Earthquake Research Program. These studies were performed in Japan at the Building Research Institute in Tsukuba, and in the U.S. at both the University of California at Berkeley and the University of Michigan, Ann Arbor. These feasibility studies yielded theoretical and practical information useful for test implementation (Refs. 1,3,5,11,12). Several summary papers have been published (Refs. 9,10,13) which discuss progress in a variety of areas related to pseudodynamic testing. In this paper, recent developments at Berkeley will be presented, together with possible new application areas that may now be feasible due to recent breakthroughs.

BASIS OF THE PSEUDODYNAMIC METHOD

The pseudodynamic method is a an integrated experimental-analytical procedure. It is similar to standard step by step dynamic analysis procedures in that the controlling software consideres the response to be discretized into a series of time steps. The pseudodynamic algorithm can be described as: calculate the displacement state at the next time step using a suitable numerical integration technique, move the specimen into the new configuration, measure the restoring forces, solve the equations of motion for the time step to get the acceleration and velocity of the specimen. These operations are then repeated for each step of the input earthquake. The governing equation of motion in this case is :

$$\mathbf{M}\mathbf{a}_i + \mathbf{C}\mathbf{v}_i + \mathbf{r}_i = -\mathbf{M}\mathbf{B}a_g \qquad (1)$$

where M and C are the mass and damping matrices; $\mathbf{a}_i$ and $\mathbf{v}_i$, are the acceleration and velocity respectively at time step i; $\mathbf{r}_i$ is the measured restoring force; and B and $\mathbf{a}_g$ are the ground acceleration transformation matrix and the ground acceleration vector respectively.

In order to perform such a test, the user must specify the inertial and damping properties of the specimen in terms of the mass and damping matrices, as well as the duration of a time step and a time history representing an earthquake record. Since experimental errors can be introduced at each step and propagate throughout a test, the pseudodynamic method has been found to be quite sensitive to errors, but a wide variety of error mitigation techniques have been proposed (Refs. 4,6,7,8).

Previous tests have used planar structures subjected to single components of earthquake excitation in order to be able to correlate the results to those obtainable from existing shaking tables. A recent verification study (Ref. 13) has lifted this restriction, and subjected a three degree of freedom nonplanar structure to a fixed base five component earthquake motion. A sample of the correlation between pseudodynamic and shaking table results during a severe earthquake can be see in Fig. 1.

IMPLICIT NUMERICAL INTEGRATION TECHNIQUES

In previous pseudodynamic tests, an explicit numerical integration operator had been used so that displacements could be directly calculated at each step. However, the use of an explicit integration operator results in stability bounds on the time step. In particular, $\omega \Delta t \leq 2$ must be satisfied for all natural frequencies (ω) of a structure. This means that the maximum size of the time step is determined by the highest natural frequency of a specimen. For specimens with a large number of degrees of freedom, the small step time determined by the highest modal frequency would aggravate error propagation problems, since error accumulation is related to the total number of time steps in a test. Test duration would also increase as the number of steps increased.

The use of an implicit integration technique can guarantee numerical stability regardless of the step size. Furthermore, there are globally stable techniques with dissipative properties that are suitable for error mitigation (Ref. 2). Implicit techniques have not been used to date in pseudodynamic testing because they require either iteration to converge on the next step displacement, which is intolerable since a real specimen is involved, or knowledge of the tangent stiffness characteristics of the specimen, which has proven extremely difficult to estimate. The initial stiffness matrix of a specimen is difficult enough to measure, the changes to the tangent stiffness matrix as the structure undergoes nonlinear deformation can be expected to be even more difficult to measure accurately.

A new method has been developed (Ref. 13), that allows a fully implicit numerical integration technique to be used without the need for iteration and without any need for estimates of the tangent stiffness matrix. The new algorithm can best be understood by examining the equations of motion together with an implicit integration algorithm proposed by Hilber, Taylor and Hughes (Ref. 2). step.

$$\mathbf{M}\mathbf{a}_{i+1} + \mathbf{C}\mathbf{v}_{i+1} + (1+\alpha)\mathbf{r}_{i+1} - \alpha\mathbf{r}_i = \mathbf{f}_{i+1} \tag{2}$$

$$\mathbf{d}_{i+1} = \mathbf{d}_i + \Delta t\,\mathbf{v}_i + (\tfrac{1}{2} - \beta)\Delta t^2\mathbf{a}_i + \beta\Delta t^2\mathbf{a}_{i+1} \tag{3}$$

$$\mathbf{v}_{i+1} = \mathbf{v}_i + (1-\gamma)\Delta t\,\mathbf{a}_i + \gamma\Delta t\,\mathbf{a}_{i+1} \tag{4}$$

where α, β and γ are parameters of the integration method.

The key to the new method is in the realization that as the new displacements are being applied as voltages sent out from the computer, the actual restoring force is available in terms of the voltages measured by the load cells. Although the computer does not explicitly know what restoring force will result from a given displacement, the voltage representing the actual restoring force exists as the displacements are changing. The new method consists of calculating the explicit terms of the new displacement and sending this signal to the actuators, and in addition, summing a portion of the measured restoring force voltage into the desired command signal. The portion of the forces needed becomes apparent when the equations of motion are recast as :

$$\mathbf{d}_{i+1} = \mathbf{d}_i + \Delta t\,\mathbf{v}_i + (\tfrac{1}{2} - \beta)\Delta t^2\mathbf{a}_i - \beta\Delta t^2\mathbf{B}\mathbf{a}_g + \beta\alpha\Delta t^2\mathbf{M}^{-1}\mathbf{r}_i - \beta(1+\alpha)\Delta t^2\mathbf{M}^{-1}\mathbf{r}_{i+1} \tag{5}$$

The last term of Equation 5 gives the portion of the restoring force signal that must be added to the explicit portion of the displacements to complete the implicit form. Using the calibration constants one can then sum this value into the desired displacement signal. Thus, the computer never knows where the specimen will go in this scheme, it only calculates the explicit portion and imposes it as a

command voltage, the implicit component is summed to this voltage in analog form to give the actual displacement which are measured and recorded.

A two degree of freedom specimen, shown in Fig. 2 was constructed to test this technique. The explicit integration method had a critical time step of 0.016 sec., so time steps of 0.01 and 0.02 sec. were used to judge the behavior of the new method. It can be seen that the explicit analytical method goes unstable with a time step of 0.02 (in Fig. 4), while the implicit method gives good results with the same time step (Fig. 5). The period elongation is due to the characteristics of the integration scheme and the very long time step chosen in this test. In a real test, one would select the time step to accurately trace the response, in this test it was chosen primarily to demonstrate stability of the procedure. The small magnitude of the implicit portion of the overall displacement can be seen in Fig. 3.

CONCLUSIONS

The pseudodynamic method has been successfully extended to nonplanar tests with multiple components of excitation. A new fully implicit integration scheme has successfully been implemented and tested. This new method makes it possible to use implicit substructuring techniques and, by rearranging the equations of motion, the new method could be used to run tests under force control, making the testing of extremely stiff structures possible for the first time.

The support of the National Science Foundation is gratefully acknowledge, but the findings and opinions described in this paper are those of the authors, and do not necessarily reflect the views of the National Science Foundation.

REFERENCES

1. Hanson, R.D., and McClamroch, N.H., "Pseudodynamic Test Method for Inelastic Building Response", *Proceedings*, Eighth World Conference on Earthquake Engineering, San Francisco, July 1984.
2. Hilber, H.M., Hughes, T.J.R., and Taylor, R.L., "Improved Numerical Dissipation for Time Integration Algorithms in Structural Dynamics", *Earthquake Engineering and Structural Dynamics*, Vol. 5, 1977, pp. 283-292.
3. Mahin, S.A., and Shing, P.B., "Pseudodynamic Methods for Seismic Testing", *Journal of Structural Engineering*, ASCE, Vol. 111 No. 7, July 1985.
4. Nakashima, M., and Kato, H., "Experimental Error Growth Behavior and Error Growth Control in On-Line Computer Test Control Method", Building Research Institute, Ministry of Construction, Japan, March 1987.
5. Shing P.B. and Mahin S.A., "Pseudodynamic Test Method for Seismic Performance Evaluation: Theory and Implementation", *UCB/EERC-84/01*, Earthquake Engineering Research Center, University of California, Berkeley, 1984.
6. Shing, P.B., and Mahin, S.A., "Computational Aspects of a Seismic Performance Test Method Using On-Line Computer Control", *Earthquake Engineering and Structural Dynamics*, Vol. 13, 1985, pp. 507-526.
7. Shing, P.B., and Mahin, S.A., "Cumulative Experimental Errors in Pseudodynamic Tests", *Journal of Earthquake Engineering and Structural Dynamics*, Vol. 15, No. 4, May 1987, pp 409-424.
8. Shing, P.B., and Mahin, S.A., "Elimination of Spurious Higher-Mode Response in Pseudodynamic Tests", *Journal of Earthquake Engineering and Structural Dynamics*, May 1987.
9. Takanashi, K., et al., "Nonlinear Earthquake Response Analysis of Structures by a Computer-Actuator On-Line System", *Bull. of Earthquake Resistant Structure Research Center*, Institute of Industrial Science, University of Tokyo, No. 8, 1975.
10. Takanashi, K, and Nakashima, M., "A State of the Art: Japanese Activities on On-Line Computer Test Control Method", *Report of the Institute of Industrial Science*, University of Tokyo, Vol. 32, No. 3, June 1986.
11. Takanashi, K, and Nakashima, M., "Japanese Activities on On-Line Testing", *Journal of Engineering Mechanics*,, ASCE, Vol. 113, No. 7, July 1987.
12. Thewalt, C.R., Mahin, S.A., and Dermitzakis, S.N., "Advanced On-Line Computer Control Methods for Seismic Performance Testing", *Third U.S. National Conference on Earthquake Engineering*, Charleston, SC, August 1986.
13. Thewalt, C.R., and Mahin, S.A., "Hybrid Solution Techniques for Generalized Pseudodynamic Testing", *UCB/EERC-87/09*, Earthquake Engineering Research Center, University of California, Berkeley, July 1987.

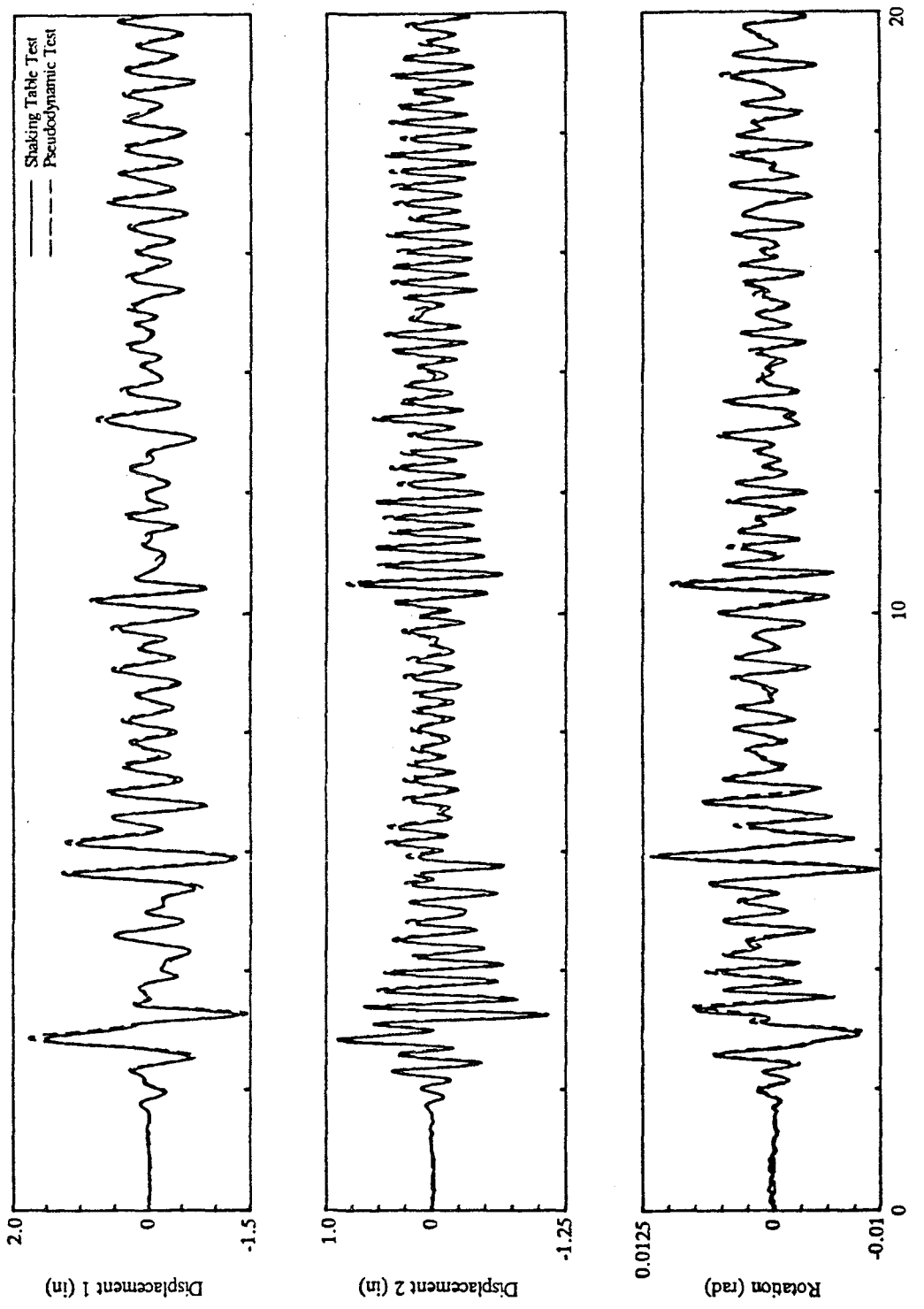

Figure 1 - Displacement Response of Non-Planar Structure

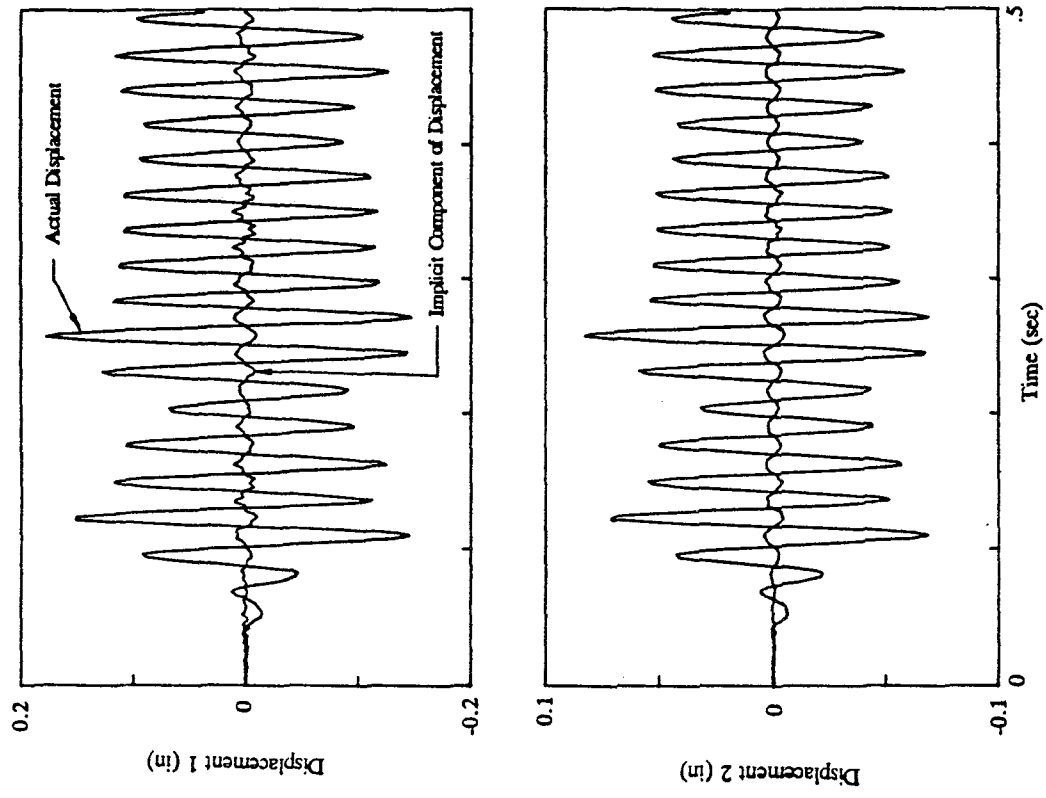

Figure 3 - Implicit Contribution to Displacement

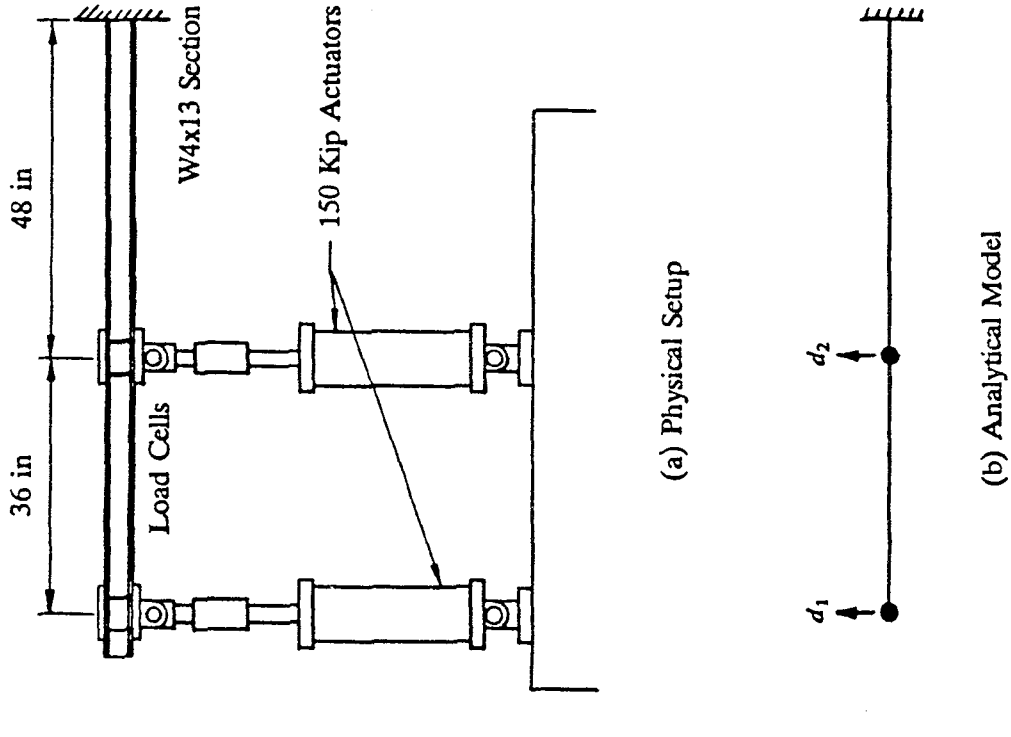

Figure 2 - Two Degree of Freedom Setup for Implicit Verification Test

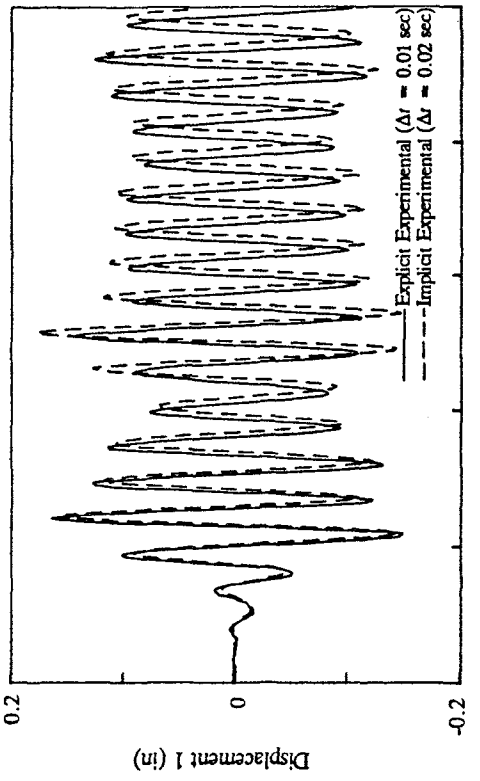

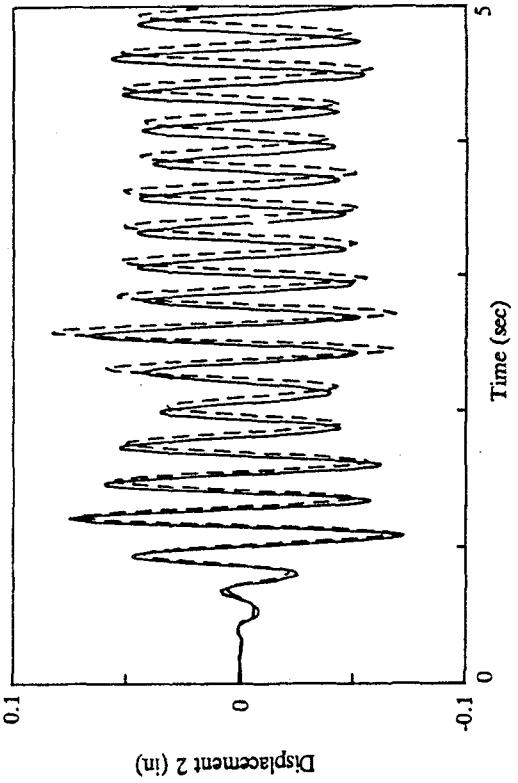

Figure 4 - Displacement Response (Explicit Test)

Figure 5 - Displacement Response (Implicit Test)

NONLINEAR RESPONSE OF CONCRETE GRAVITY DAMS

Luis M. VARGAS-LOLI[1] and Gregory L. FENVES[2]

[1]Department of Civil Engineering, The University of Texas at Austin, Austin, Texas, U.S.A.
[2]Department of Civil Engineering, University of California, Berkeley, California, U.S.A.

SUMMARY

The earthquake response of a typical concrete gravity dam-water system is studied to assess the importance of cavitation in the impounded water. The results indicate that water cavitation has little influence on the maximum displacement and stresses in dams. Cavitation increases the maximum acceleration at the dam crest. The amplified accelerations may affect the response of stiff appurtenant equipment or the stability of the upper portion of a dam after extensive cracking of the concrete.

INTRODUCTION

Linear dynamic analysis provides important information on the earthquake response of concrete gravity dams, in particular the significance of dam-water interaction and water compressibility. However, the realistic dynamic analysis of dams should include the effects of various nonlinearities in the response to earthquake ground motion. One nonlinear effect is cavitation, the formation of gaseous regions in the water that occur when the dam acceleration is large enough for the absolute pressure in the water to reach the vapor pressure.

Early studies of water cavitation and concrete gravity dams used simplifying assumptions of a rigid dam and incompressible water. In such cases, the ground acceleration needed to produce water cavitation in a full reservoir is inversely proportional to the square root of the dam height (Ref. 2). This criterion does not apply to flexible dams impounding a compressible fluid because the acceleration along the dam height depends on the vibration properties of the dam-water system and the ground motion. Previous investigations of cavitation effects on the earthquake response of concrete gravity dams are limited and with differences in conclusions (Refs. 2 and 5).

In this study, a typical concrete gravity dam is analyzed to determine the significance of water cavitation on the response to earthquake ground motion. The complete dam-water system is modeled including water compressibility.

ANALYSIS PROCEDURE

A numerical procedure for computing the nonlinear dynamic response of fluid-structure systems (Ref. 3) is applied to a two-dimensional model of a

concrete gravity dam impounding a reservoir of compressible water. The water is idealized as an inviscid fluid undergoing small amplitude, irrotational motion. The equation of state for water represents the effects of cavitation by a bi-linear pressure-density relationship (Ref. 1). The water is linearly compressible for pressures greater than the vapor pressure, but the water can expand at the constant vapor pressure. The equation of state is shown in Fig. 1 in terms of hydrodynamic pressure and change in density, where c is the velocity of wave propagation, p_v is the vapor pressure, and p_0 is the hydrostatic pressure.

The semi-infinite extent of water in the upstream direction is modeled by a finite fluid domain with an approximate radiating boundary condition at the upstream end. Sediments deposited at the reservoir bottom are represented by an absorbing boundary condition. Linear surface waves at the free surface are allowed, although they have a small effect on the earthquake response of dams.

The dynamic analysis procedure uses a displacement finite element formulation for the structure and a mixed pressure-displacement formulation for the fluid. Enforcing equilibrium and normal compatibility at the fluid-structure interface results in coupled, symmetric, nonlinear equations of motion for the fluid-structure system (Ref. 3):

$$\mathbf{M}\ddot{\mathbf{X}} + \mathbf{C}\dot{\mathbf{X}} + \mathbf{K}\mathbf{X} + \mathbf{F} = -\mathbf{M}\mathbf{R}\ddot{\mathbf{u}}_g - \mathbf{C}_F\mathbf{R}\dot{\mathbf{u}}_g - \mathbf{K}_F\mathbf{u}_g \qquad (1)$$

where $\mathbf{X}$ is the vector of nodal displacements in the structure and fluid; $\mathbf{M}$, $\mathbf{C}$, and $\mathbf{F}=\mathbf{F}(\mathbf{X})$ are the mass, damping, and vector of nonlinear restoring forces for the coupled system, respectively; and $\mathbf{K}$ is the stiffness matrix required to constrain irrotational motion in the fluid. The right-hand side of Eq. (1) is the dynamic force due to the ground motion, $\mathbf{u}_g$, in which $\mathbf{R}$ is the influence matrix for the ground motion components, $\mathbf{C}_F$ is a matrix that represents radiation of waves at the truncated fluid boundary, and $\mathbf{K}_F$ accounts for linear surface waves at the free surface.

In a typical two-dimensional analysis four node non-conforming elements are used for the structure and four node constant pressure elements are used for the fluid. The equations of motion are solved in the time domain using an implicit time integration procedure with equilibrium iterations based on the Newton-Raphson method. Time steps of 0.02 sec and 0.01 sec for dams with linear fluid and cavitating fluid, respectively, were found adequate for accurate response.

Material nonlinearities in the dam, such as tensile cracking of concrete, can be included in the analysis procedure. The effects of concrete tensile cracking on the earthquake response of dams are not presented here, although they are available in Ref. 4.

SYSTEM CONSIDERED

The tallest, nonoverflow monolith of Pine Flat dam is taken as a typical example of a concrete gravity dam to study water cavitation. The finite element model of the dam-water system is shown in Fig. 2, in which the upstream length of the reservoir is three times the dam height of 400 ft and the water depth is 381 ft. For showing the earthquake response, Point 1 is on the upstream side of the dam crest and point A is in the water at a depth of 34.5 ft. Positive displacements and accelerations are in the upstream direction.

The concrete in the dam is assumed homogeneous, isotropic, and linear elastic, with the following properties: elastic modulus, 3.25×10^6 psi; Poisson ratio, 0.20; and unit weight, 155 lb/ft^3. Assumed stiffness proportional damping provides five percent of critical damping at the fundamental vibration frequency of the dam alone. The water has the following properties: velocity of wave

propagation, 4720 ft/sec; unit weight, 62.4 lb/ft^3; and vapor pressure, measured with respect to atmospheric pressure, -15 lb/in^2.

Two earthquake ground motions, Taft Lincoln School Tunnel (1952 Kern County) and Pacoima dam (1971 San Fernando), are selected for evaluation of cavitation effects. The S69E horizontal component of the Taft ground motion is scaled from a peak ground acceleration of 0.18 g to 1.0 g to induce cavitation in the water. The S16E horizontal component of the Pacoima ground motion, with a peak ground acceleration of 1.17 g, is not scaled.

RESPONSE RESULTS

The response of the 400 ft. dam-water system due to the S69E horizontal component of the Taft ground motion is shown in Fig. 4. The hydrodynamic pressure at Point A, as shown in Fig. 4(a), demonstrates that the water will not sustain a pressure less than the vapor pressure with the bilinear equation of state. Cavitation initiates at 3.95 sec when the dam is displaced in the upstream direction. The acceleration in the downstream direction produces a cutoff in hydrodynamic force on the upstream face of the dam. One-half cycle of vibration later, as the velocity of the dam decreases from the maximum value, the cavitated region collapses, producing a pressure pulse of high amplitude and short duration. The pressure pulse, caused by impact of the water as the cavitated region collapses, subsequently produces a large amount of additional cavitation. Fig. 3(b) shows the count of cavitation events in the fluid elements during the ground motion, where the intensity of the shading in the fluid elements is proportional to the number of times the absolute pressure in the element reaches the vapor pressure. The amount of cavitation decreases with depth because the hydrostatic pressure increases with depth; cavitation decreases in the upstream direction because the hydrodynamic pressure decreases exponentially in the upstream direction.

Although there is severe cavitation in the water, Fig. 4(b) reveals that the effect on the maximum dam displacement is very small. The cutoff of hydrodynamic force in the upstream direction slightly reduces later displacement peaks. The maximum principal stresses at several locations in the dam are shown in Fig. 3(a) with and without cavitation. The maximum stresses occur near geometric discontinuities in the cross section. As with displacements, cavitation has a very small effect on stresses. The maximum principal stresses exceed the tensile strength of concrete, indicating that tensile cracking is a more important nonlinear effect in concrete dams.

Cavitation has a major effect on the acceleration of the dam crest. Fig. 4(c) shows the maximum crest acceleration is 2.5 g for the linear fluid, whereas the crest acceleration, more than doubles to 5.5 g for the cavitating fluid. The peak acceleration occurs at the same time (8.2 sec) as the largest pressure pulse from cavitation collapse.

The response of the 400 ft dam-water system to the S16E horizontal component of the Pacoima ground motion is shown in Fig. 5. Compared to the scaled Taft ground motion, the Pacoima ground motion produces less cavitation even though the peak ground acceleration is greater. The observations on the small effect of cavitation on the displacement and stresses in the dam are the same as noted for the Taft ground motion. As before, the increase in peak acceleration at the crest due to cavitation of the water is significant.

To investigate the effect of dam height on cavitation, a 600 ft high dam-water system was obtained by uniformly scaling the finite element model in Fig. 2. Less cavitation occurs when the taller dam is subjected to the Taft ground

motion, and no cavitation occurs when subjected to the Pacoima ground motion. The reduction in cavitation with increasing dam height contradicts the conclusion for rigid dams. The reduction in cavitation results from a decrease in the response spectrum ordinate for the two ground motions as the period of the dam-water system lengthens with height.

More extensive results are given in Ref. 4, including the effects of reservoir bottom absorption and the response to vertical ground motion.

SUMMARY AND CONCLUSIONS

The level of earthquake ground motion that produces cavitation in water impounded by a concrete gravity dam generally produces tensile stresses in the dam that exceed the tensile strength of concrete. When cavitation of the water occurs, it has little effect on the maximum displacements and stresses in dams because the reduction in hydrodynamic force in the upstream direction is small compared to the inertial and elastic forces. The large pressure pulses that result from cavitation collapse do not affect the displacement and stresses in the dam. However, the pressure pulses can significantly amplify the peak accelerations of the dam because (1) the pulses are resisted by dam inertia, and (2) the acceleration of the upstream face is proportional to the large pressure gradients that develop in the water.

The amplified accelerations from water cavitation may affect the response of stiff appurtenant equipment attached to a dam crest. Also, if the upper portion of a dam cracks extensively during an earthquake, the amplified accelerations may reduce post-cracking stability of the dam.

ACKNOWLEDGEMENTS

The National Science Foundation supported this work under Grant ECE-850449 to The University of Texas at Austin. The Center for High Performance Computing, The University of Texas, allocated time on the Cray X-MP/24 for the computations.

REFERENCES

1. Bleich, H.H., and Sandler, I.S., "Interaction Between Structures and Bilinear Fluids," Inter. Jour. Solids and Struct., 6, 617-639, (1970).

2. Clough, R.W., and Chang, C.H., "Seismic Cavitation Effects on Gravity Reservoirs," Numerical Methods in Coupled Systems, R.W. Lewis, et al, eds., John Wiley, (1984).

3. Fenves, G., and Vargas-Loli, L.M., "Nonlinear Dynamic Analysis of Fluid-Structure Systems," Jour. Eng. Mechanics, ASCE, 114, 219-240, (1988).

4. Vargas-Loli, L.M., and Fenves, G., "Nonlinear Earthquake Response of Concrete Gravity Dams," Report to NSF, Depart. of Civil Eng., The University of Texas at Austin, (1987).

5. Zienkiewicz, O.C., Paul, D.K., and Hinton, E., "Cavitation in Fluid-Structure Response (with Particular Reference to Dams Under Earthquake Loading)," Earthquake Eng. and Struct. Dynamics, 11, 463-481, (1983).

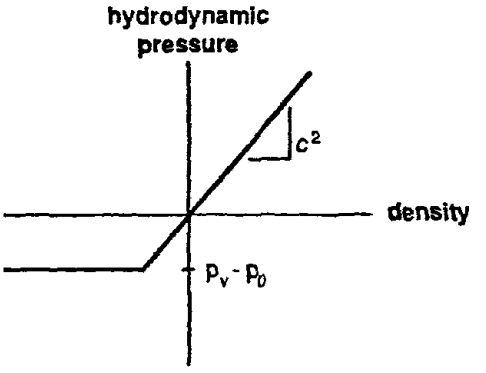

Fig. 1 Bilinear Equation of State for Fluid

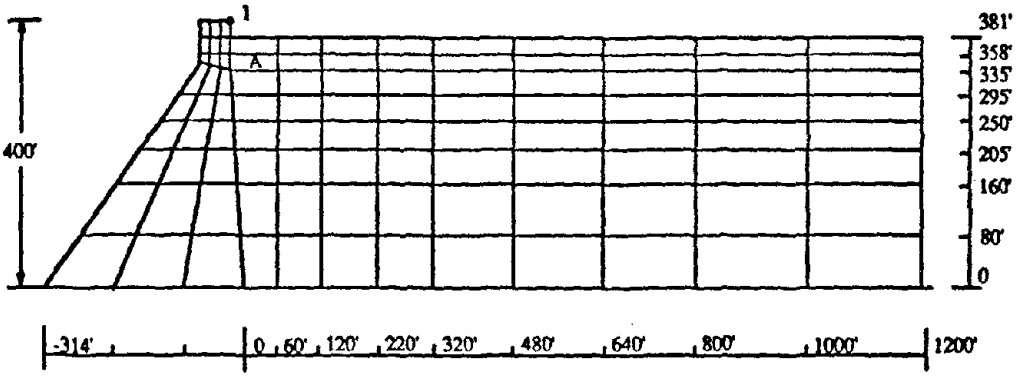

Fig. 2 Finite Element Model of Concrete Gravity Dam-Water System

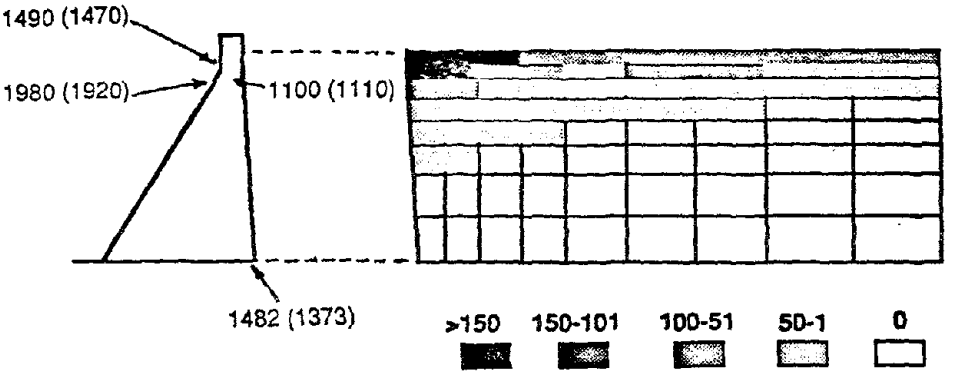

a) Maximum Principal Stress in Dam, psi

b) Number of Cavitation Events in Water

Fig. 3 a) Maximum Principal Stresses in Dam Without Cavitation (with Cavitation), and b) Number of Cavitation Events in Water, Due to S69E Component of Taft Ground Motion, Scaled to 1.0 g Peak Acceleration

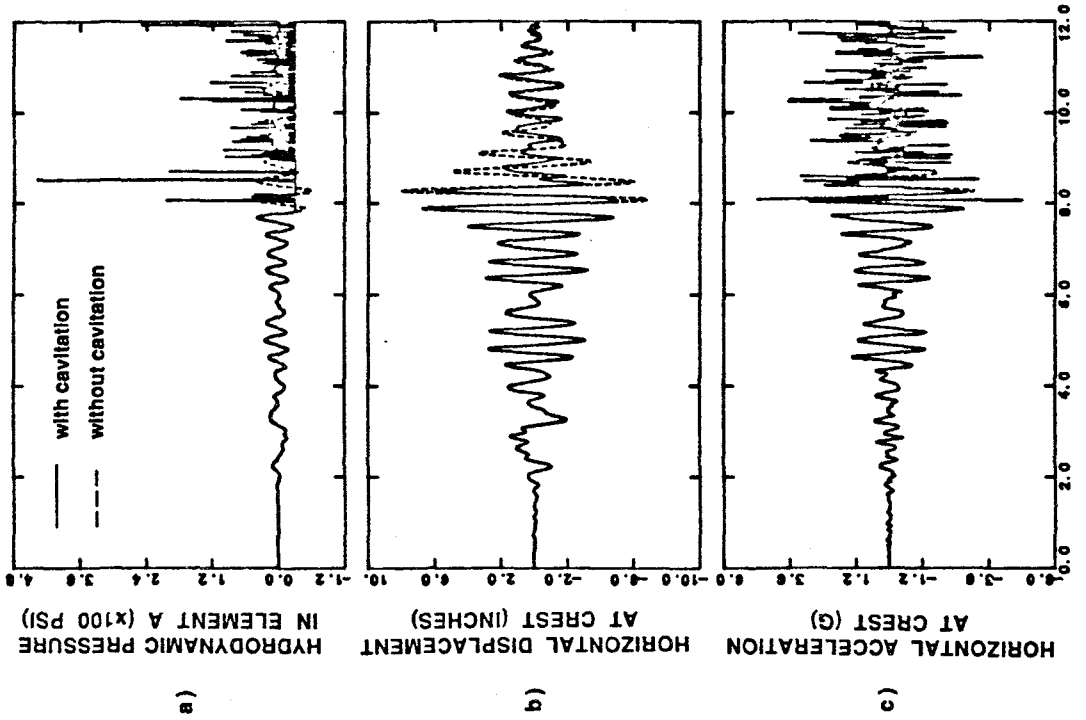

Fig. 4 Effects of Cavitation in Dam-Water System Due to S69E Component of Taft Ground Motion, Scaled to 1.0 g Peak Acceleration

Fig. 5 Effects of Cavitation in Dam-Water System Due to S16E Component of Pacoima Ground Motion

ANALYTICAL MODELING OF R/C STRUCTURAL WALLS

Alfonso VULCANO[1], Vitelmo V. BERTERO[2] and Vincenzo COLOTTI[1]

[1] Dipartimento di Strutture, Università della Calabria, Arcavacata di Rende (Cosenza), Italy
[2] Department of Civil Engineering, University of California, Berkeley, U.S.A.

SUMMARY

A relatively simple and reasonably reliable wall model is proposed, which is suitable to be efficiently incorporated in a practical nonlinear seismic analysis of R/C frame-wall structural systems. A numerical investigation, conducted with reference to a series of R/C structural walls tested at the University of California at Berkeley, shows that the proposed model accurately predicts the measured flexural response. However, under high shear stresses, further improvements of the wall model are needed to accurately predict the hysteretic shear response as well as the flexural and shear displacement components.

INTRODUCTION

R/C frame-wall structural systems prove to be very effective during severe earthquake ground motions, particularly when adopted for tall buildings. In order to predict the inelastic response of such structural systems under seismic loads, the hysteretic behaviour of the structural members and their interaction should be accurately described by reliable analytical models. Nevertheless, relatively simple models should be used such that the analysis could be performed with a reasonable computational effort.

As emphasized in Ref. 1, the nonlinear analysis of complex structural systems can be efficiently carried out by using analytical models based on a macroscopic approach rather than detailed models. Although suitable analytical models have been proposed for realistic and practical prediction of the hysteretic behaviour of R/C beam members, many uncertainties about the formulation of a reliable model for a practical analysis of R/C structural walls persist.

The use of wall models based on the concept of equivalent beam or equivalent truss involves many limitations pointed out in the mentioned Ref. 1. Many important features of the hysteretic behaviour observed during experiments on a full-scale model of a seven-story R/C frame-wall structure have been incorporated in the Three-Vertical-Line-Element Model (TVLEM) proposed by Kabeyasawa et al. (Ref. 2) to simulate the inelastic response or R/C structural walls. Even though there is good correlation between observed and computed responses for the overall structure, further improvements in the TVLEM are believed possible. In Ref. 1 the TVLEM was modified by incorporation of an axial-stiffness

hysteresis model (ASHM) consisting of two axial elements in series whose hysteretic behaviour was described by considerably simple laws. The results of an extensive numerical investigation, besides showing some limitations of the modified TVLEM, indicated the opportunity of obtaining a more refined description of the flexural behaviour of the wall from one or both the following approaches: a) use of more refined laws, based on the actual behaviour of the materials and their interaction, to describe the response of the two elements in series constituting the ASHM; b) modification of geometry of the wall model to gradually account for the progressive yielding of the steel.

In this paper a wall model is proposed by following both these approaches. In order to check effectiveness and reliability of the proposed wall model, a numerical investigation is carried out with reference to a series of R/C structural walls tested at the University of California at Berkeley (Ref. 3).

PROPOSED WALL MODEL

The model in Fig. 1 is proposed to simulate the response of the generic wall member. The flexural response is simulated by a multi-uniaxial-element-in-parallel model with infinitely rigid beams at the top and bottom floor levels: the two external elements represent the axial stiffnesses (K_1 and K_2) of the boundary columns, while the interior elements (at least two, with stiffnesses $K_3,..,K_n$) represent the axial and flexural stiffnesses of the central panel. A horizontal spring, with stiffness K_H and hysteretic behaviour described by the origin-oriented hysteresis model (OOHM) proposed in the mentioned Ref. 2, simulates the shear response of the wall member. The relative rotation $\Delta\phi$ is intended around the point placed on the central axis of the wall member at height ch. A suitable value of the parameter c can be selected on the basis of the expected curvature distribution along the inter-storey height h: for instance, $0 \leqslant c \leqslant 1$, if the curvature sign does not change along h.

The two-element-in-series model shown in Fig. 2 describes the response of the generic uniaxial element in Fig. 1. The two elements in series are representative of the axial stiffness of the column segments in which the bond remains active (element 1) and those segments for which the bond stresses are negligible (element 2). Each element consists of two parallel components to account for the mechanical behaviour of the concrete (C) and the steel (S); a suitable law for the dimensionless parameter λ defining the length of the two elements permits an accurate description of the measured tension-stiffening effect. It should be noted that the model in Fig. 2, though similar to the ASHM adopted in Ref. 1 with a one-component element 1, differs from this model in having also the element 1 constituted by two components C and S. Moreover, unlike the considerably simple assumptions for the ASHM in Ref. 1, refined constitutive laws are herein adopted to idealize the hysteretic behaviour of the materials and the tension-stiffening effect.

Concrete Model A different uniaxial stress-strain relationship is adopted for cracked and uncracked concrete, that is for component C of the elements 2 and 1 in Fig. 2, respectively. Even though many models are available, the Bolong's et al. model (Ref. 4) is here considered for the cracked concrete, because it also accounts for the contact stresses due to the progressive closure of cracks. However, a limitation of this model consists in the lack of knowledge of the effect of the longitudinal and transverse steel ratios on shape and parameters of the characteristic curves of the model. Therefore, the same shape

of these curves is assumed for confined and unconfined concrete, but for this last one a skeleton compressive curve of the kind assumed in Ref. 3 is adopted. The stress-strain relationship for uncracked concrete and a set of rules allowing for a generalized load history, both previously proposed in Ref. 5, are adopted in these studies.

Steel Model The stress-strain relationship originally proposed by Giuffrè and Pinto and later implemented in Ref. 6 is adopted to describe the hysteretic response of the reinforcing steel. In order to avoid the storage of all parameters required for a generalized load history to retrace all previous reloading curves which were left incomplete, in this paper the set of simple rules suggested by Jennings (Ref. 7) is used.

Modeling of the Tension-Stiffening Effect Under monotonic tensile loading the tension-stiffening effect is taken into account by calculating the value of λ such that the tensile stiffness of the uniaxial model in Fig. 2 would be equal to the actual tensile stiffness of the uniaxial R/C member which is intended to be idealized. The actual tensile stiffness of this member is evaluated on the basis of the empirical law suggested by Rizkalla and Hwang (Ref. 8). Due to these assumptions, until the concrete remains uncracked or successively to the steel yielding, the model in Fig. 2 specializes in the element 1 (λ=0) or in the element 2 (λ=1), respectively. Under cyclic loadings it is here assumed that, during an unloading from a tensile stress state, the value of λ is maintained constant, equal to the value corresponding to the maximum tensile strain which has been previously attained; if this maximum strain is exceeded during a tensile reloading, the value of λ is updated as for the case of monotonic tensile loading. Further detail can be found in Ref. 5.

NUMERICAL RESULTS AND CONCLUDING REMARKS

On the basis of the models in Figs. 1 and 2, a numerical procedure analogous to that described in detail in Ref. 1 has been coded as a computer program for the nonlinear analysis of R/C structural walls and uniaxial members.

A first test has been conducted to check the reliability of the uniaxial element model in Fig. 2 with reference to a R/C prism under axial load reversals tested by Morita et al. (Ref. 9). A good correlation of numerical and experimental results is shown in Fig. 3, except for the branches corresponding to the progressive closure of cracks. This discrepancy is due to the fact that, as previously pointed out, the adopted concrete model does not account for the effects produced by different values of the actual longitudinal and transversal steel ratios: e.g., the effects on the stress-strain relationship during the closure of cracks.

Many numerical tests have been conducted in order to check effectiveness and reliability of the wall model in Fig. 1 with reference to four 1/3-scale R/C wall specimens previously tested by Vallenas et al. (Ref. 3). Test walls and loading patterns are schematically shown in Fig. 4.

The same test walls, which were subjected to high shear stresses, were considered in Ref. 1, where parametric studies shown the difficulty of describing accurately by the modified TVLEM, already mentioned, the measured flexural and shear displacement components, which proved to be sensitive to the choice of many parameters. A difficulty of the same kind has been met in these studies. This is shown in Fig. 5, where the measured displacement components at the

third floor of specimens 3 and 5 are compared with the analogous analytical components obtained by assuming different values of the parameter c for the wall model in Fig. 1. All the analytical curves have been obtained for an adequate number of uniaxial elements (n=8); however, also for n=4, minimum value to be assumed, the analogous curves, here not shown for sake of brevity, proved to be practically the same of those in Fig. 5. In Ref. 1 it was also pointed out the inadequacy of the OOHM, adopted also herein, if a refined description of the shear hysteretic behaviour is required under high shear stresses, as was the case for the test walls. For this reason, in these studies the attention is focused on the flexural response of the wall model in Fig. 1.

In Figs. 6a and 6b the experimental and analytical results in terms of base shear V versus the flexural displacement $\delta_{3flex.}$ at the third floor are compared for specimens 3 and 5, respectively. The numerical results shown by full line have been obtained by assuming n=4 for different values of the parameter c. Apart from a slight discrepancy, good correlation of the experimental curve and the analytical curve corresponding to the value c=0.4 is observed for both the mentioned specimens. The correlation of experimental and analytical curves becomes excellent when adopting the values c=0.4 and n=8 for the analytical model (see dashed lines in Fig. 6). A good correlation of experimental and analytical curves corresponding to c=0.4 and n=4 is also shown in Figs. 7a and 7b for specimens 4 and 6, respectively.

It is worth-while to note that the choice of the minimum value for n (n=4), which, as shown in Figs. 6 and 7, allowed to obtain by the analytical wall model a good prediction of the flexural response provided that a suitable value of c has been chosen, is the most advantageous in terms of computational effort. This is still more evident if, as it can be observed in Fig. 8 with reference to a particular cycle of flexural response of the specimen 4, the accuracy of the proposed wall model in predicting the measured flexural response is comparable with that of a F.E. analysis conducted by ANSR-I computer program, which however requires a considerably greater computational effort.

It can be concluded that, on the basis of the refined constitutive laws adopted for the materials and the tension-stiffening effect, the proposed wall model can reliably predict the flexural response, even assuming the minimum of uniaxial elements (n=4), which is the most advantageous choice to reduce the computational effort. The accuracy in predicting the flexural response can be efficiently improved, rather than assuming a greater number of uniaxial elements, by calibrating adequately the parameter c defining the relative rotation center of the generic wall number. For a comparable level of accuracy the proposed wall model is considerably less time-consuming than detailed models. Therefore, the use of simplified, yet reasonably accurate, constitutive laws for the materials and the tension-stiffening effect should provide a reliable wall model particularly suitable for incorporation in a practical seismic nonlinear analysis of complex R/C structural systems.

However, under high shear stresses, the OOHM gives only an approximate description of the shear hysteretic response; moreover, the prediction by the proposed wall model of the shear and flexural displacement components is very difficult , depending on the choice of many parameters. Thus, when high shear stresses are expected, the reliability of the proposed wall model should be improved by revising the OOHM and relating in some way flexural and shear responses, which at the present are independently described by the wall model.

ACKNOWLEDGMENTS

A large portion of the results reported herein was obtained as part of a cooperative research program between Italy and the U.S.A., sponsored by the C.N.R. (Italian Research Council). Professor Bertero gratefully acknowledges the financial support of the National Science Foundation (U.S.A.).

REFERENCES

1. Vulcano, A. and Bertero, V.V., "Analytical Models for Predicting the Lateral Response of R/C Shear Walls: Evaluation of Their Reliability", Earth. Eng. Research Center Report UCB/EERC-87/19, Univ. of California, Berkeley, (1987).
2. Kabeyasawa, T., Shioara, H., Otani, S., and Aoyama, H., "Analysis of the Full-Scale Seven-Story Reinforced Concrete Test Structure: Test PSD3", Procs. 3rd Joint Tech. Coord. Committee, Tsukuba, Japan, (1982).
3. Vallenas, J.M., Bertero, V.V., and Popov, E.P., "Hysteretic Behavior of Reinforced Concrete Structural Walls", Earth. Eng. Research Center Report UCB/EERC-79/20, Univ. of California, Berkeley, (1979).
4. Bolong, Z., Mingshun, W., and Kunlian, Z., "A Study of Hysteretic Curve of Reinforced Concrete Members Under Cyclic Loading", Procs. 7th W.C.E.E., Vol.6, Istanbul, Turkey, (1980).
5. Colotti, V. and Vulcano, A., "Behaviour of R/C Structural Walls Subjected to Severe Cyclic Loadings" (in Italian), Procs. AICAP (Italian Association of Reinforced and Prestressed Concrete) Conference, Stresa, Italy, (1987).
6. Menegotto, M. and Pinto, P.E., "Method of Analysis for Ciclically Loaded Reinforced Concrete Plane Frames Including Changes in Geometry and Nonelastic Behavior of Elements Under Combined Normal Force and Bending", Procs. IABSE Symp., Lisbon, (1973).
7. Jennings, P.C., "Response of Simple Yielding Structures to Earthquake Excitations", California Inst. of Technology, Pasadena, California, (1963).
8. Rizkalla, S.H. and Hwang, L.S., "Crack Prediction for Members in Uniaxial Tension", ACI Journal, Nov.-Dec. (1984).
9. Morita, S., Kaku, T., and Sudo, E., "Force-Strain Relationship of Reinforcing Bars Embedded in Concrete Under Reversed Loadings", CEB, Bull. d'Inf. N. 132, AICAP-CEB Symp., Rome, (1979).

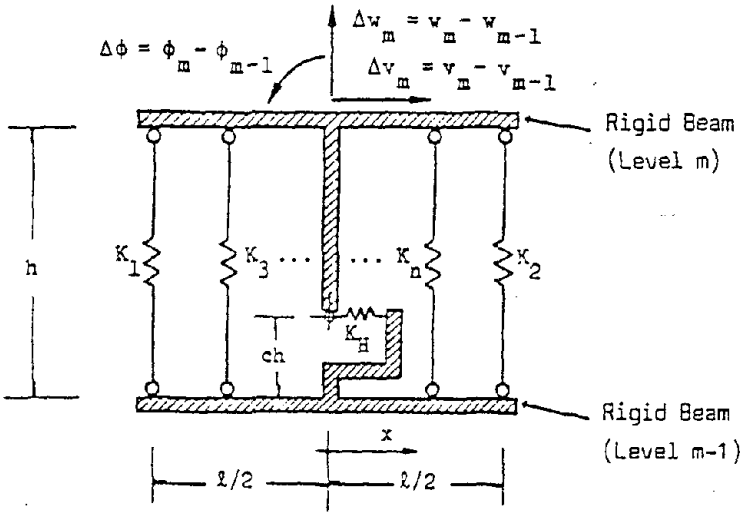

Fig. 1 Proposed Wall Model

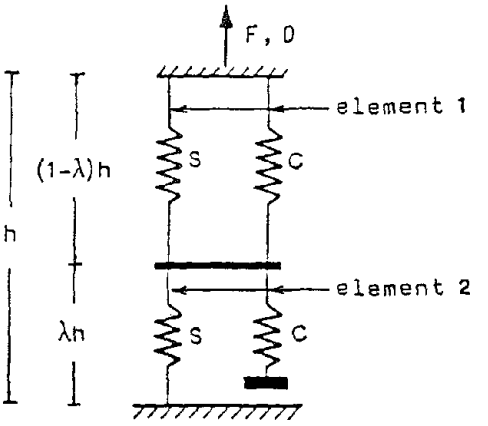

Fig. 2 Uniaxial Element Model

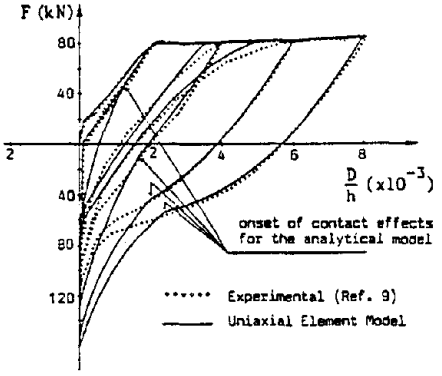

Fig. 3 Analytical and Experimental Curves for a R/C Uniaxial Member

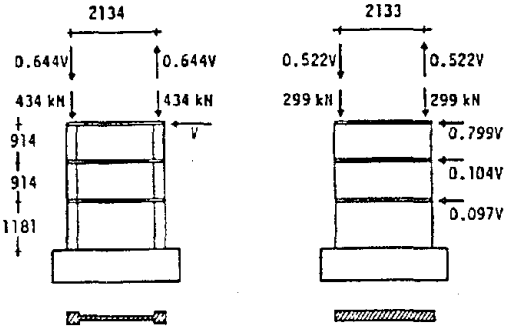

(a) Specimens 3, 4 (b) Specimens 5, 6

Fig. 4 Test Walls and Loading Patterns

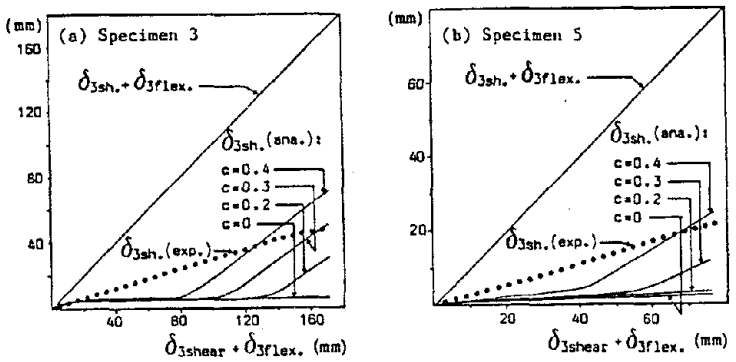

Fig. 5 Third Floor Displacement Components of Test Walls (Monotonic Loading)

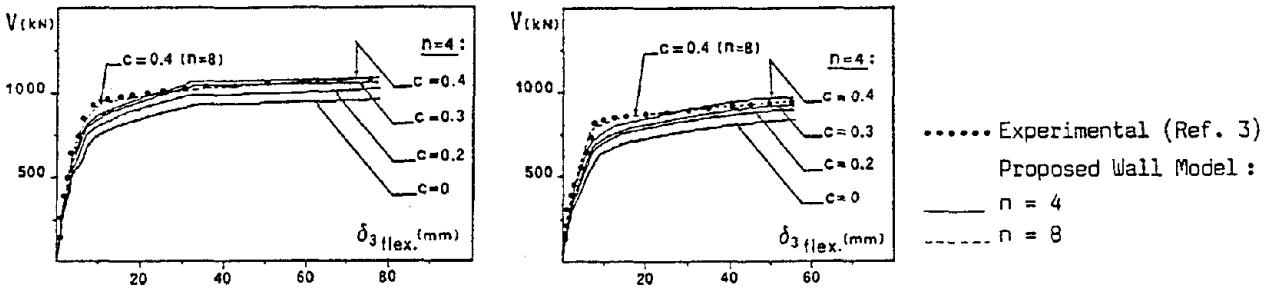

(a) Specimen 3 (b) Specimen 5

Fig. 6 Flexural Response of Test Walls Under Monotonic Loading

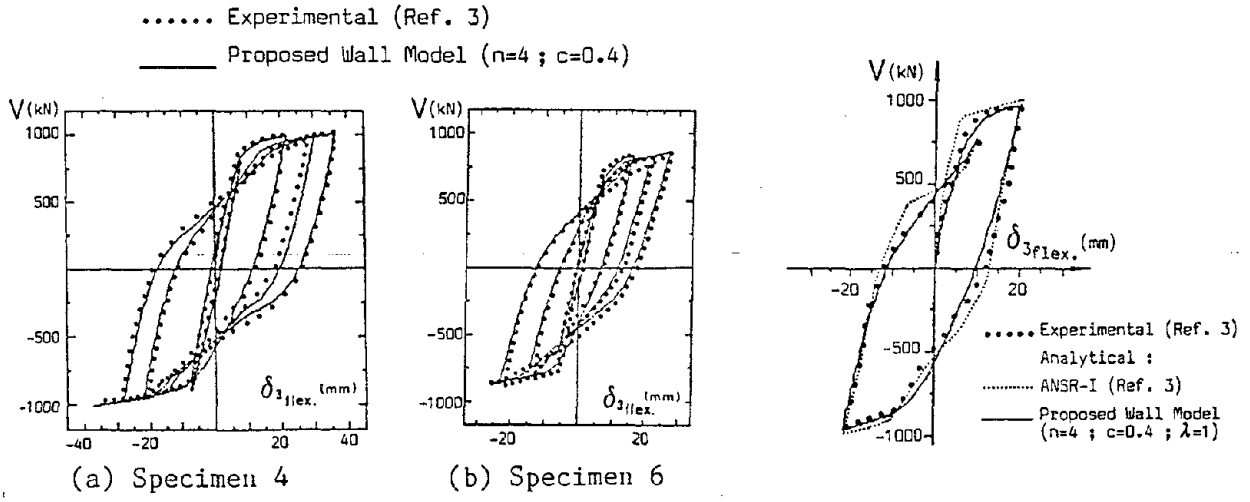

(a) Specimen 4 (b) Specimen 6

Fig. 7 Flexural Response of Test Walls Under Cyclic Loading

Fig. 8 Experimental and Analytical Results for Specimen 4

ANALYTICAL MODELS FOR THE BIAXIAL RESPONSE OF REINFORCED CONCRETE BUILDINGS

Christos ZERIS[1] and Stephen MAHIN[2]

[1]Department of Civil Engineering, National Technical University of Athens, Athens 10683, Greece.
[2]Department of Civil Engineering, University of California, Berkeley, CA 94720, U.S.A.

SUMMARY

A refined element model is presented for the analysis of reinforced concrete beam-columns under generalized bi-directional flexural and axial load fluctuations. A section/fiber idealization is adopted. The formulation is capable of describing the internal damage distribution and the finite deformability and softening characteristics of the member. The element, which is implemented in a general purpose space frame analysis program, is used herein for correlations of column experiments under biaxial bending and the analysis of a test frame under oblique uniaxial earthquake base excitation. The analyses demonstrate the reliability of the formulation and the biaxial response characteristics of columns that influence global structural response and concentration of damage.

INTRODUCTION

Refined finite element discretizations are often computationally prohibitive for the analysis of entire building systems and they may be unsuitable for cyclic response analysis. For the analysis of entire structural systems different approaches usually have been followed for modelling the biaxial bending of individual beam-columns; these range from the lumped plasticity representations that assume all nonlinearity is confined to idealized end springs (3,6, and 13), to distributed damage models which account for the spread of damage along the length (2,5,7,9, and 12). A detailed review of alternative models and their restrictions is given in Refs. 8 and 15. The applicability of existing analytical models is often limited because they may oversimplify some key aspects of physical behavior, or may employ restrictive theoretical assumptions. Similarly, most formulations suffer from numerical problems when a drop in resistance is encountered with increasing deformation. A refined formulation which overcomes some of these deficiencies is presented herein.

ELEMENT FORMULATION

A series of nonlinear models has been developed for the static and dynamic analysis of individual biaxially loaded columns. The section discretization employed in the finite element models is similar to that adopted in the interactive program BICOLA, used for the analysis of arbitrary-shaped column sections under generalized biaxial bending-axial load (or deformation) control (16). The member models have been implemented in ANSR, a general purpose finite element analysis program for the nonlinear static and dynamic analysis of three-dimensional structural systems (10).

Section Idealization The section can be arbitrarily shaped and is defined as an assemblage of uniaxially stressed steel and concrete fibers in an orthonormal right-hand coordinate system. The coordinate set is normal to the reference axis of the member and the section origin is located on the member axis (Fig. 1). Following the usual fiber model assumptions, plane sections are assumed to remain plane and normal to the member axis while full compatibility is enforced between neighboring steel and concrete fibers. Therefore, the section state is completely defined by the reference strain at the origin and two orthogonal curvatures in the orthonormal system.

Different material constitutive models for the steel and concrete can be used within the section. For the steel three different models are implemented (Ref. 15). For the concrete a general model is adopted, capable of describing unconfined as well as confined behavior.

Member Idealization The element models prismatic members with a straight longitudinal axis. A column is monitored at sections located along its length (Fig. 1). At least two sections (at the ends of the member) must be defined. The member degrees of freedom are shown in Fig. 1.

Small displacement theory defines all interior kinematic transformations; however, the distribution of damage within the element is taken into account in the definition of these transformations. Global level second order geometric effects are considered assuming a simple truss mechanism. Shear deformations at the global level, as well as shear force-flexure interaction, are ignored. Under the plane sections assumption, effects due to bond slip are neglected within the element. However, fixed end rotations at the column ends can be included in the analysis of the entire structure through additional joint spring elements especially developed for this purpose (15).

Distributed transverse loads are not considered; this assumption is typically correct for columns. Variation of section properties is permitted along the longitudinal axis; however, interior sections must be at least as strong as the end sections to avoid convergence problems.

Member Stiffness For computational economy a linear flexibility variation is assumed between monitored sections. Therefore, the location of internal sections is dictated by the need for realism in establishing an adequate flexibility distribution. The member tangent stiffness matrix is obtained by inverting the local element tangent flexibility F_m. Following established virtual work procedures, this is evaluated during changes of fiber state through a weighted integration of the current section flexibilities $f_s(z)$,

$$F_m = \int_0^L b_s^m(z)^T f_s(z) b_s^m(z) dz \tag{1}$$

where $b_s^m(z)$ is the equilibrium transformation matrix of a simply supported member. Section flexibilities $f_s(z)$ are calculated by inverting the individual section stiffnesses (17).

State Determination Numerical problems with displacement advancement strategies due to negative definite stiffness following section disintegration, as well as due to nonproportional loading, have been reported in Ref. 5 and were examined in Ref. 16. In order to account for possible deformation softening of the critical regions, the process of determining the internal fiber stresses and section forces differs from conventional displacement formulations.

Changes in the end section fiber states within a time step are monitored through a modified event-to-event step advancement (15). During each event, section deformations and fiber strains are evaluated from end section deformations (dv_s) using displacement transformation matrices $a_s^m(z)$ that account for the current internal flexibility distribution, following

$$dv_s(z) = f_s(z) b_s^m(z) F_m^{-1} dr_m = a_s^m(z) dr_m \tag{2}$$

where F_m is the current tangent member flexibility. The use of the above variable transformation functions has been introduced in Ref. 7 for modelling steel tubular members.

After the section resistance vectors are obtained, remaining interior sections are updated iteratively to conform to the equilibrium diagram defined by the end section forces. As a result, numerical instability problems of the displacement formulation (illustrated in Refs. 8, 15, and 17) are resolved. For positive definite section behavior the adopted procedure is entirely equivalent to standard displacement formulations (15).

The equilibrium iteration procedure (15) consists of a three-level nested iteration loop establishing the section strain state (given the past history) that equilibrates the target section forces. At the upper level a bisection scheme is adopted in the two-dimensional moment space in order to establish the section deformation state that minimizes the difference between applied and resisting section moments. Using the lower level iterations, the evaluation of each trial point satisfies axial load equilibrium. A similar displacement controlled advancement of the critical end section is enforced in the event of instability under nonproportional loading associated with the onset of deformation softening.

VERIFICATION STUDIES

Several column tests have been used for element verification (11 and 13). A square, symmetrically reinforced column tested under a constant axial load of sixteen tons is considered here. The specimen is displaced in a square pattern in plan with cycles of gradually increasing amplitude. Reported material characteristics are used in modelling the member. The element is monitored at four unequally spaced sections, with approximately 200 fibers per section. Steel is modelled using an explicit exponential idealization.

The predicted base shear-tip displacement characteristics are compared with experimental results in Fig. 2. Analytical correlations of the above tests have also been reported, using other plasticity or lumped nonlinearity formulations in Refs. 3 and 13. The correlations between recorded and predicted responses demonstrate that the model is able to adequately simulate the biaxial bending phenomena observed experimentally in the variation of stiffness, strength, and hysteretic response.

Following the projected hysteretic shapes, several phenomena associated with biaxial response can be identified which are not encountered in strictly uniaxial response. As a consequence of the biaxial strength interaction, increase in the out-of-plane deformation (while keeping the in-plane displacement fixed) causes a significant reduction of the in-plane resistance due to the influence of a maximum capacity surface. Comparing subsequent cycles through the same displacement level with intervening out-of-plane excursions, a reduction is observed in the flexural stiffness of the member as a consequence of intermediate out-of-plane bending cycles.

ANALYSIS OF A SIMPLE FRAME

A two-story test frame was analyzed under the first seven seconds of the Taft earthquake record, scaled to 0.57g (Test W2, Ref. 4). Different inclinations (Θ) of the base input relative to the structural principal axes were considered, from 0° through 90° at increments of 15°, assuming full correlation of the base input orthogonal components. The recorded acceleration records acting simultaneously (the transverse motion acceleration being scaled with the same scale factor as the longitudinal one) and the longitudinal component acting simultaneously along both axes (cases UNC and 0+90, in Figs. 3 and 5, respectively). The detailing of the members conformed with standard ductile moment-resisting frame practices. Columns were rectangular in section, oriented such that strong bending occurs for longitudinal (denoted as x) motion. The diaphragm was assumed to be rigid in its own plane. Beams were modelled as simple two-component elements while columns were modelled by the fiber element, monitored at six unequally spaced sections. Rigid zones were specified to approximate the beam-column joints.

The predicted particle motions at the roof centroid are compared in Fig. 3 for the different Θ's. Overall, drifts are higher in the transverse direction due to the relatively higher flexibility of the structure in this direction, as well as due to a different pattern of member hinging. For this particular earthquake, centroidal drifts are comparable to those attained under uniaxial excitation in either direction. The maximum predicted drift (case 0+90) is 2.5 in (6.3cm), corresponding to an interstory drift of 1.8%. Projected column drifts exceed somewhat the corresponding centroidal values as a result of torsion.

The initial response loops are strongly affected by Θ, although this dependence breaks down as significant nonlinearity is induced in the system. Most nonlinear action is confined to the ground floor columns, with the first story gradually turning into a soft story. The maximum vectorial displacement ductility at this level, accounting for the reduction in yield deformation due to biaxial effects, is equal to 5.3, compared to the maximum uniaxial demand of 3 (obtained in y excitation). Despite the initial symmetry of the frame, torsional response is induced as a result of unsymmetric inelastic distributions of lateral stiffnesses between columns due to biaxial bending; this is further accentuated by axial load fluctuations.

Projected x motion bending moment-chord rotation characteristics for a typical ground corner column are compared in Fig. 4. Projected chord rotation demands are comparable for different Θ's. However, due to higher axial load fluctuation and biaxial bending, flexural strengths are reduced by up to 40% compared to uniaxial excitation.

Despite the near equality of global drifts, the presence of biaxial demands in the column critical regions produces a significant difference in the local damage. Comparing the energy dissipated by the reinforcement at the base critical section of this column normalized by the energy at yield in pure tension (Fig. 5), it can be seen that the induced damage is considerably higher than that induced under uniaxial excitation.

CONCLUSIONS

A fiber element model is proposed for the cyclic analysis of reinforced concrete beam-columns under biaxial bending and axial load fluctuations. The formulation adopted can reliably model members that exhibit deformation softening. Detailed information can be obtained on the internal curvature and strain demands, as well as the concentration of damage within the member.

The analyses of the test members indicate that biaxial bending of columns results in a reduction of strength and flexural stiffness relative to their uniaxial response counterparts. As a result of biaxial excitation, unusually high strains can be locally induced.

ACKNOWLEDGEMENTS

This research was funded by the National Science Foundation. The findings are, however, those of the authors above.

REFERENCES

1. Abrams D.P., Influence of Axial Force Variations on Flexural Behavior of Reinforced Concrete Columns, *Structural Journal*, ACI, Vol. 84, No. 3, May-June 1987.
2. Aktan A., D. Pecknold and M.A. Sozen, Effects of Two Dimensional Earthquake Motion on a Reinforced Concrete Column, *Rep. No. UILU-ENG 73-2009*, Univ. of Illinois, Urbana, May 1973.
3. Chen P., Generalized Plastic Hinge Concepts for 3D Beam Column Elements, Ph.D. thesis, Univ. of California, Berkeley, 1981.
4. Clough R.W. and J. Gidwani, Reinforced Concrete Frame 2: Seismic Testing and Analytical Correlation, *Rep. No. UCB/EERC-76/15*, University of California, Berkeley, June 1976.
5. Kang Y. and A.C. Scordelis, Nonlinear Geometric, Material and Time Dependent Analysis of Reinforced and Prestressed Concrete Frames, *Rep. UC-SESM No. 77-1*, University of California, Berkeley, Jan. 1977.
6. Lai S., G. Will and S. Otani, Model for Inelastic Biaxial Bending of Concrete Members, *Journal of the Structures Division*, ASCE, Vol. 110, No. ST11, Nov. 1984.
7. Mahasurevachai M., Inelastic Analysis of Piping and Tubular Structures, *Rep. No. UCB/EERC-82/27*, University of California, Berkeley, 1982.
8. Mahin S.A., Inelastic Behavior and Modeling of Reinforced Concrete Columns under Multidirectional Seismic Excitations, *Proceedings*, Ninth World Conference on Earthquake Engineering, Japan, Aug. 1988.
9. Menegotto M. and P. Pinto, Slender RC Compressed Members in Biaxial Bending, *Journal of the Structures Division*, ASCE, Vol. 103, No. ST3, March 1977.
10. Mondkar D. and G.H. Powell, ANSR-I General Purpose Computer Program for Analysis of Non-Linear Structural Response, *Rep. No. UCB/EERC-75/37*, University of California, Berkeley, 1975.
11. Otani S. and V.W. Cheung, Behavior of Reinforced Concrete Columns Under Biaxial Lateral Load Reversals, (ii) Test Without Axial Loads, *Publ.81-02*, Univ. of Toronto, Toronto, Feb. 1982.
12. Suharwardy M. and D. Pecknold, Inelastic Response of Reinforced Concrete Columns Subjected to Two-Dimensional Response, *Rep. No. UILU-ENG 78-2022*, Univ. of Illinois, Urbana, Oct. 1978.
13. Takizawa H. and H. Aoyama, Biaxial Effects in Modelling Earthquake Response of R/C Structures, *Earthquake Engineering and Structural Dynamics*, Vol. 4, 1976.
14. Zeris C., S.A. Mahin and V.V. Bertero, Analysis of the Seismic Performance of the Imperial County Services Buildings, Proceedings, IIIrd U.S. National Conference on Earthquake Engineering, Charleston, Aug. 1986.
15. Zeris C.A., Three Dimensional Nonlinear Response of Reinforced Concrete Buildings, Ph.D. thesis, Univ. of California, Berkeley, 1986.
16. Zeris C.A. and S.A. Mahin, Biaxial Column Analysis Program (BICOLA) User's Guide, *SEMM Report*, Univ. of California, Berkeley, Oct. 1987.
17. Zeris C.A. and S.A. Mahin, Analysis of Reinforced Concrete Beam-Columns Under Uniaxial Excitation, *Journal of the Structures Division*, ASCE, Vol. 114, No. ST4, April 1988.

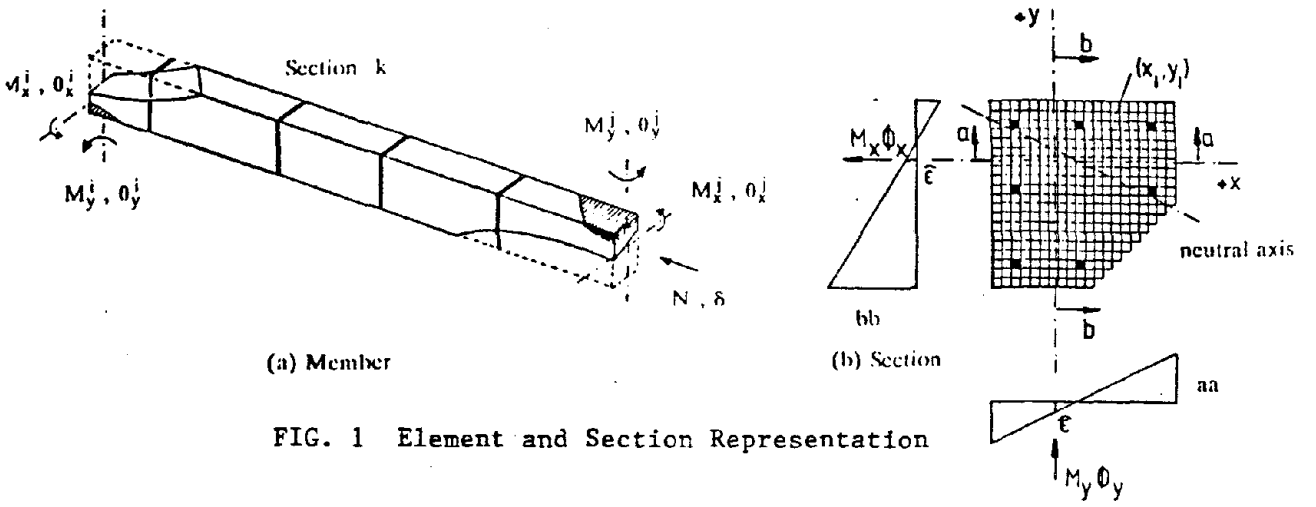

FIG. 1 Element and Section Representation

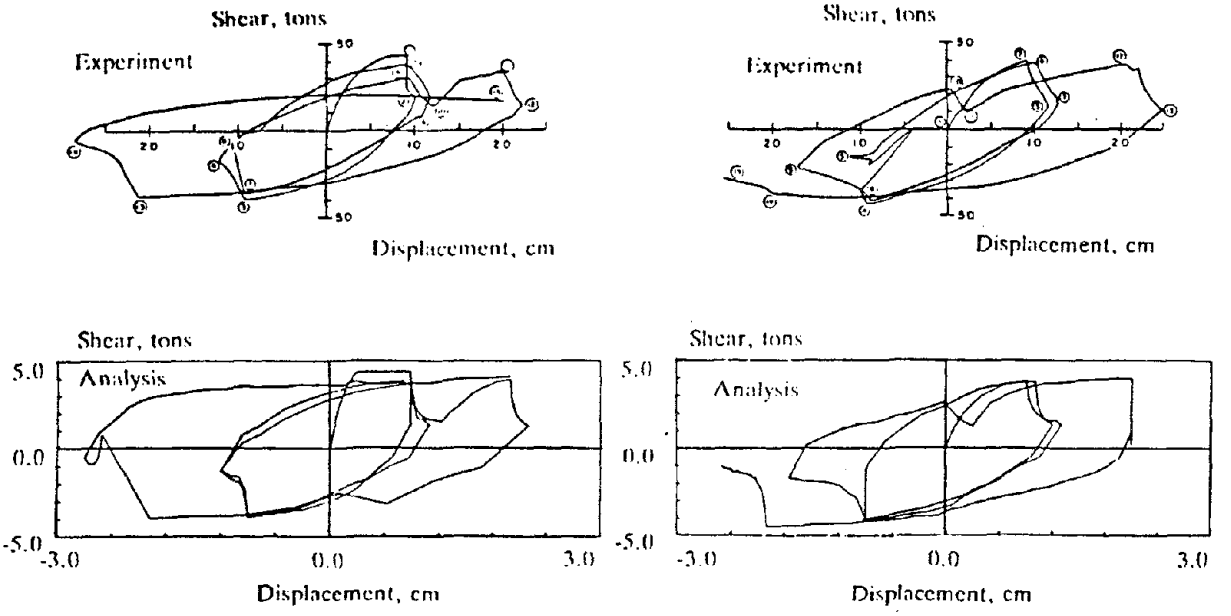

FIG. 2 Correlations With Experiments, Takizawa and Aoyama Column

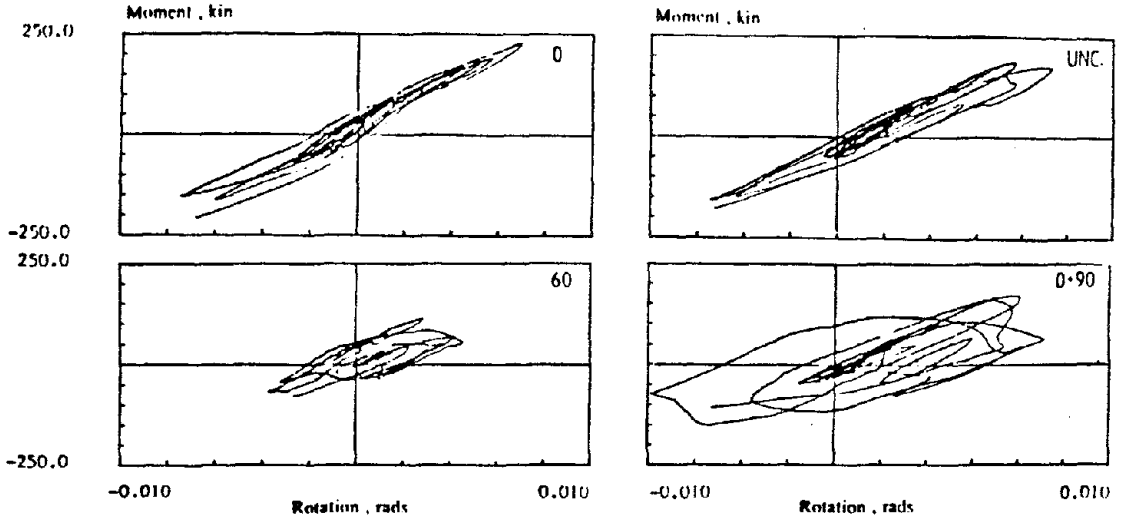

FIG. 3 Roof Centroidal Motions for Different Incident Angles

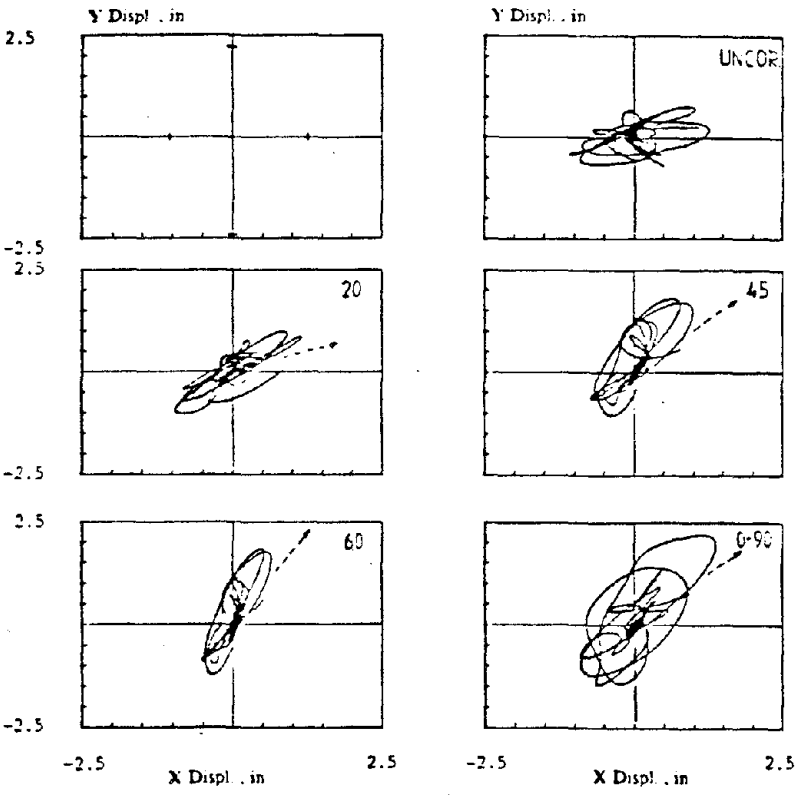

FIG. 4 Column Base Moment - Chord Rotation for Different Incident Angles

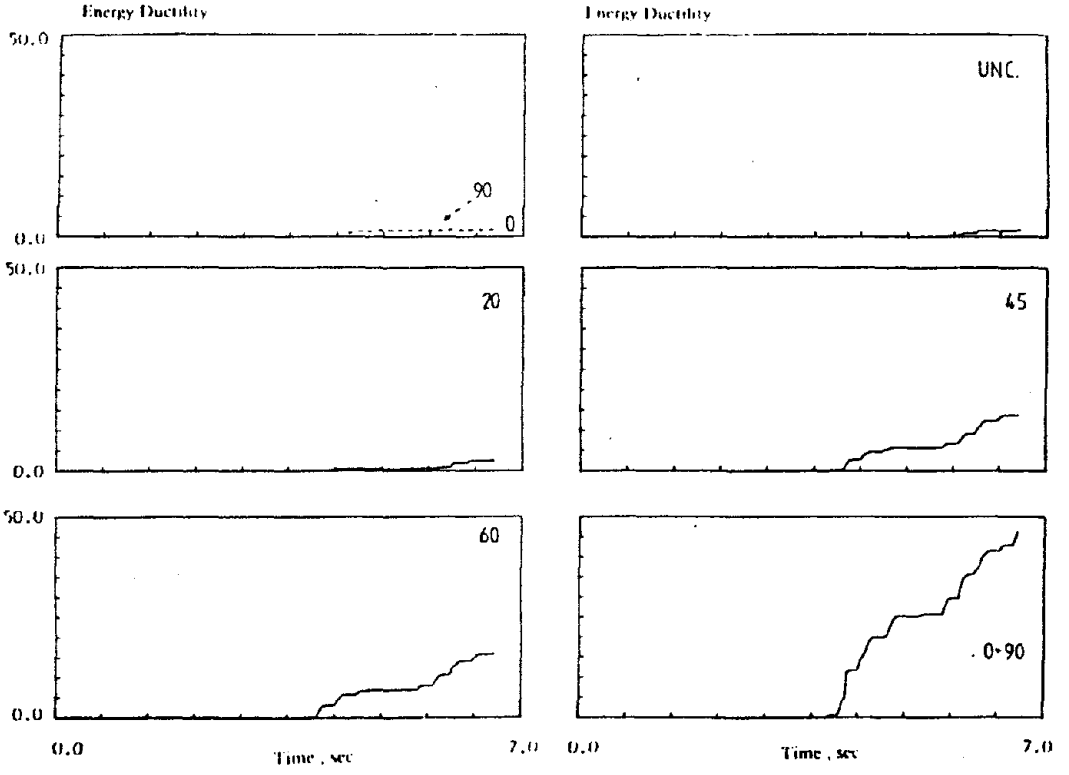

FIG. 5 Cumulative Inelastic Energy Ductility, Ground Story Column, For Different Incident Angles

EARTHQUAKE ENGINEERING RESEARCH CENTER REPORT SERIES

EERC reports are available from the National Information Service for Earthquake Engineering(NISEE) and from the National Technical Information Service(NTIS). Numbers in parentheses are Accession Numbers assigned by the National Technical Information Service; these are followed by a price code. Contact NTIS, 5285 Port Royal Road, Springfield Virginia, 22161 for more information. Reports without Accession Numbers were not available from NTIS at the time of printing. For a current complete list of EERC reports (from EERC 67-1) and availablity information, please contact University of California, EERC, NISEE, 1301 South 46th Street, Richmond, California 94804.

UCB/EERC-80/01 "Earthquake Response of Concrete Gravity Dams Including Hydrodynamic and Foundation Interaction Effects," by Chopra, A.K., Chakrabarti, P. and Gupta, S., January 1980, (AD-A087297)A10.

UCB/EERC-80/02 "Rocking Response of Rigid Blocks to Earthquakes," by Yim, C.S., Chopra, A.K. and Penzien, J., January 1980, (PB80 166 002)A04.

UCB/EERC-80/03 "Optimum Inelastic Design of Seismic-Resistant Reinforced Concrete Frame Structures," by Zagajeski, S.W. and Bertero, V.V., January 1980, (PB80 164 635)A06.

UCB/EERC-80/04 "Effects of Amount and Arrangement of Wall-Panel Reinforcement on Hysteretic Behavior of Reinforced Concrete Walls," by Iliya, R. and Bertero, V.V., February 1980, (PB81 122 525)A09.

UCB/EERC-80/05 "Shaking Table Research on Concrete Dam Models," by Niwa, A. and Clough, R.W., September 1980, (PB81 122 368)A06.

UCB/EERC-80/06 "The Design of Steel Energy-Absorbing Restrainers and their Incorporation into Nuclear Power Plants for Enhanced Safety (Vol 1a): Piping with Energy Absorbing Restrainers: Parameter Study on Small Systems," by Powell, G.H., Oughourlian, C. and Simons, J., June 1980.

UCB/EERC-80/07 "Inelastic Torsional Response of Structures Subjected to Earthquake Ground Motions," by Yamazaki, Y., April 1980, (PB81 122 327)A08.

UCB/EERC-80/08 "Study of X-Braced Steel Frame Structures under Earthquake Simulation," by Ghanaat, Y., April 1980, (PB81 122 335)A11.

UCB/EERC-80/09 "Hybrid Modelling of Soil-Structure Interaction," by Gupta, S., Lin, T.W. and Penzien, J., May 1980, (PB81 122 319)A07.

UCB/EERC-80/10 "General Applicability of a Nonlinear Model of a One Story Steel Frame," by Sveinsson, B.I. and McNiven, H.D., May 1980, (PB81 124 877)A06.

UCB/EERC-80/11 "A Green-Function Method for Wave Interaction with a Submerged Body," by Kioka, W., April 1980, (PB81 122 269)A07.

UCB/EERC-80/12 "Hydrodynamic Pressure and Added Mass for Axisymmetric Bodies.," by Nilrat, F., May 1980, (PB81 122 343)A08.

UCB/EERC-80/13 "Treatment of Non-Linear Drag Forces Acting on Offshore Platforms," by Dao, B.V. and Penzien, J., May 1980, (PB81 153 413)A07.

UCB/EERC-80/14 "2D Plane/Axisymmetric Solid Element (Type 3-Elastic or Elastic-Perfectly Plastic)for the ANSR-II Program," by Mondkar, D.P. and Powell, G.H., July 1980, (PB81 122 350)A03.

UCB/EERC-80/15 "A Response Spectrum Method for Random Vibrations," by Der Kiureghian, A., June 1981, (PB81 122 301)A03.

UCB/EERC-80/16 "Cyclic Inelastic Buckling of Tubular Steel Braces," by Zayas, V.A., Popov, E.P. and Mahin, S.A., June 1981, (PB81 124 885)A10.

UCB/EERC-80/17 "Dynamic Response of Simple Arch Dams Including Hydrodynamic Interaction," by Porter, C.S. and Chopra, A.K., July 1981, (PB81 124 000)A13.

UCB/EERC-80/18 "Experimental Testing of a Friction Damped Aseismic Base Isolation System with Fail-Safe Characteristics," by Kelly, J.M., Beucke, K.E. and Skinner, M.S., July 1980, (PB81 148 595)A04.

UCB/EERC-80/19 "The Design of Steel Energy-Absorbing Restrainers and their Incorporation into Nuclear Power Plants for Enhanced Safety (Vol.1B): Stochastic Seismic Analyses of Nuclear Power Plant Structures and Piping Systems Subjected to Multiple Supported Excitations," by Lee, M.C. and Penzien, J., June 1980, (PB82 201 872)A08.

UCB/EERC-80/20 "The Design of Steel Energy-Absorbing Restrainers and their Incorporation into Nuclear Power Plants for Enhanced Safety (Vol 1C): Numerical Method for Dynamic Substructure Analysis," by Dickens, J.M. and Wilson, E.L., June 1980.

UCB/EERC-80/21 "The Design of Steel Energy-Absorbing Restrainers and their Incorporation into Nuclear Power Plants for Enhanced Safety (Vol 2): Development and Testing of Restraints for Nuclear Piping Systems," by Kelly, J.M. and Skinner, M.S., June 1980.

UCB/EERC-80/22 "3D Solid Element (Type 4-Elastic or Elastic-Perfectly-Plastic) for the ANSR-II Program," by Mondkar, D.P. and Powell, G.H., July 1980, (PB81 123 242)A03.

UCB/EERC-80/23 "Gap-Friction Element (Type 5) for the Ansr-II Program," by Mondkar, D.P. and Powell, G.H., July 1980, (PB81 122 285)A03.

UCB/EERC-80/24 "U-Bar Restraint Element (Type 11) for the ANSR-II Program," by Oughourlian, C. and Powell, G.H., July 1980, (PB81 122 293)A03.

UCB/EERC-80/25 "Testing of a Natural Rubber Base Isolation System by an Explosively Simulated Earthquake," by Kelly, J.M., August 1980, (PB81 201 360)A04.

UCB/EERC-80/26 "Input Identification from Structural Vibrational Response," by Hu, Y., August 1980, (PB81 152 308)A05.

UCB/EERC-80/27 "Cyclic Inelastic Behavior of Steel Offshore Structures," by Zayas, V.A., Mahin, S.A. and Popov, E.P., August 1980, (PB81 196 180)A15.

UCB/EERC-80/28 "Shaking Table Testing of a Reinforced Concrete Frame with Biaxial Response," by Oliva, M.G., October 1980, (PB81 154 304)A10.

UCB/EERC-80/29 "Dynamic Properties of a Twelve-Story Prefabricated Panel Building," by Bouwkamp, J.G., Kollegger, J.P. and Stephen, R.M., October 1980, (PB82 138 777)A07.

UCB/EERC-80/30 "Dynamic Properties of an Eight-Story Prefabricated Panel Building," by Bouwkamp, J.G., Kollegger, J.P. and Stephen, R.M., October 1980, (PB81 200 313)A05.

UCB/EERC-80/31 "Predictive Dynamic Response of Panel Type Structures under Earthquakes," by Kollegger, J.P. and Bouwkamp, J.G., October 1980, (PB81 152 316)A04.

UCB/EERC-80/32 "The Design of Steel Energy-Absorbing Restrainers and their Incorporation into Nuclear Power Plants for Enhanced Safety (Vol 3): Testing of Commercial Steels in Low-Cycle Torsional Fatique," by Spanner, P., Parker, E.R., Jongewaard, E. and Dory, M., 1980.

UCB/EERC-80/33 "The Design of Steel Energy-Absorbing Restrainers and their Incorporation into Nuclear Power Plants for Enhanced Safety (Vol 4): Shaking Table Tests of Piping Systems with Energy-Absorbing Restrainers," by Stiemer, S.F. and Godden, W.G., September 1980, (PB82 201 880)A05.

UCB/EERC-80/34 "The Design of Steel Energy-Absorbing Restrainers and their Incorporation into Nuclear Power Plants for Enhanced Safety (Vol 5): Summary Report," by Spencer, P., 1980.

UCB/EERC-80/35 "Experimental Testing of an Energy-Absorbing Base Isolation System," by Kelly, J.M., Skinner, M.S. and Beucke, K.E., October 1980, (PB81 154 072)A04.

UCB/EERC-80/36 "Simulating and Analyzing Artificial Non-Stationary Earth Ground Motions," by Nau, R.F., Oliver, R.M. and Pister, K.S., October 1980, (PB81 153 397)A04.

UCB/EERC-80/37 "Earthquake Engineering at Berkeley - 1980," by , September 1980, (PB81 205 674)A09.

UCB/EERC-80/38 "Inelastic Seismic Analysis of Large Panel Buildings," by Schricker, V. and Powell, G.H., September 1980, (PB81 154 338)A13.

UCB/EERC-80/39 "Dynamic Response of Embankment, Concrete-Gavity and Arch Dams Including Hydrodynamic Interation," by Hall, J.F. and Chopra, A.K., October 1980, (PB81 152 324)A11.

UCB/EERC-80/40 "Inelastic Buckling of Steel Struts under Cyclic Load Reversal.," by Black, R.G., Wenger, W.A. and Popov, E.P., October 1980, (PB81 154 312)A08.

UCB/EERC-80/41 "Influence of Site Characteristics on Buildings Damage during the October 3,1974 Lima Earthquake," by Repetto, P., Arango, I. and Seed, H.B., September 1980, (PB81 161 739)A05.

UCB/EERC-80/42 "Evaluation of a Shaking Table Test Program on Response Behavior of a Two Story Reinforced Concrete Frame," by Blondet, J.M., Clough, R.W. and Mahin, S.A., December 1980, (PB82 196 544)A11.

UCB/EERC-80/43 "Modelling of Soil-Structure Interaction by Finite and Infinite Elements," by Medina, F., December 1980, (PB81 229 270)A04.

UCB/EERC-81/01 "Control of Seismic Response of Piping Systems and Other Structures by Base Isolation," by Kelly, J.M., January 1981, (PB81 200 735)A05.

UCB/EERC-81/02 "OPTNSR- An Interactive Software System for Optimal Design of Statically and Dynamically Loaded Structures with Nonlinear Response," by Bhatti, M.A., Ciampi, V. and Pister, K.S., January 1981, (PB81 218 851)A09.

UCB/EERC-81/03 "Analysis of Local Variations in Free Field Seismic Ground Motions," by Chen, J.-C., Lysmer, J. and Seed, H.B., January 1981, (AD-A099508)A13.

UCB/EERC-81/04 "Inelastic Structural Modeling of Braced Offshore Platforms for Seismic Loading," by Zayas, V.A., Shing, P.-S.B., Mahin, S.A. and Popov, E.P., January 1981, (PB82 138 777)A07.

UCB/EERC-81/05 "Dynamic Response of Light Equipment in Structures," by Der Kiureghian, A., Sackman, J.L. and Nour-Omid, B., April 1981, (PB81 218 497)A04.

UCB/EERC-81/06 "Preliminary Experimental Investigation of a Broad Base Liquid Storage Tank," by Bouwkamp, J.G., Kollegger, J.P. and Stephen, R.M., May 1981, (PB82 140 385)A03.

UCB/EERC-81/07 "The Seismic Resistant Design of Reinforced Concrete Coupled Structural Walls," by Aktan, A.E. and Bertero, V.V., June 1981, (PB82 113 358)A11.

UCB/EERC-81/08 "Unassigned," by Unassigned, 1981.

UCB/EERC-81/09 "Experimental Behavior of a Spatial Piping System with Steel Energy Absorbers Subjected to a Simulated Differential Seismic Input," by Stiemer, S.F., Godden, W.G. and Kelly, J.M., July 1981, (PB82 201 898)A04.

UCB/EERC-81/10 "Evaluation of Seismic Design Provisions for Masonry in the United States," by Sveinsson, B.I., Mayes, R.L. and McNiven, H.D., August 1981, (PB82 166 075)A08.

UCB/EERC-81/11 "Two-Dimensional Hybrid Modelling of Soil-Structure Interaction," by Tzong, T.-J., Gupta, S. and Penzien, J., August 1981, (PB82 142 118)A04.

UCB/EERC-81/12 "Studies on Effects of Infills in Seismic Resistant R/C Construction," by Brokken, S. and Bertero, V.V., October 1981, (PB82 166 190)A09.

UCB/EERC-81/13 "Linear Models to Predict the Nonlinear Seismic Behavior of a One-Story Steel Frame," by Valdimarsson, H., Shah, A.H. and McNiven, H.D., September 1981, (PB82 138 793)A07.

UCB/EERC-81/14 "TLUSH: A Computer Program for the Three-Dimensional Dynamic Analysis of Earth Dams," by Kagawa, T., Mejia, L.H., Seed, H.B. and Lysmer, J., September 1981, (PB82 139 940)A06.

UCB/EERC-81/15 "Three Dimensional Dynamic Response Analysis of Earth Dams," by Mejia, L.H. and Seed, H.B., September 1981, (PB82 137 274)A12.

UCB/EERC-81/16 "Experimental Study of Lead and Elastomeric Dampers for Base Isolation Systems," by Kelly, J.M. and Hodder, S.B., October 1981, (PB82 166 182)A05.

UCB/EERC-81/17 "The Influence of Base Isolation on the Seismic Response of Light Secondary Equipment," by Kelly, J.M., April 1981, (PB82 255 266)A04.

UCB/EERC-81/18 "Studies on Evaluation of Shaking Table Response Analysis Procedures," by Blondet, J. M., November 1981, (PB82 197 278)A10.

UCB/EERC-81/19 "DELIGHT.STRUCT: A Computer-Aided Design Environment for Structural Engineering," by Balling, R.J., Pister, K.S. and Polak, E., December 1981, (PB82 218 496)A07.

UCB/EERC-81/20 "Optimal Design of Seismic-Resistant Planar Steel Frames," by Balling, R.J., Ciampi, V. and Pister, K.S., December 1981, (PB82 220 179)A07.

UCB/EERC-82/01 "Dynamic Behavior of Ground for Seismic Analysis of Lifeline Systems," by Sato, T. and Der Kiureghian, A., January 1982, (PB82 218 926)A05.

UCB/EERC-82/02 "Shaking Table Tests of a Tubular Steel Frame Model," by Ghanaat, Y. and Clough, R.W., January 1982, (PB82 220 161)A07.

UCB/EERC-82/03 "Behavior of a Piping System under Seismic Excitation: Experimental Investigations of a Spatial Piping System supported by Mechanical Shock Arrestors," by Schneider, S., Lee, H.-M. and Godden, W. G., May 1982, (PB83 172 544)A09.

UCB/EERC-82/04 "New Approaches for the Dynamic Analysis of Large Structural Systems," by Wilson, E.L., June 1982, (PB83 148 080)A05.

UCB/EERC-82/05 "Model Study of Effects of Damage on the Vibration Properties of Steel Offshore Platforms," by Shahrivar, F. and Bouwkamp, J.G., June 1982, (PB83 148 742)A10.

UCB/EERC-82/06 "States of the Art and Pratice in the Optimum Seismic Design and Analytical Response Prediction of R/C Frame Wall Structures," by Aktan, A.E. and Bertero, V.V., July 1982, (PB83 147 736)A05.

UCB/EERC-82/07 "Further Study of the Earthquake Response of a Broad Cylindrical Liquid-Storage Tank Model," by Manos, G.C. and Clough, R.W., July 1982, (PB83 147 744)A11.

UCB/EERC-82/08 "An Evaluation of the Design and Analytical Seismic Response of a Seven Story Reinforced Concrete Frame," by Charney, F.A. and Bertero, V.V., July 1982, (PB83 157 628)A09.

UCB/EERC-82/09 "Fluid-Structure Interactions: Added Mass Computations for Incompressible Fluid," by Kuo, J.S.-H., August 1982, (PB83 156 281)A07.

UCB/EERC-82/10 "Joint-Opening Nonlinear Mechanism: Interface Smeared Crack Model," by Kuo, J.S.-H., August 1982, (PB83 149 195)A05.

UCB/EERC-82/11 "Dynamic Response Analysis of Techi Dam," by Clough, R.W., Stephen, R.M. and Kuo, J.S.-H., August 1982, (PB83 147 496)A06.

UCB/EERC-82/12 "Prediction of the Seismic Response of R/C Frame-Coupled Wall Structures," by Aktan, A.E., Bertero, V.V. and Piazzo, M., August 1982, (PB83 149 203)A09.

UCB/EERC-82/13 "Preliminary Report on the Smart 1 Strong Motion Array in Taiwan," by Bolt, B.A., Loh, C.H., Penzien, J. and Tsai, Y.B., August 1982, (PB83 159 400)A10.

UCB/EERC-82/14 "Shaking-Table Studies of an Eccentrically X-Braced Steel Structure," by Yang, M.S., September 1982, (PB83 260 778)A12.

UCB/EERC-82/15 "The Performance of Stairways in Earthquakes," by Roha, C., Axley, J.W. and Bertero, V.V., September 1982, (PB83 157 693)A07.

UCB/EERC-82/16 "The Behavior of Submerged Multiple Bodies in Earthquakes," by Liao, W.-G., September 1982, (PB83 158 709)A07.

UCB/EERC-82/17 "Effects of Concrete Types and Loading Conditions on Local Bond-Slip Relationships," by Cowell, A.D., Popov, E.P. and Bertero, V.V., September 1982, (PB83 153 577)A04.

UCB/EERC-82/18 "Mechanical Behavior of Shear Wall Vertical Boundary Members: An Experimental Investigation," by Wagner, M.T. and Bertero, V.V., October 1982, (PB83 159 764)A05.

UCB/EERC-82/19 "Experimental Studies of Multi-support Seismic Loading on Piping Systems," by Kelly, J.M. and Cowell, A.D., November 1982.

UCB/EERC-82/20 "Generalized Plastic Hinge Concepts for 3D Beam-Column Elements," by Chen, P. F.-S. and Powell, G.H., November 1982, (PB83 247 981)A13.

UCB/EERC-82/21 "ANSR-II: General Computer Program for Nonlinear Structural Analysis," by Oughourlian, C.V. and Powell, G.H., November 1982, (PB83 251 330)A12.

UCB/EERC-82/22 "Solution Strategies for Statically Loaded Nonlinear Structures," by Simons, J.W. and Powell, G.H., November 1982, (PB83 197 970)A06.

UCB/EERC-82/23 "Analytical Model of Deformed Bar Anchorages under Generalized Excitations," by Ciampi, V., Eligehausen, R., Bertero, V.V. and Popov, E.P., November 1982, (PB83 169 532)A06.

UCB/EERC-82/24 "A Mathematical Model for the Response of Masonry Walls to Dynamic Excitations," by Sucuoglu, H., Mengi, Y. and McNiven, H.D., November 1982, (PB83 169 011)A07.

UCB/EERC-82/25 "Earthquake Response Considerations of Broad Liquid Storage Tanks," by Cambra, F.J., November 1982, (PB83 251 215)A09.

UCB/EERC-82/26 "Computational Models for Cyclic Plasticity, Rate Dependence and Creep," by Mosaddad, B. and Powell, G.H., November 1982, (PB83 245 829)A08.

UCB/EERC-82/27 "Inelastic Analysis of Piping and Tubular Structures," by Mahasuverachai, M. and Powell, G.H., November 1982, (PB83 249 987)A07.

UCB/EERC-83/01 "The Economic Feasibility of Seismic Rehabilitation of Buildings by Base Isolation," by Kelly, J.M., January 1983, (PB83 197 988)A05.

UCB/EERC-83/02 "Seismic Moment Connections for Moment-Resisting Steel Frames.," by Popov, E.P., January 1983, (PB83 195 412)A04.

UCB/EERC-83/03 "Design of Links and Beam-to-Column Connections for Eccentrically Braced Steel Frames," by Popov, E.P. and Malley, J.O., January 1983, (PB83 194 811)A04.

UCB/EERC-83/04 "Numerical Techniques for the Evaluation of Soil-Structure Interaction Effects in the Time Domain," by Bayo, E. and Wilson, E.L., February 1983, (PB83 245 605)A09.

UCB/EERC-83/05 "A Transducer for Measuring the Internal Forces in the Columns of a Frame-Wall Reinforced Concrete Structure," by Sause, R. and Bertero, V.V., May 1983, (PB84 119 494)A06.

UCB/EERC-83/06 "Dynamic Interactions Between Floating Ice and Offshore Structures," by Croteau, P., May 1983, (PB84 119 486)A16.

UCB/EERC-83/07 "Dynamic Analysis of Multiply Tuned and Arbitrarily Supported Secondary Systems," by Igusa, T. and Der Kiureghian, A., July 1983, (PB84 118 272)A11.

UCB/EERC-83/08 "A Laboratory Study of Submerged Multi-body Systems in Earthquakes," by Ansari, G.R., June 1983, (PB83 261 842)A17.

UCB/EERC-83/09 "Effects of Transient Foundation Uplift on Earthquake Response of Structures," by Yim, C.-S. and Chopra, A.K., June 1983, (PB83 261 396)A07.

UCB/EERC-83/10 "Optimal Design of Friction-Braced Frames under Seismic Loading," by Austin, M.A. and Pister, K.S., June 1983, (PB84 119 288)A06.

UCB/EERC-83/11 "Shaking Table Study of Single-Story Masonry Houses: Dynamic Performance under Three Component Seismic Input and Recommendations," by Manos, G.C., Clough, R.W. and Mayes, R.L., July 1983, (UCB/EERC-83/11)A08.

UCB/EERC-83/12 "Experimental Error Propagation in Pseudodynamic Testing," by Shiing, P.B. and Mahin, S.A., June 1983, (PB84 119 270)A09.

UCB/EERC-83/13 "Experimental and Analytical Predictions of the Mechanical Characteristics of a 1/5-scale Model of a 7-story R/C Frame-Wall Building Structure," by Aktan, A.E., Bertero, V.V., Chowdhury, A.A. and Nagashima, T., June 1983, (PB84 119 213)A07.

UCB/EERC-83/14 "Shaking Table Tests of Large-Panel Precast Concrete Building System Assemblages," by Oliva, M.G. and Clough, R.W., June 1983, (PB86 110 210/AS)A11.

UCB/EERC-83/15 "Seismic Behavior of Active Beam Links in Eccentrically Braced Frames," by Hjelmstad, K.D. and Popov, E.P., July 1983, (PB84 119 676)A09.

UCB/EERC-83/16 "System Identification of Structures with Joint Rotation," by Dimsdale, J.S., July 1983, (PB84 192 210)A06.

UCB/EERC-83/17 "Construction of Inelastic Response Spectra for Single-Degree-of-Freedom Systems," by Mahin, S. and Lin, J., June 1983, (PB84 208 834)A05.

UCB/EERC-83/18 "Interactive Computer Analysis Methods for Predicting the Inelastic Cyclic Behaviour of Structural Sections," by Kaba, S. and Mahin, S., July 1983, (PB84 192 012)A06.

UCB/EERC-83/19 "Effects of Bond Deterioration on Hysteretic Behavior of Reinforced Concrete Joints," by Filippou, F.C., Popov, E.P. and Bertero, V.V., August 1983, (PB84 192 020)A10.

UCB/EERC-83/20 "Analytical and Experimental Correlation of Large-Panel Precast Building System Performance," by Oliva, M.G., Clough, R.W., Velkov, M. and Gavrilovic, P., November 1983.

UCB/EERC-83/21 "Mechanical Characteristics of Materials Used in a 1/5 Scale Model of a 7-Story Reinforced Concrete Test Structure," by Bertero, V.V., Aktan, A.E., Harris, H.G. and Chowdhury, A.A., October 1983, (PB84 193 697)A05.

UCB/EERC-83/22 "Hybrid Modelling of Soil-Structure Interaction in Layered Media," by Tzong, T.-J. and Penzien, J., October 1983, (PB84 192 178)A08.

UCB/EERC-83/23 "Local Bond Stress-Slip Relationships of Deformed Bars under Generalized Excitations," by Eligehausen, R., Popov, E.P. and Bertero, V.V., October 1983, (PB84 192 848)A09.

UCB/EERC-83/24 "Design Considerations for Shear Links in Eccentrically Braced Frames," by Malley, J.O. and Popov, E.P., November 1983, (PB84 192 186)A07.

UCB/EERC-84/01 "Pseudodynamic Test Method for Seismic Performance Evaluation: Theory and Implementation," by Shing, P.-S.B. and Mahin, S.A., January 1984, (PB84 190 644)A08.

UCB/EERC-84/02 "Dynamic Response Behavior of Kiang Hong Dian Dam," by Clough, R.W., Chang, K.-T., Chen, H.-Q. and Stephen, R.M., April 1984, (PB84 209 402)A08.

UCB/EERC-84/03 "Refined Modelling of Reinforced Concrete Columns for Seismic Analysis," by Kaba, S.A. and Mahin, S.A., April 1984, (PB84 234 384)A06.

UCB/EERC-84/04 "A New Floor Response Spectrum Method for Seismic Analysis of Multiply Supported Secondary Systems," by Asfura, A. and Der Kiureghian, A., June 1984, (PB84 239 417)A06.

UCB/EERC-84/05 "Earthquake Simulation Tests and Associated Studies of a 1/5th-scale Model of a 7-Story R/C Frame-Wall Test Structure," by Bertero, V.V., Aktan, A.E., Charney, F.A. and Sause, R., June 1984, (PB84 239 409)A09.

UCB/EERC-84/06 "R/C Structural Walls: Seismic Design for Shear," by Aktan, A.E. and Bertero, V.V., 1984.

UCB/EERC-84/07 "Behavior of Interior and Exterior Flat-Plate Connections subjected to Inelastic Load Reversals," by Zee, H.L. and Moehle, J.P., August 1984, (PB86 117 629/AS)A07.

UCB/EERC-84/08 "Experimental Study of the Seismic Behavior of a Two-Story Flat-Plate Structure," by Moehle, J.P. and Diebold, J.W., August 1984, (PB86 122 553/AS)A12.

UCB/EERC-84/09 "Phenomenological Modeling of Steel Braces under Cyclic Loading," by Ikeda, K., Mahin, S.A. and Dermitzakis, S.N., May 1984, (PB86 132 198/AS)A08.

UCB/EERC-84/10 "Earthquake Analysis and Response of Concrete Gravity Dams," by Fenves, G. and Chopra, A.K., August 1984, (PB85 193 902/AS)A11.

UCB/EERC-84/11 "EAGD-84: A Computer Program for Earthquake Analysis of Concrete Gravity Dams," by Fenves, G. and Chopra, A.K., August 1984, (PB85 193 613/AS)A05.

UCB/EERC-84/12 "A Refined Physical Theory Model for Predicting the Seismic Behavior of Braced Steel Frames," by Ikeda, K. and Mahin, S.A., July 1984, (PB85 191 450/AS)A09.

UCB/EERC-84/13 "Earthquake Engineering Research at Berkeley - 1984," by , August 1984, (PB85 197 341/AS)A10.

UCB/EERC-84/14 "Moduli and Damping Factors for Dynamic Analyses of Cohesionless Soils," by Seed, H.B., Wong, R.T., Idriss, I.M. and Tokimatsu, K., September 1984, (PB85 191 468/AS)A04.

UCB/EERC-84/15 "The Influence of SPT Procedures in Soil Liquefaction Resistance Evaluations," by Seed, H.B., Tokimatsu, K., Harder, L.F. and Chung, R.M., October 1984, (PB85 191 732/AS)A04.

UCB/EERC-84/16 "Simplified Procedures for the Evaluation of Settlements in Sands Due to Earthquake Shaking," by Tokimatsu, K. and Seed, H.B., October 1984, (PB85 197 887/AS)A03.

UCB/EERC-84/17 "Evaluation of Energy Absorption Characteristics of Bridges under Seismic Conditions," by Imbsen, R.A. and Penzien, J., November 1984.

UCB/EERC-84/18 "Structure-Foundation Interactions under Dynamic Loads," by Liu, W.D. and Penzien, J., November 1984, (PB87 124 889/AS)A11.

UCB/EERC-84/19 "Seismic Modelling of Deep Foundations," by Chen, C.-H. and Penzien, J., November 1984, (PB87 124 798/AS)A07.

UCB/EERC-84/20 "Dynamic Response Behavior of Quan Shui Dam," by Clough, R.W., Chang, K.-T., Chen, H.-Q., Stephen, R.M., Ghanaat, Y. and Qi, J.-H., November 1984, (PB86 115177/AS)A07.

UCB/EERC-85/01 "Simplified Methods of Analysis for Earthquake Resistant Design of Buildings," by Cruz, E.F. and Chopra, A.K., February 1985, (PB86 112299/AS)A12.

UCB/EERC-85/02 "Estimation of Seismic Wave Coherency and Rupture Velocity using the SMART 1 Strong-Motion Array Recordings," by Abrahamson, N.A., March 1985, (PB86 214 343)A07.

UCB/EERC-85/03 "Dynamic Properties of a Thirty Story Condominium Tower Building," by Stephen, R.M., Wilson, E.L. and Stander, N., April 1985, (PB86 118965/AS)A06.

UCB/EERC-85/04 "Development of Substructuring Techniques for On-Line Computer Controlled Seismic Performance Testing," by Dermitzakis, S. and Mahin, S., February 1985, (PB86 132941/AS)A08.

UCB/EERC-85/05 "A Simple Model for Reinforcing Bar Anchorages under Cyclic Excitations," by Filippou, F.C., March 1985, (PB86 112 919/AS)A05.

UCB/EERC-85/06 "Racking Behavior of Wood-framed Gypsum Panels under Dynamic Load," by Oliva, M.G., June 1985.

UCB/EERC-85/07 "Earthquake Analysis and Response of Concrete Arch Dams," by Fok, K.-L. and Chopra, A.K., June 1985, (PB86 139672/AS)A10.

UCB/EERC-85/08 "Effect of Inelastic Behavior on the Analysis and Design of Earthquake Resistant Structures," by Lin, J.P. and Mahin, S.A., June 1985, (PB86 135340/AS)A08.

UCB/EERC-85/09 "Earthquake Simulator Testing of a Base-Isolated Bridge Deck," by Kelly, J.M., Buckle, I.G. and Tsai, H.-C., January 1986, (PB87 124 152/AS)A06.

UCB/EERC-85/10 "Simplified Analysis for Earthquake Resistant Design of Concrete Gravity Dams," by Fenves, G. and Chopra, A.K., June 1986, (PB87 124 160/AS)A08.

UCB/EERC-85/11 "Dynamic Interaction Effects in Arch Dams," by Clough, R.W., Chang, K.-T., Chen, H.-Q. and Ghanaat, Y., October 1985, (PB86 135027/AS)A05.

UCB/EERC-85/12 "Dynamic Response of Long Valley Dam in the Mammoth Lake Earthquake Series of May 25-27, 1980," by Lai, S. and Seed, H.B., November 1985, (PB86 142304/AS)A05.

UCB/EERC-85/13 "A Methodology for Computer-Aided Design of Earthquake-Resistant Steel Structures," by Austin, M.A., Pister, K.S. and Mahin, S.A., December 1985, (PB86 159480/AS)A10 .

UCB/EERC-85/14 "Response of Tension-Leg Platforms to Vertical Seismic Excitations," by Liou, G.-S., Penzien, J. and Yeung, R.W., December 1985, (PB87 124 871/AS)A08.

UCB/EERC-85/15 "Cyclic Loading Tests of Masonry Single Piers: Volume 4 - Additional Tests with Height to Width Ratio of 1," by Sveinsson, B., McNiven, H.D. and Sucuoglu, H., December 1985.

UCB/EERC-85/16 "An Experimental Program for Studying the Dynamic Response of a Steel Frame with a Variety of Infill Partitions," by Yanev, B. and McNiven, H.D., December 1985.

UCB/EERC-86/01 "A Study of Seismically Resistant Eccentrically Braced Steel Frame Systems," by Kasai, K. and Popov, E.P., January 1986, (PB87 124 178/AS)A14.

UCB/EERC-86/02 "Design Problems in Soil Liquefaction," by Seed, H.B., February 1986, (PB87 124 186/AS)A03.

UCB/EERC-86/03 "Implications of Recent Earthquakes and Research on Earthquake-Resistant Design and Construction of Buildings," by Bertero, V.V., March 1986, (PB87 124 194/AS)A05.

UCB/EERC-86/04 "The Use of Load Dependent Vectors for Dynamic and Earthquake Analyses," by Leger, P., Wilson, E.L. and Clough, R.W., March 1986, (PB87 124 202/AS)A12.

UCB/EERC-86/05 "Two Beam-To-Column Web Connections," by Tsai, K.-C. and Popov, E.P., April 1986, (PB87 124 301/AS)A04.

UCB/EERC-86/06 "Determination of Penetration Resistance for Coarse-Grained Soils using the Becker Hammer Drill," by Harder, L.F. and Seed, H.B., May 1986, (PB87 124 210/AS)A07.

UCB/EERC-86/07 "A Mathematical Model for Predicting the Nonlinear Response of Unreinforced Masonry Walls to In-Plane Earthquake Excitations," by Mengi, Y. and McNiven, H.D., May 1986, (PB87 124 780/AS)A06.

UCB/EERC-86/08 "The 19 September 1985 Mexico Earthquake: Building Behavior," by Bertero, V.V., July 1986.

UCB/EERC-86/09 "EACD-3D: A Computer Program for Three-Dimensional Earthquake Analysis of Concrete Dams," by Fok, K.-L., Hall, J.F. and Chopra, A.K., July 1986, (PB87 124 228/AS)A08.

UCB/EERC-86/10 "Earthquake Simulation Tests and Associated Studies of a 0.3-Scale Model of a Six-Story Concentrically Braced Steel Structure," by Uang, C.-M. and Bertero, V.V., December 1986, (PB87 163 564/AS)A17.

UCB/EERC-86/11 "Mechanical Characteristics of Base Isolation Bearings for a Bridge Deck Model Test," by Kelly, J.M., Buckle, I.G. and Koh, C.-G., 1987.

UCB/EERC-86/12 "Effects of Axial Load on Elastomeric Isolation Bearings," by Koh, C.-G. and Kelly, J.M., 1987.

UCB/EERC-87/01 "The FPS Earthquake Resisting System: Experimental Report," by Zayas, V.A., Low, S.S. and Mahin, S.A., June 1987.

UCB/EERC-87/02 "Earthquake Simulator Tests and Associated Studies of a 0.3-Scale Model of a Six-Story Eccentrically Braced Steel Structure," by Whittaker, A., Uang, C.-M. and Bertero, V.V., July 1987.

UCB/EERC-87/03 "A Displacement Control and Uplift Restraint Device for Base-Isolated Structures," by Kelly, J.M., Griffith, M.C. and Aiken, I.D., April 1987.

UCB/EERC-87/04 "Earthquake Simulator Testing of a Combined Sliding Bearing and Rubber Bearing Isolation System," by Kelly, J.M. and Chalhoub, M.S., 1987.

UCB/EERC-87/05 "Three-Dimensional Inelastic Analysis of Reinforced Concrete Frame-Wall Structures," by Moazzami, S. and Bertero, V.V., May 1987.

UCB/EERC-87/06 "Experiments on Eccentrically Braced Frames with Composite Floors," by Ricles, J. and Popov, E., June 1987.

UCB/EERC-87/07 "Dynamic Analysis of Seismically Resistant Eccentrically Braced Frames," by Ricles, J. and Popov, E., June 1987.

UCB/EERC-87/08 "Undrained Cyclic Triaxial Testing of Gravels-The Effect of Membrane Compliance," by Evans, M.D. and Seed, H.B., July 1987.

UCB/EERC-87/09 "Hybrid Solution Techniques for Generalized Pseudo-Dynamic Testing," by Thewalt, C. and Mahin, S.A., July 1987.

UCB/EERC-87/10 "Ultimate Behavior of Butt Welded Splices in Heavy Rolled Steel Sections," by Bruneau, M. Mahin, S.A. and Popov, E., September 1987.

UCB/EERC-87/11 "Residual Strength of Sand from Dam Failures in the Chilean Earthquake of March 3, 1985," by De Alba, P., Seed, H.B., Retamal, E. and Seed, R.B., September 1987.

UCB/EERC-87/12 "Inelastic Seismic Response of Structures with Mass or Stiffness Eccentricities in Plan," by Bruneau, M. and Mahin, S.A., September 1987.

UCB/EERC-87/13 "CSTRUCT: An Interactive Computer Environment for the Design and Analysis of Earthquake Resistant Steel Structures," by Austin, M.A., Mahin, S.A. and Pister, K.S., September 1987.

UCB/EERC-87/14 "Experimental Study of Reinforced Concrete Columns Subjected to Multi-Axial Loading," by Low, S.S. and Moehle, J.P., September 1987.

UCB/EERC-87/15 "Relationships between Soil Conditions and Earthquake Ground Motions in Mexico City in the Earthquake of Sept. 19, 1985," by Seed, H.B., Romo, M.P., Sun, J., Jaime, A. and Lysmer, J., October 1987.

UCB/EERC-87/16 "Experimental Study of Seismic Response of R. C. Setback Buildings," by Shahrooz, B.M. and Moehle, J.P., October 1987.

UCB/EERC-87/17 "The Effect of Slabs on the Flexural Behavior of Beams," by Pantazopoulou, S.J. and Moehle, J.P., October 1987.

UCB/EERC-87/18 "Design Procedure for R-FBI Bearings," by Mostaghel, N. and Kelly, J.M., November 1987.

UCB/EERC-87/19 "Analytical Models for Predicting the Lateral Response of R C Shear Walls: Evaluation of their Reliability," by Vulcano, A. and Bertero, V.V., November 1987.

UCB/EERC-87/20 "Earthquake Response of Torsionally-Coupled Buildings," by Hejal, R. and Chopra, A.K., December 1987.

UCB/EERC-87/21 "Dynamic Reservoir Interaction with Monticello Dam," by Clough, R.W., Ghanaat, Y. and Qiu, X-F., December 1987.

UCB/EERC-87/22 "Strength Evaluation of Coarse-Grained Soils," by Siddiqi, F.H., Seed, R.B., Chan, C.K., Seed, H.B. and Pyke, R.M., December 1987.

UCB/EERC-88/01 "Seismic Behavior of Concentrically Braced Steel Frames," by Khatib, I., Mahin, S.A. and Pister, K.S., January 1988.

UCB/EERC-88/02 "Experimental Evaluation of Seismic Isolation of Medium-Rise Structures Subject to Uplift," by Griffith, M.C., Kelly, J.M., Coveney, V.A. and Koh, C.G., January 1988.

UCB/EERC-88/03 "Cyclic Behavior of Steel Double Angle Connections," by Astaneh-Asl, A. and Nader, M.N., January 1988.

UCB/EERC-88/04 "Re-evaluation of the Slide in the Lower San Fernando Dam in the Earthquake of Feb. 9, 1971," by Seed, H.B., Seed, R.B., Harder, L.F. and Jong, H.-L., April 1988.

UCB/EERC-88/05 "Experimental Evaluation of Seismic Isolation of a Nine-Story Braced Steel Frame Subject to Uplift," by Griffith, M.C., Kelly, J.M. and Aiken, I.D., May 1988.

UCB/EERC-88/06 "DRAIN-2DX User Guide.," by Allahabadi, R. and Powell, G.H., March 1988.

UCB/EERC-88/07 "Cylindrical Fluid Containers in Base-Isolated Structures," by Chalhoub, M.S. and Kelly, J.M., April 1988.

UCB/EERC-88/08 "Analysis of Near-Source Waves: Separation of Wave Types using Strong Motion Array Recordings," by Darragh, R.B., June 1988.

UCB/EERC-88/09 "Alternatives to Standard Mode Superposition for Analysis of Non-Classically Damped Systems," by Kusainov, A.A. and Clough, R.W., June 1988.

UCB/EERC-88/10 "The Landslide at the Port of Nice on October 16, 1979," by Seed, H.B., Seed, R.B., Schlosser, F., Blondeau, F. and Juran, I., June 1988.

UCB/EERC-88/11 "Liquefaction Potential of Sand Deposits Under Low Levels of Excitation," by Carter, D.P. and Seed, H.B., August 1988.

UCB/EERC-88/12 "Analysis of Nonlinear Response of Reinforced Concrete Frames to Cyclic Load Reversals," by Filippou, F.C. and Issa, A., September 1988.

UCB/EERC-88/13 "Earthquake-Resistant Design of Building Structures: An Energy Approach," by Uang, C.-M. and Bertero, V.V., September 1988.

UCB/EERC-88/14 "An Experimental Study of the Behavior of Dual Steel Systems," by Whittaker, A.S., Uang, C.-M. and Bertero, V.V., September 1988.

UCB/EERC-88/15 "Dynamic Moduli and Damping Ratios for Cohesive Soils," by Sun, J.I., Golesorkhi, R. and Seed, H.B., August 1988.

UCB/EERC-88/16 "Reinforced Concrete Flat Plates Under Lateral Load: An Experimental Study Including Biaxial Effects," by Pan, A. and Moehle, J., November 1988.

UCB/EERC-88/17 "Earthquake Engineering Research at Berkeley - 1988," November 1988.